Coordination of Endoplasmic Reticulum–Associated RNA and Protein Degradation Pathways

Inaugural–Dissertation
zur
Erlangung des Doktorgrades
der Mathematisch–Naturwissenschaftlichen Fakultät
der Universität zu Köln

vorgelegt von
Sotirios Efstathiou
geboren am 20.09.1994 in Köln, DE

Köln, 2024

Gutachter: **Prof. Dr. Thorsten Hoppe**
Institut für Genetik, CECAD Forschungszentrum, Universität zu Köln

Prof. Dr. David Vilchez
Institut für Genetik, CECAD Forschungszentrum, Universität zu Köln

Prof. Dr. Gunter Meister
Institut für Biochemie,
Universität Regensburg

Vorsitzender der Prüfungskommission: **Prof. Dr. Jan Riemer**
Institut für Biochemie,
Universität zu Köln

Tag der letzten mündlichen Prüfung: **08 Juli 2024**

Contents

Abstract I
Zusammenfassung II
Acknowledgements III
List of Publications IV
List of Figures VI
List of Tables VII
List of Abbreviations VIII
List of Gene Orthologues X

1 Introduction 1
1.1 Coordination of Eukaryotic Gene Expression . . . 2
1.1.1 RNA Quality Control and Degradation Pathways . . . 3
1.1.1.1 Principles of RNA Destabilization and Degradation. . . . 3
1.1.1.2 AGO-dependent RNA Silencing. . . . 5
1.1.1.3 UPF1-dependent RNA Decay . . . 9
1.1.1.4 IRE1-dependent RNA Decay . . . 12
1.1.2 Protein Quality Control and Degradation Pathways . . . 14
1.1.2.1 Ubiquitin-Conjugation . . . 14
1.1.2.2 The Ubiquitin-Proteasome System and Autophagy . . . 14
1.1.2.3 Ribosome-associated Quality Control . . . 16
1.2 Endoplasmic Reticulum Function and Homeostasis . . . 16
1.2.1 ER Protein Targeting and Cotranslational Translocation. . . . 16
1.2.2 ER Protein Quality Control and Degradation Pathways . . . 18
1.2.2.1 ER UFMylation System . . . 19
1.2.2.2 ER Chaperon Systems . . . 20
1.2.2.3 ER Proteolytic Systems . . . 22
1.2.2.4 ER-Associated Protein Degradation . . . 22
1.2.2.5 ER-to-Lysosome-Associated Degradation | ER-Phagy . . . 24
1.2.3 Cytoprotective Stress Responses of the ER . . . 25
1.2.3.1 The Unfolded Protein Response of the ER. . . . 25
1.2.3.2 The Integrated Stress Response . . . 26
1.3 Molecular Tools to Study ER Homeostasis in *C.elegans* . . . 27
1.3.1 *C. elegans* as Model Organism to Study ER Homeostasis . . . 27
1.3.2 COPAS Large Particle Flow Cytometry for *C. elegans* . . . 29
1.4 Objectives of the Dissertation . . . 31

2 Results **32**
2.1 Publication A: ER-Associated RNA Silencing Promotes ER Quality Control. 33
2.1.1 Summary Publication A 33
2.1.2 Contribution to Publication A. 34
2.1.3 Follow-up of publication A 35
2.1.3.1 ERAS and ERAD regulate human alpha-1-antitrypsin in *C. elegans* 35
2.1.3.2 SEL-11 auto-ubiquitination does not impact ERAD function . . 39
2.2 Publication B: Cutting through the Stress: RNA Decay Pathways at the Endoplasmic Reticulum 43
2.2.1 Summary publication B 43
2.2.2 Contribution to publication B. 44
2.2.3 Follow-up of publication B 45
2.2.3.1 Epistasis knockdown screen of ERAS and ERQC factors. 45

3 Discussion **55**
3.1 What makes an ERAS target? 56
3.1.1 Reevaluating ER stress as a primary trigger for ERAS activation . . 57
3.1.2 Could the transgene composition influence ERAS target specificity? 58
3.1.3 Is ERAD participation a more accurate indicator of ERAS activation? 62
3.1.4 Emerging AGO-dependent and ER-associated RNA and protein degradation pathway 63
3.2 What is the source of the small guide RNA species in ERAS? 64
3.3 Conclusion and outlook 66

4 Material and Methods **68**
4.1 Consumables and Instruments. 69
4.2 Software and Resources 69
4.3 Antibodies. 70
4.4 Microbiology 70
4.4.1 Media and Solutions 70
4.4.2 Antibiotics. 71
4.4.3 Bacterial Strains. 71
4.4.4 Cultivation of Bacteria 71
4.5 Molecular Biology 72
4.5.1 Solutions 72
4.5.2 Oligonucleotides 72

4.5.3 Polymerase chain reactions (PCR) 75
4.5.4 Agarose gel electrophoresis 75
4.5.5 Sodium-dodecyl sulfate polyacrylamid gel electrophoresis (SDS-PAGE) 76
4.5.6 Quantitative Western Blotting 76
4.6 *C.elegans* Techniques 77
4.6.1 Buffer and Solutions 77
4.6.2 Strains 77
4.6.3 Age synchronization of *C.elegans* 81
4.6.4 Preparation of protein lysates for Western Blotting 81
4.6.5 Single worm lysis 81
4.6.6 Generation of *C.elegans* males 81
4.6.7 Crossing of *C.elegans* strains 81
4.6.8 RNA isolation 82
4.6.9 cDNA synthesis and real time quantitative PCR (RT-qPCR) 82
4.6.10 RNA Interference (RNAi) 83
4.6.11 Cellular microsomal fractionation assay 83
4.6.12 UV cross-link immunoprecipitation (CLIP) 83
4.6.13 COPAS quantification of fluorescence and extinction 84

5 References **85**

6 Erklärung zur Dissertation **110**

7 Curriculum Vitae **112**

A Appendix **114**
A.1 Epistasis knockdown screen of ERQC and ERAS factors 115
A.2 Publication A: ER-associated RNA silencing promotes ER quality control 120
A.3 Publication B: Cutting through the stress: RNA decay pathways at the endoplasmic reticulum 151

Abstract

The endoplasmic reticulum (ER) is crucial for the translation, maturation, and sorting of luminal, transmembrane, and secretory proteins. A decline in ER-localized gene expression fidelity can lead to the production of mRNAs and proteins in harmful quantities and compromised quality, characterized by sequence errors, incorrect localization, and improper folding. Downstream consequences of this decline in fidelity include ER stress and an overwhelming protein-folding burden, which together compromise ER function and lead to severe impairments at the cellular, tissue, and organismal levels. Beyond the well-known IRE1α-dependent mRNA decay (RIDD) and ER-associated degradation (ERAD), the mechanisms that coordinate the maintenance of ER-associated gene expression fidelity are not well understood.

In this study, through genetic screening in *Caenorhabditis elegans (C. elegans)* expressing an ERAD model substrate, we identified a somatic RNA silencing process that enhances ER quality control (ERQC). This process, which we named ER-associated RNA silencing (ERAS), works in tandem with ERAD to maintain ERQC. Triggered by ER stress, ERAS is facilitated by the Argonaute protein RDE-1/AGO2, promoting the turnover of ER-associated RNAs and is conserved in mammals. Our findings reveal ERAS and ERAD as complementary systems; their simultaneous inactivation leads to increased ER stress, reduced protein quality control, and impaired intestinal integrity. These results underscore the protective synergy between ERAS and ERAD in maintaining ER homeostasis and overall organismal health.

This study further reviews various ER-associated RNA decay pathways, including RIDD, nonsense-mediated mRNA decay (NMD), and AGO2-dependent RNA silencing. It then explores the coordination between those ER-associated RNA and protein degradation mechanisms by conducting a genetic epistasis screen to analyze the interactions of these pathways with ERAS. Collectively, this work offers a comprehensive view of mechanisms governing the 'Coordination of ER-Associated RNA and Protein Degradation Pathways'.

Zusammenfassung

Das endoplasmatische Retikulum (ER) ist entscheidend für die Translation, Prozessierung und Sortierung von ER-luminalen, sekretorischen und Transmembranproteinen. Eine beeinträchtigte Präzision der am ER lokalisierten Genexpression kann zur Produktion von mRNAs und Proteinen in schädlicher Menge und beeinträchtigter Qualität führen, die durch Sequenzfehler, falsche Lokalisierung und falsche Faltung gekennzeichnet ist. Zu den Konsequenzen gehören ER-Stress und eine Überlastung der Proteinfaltungskapazität, die zusammen die ER-Funktion erschweren und zu schwerwiegenden Beeinträchtigungen auf Zell-, Gewebe- und Organismusebene führen. Neben den bekannten Prozessen wie dem IRE1α-dependent mRNA decay (RIDD) und der ER-associated degradation (ERAD) sind die Mechanismen, welche die Präzision der ER-assoziierten Genexpression koordinieren, noch nicht gut verstanden.

In dieser Dissertaton haben wir durch genetisches Screening in *Caenorhabditis elegans (C. elegans)*, welches ein ERAD-Modellsubstrat exprimiert, einen somatischen RNA-Silencing-Prozess identifiziert, der die ER quality control (ERQC) verbessert. Dieser Prozess, den wir ER-associated RNA silencing (ERAS) genannt haben, arbeitet mit ERAD zusammen, um ERQC aufrechtzuerhalten. Ausgelöst durch ER-Stress, werden im ERAS-Prozess ER-assoziierte RNAs durch das Argonaute-Protein RDE-1/AGO2 abgebaut, ein Mechanismus, der auch in Säugetieren konserviert ist. Unsere Ergebnisse zeigen, dass ERAS und ERAD komplementäre Systeme sind; ihre gleichzeitige Inaktivierung führt in *C. elegans* zu erhöhtem ER-Stress, verminderter Proteinqualitätskontrolle und beeinträchtigter intestinaler Integrität. Diese Ergebnisse unterstreichen die protektive Synergie zwischen ERAS und ERAD bei der Aufrechterhaltung der ER-Homöostase und der allgemeinen Gesundheit des Organismus.

Im zweiten Teil dieser Dissertation haben wir ein Review der verschiedenen ER-assoziierten RNA-Abbauprozesse verfasst, welches RIDD, den Nonsense-mediated mRNA decay (NMD) und das AGO2-abhängigen RNA-Silencing einschliesst. Anschließend wird die Koordination zwischen diesen ER-assoziierten RNA- und Proteinabbaumechanismen untersucht, indem ein genetischer Epistasis-Screen durchgeführt wird, um die Interaktionen dieser Mechanismen mit ERAS zu analysieren. Insgesamt zeigt diese Arbeit auf, wie ER-assoziierte RNA- und Proteinabbaupfade zur Aufrechterhaltung der präzisen ER-lokalisierten Genexpression beitragen.

Acknowledgements

I am profoundly grateful to Prof. Dr. Thorsten Hoppe for the opportunity to work under his guidance and for his mentorship throughout my PhD journey. There are many aspects of our collaboration that have reassured me of my decision to conduct my dissertation in his lab, but one example stands out as particularly impactful. I vividly remember a period of intense self-doubt when I questioned my role in the project and my capacity as a PhD candidate. During this crucial time, Thorsten's unwavering support and his ability to put things into perspective were pivotal. His supportive attitude not only guided me through my difficulties in the project but also reignited my confidence and dedication to my work. Oh, and I truly appreciated how Thorsten gave me the freedom to think and work creatively and independently, often placing me behind the wheel of a race car at full throttle—to see if I could acclimate and learn during the race. I believe that I managed to do just that.

I am sincerely grateful to Prof. Dr. David Vilchez for his guidance and realistic insights during my TAC meetings, alongside Prof. Dr. Martin Graef, who not only helped shape my project and maintain my focus but also streamlined the dissertation process. I particularly thank David for his willingness to serve as the second reviewer of my dissertation.

I am also thankful to Prof. Dr. Jan Riemer for agreeing to chair my thesis defense and for the mentoring advice he provided during my studies in Cologne. Further, I want to thank two special colleagues and friends, Franzi and André, for the countless hours of seemingly endless but thoroughly enjoyable scientific and personal discussions that greatly enriched my time during the PhD. At this point, I want to extend my heartfelt thanks to all the members of the Hoppe lab for the wonderful and challenging times we shared together. I want to thank Agata, the distributor of hugs, guardian of the worm database, and sweetest person alive, for her unwavering positive attitude and her unconditional warmth, regardless of my mishaps with her beloved database.

I want to thank the thick net of family and friends around me, whose importance in my life goes beyond the scope of this page to describe.

Most importantly, I want to express my deepest gratitude to Nina, my partner and greatest ally. Her unique perspective nudged me to appreciate life beyond academic achievements, finding joy, irony, and humor on the go, which has profoundly enriched my PhD journey. A path forward is always just one thoughtful conversation away and I am curious to see where it ends up going.

List of Publications

The following peer-reviewed and published research (I) and review (II) articles form the basis of this dissertation:

(I) **Efstathiou, S***., Ottens, F.*, Schütter, L. S.*, Ravanelli, S., Charmpilas, N., Gutschmidt, A., le Pen, J., Gehring, N. H., Miska, E. A., Bouças, J., & Hoppe, T. (2022). ER-associated RNA silencing promotes ER quality control. *Nature Cell Biology*, 24(12), 1714–1725. https://doi.org/10.1038/S41556-022-01025-4

(II) Ottens, F.*, **Efstathiou, S***., & Hoppe, T. (2023). Cutting through the stress: RNA decay pathways at the endoplasmic reticulum. In *Trends in Cell Biology*. Elsevier Ltd. https://doi.org/10.1016/j.tcb.2023.11.003

* These authors contributed equally

List of Figures

1 Coordination of eukaryotic gene expression: the journey from DNA to the protein . . . 2
2 Eukaryotic mRNA structure and mRNA decay processes . . . 4
3 Dicer and AGO in somatic RNA silencing . . . 5
4 The siRNA pathway in *C. elegans* . . . 6
5 The miRNA pathway in mammalian translational repression and mRNA decay . . . 8
6 Nonsense-mediated mRNA decay in mammals . . . 11
7 IRE1-dependent decay in mammals . . . 13
8 The ubiquitin conjugation pathway . . . 14
9 Pathway choice between the ubiquitin-proteasome system and autophagy . . . 15
10 Substrate-driven composition of the SEC61 translocon . . . 17
11 ER-associated degradation . . . 23
12 The unfolded protein response of the ER . . . 26
13 ERQC, ER homeostasis and ISR reporter strains in *C. elegans* . . . 28
14 Schematic overview of the COPAS flow cell . . . 29
15 ERAS and ERAD maintain ERQC . . . 33
16 ERAS and ERAD reduce *ATM* and *ATZ* protein levels . . . 37
17 ERAS degrades the mRNA of *ATM* and *ATZ* . . . 38
18 Sequence alignment of SEL-11 reveals a single conserved lysine in the RING domain . . . 39
19 *sel-11(K306R)* mutation does not lead to impaired ERAD . . . 41
20 *sel-11(K306R)* does not trigger UPR^{ER} . . . 42
21 Model of ER-associated RNA decay pathways and their ERQC integration . . . 44
22 Examining the interplay between ER-associated RNA and protein degradation machinery with ERAS . . . 45
23 Generation of ERQC knockdown library in conjunction with *rde-1* 46
24 Fluorescence quantification strategy with COPAS . . . 47
25 Extinction quantification strategy with COPAS . . . 48
26 ERQC RNAi screen: reporter activation and developmental delay 49
27 ERQC RNAi screen: correlation between UPR^{ER} and $CPL\text{-}1^{WT}$ levels 51
28 ERQC RNAi screen: $CPL\text{-}1^{WT}$ levels under ER stress inducing knockdowns . . . 51
29 ERQC RNAi screen: correlation analysis between UPR^{ER}, ISR and ERQC . . . 52

30 ERQC RNAi screen: strain-specific developmental delay 53
31 ERQC RNAi screen: extinction correlation analysis between CPL-1* and CPL-1^{WT} 54
32 Two models of ERAS activation 56
33 Model of trans-acting ERAS activation by miRNAs or endo-siRNAs 60
34 Comparison of ER-targeted reporter substrates 63
35 Model of ER-RQC, ERAD, and RNA silencing cooperation 64
36 Speculative model of RIDD(LE)-mediated generation of RNA Fragments for RNA silencing 66
A. 1 Knockdown screen: ER-associated E3 ligases 115
A. 2 Knockdown screen: ER-associated NMD 116
A. 3 Knockdown screen: ER-resident signal peptidase complex 117
A. 4 Knockdown screen: UFMylation machinery 118
A. 5 Knockdown screen: miRNA silencing 119

List of Tables

1 List of primary and secondary antibodies used in this study. . . . 70
2 List of media and solutions used in this study. 70
3 List of antibiotics used in this study. 71
4 List of *E. coli* strains used in this study. 71
5 List of solutions used for experiments in molecular biology in this study. 72
6 List of oligonucleotides for genotyping experiments in this study 73
7 List of oligonucleotides for RT-qPCR experiments used in this study 74
8 Genotyping reaction mix components. 75
9 Standard protocol of the thermocycler for genotyping PCR. . . . 75
10 List of solutions and buffers used for experiments with *C. elegans* in this study. 77
11 List of *C. elegans* strains in this study 77

List of Abbreviations

AGO	Argonaute
AGO-RQC	Argonaute-dependent ribosome-associated quality control
ATT	Alpha-1 antitrypsin
Cas9	CRISPR-associated protein 9
CDS	Coding sequence
CHX	Cycloheximide
CRISPR	Clustered regularly interspaced short palindromic repeats
DNA	Deoxyribonucleic acid
DUB	Deubiquitinase enzyme
dsRNA	Double-stranded RNA
EMC	ER membrane complex
ER	Endoplasmic reticulum
ERAD	ER-associated degradation
ERAS	ER-associated RNA silencing
ER-E3	Endoplasmic reticulum-associated ubiquitin ligase
ERLAD	ER-to-lysosome-associated degradation
ER-NMD	ER-associated Nonsense-mediated RNA decay
E1	Ubiquitin-activating enzyme
E2	Ubiquitin-conjugating enzyme
E3	Ubiquitin ligase
EJC	Exon junction complex
GET	Guided entry of tail-anchored proteins
GMD	Glucocorticoid receptor-mediated mRNA decay
GOF	Gain-of-function
HMD	Replication-dependent histone mRNA decay

ISR	Integrated stress response
miRNA	MicroRNA
mRNA	Messenger RNA
NAC	Nascent chain-associated complex
NC	Nascent chain
NGD	No-go decay
NSD	Non-stop decay
PTC	Premature termination codons
PTGS	Transcriptional gene silencing system
RdRP	RNA-dependent RNA polymerase
RIDD	IRE1α-dependent mRNA decay
RIDDLE	IRE1α-dependent mRNA decay lacking endomotif
RMD	Regnase 1-mediated mRNA decay
RNA	Ribonucleic acid
RNAi	RNA interference
RQC	Ribosome-associated quality control
SMD	Staufen-mediated mRNA decay
SBS	Staufen-binding sites
siRNA	Short interfering RNA
TOF	Time-of-flight
TumiD	Tudor-SN-mediated endonucleolytic decay
uORF	Upstream open reading frames
UPS	Ubiquitin-proteasome system
UTR	Untranslated region
UPR^{ER}	Unfolded protein response of the endoplasmic reticulum
C. elegans	*Caenorhabditis elegans*
D. melanogaster	*Drosophila melanogaster*
H. sapiens	*Homo sapiens*
S. cerevisiae	*Saccharomyces cerevisiae*

List of Gene Orthologues

H. sapiens	*C. elegans*	Pathway
AGO2	RDE-1	ERAS
DICER	DCR-1	ERAS
RIG-I	DRH-1	ERAS
SIDT1	SID-1	siRNA
-	SID-2	siRNA
TRBP/PACT^{X}	RDE-4	siRNA
-	RRF-1	siRNA
-	WAGO-1	siRNA
AGO1-4^{X}	ALG-1	miRNA
AGO1-4^{X}	ALG-2	miRNA
GW182^{X}	AIN-1	miRNA
GW182^{X}	AIN-2	miRNA
eIF4E^{X}	IFE-1	miRNA
eIF4E^{X}	IFE-2	miRNA
SMG1	SMG-1	NMD
UPF1	SMG-2	NMD
NBAS	SMGL-1	ER-NMD
DHX32	SMGL-2	ER-NMD
STAUFEN1	STAU-1	ER-NMD
IRE1	IRE-1	UPR^{ER}
ATF6	ATF-6	UPR^{ER}
PERK	PEK-1	UPR^{ER}
XBP1s	XBP-1s	UPR^{ER}

H. sapiens	*C. elegans*	Pathway
TRAP^{X}	TRAP-1,3	ER-Translation
SEC61	SEC-61	ER-Translation
BIP	HSP-4	ERAD | UPR^{ER}
CANX	CNX-1	ERAD
CALR	CRT-1	ERAD
OS9	F48E8.4	ERAD
DERL2	DER-2	ERAD
HERP	-	ERAD
VCP	CDC-48	ERAD | RQC
HRD1	SEL-11	ERAD
SEL1L	SEL-1	ERAD
MARCH6F	MARC-6	ERAD
LTN1	LTN-1	RQC
SPCS1	SPCS-1	SPP
SPCS2	SPCS-2	SPP
SPCS3	SPCS-3	SPP
RPL26	RPL-26	UFMylation
UFM1	UFM-1	UFMylation
UFL1	UFL-1	UFMylation
ATF4	ATF-5	ISR
eIF2α	eIF-2α	ISR

^{X}: Instead of the specific gene name of the orthologues factor, this entry denotes the corresponding functional orthologues protein class or complex within the pathway

1 Introduction

1.1 Coordination of Eukaryotic Gene Expression

Eukaryotic cells exert tremendous control over their protein production through multiple regulatory mechanisms. These mechanisms function at six key stages of gene expression and protein synthesis, ensuring precise control over cellular function: ① Transcriptional control involves regulating the timing and frequency of gene transcription. ② pre-mRNA processing control manages the splicing and processing of mRNA transcripts. ③ RNA transport and localization control govern the export of mRNAs from the nucleus to the cytosol and their final subcellular localization. ④ Translational control selects which mRNAs are translated. ⑤ mRNA degradation control involves the selective destabilization of mRNAs. ⑥ Protein activity control encompasses the activation, inactivation, degradation, or localization of proteins (Figure 1).

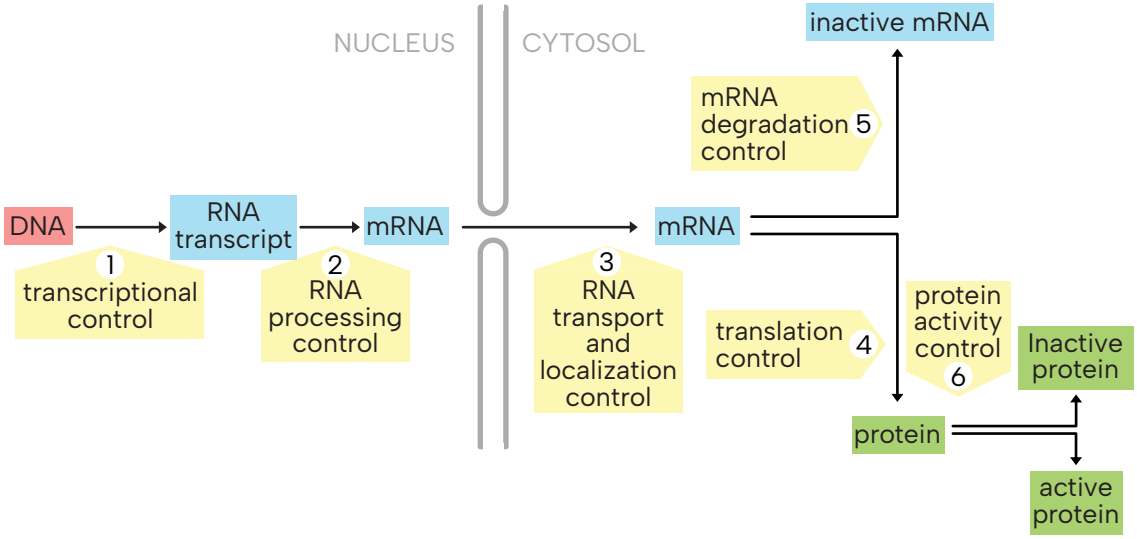

Figure 1: **Coordination of eukaryotic gene expression: the journey from DNA to the protein**. For protein-coding genetic information to be translated into an active protein, it must navigate through multiple regulatory checkpoints (yellow). The genetic information is encoded in DNA (red), which is transcribed into mRNA (blue), and translated into a protein (green). The flow of genetic information is shaped at any of these regulatory checkpoints, ensuring the fidelity of gene expression through both the quantity and quality of DNA, mRNA, and protein. Figure reproduced from [1].

The fidelity of mRNA and protein biosynthesis declines with age and in response to external stressors, a phenomenon that has only recently been captured on the global level for both transcription [2, 3] and translation [4, 5]. This decline in fidelity results in the production of mRNAs and proteins in detrimental quantities and compromised quality, characterized by sequence errors, improper folding, and incorrect localization. Over time, these anomalies can overwhelm proteostasis networks, leading to an accumulation of dysfunctional, misfolded, and aggregating proteins, ultimately causing proteostasis collapse and resulting in cell death [6, 7].

This dissertation focuses on the "Coordination of ER-Associated RNA and Protein Degradation Pathways". A wide array of regulatory mechanisms are employed to regulate the fidelity of gene expression to the ER, a subcellular compartment that is tasked with the translation, folding, and maturation of up to one-third of the cellular proteome [8]. In particular, this dissertation focuses on post-transcriptional processes related to RNA ③ localization and ⑤ degradation control, as well as, protein ④ translation and ⑥ activity control through protein degradation. The subsequent chapters of the introduction systematically outline the key post-transcriptional pathways that maintain the fidelity of gene expression at both the RNA (1.1.1) and protein (1.1.2) levels, and describe how these pathways are integrated within the ER (1.2.2). After introducing the complex machinery that regulates gene expression fidelity, the final two chapters of the introduction explore how this machinery can be studied using the multicellular model organism *C. elegans* (1.3) and outline the objectives of this dissertation (1.4).

1.1.1 RNA Quality Control and Degradation Pathways

1.1.1.1 Principles of RNA Destabilization and Degradation

After pre-mRNA splicing and processing, mRNA molecules exported to the cytosol are characterized by a 5′ cap, a 5′ untranslated region (UTR), a coding sequence, a 3′ UTR, and a poly(A) tail (Figure 2). To translate these mRNAs into functional proteins, they must interact effectively with numerous quantity and quality control mechanisms, that post-transcriptionally fine-tune gene expression and select against erroneous mRNAs, respectively [9]. These quality control mechanisms scrutinize potential inefficiencies in the sequence, localization, translation, or folding of encoded proteins. Upon detecting any conspicuous anomalies, they initiate the processes of mRNA destabilization and degradation [10, 9]. Conversely, successful interactions with these same factors ensure productive translation into an active protein. The key cytosolic factors involved in the destabilization and degradation of mRNA are classified by their mechanism of action into five categories: ① 5′ decapping, ② 5′ to 3′ decay, ③ endonucleolytic decay, ④ 3′ deadenylation, and ⑤ 3′ to 5′ decay [10]. The destabilization of mRNA can be initiated through three main mechanisms: 5′ decapping, endonucleolytic cleavage, or 3′ deadenylation, each rendering the mRNA susceptible to degradation via exonucleolytic degradation [10] (Figure 2).

Exonucleolytic degradation is primarily performed by the enzyme XRN1 (5′–3′) and the multiprotein complex known as the SKIV2L Exosome (3′–5′), with recent indications that XRN1 is deployed primarily in cytosolic bulk mRNA degradation while the SKIV2L Exosome is universally recruited to ribosomes during translation [11]. In this dissertation, the terms 'destabilization,' 'degradation,' and 'decay' are specifically defined to delineate distinct stages in the process of RNA stability regulation. 'Destabilization' refers to the initial modifications of mRNA, which include 5′ decapping, endonucleolytic cleavage, or 3′ deadenylation. This is followed by 'degradation,' which involves the bulk exonucleolytic breakdown, either from the 5′ or 3′ end. Together, 'destabilization' and 'degradation' lead to 'decay,' the complete breakdown of an mRNA molecule (Figure 2).

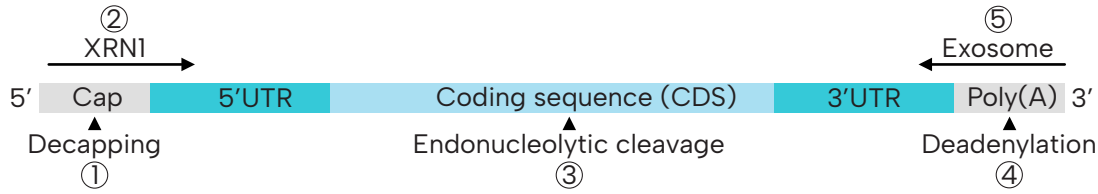

Figure 2: **Eukaryotic mRNA structure and mRNA decay processes**. Eukaryotic mRNA structure from 5′–3′: 5′ cap, 5′ UTR, coding sequence, 3′ UTR, and poly(A) tail. The mRNA destabilizing processes are indicated with triangles: decapping, endonucleolytic cleavage, and deadenylation. Destabilized mRNAs are degraded through exonucleolytic breakdown by XRN1 (5′–3′) and the Exosome (3′–5′). Figure created based on [10]

.

The primary mRNA sequence provides not only the codon triplets necessary for translation into the primary polypeptide sequence but also includes additional sequences and structural elements that regulate various stages of gene expression [12]. These stages include mRNA localization, translation efficiency, and mRNA stability control. Such regulatory elements are located within UTRs or in the CDS (Figure 2), for example, upstream open reading frames (uORFs; see 1.2.3.2) in the 5′ UTR, microRNA (miRNA) binding sites in the 3′ UTR (see 1.1.1.2), and differential codon usage in the CDS [13]. Another example are secondary structures such as stem–loops that can reduce translation efficiency [14] or can serve as motifs for RNA endonucleases as in regulated Ire1–dependent decay (RIDD) (see 1.1.1.4). This dissertation focuses on three highly regulated mRNA destabilization pathways that will be introduced in subsequent sections: somatic RNA silencing (1.1.1.2), UPF1–mediated (1.1.1.3), and IRE1–mediated (1.1.1.4) mRNA decay and examines how these pathways are involved in the coordination of ER–associated RNA and protein degradation.

1.1.1.2 AGO-dependent RNA Silencing

RNA silencing represents one of the most potent tools in eukaryotic cells for regulating both the quantity and the temporal availability of specific mRNAs, especially under stress conditions, allowing cells to adapt rapidly to new challenges [15, 16]. The RNA silencing pathway is a post-transcriptional mechanism that converts double-stranded RNA (dsRNA) into small guide RNA species, which are then used to identify and destabilize RNAs with complementary sequences. This silencing activity is orchestrated by two key players: Dicer and Argonaute (AGO). As input, Dicer recognizes a wide range of dsRNAs and processes them into ~20–30 nt small guide RNA species that are competent for AGO loading (dicing) [17, 18]. Through the complementary base pairing of the guide and target RNAs, AGO proteins selectively silence target mRNAs within the RNA-induced silencing complex (RISC)(Figure 3). Mammalian genomes encode four distinct AGO proteins, AGO1–4, sharing 80 % sequence homology. These proteins have a consistent domain structure that ranges from the N-terminal (N), MID, PIWI/ Argonaute/ Zwille (PAZ) to the P-element-induced wimpy testis (PIWI) domain. To achieve catalytic activity, the MID and PAZ domains bind to the 5′ and 3′ ends of the guide RNA, respectively. The N domain unwinds the guide RNA duplex, and the PIWI domain orchestrates the endonucleolytic cleavage of the target mRNA through a catalytic DEDX (X for H or D) tetrad [19, 20]. AGO2 stands out as the sole mammalian AGO protein with guide RNA-dependent endonucleolytic cleavage activity (slicing), indicating functional similarities to slicer-active AGO proteins found in invertebrates such as RDE-1 *C. elegans* [20, 21].

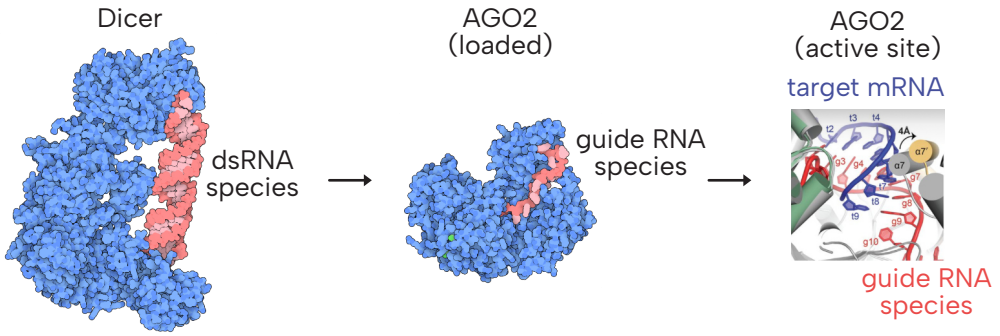

Figure 3: **Structures of Dicer and AGO in somatic RNA silencing**. This figure illustrates the structural basis for sequence-specific silencing of target mRNAs via the two key players in somatic RNA silencing: Dicer and AGO2. Dicer with partner protein R2D2 PBD: 5ZAL [22]; AGO2 (loaded) PBD: 4W5N [23]; AGO2 (active site) PDB: 4W5T [24]. 5ZAL and 4W5N were illustrated with 'Illustrate' by David Goodsell [25].

The somatic RNA silencing pathway includes two well-defined functional manifestations of RISC: the small interfering RNA (siRNA) and miRNA path-

ways. The distinction between these pathways is based primarily on three key factors: ① the origin and structure of the input dsRNA, ② the degree of complementarity between the guide RNA and the target RNAs, and ③ the functional outcome achieved by either mRNA destabilization or translational repression. While AGO 'slicing' involves endonucleolytic cleavage and thus is an mRNA destabilization mechanism, the process of 'silencing' refers to the complete mRNA decay. Somatic RNA silencing utilizes both mRNA destabilization and degradation mechanisms to efficiently mediate the decay of target mRNAs.

siRNA Pathway

The evolutionary roots of the siRNA pathway date back to the last common ancestor of eukaryotes, where it served as an antiviral defense mechanism against deleterious gene sequences from transposable elements and viruses [26, 27]. Silencing by siRNAs is achieved by ① utilizing exogenous dsRNA sources e.g. from viruses, ② producing fully complementary siRNA guide RNA species, and ③ by potently slicing the RNA sources [18]. In *C. elegans*, the transport of dsRNA across the plasma membrane is facilitated by the dsRNA transporters SID-1 and SID-2. While SID-1 is ubiquitously expressed, SID-2 is expressed primarily in intestinal cells [28]. dsRNA is recognized and cut into small 21-25 nt primary siRNA fragments by a protein complex consisting of DRH-1, RDE-1, RDE-4, and DCR-1 [29]. The slicer-competent argonaute protein RDE-1 loads these primary siRNA fragments and selectively binds to the target mRNA within the RISC [30]. From there, target mRNA is either directly sliced or used by RNA-dependent RNA polymerase (RdRP) like RRF-1 to generate secondary siRNA fragments, which are then recognized by secondary argonaute effectors like WAGO-1 to further increase target mRNA decay [18]. Notably, in *C. elegans* the siRNA pathway is functionally multifaceted and can use endogenously derived siRNAs to regulate gene expression [31], can distribute small RNAs across tissues [32], and can propagate small RNA species for several generations in the germline [33].

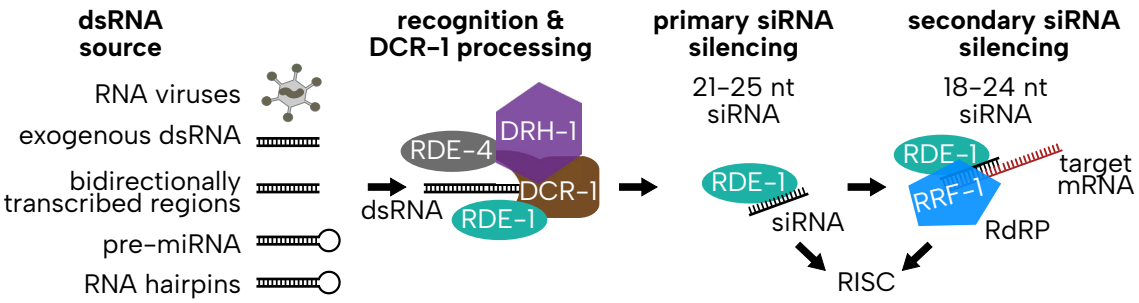

Figure 4: **The siRNA pathway in *C. elegans***. Overview of the siRNA pathway, detailing how dsRNA is processed into primary and secondary siRNAs for RISC-mediated silencing. RDE-4: RNAi DEfective-4, DRH-1: Dicer Related Helicase-1, DCR-1: DiCer Related-1, RDE-1: RNAi DEfective-1, RRF-1: RNA-dependent RNA polymerase Family-1.

Recent findings indicate that mammalian siRNA silencing may exhibit functional diversity similar to that observed in *C. elegans*. Endogenously derived small guide RNA species are used to control gene expression [18, 34, 35], are shared between different tissues to support viral defense [36, 37], and the interferon response might work in conjunction with siRNA silencing to combat viruses [38, 39]. However, secondary siRNA amplification through RdRPs is functionally lost in mammals [40](Figure 4), and it remains an open question whether transgenerational inheritance via siRNAs occurs in mammalian cells [41]. In mammals, the activity of siRNA silencing operates independently of translation and may even intensify in its absence [42]. This independence in translation marks a significant distinction between siRNA-mediated silencing and miRNA-mediated silencing, the latter being strictly dependent on translation [43].

miRNA Pathway

The miRNA pathway regulates gene expression through ① the transcription and processing of dsRNAs (primary miRNAs) from genome-encoded sequences into mature miRNAs, ② the binding of these miRNAs to several mRNAs through imperfect base pairing, primarily within the 3′ untranslated regions, and ③ the subsequent translational repression or mRNA destabilization, resulting in quantity control of gene expression [18]. While the minimal siRNA-driven RISC (siRISC) consists solely of the small guide RNA and the slicing-competent Argonaute RDE-1/AGO2, the miRNA-driven RISC (miRISC) additionally requires GW182 effectors, highlighting the dependency of the miRNA silencing pathway on translation [44]. GW182 proteins serve as intermediary platforms that connect AGO proteins to translation factors and downstream mRNA destabilization and degradation factors. The miRNA silencing process is initiated through the miRISC, comprising a miRNA-loaded AGO protein (AGO1, AGO2, AGO3 or AGO4) and GW182 binding to a miRNA recognition site on the 3′ UTR of the target mRNA. Once the GW182 protein recruits downstream effectors, the translational repression and mRNA decay occurs through several steps: ① inhibition of cap-dependent translation at the initiation phase (eIF4A, eIF4E, and eIF4G) by the CCR4–NOT complex; ② mRNA deadenylation, primarily facilitated by the CCR4–NOT complex; ③ removal of the 5′ cap by the decapping complex by DCP1-2; ④ mRNA degradation by the XRN1 5′-3′ exonuclease (Figure 5).

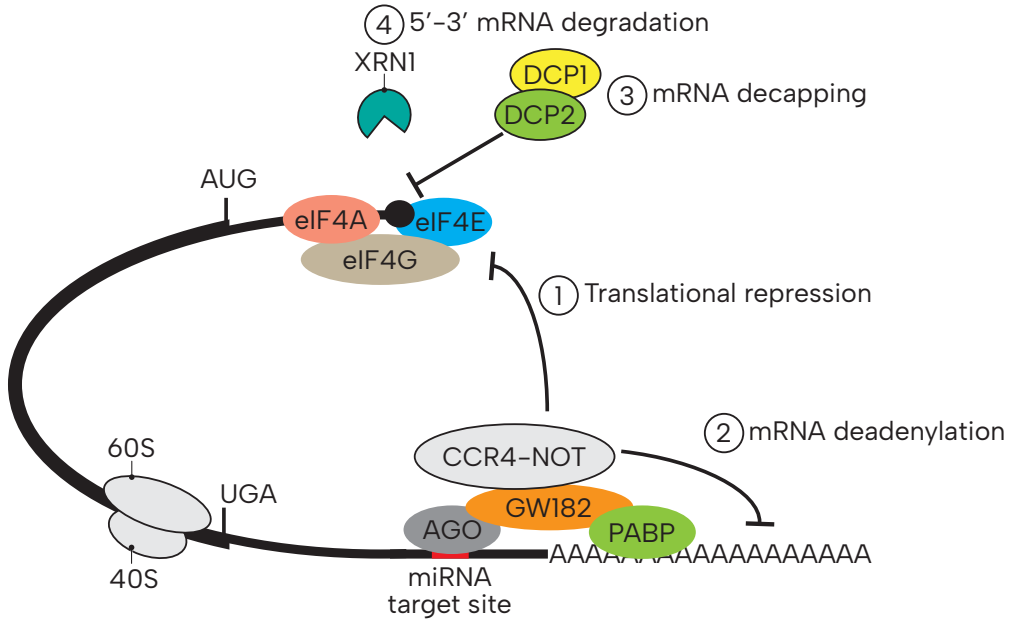

Figure 5: **The miRNA pathway in mammalian translational repression and mRNA decay**. AUG: start codon, UGA: stop codon, eIF4A/E/G: eukaryotic Initiation Factor 4A/E/G, DCP1/2: DeCapping Enzyme 1/2, GW182: multiple glycine-tryptophan (GW) repeats 182kDa protein, PABP: PolyAdenylate-Binding Protein, CCR4-NOT: Carbon Catabolite Repression 4 -Negative On TATA-less, XRN1: 5′–3′ eXoRiboNuclease 1 Figure adapted and modified from [44].

In *C. elegans*, the miRISC is functionally orthologues to that in mammals, with ALG-1/2 acting as slicer-incompetent argonautes. These rely on downstream GW182 effectors, AIN-1/2, which recruit factors that execute translational repression, mRNA deadenylation, decapping, and bulk mRNA degradation [45, 46, 47, 48, 49, 50]. For example, IFE-1 and IFE-2 contribute to the eIF4E complex (Figure 5), which is crucial in the process of cap-dependent translation initiation. In *C. elegans*, miRISCs can also regulate translational suppression by competing with the eIF4E complex for binding to the mRNA cap structure, thereby diminishing translational initiation [51, 52, 53]. This mechanism mirrors the mammalian miRISC approach to translational repression (Figure 5). However, the specific mechanistic details of miRISC downstream effectors in *C. elegans* remain less well understood in comparison to those in mammals.

Taken together, the siRNA and miRNA pathways constitute a potent post-transcriptional gene silencing system (PTGS) that utilizes dsRNA species to regulate the quantity of target mRNA either pre-translationally (siRNA) or co-translationally (miRNA). This system operates through AGOs that either directly slice the mRNA (siRNA) or recruit additional factors to destabilize the mRNA (miRNA) (Figure 5).

In addition to the PTGS, cells implement several mechanisms to monitor the quantity and quality of their transcriptome, particularly during mRNA translation [9]. For instance, translation efficiency is continuously monitored by various translation-dependent mRNA surveillance pathways, such as nonsense-mediated decay (NMD), no-go decay (NGD), and non-stop decay (NSD). These pathways specifically target and degrade mRNAs with premature stop codons causing translational stalling, and mRNAs encoding poly(A) sequences within their CDS, respectively [12]. NMD, NGD, and NSD work in conjunction with the ribosome-associated quality control (RQC; see 1.1.2.3) pathway [54]. Together, mRNA surveillance and RQC not only ensure the degradation of erroneous mRNAs and potentially toxic peptides but also facilitate the recovery and recycling of ribosomes.

Recently, ER-specific adaptations of RNA surveillance and RQC have been postulated [55], with initial steps toward their identification already achieved [56, 57, 58, 59, 21]. These developments, along with AGO-mediated (1.1.1.2), UPF1-mediated (1.1.1.3), and IRE1-mediated (1.1.1.4) ER-associated RNA decay pathways, are integrated and reviewed in Publication (II) of this dissertation.

1.1.1.3 UPF1-dependent RNA Decay

The ATP-dependent RNA helicase UPF1 acts as a pivotal regulator of mRNA quantity and quality, serving as an assemblage platform for various downstream RNA decay pathways [60]. It binds broadly to physically accessible mRNAs, overseeing a wide range of transcripts [61, 62, 63]. By engaging RNA decay pathways that eliminate erroneous mRNAs, UPF1 prevents the cellular damage caused by the production of harmful truncated or misfolded proteins. Known UPF1-dependent pathways include NMD, staufen-mediated mRNA decay (SMD), replication-dependent histone mRNA decay (HMD), glucocorticoid receptor-mediated mRNA decay (GMD), regnase 1-mediated mRNA decay (RMD), and tudor-S/M-like nuclease (TSN)-mediated microRNA decay (TumiD) [60]. This dissertation focuses on the well-studied NMD and the specialized and double-stranded RNA binding SMD pathways, which recognize mRNAs with premature termination codons (PTCs) or double-stranded RNA motifs in their 3′ UTRs, respectively.

Nonsense-mediated mRNA Decay

An estimated 5 %–30 % of human transcripts are faulty because they harbor PTCs, some of which may yield truncated polypeptides [60]. NMD is a co-translational RNA surveillance pathway found across eukaryotes that identifies and degrades mRNAs containing PTCs or abnormally long 3′ UTRs. PTCs can

emerge from genetic mutations or as a consequence of alternative splicing, posing risks to cellular proteostasis networks due to the synthesis of truncated proteins exhibiting dominant negative functions [9]. In addition to PTCs, specific mRNA features such as 5′ UTR uORFs, extended 3′ UTRs, or non-canonical exon junction complexes (EJCs) downstream of the PTC have been identified as additional triggers for initiating NMD [61]. Interestingly, NMD directly or indirectly influences the stability of approximately 10–30 % of eukaryotic transcripts, including mRNAs without known NMD-inducing features [64, 65, 66]. Accordingly, NMD acts beyond mRNA quality control and is involved in mRNA quantity control of a significant portion of the transcriptome.

UPF1, the centerpiece of NMD, binds transiently to mRNAs with limited sequence specificity and no apparent discrimination between PTC-containing and canonical mRNAs [61, 62, 63]. However, the initiation of NMD is closely linked to translation, particularly at the stage of translation termination. During efficient translation termination, eRF1 and eRF3, along with the ribosome at the stop codon, engage with the PABP and the 5′ cap-bound eIF4G. These components, which are accessible within the closed-loop structure of mRNA (as seen in Figure 5), facilitate the translation termination process [61] and prepare the mRNA for another round of translation, thus preventing NMD. When translation efficiency slows at a PTC, it triggers the assembly of a group of proteins known as the SURF complex. This emerging complex includes UPF1, SMG1, DHX34, eRF1 and eRF3. Productive NMD is initiated – either due to the absence of interactions with PABP and eIF4G or due to the presence of an exon junction complex (EJC) downstream – by recruitment of additional NMD factors such as the bridging NMD factors UPF2 and UPF3B. This marks the transition from the SURF complex to the decay-inducing complex (DECID), where UPF1 is phosphorylated by SMG1 kinase (Figure 6). Once UPF1 is phosphorylated by SMG1, several downstream mRNA degradation effectors are recruited to perform ① endonucleolytic cleavage (SMG6), ② 3′ deadenylation (SMG5/7, CCR4-NOT, not shown), and ③ 5′ decapping (decapping complex DCP and PNRC2, not shown).

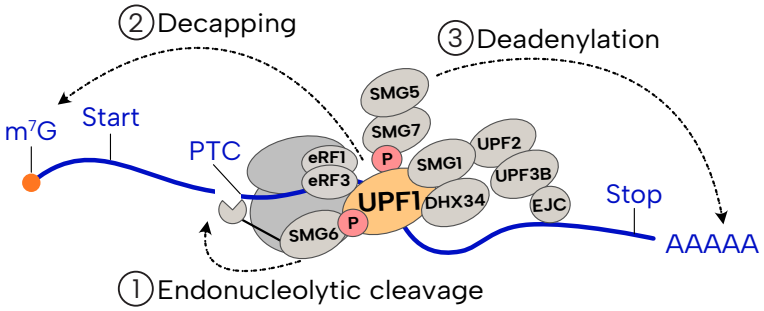

Figure 6: **Nonsense-mediated mRNA decay in mammals**. m^7G: 5′-cap, Start: start codon, PTC: premature termination codon, Stop: stop codon, EJC: Excon Junction Complex, SMG1/5/6/7: Suppressor with Morphological effect on Genitalia 1/5/6/7, eRF1/3: eukaryotic peptide chain Release Factor 1/3. UPF1/2/3: UP-Frameshift suppressor 1/2/3, DHX34: DExH-Box Helicase 34, Ⓟ: Phosphorylation. Scheme modified from [19] and further supplemented from [67, 61].

Factors required for NMD have been identified in all tested eukaryotes, underscoring the evolutionary significance of the pathway in eukaryotic gene expression [68]. Orthologues to mammals, the *C. elegans* UPF1/SMG-2 protein resembles the centerpiece of the SURF complex and the downstream kinase SMG1/SMG-1 marks the transition to the DECID complex through UPF1 phosphorylation [68, 69, 70, 71]. Recent research has identified a set of endogenous NMD targets in *C. elegans*, which represent nearly 5 % of the total transcriptome [68], demonstrating the potential to study NMD in *C. elegans*. Indeed, knockdown screening in *C. elegans* revealed the novel NMD factors SMGL-1 and SMGL-2, with their mammalian orthologues NBAS and DHX34, respectively. While DHX34 is a known component of the SURF complex (Figure 6), NBAS was only then confirmed to be also a novel mammalian NMD factor, especially for the ER-association of NMD (ER-NMD) and degradation of ER-targeted mRNAs [72, 67].

Staufen-mediated mRNA Decay

Staufen-mediated mRNA decay (SMD) is an mRNA destabilization process driven by dsRNA binding Staufen proteins (STAU1 and STAU2), which bind to Staufen-binding sites (SBSs) on 3′ UTRs of target mRNAs. This interaction facilitates the recruitment of UPF1, to initiate mRNA decay. A typical SMD target contains structured 3′ UTRs, that form SBSs, facilitated either by intramolecular base pairing in the 3′ UTR or by intermolecular interactions of the 3′ UTR with long-noncoding RNAs. These SBSs are often generated by Alu elements in humans, which can lead to the formation of the necessary dsRNA regions for SBSs [73]. SMD regulates the decay of approximately 1 % of cellular mRNAs, impacting genes involved in crucial cellular processes like differentiation and stress response [74]. Based on its dependency on UPF1 SMD competes with NMD for the recruitment of downstream mRNA decay factors [73]. STAU1

localizes to the ER [75] and interacts with the dsRNA-binding protein PACT, which itself binds to Dicer and AGO2, the two main components of somatic RNA silencing [76].

In *C. elegans*, there is only one Staufen orthologue, STAU-1. It has been shown to have a high binding affinity for double-stranded RNA and is expressed at all developmental stages. In addition, partial *LOF* mutants exhibit phenotypes that include enhanced siRNA and miRNA silencing, and mild germline defects [77, 78]. This modulation does not occur through changes in miRNA levels but rather through potential competitive interactions at the 3′ UTR of miRNA target mRNAs, where miRNAs bind to exert their silencing effects, thus modulating the activity of miRNAs downstream of their biogenesis [78].

Overall, the UPF1 platform functions as a robust post-transcriptional gene regulatory system that controls mRNA quality and quantity through various RNA decay pathways. NMD and SMD are just two examples of UPF1-mediated mRNA decay, where mRNAs containing PTCs or form dsRNA intermediates within their 3′ UTRs are targeted, respectively. The last RNA decay pathway relevant to this dissertation likewise recognizes dsRNA motifs and is additionally noted as a prime example of an ER-associated RNA decay mechanism.

1.1.1.4 IRE1-dependent RNA Decay

IRE1 is a multifunctional protein located in the ER membrane, that plays a critical role in maintaining cellular and ER homeostasis. Depending on the levels of ER stress, IRE1 can form diverse complexes and achieve varying autophosphorylation states, thereby executing endonucleolytic cleavage reactions with distinct substrate affinities (Figure 7). For instance, autophosphorylation and dimerization of IRE1 initiate the unconventional splicing of *xbp1* mRNA. This process leads to the production of the potent transcription factor XBP1s (spliced), which upregulates genes involved in reestablishing ER homeostasis ([79]; for details, see 1.2.3.1). Further oligomerization and autophosphorylation enhance the endonucleolytic capabilities of IRE1, enabling it to carry out IRE1-dependent decay (RIDD) and RIDD lacking endomotif (RIDDLE) ([80, 81]). RIDD typically targets mRNAs harboring specific stem-loop structures (endomotif) similar to those found in XBP1 mRNA. In contrast, RIDDLE does not require specific XBP1-like stem-loop endomotifs and targets a broader range of mRNAs (Figure 7. Therefore, upon ER stress induction, IRE1 (phospho)-dimers cleave ① stem-loop containing XBP1 mRNA and ② endomotif specific RIDD targets. IRE1 phospho-oligomers degrade ③ RIDDLE targets at minimal G^C sites but can also further process RIDD cleavage products or degrade miRNAs at G^C sites

[82]. These observations have led to the development of rheostatic models of IRE1-dependent mRNA decay, where increasing ER stress levels facilitate more potent RNA decay, with progressively less substrate specificity (Figure 7).

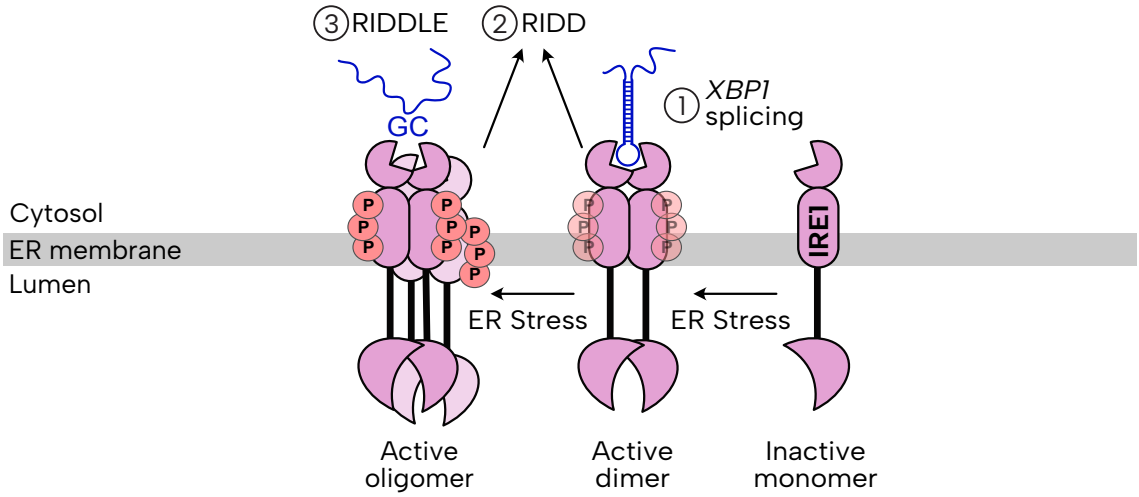

Figure 7: **IRE1-dependent decay in mammals**. IRE1: Inositol-Requiring Enzyme 1, XBP1: X-Box Binding Protein 1, Ⓟ: Phosphorylation, GC: G^C sites for RIDDLE. Figure modified from [19, 81]

The first part of the introduction elucidated the key concepts of 'Coordination of Eukaryotic Gene Expression', focusing on the post-transcriptional 'RNA Quality Control and Degradation Pathways'. The 'Principles of RNA Destabilization and Degradation' laid then the groundwork for exploring three influential RNA decay pathways: 'AGO-dependent', 'UPF1-dependent', and 'IRE1-dependent RNA decay'. The next section shifts focus to cellular strategies for 'Protein Quality Control and Degradation Pathways', specifically introducing the two dominant cytosolic degradation systems: the 'Ubiquitin-Proteasome System' and 'Autophagy'. A broad understanding of these cytosolic RNA and protein quality control mechanisms is essential for the third part, which examines how these pathways are co-opted to the ER and how they are regulated by 'Cytoprotective Stress Responses of the ER'

1.1.2 Protein Quality Control and Degradation Pathways

1.1.2.1 Ubiquitin-Conjugation

To maintain cellular protein homeostasis, two major protein degradation pathways, the ubiquitin-proteasome system (UPS) and macroautophagy (hereafter called autophagy), facilitate the breakdown of proteins to either actively regulate protein quantity or enforce protein quality control. Both pathways depend on the process of covalently attaching a conserved small protein called ubiquitin (Ub) to substrate proteins [83]. This process is a reversible reaction carried out by a hierarchical enzymatic cascade that leads to ① activation, ② conjugation, and ③ ligation of Ub to substrate proteins [84] (Figure 8). Initially, a ubiquitin-activating enzyme (E1; n ≥ 2 in humans) activates Ub in an ATP-dependent manner. Subsequently, activated Ub is transferred to a ubiquitin-conjugating enzyme (E2; n > 40 in humans) and covalently ligated to the substrate by a ubiquitin ligase (E3; n > 500 in humans) [83, 85]. Conjugated Ub can be removed by a deubiquitinase enzyme (DUB; n > 100 in humans) [86].

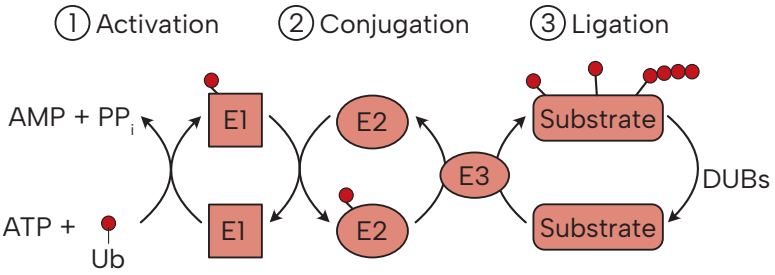

Figure 8: **The ubiquitin conjugation pathway**. ATP: Adenosine triphosphate; AMP: Adenosine monophosphate; PP: Diphosphate; Ub: Ubiquitin; E1: Ubiquitin-activating enzymes; E2: Ubiquitin-conjugating enzymes; E3: Ubiquitin ligases; DUB: Deubiquitinating enzyme. Modified figure from [87]

1.1.2.2 The Ubiquitin-Proteasome System and Autophagy

The substrate specificity of the ubiquitination process is largely mediated by the diversity of E3 ligases and their diverse interactions with substrates. Additionally, the simplicity of the E1, E2, and E3 system is complemented by the complexity of substrate polyubiquitination and the specificity of the linkage of the Ub moieties, which has been described as "Ubiquitin Code" [88]. For poly-ubiquitination, Ub can be conjugated to another Ub molecule either at its N terminus or at one of several specific lysine residues (Lys^{6}, Lys^{11}, Lys^{27}, Lys^{29}, Lys^{33}, Lys^{48}, Lys^{63}) of Ub, leading to the formation of various linear or branched Ub chains. Different Ub chain formations resemble the ubiquitin code and can recruit a diverse range of factors with Ub-binding domains (UBD), including shuttle factors and autophagy receptors that direct substrates to the UPS or

autophagy, respectively. For instance, polyubiquitin chains linked by Lys^{48}, and branched chains that combine Lys^{48} and Lys^{11}, serve as the most potent signals to target proteins to the UPS for degradation [83, 88]. On the other hand, polyubiquitin chains linked through Lys^{63} typically modulate protein functions or serve as platforms for subsequent signaling steps, and are preferably bound by autophagy receptors over those linked via Lys^{48}[88, 89]. Thus, different polyubiquitin chain morphologies can also lead to non-proteolytic changes, affecting protein interactions, localization, and activity. [90, 91]. Beyond the E3 ligases and the Ub linkage types that regulate substrate specificity and the choice of degradation pathway, the oligomerization state of Ub receptors has emerged as an additional layer to determine the pathway choice between the UPS or autophagy for protein degradation (Figure 9). [92, 83, 93]. For example, shuttling factors, which bind to soluble ubiquitinated proteins and guide these substrates to the proteasome, bind to Ub moieties more efficiently than autophagy receptors. However, autophagy receptors may become more effective after substrate aggregation, especially when the autophagy receptors clump together and oligomerize, targeting the aggregated substrate for autophagy [92, 83].

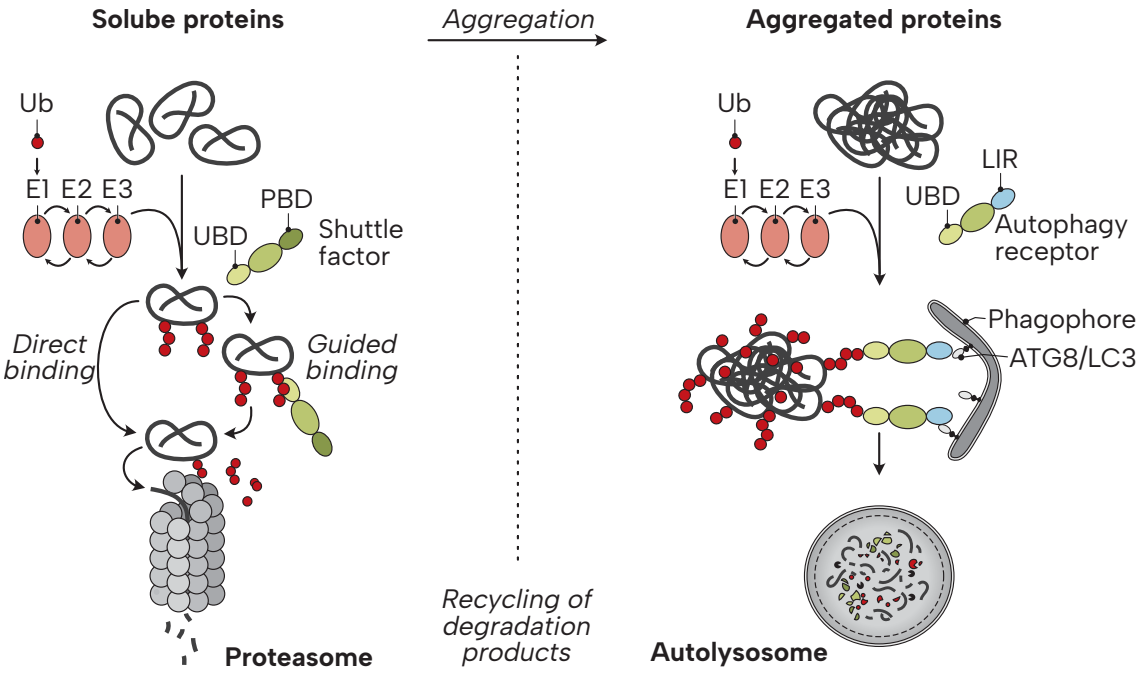

Figure 9: **Pathway choice between the ubiquitin–proteasome system and autophagy**. Ub: Ubiquitin; E1: Ubiquitin-activating enzymes; E2: Ubiquitin-conjugating enzymes; E3: Ubiquitin ligases; PBD: Proteasome binding domain; UBD: Ubiquitin binding domain; LIR: LC3-interacting region. The figure is adapted and modified from [83]

1.1.2.3 Ribosome-associated Quality Control

Besides post-translational protein quality control (PQC) mechanisms such as the UPS and autophagy, eukaryotic cells also utilize a co-translational ribosome-associated quality control (RQC) system that actively monitors the translational efficiency of nascent proteins. This RQC system identifies aberrant translation events such as slow decoding, ribosome pauses, or ribosome collisions. Depending on the severity of these disruptions, it triggers a range of responses from translation repression and mRNA decay to ribosome splitting and polypeptide nascent chain (NC) degradation [94, 19, 95]. The recruitment of RNA decay factors involved in destabilizing and degrading mRNAs during the RQC process remains poorly understood [96]. However, factors such as CCR4-NOT, DCP1/2, XRN1, and the Exosome have been associated, along with N4BP2 in mammals and its orthologue NONU1 in *C. elegans* [94, 97, 96]. Additionally, it was suggested that RQC may cooperate with co-translational mRNA decay mechanisms such as NGD, NSD, and NMD [54]. During RQC, upon initiation of ribosome splitting and the irreversible interruption of the translation process, the E3 ligase listerin (LTN1) is recruited. LTN1 then cooperates with the segregase VCP to extract, ubiquitinate, and transport the NC from the ribosome to the UPS [94, 19, 95].

During RQC at the ER, the 'Coordination of Eukaryotic Gene Expression' encounters a crucial intersection at the membrane boundary of the ER. At this juncture, the cytosolic quality and quantity control machinery loses its direct influence over proteins as they are translocated into the endomembrane system at the ER site. The subsequent sections will introduce the key pathways that regulate the import, quality control, and degradation of ER-targeted proteins.

1.2 Endoplasmic Reticulum Function and Homeostasis

1.2.1 ER Protein Targeting and Cotranslational Translocation

Approximately one-third of the cellular proteome is targeted to the endomembrane system [8]. Various classes of proteins utilize unique routes depending on the position and characteristics of their targeting signal [98, 99]. Tail-anchored proteins, which display a single membrane-spanning domain near their C-terminus, utilize the Guided Entry of Tail-anchored proteins (GET) pathway. This post-translational mechanism involves cytosolic factors that recognize and bind the hydrophobic tail-anchor as it exits the ribosome, directing these proteins to the ER membrane for insertion [100]. The primary

and best-studied mechanism for directing the majority of proteins toward the ER involves the Signal Recognition Particle (SRP) pathway. These proteins are synthesized for up to 20 N-terminal amino acids representing a cleavable signal peptide that emerges from the ribosome and is immediately recognized by the Nascent Chain-Associated Complex (NAC), which hands over the signal peptide to the SRP [101, 102, 103]. This handover improves targeting accuracy by ensuring that SRP engages solely with nascent chains (NCs) harboring genuine signal peptides. Once the SRP binds to the signal peptide, translation is paused and the ribosome-NC complex is recruited to the SRP receptor on the ER membrane [104]. This complex is transferred to the SEC61 translocon, through which the NCs enter the ER lumen or integrate into the ER membrane, in a process called co-translational translocation [105]. The SEC61 translocon is a versatile conduit for protein translocation into the ER and recruits various accessory components to meet the specific needs of a diverse set of substrates (Figure 10) [106, 107]. ① The core translocon consists of the TRAP and SEC61 complex, resembling a 'cradle' like structure, that facilitates the general translocation and folding of nascent peptides within the ER lumen [108]. ② Multipass membrane proteins recruit the GEL, PAT, and BOS complexes to support the integration of the hard-to-fold multipass membrane proteins into the ER membrane. Additionally, the EMC may support the insertion of multipass proteins with complex topologies (not shown) [109]. ③ Secretory proteins with a need for N-glycosylation, which is crucial for their proper folding and function (see 1.2.2.2), recruit the OST complex [107].

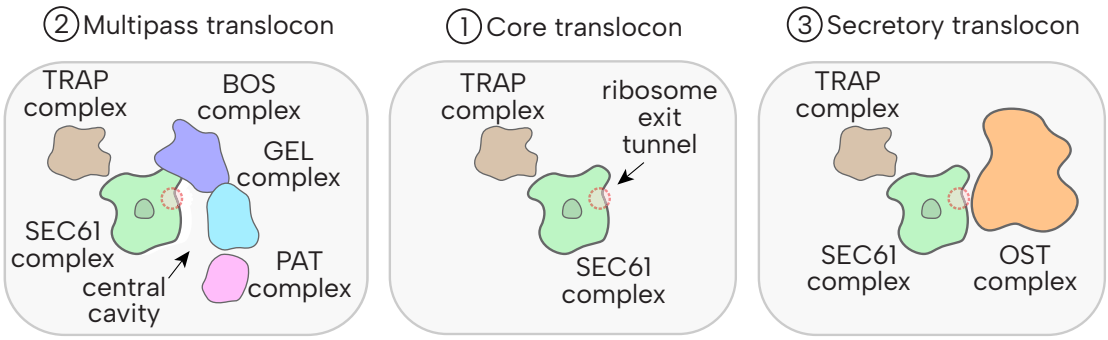

Figure 10: **Substrate-driven composition of the SEC61 translocon**. TRAP: Translocon-Associated Protein, GEL: GET- and EMC-Like, PAT: Protein Associated with Translocon (PAT), BOS: Back of SEC61, OST: Oligosaccharyl Transferase Complex. EMC: ER Membrane Complex. Figure is adapted and modified from [107]

Notably, the configuration of the multipass and the secretory translocon is structurally mutually exclusive. During the translation of multipass membrane proteins that require N-glycosylation, the OST and the BOS, GEL, and PAT are intermittently swapped for proper folding and N-glycosylation [107].

Collectively, these specialized adaptations of the SEC61 translocon underscore its dynamic capacity to accommodate the unique demands of ER-targeted proteins. After successful translocation, the final step in this pathway involves the signal peptide peptidase (SPP), which cleaves off the signal peptide, leading to the successful import and release of the mature protein into the ER [99].

1.2.2 ER Protein Quality Control and Degradation Pathways

The ER serves as the primary gateway within the endomembrane system, where the folding, post-translational modification, and maturation of secreted and membrane-bound proteins take place [110, 111]. However, once proteins cross the ER membrane, the mechanisms responsible for their quality and quantity control must traverse these ER membrane boundaries to access the cytosolic proteolytic machinery. This is necessary because the ER itself lacks internal protein degradation systems [112, 113]. For instance, soluble secretory proteins, along with their secondary structures and post-translational modifications, must traverse the hydrophobic environment of the phospholipid bilayer to reach the cytosolic UPS. Proteins with transmembrane domains embedded within the ER membrane require mechanisms for extraction and release into the cytosol [114]. Conversely, larger protein aggregates, owing to their size and charge, cannot be extracted from the ER due to the barrier posed by the hydrophobic phospholipid bilayer. Instead, they depend on organized membrane transport to the lysosome for degradation through autophagy [112, 115]. Overall, to establish the quality control of all protein species in the ER, a dedicated ER-specific chaperone system evolved to not only assist in correct folding, post-translational modification, and maturation of proteins but also to orchestrate the transfer of erroneous proteins to proteolytic degradation mechanisms for the final degradation in the cytosol.

The following section will focus on how faulty proteins are either preemptively detected during RQC before crossing the ER membrane (1.2.2.1) or detected by the ER-adapted chaperon systems (1.2.2.2), handed over to proteolytic systems (1.2.2.3), and finally how ER protein quality and quantity control is regulated by the UPR^{ER}(1.2.3.1) and the ISR (1.2.3.2).

1.2.2.1 ER UFMylation System

It has only recently been sufficiently elucidated how the RQC process has adapted to the ER, specifically how ER-targeted proteins are subjected to preemptive degradation mediated by LTN1 and VCP during the process of co-translational translocation through the help of UFMlyation [116, 117, 58]. UFMylation, akin to ubiquitination, involves the covalent attachment of a small ubiquitin-like protein, UFM1, to target proteins. This attachment forms isopeptide bonds with lysine residues on the targets through the catalytic action of specific enzymes: the E1 activating enzyme UBA5, the E2 conjugating enzyme UFC1, and a heterotrimeric E3 ligase complex composed of UFL1, DDRGK1, and CDK5RAP3 [58]. The removal of UFM1 from these proteins is facilitated by a specialized cysteine protease, UFSP2, ensuring reversible modification [58]. The principal client of UFMylation is the 60S ribosomal protein, RPL26 [118, 119], which is facing the ER membrane during co-translational translocation. The UFMylation of RPL26 has been shown to weaken the tightly sealed ribosome-translocon junction [120]. This alteration permits the RQC components NEMF, LTN1, and VCP to access ER-targeted proteins that induce translational arrest during co-translational translocation and target them towards the UPS [58]. Finally, nonstop ER-targeted soluble proteins, which become lodged at the SEC61 complex, also undergo ubiquitination by LTN1 and not by other E3 ligases that are usually known to degrade ER-targeted proteins (see 1.2.2.4) [116, 117]. Consequently, genetic disruption of UFMylation-related genes induces severe ER stress, and UFMylation genes are upregulated by the UPR^{ER} [121, 122]. Currently, it is unknown which RNA decay pathways support the degradation of the mRNAs during LTN1-driven RQC of ER-targeted proteins. There are only hints of which pathways may be involved, such as NSD in yeast [116] and AGO proteins in mammals and invertebrates [56, 57]. The UFMylation-driven RQC during co-translational translocation offers the final chance for ER-targeted proteins to engage with cytosolic quality and quantity control mechanisms before complete translocation into the ER, where they are dependent on ER-associated quality control and degradation pathways.

1.2.2.2 ER Chaperon Systems

At least three collaborative chaperons systems evolved to assist folding and enforce quality control of nascent peptide chains in the ER via the recognition of ① hydrophobic patches, ② N-glycosylation state, and the ③ quality of disulfide-bond formation. These alert systems serve both as supporters and obstacles to emerging peptide chains, where suitable and short-term engagements assist in folding, while prolonged and incorrect interactions result in transfer to ERAD.

Hydrophobic System
A hallmark of erroneous protein folding is the exposure of hydrophobic patches on the surface of soluble proteins. These hydrophobic patches are recognized by an ER-adapted chaperon of the Hsp70 family called BIP/HSP-4. BIP is recruited to hydrophobic regions of unfolded or misfolded proteins, and ATP-dependently assists protein folding by solubilizing aggregating domains and guiding native protein folding [123]. Failed attempts at substrate refolding, indicated by extended BIP interaction with hydrophobic patches, result in BIP-mediated transfer of the substrate to the ERAD factors SEL1L/SEL-1 [114], culminating in substrate degradation via the ERAD factor HRD1/SEL-11 and VCP (Figure 11). Proper ERAD handover of substrates requires the BIP-mediated solubilization and final BIP dissociation from the substrate [123, 124]. Further, BIP regulates UPR^{ER} through interaction with the luminal domains of the UPR^{ER} sensors IRE1, PERK, and ATF6 (see 1.2.3.1).

N-glycan-dependent System
Newly synthesized proteins in the ER are post-translationally modified by N-glycosylation [125]. In this process, a pre-assembled $GlcNAc_2Man_9Glc_3$ oligosaccharide (glycan) is covalently linked to the amide chain of an asparagine on the folding peptide chain (N-glycosylation). The pre-assembled glycan is readily deglucosylated into $GlcNAc_2Man_9$. Next, the proximal mannose is slowly removed by ER-mannosidase I to generate $GlcNAc_2Man_8$. During the mannose trimming, the folding peptide interacts with lectin-like chaperons like calreticulin (CALR/CRT-1) and calnexin (CANX/CNX-1), which assist in repeated cycles of protein folding attempts. Successfully folded glycoproteins leave the ER with the $GlcNAc_2Man_8$ modification. However, if multiple cycles of protein folding are unproductive, EDEM mannosidases are recruited to further trim the glycan to $GlcNAc_2Man_{5-7}$, exposing a terminal α1,6 mannose residue. This terminal α1,6 mannose is recognized by OS9/F48E8.4 and transferred via SEL1L/SEL-1 to ERAD for terminal degradation [114, 126, 127].

Disulfid Bond-dependent System

The formation of disulfide bonds is a vital post-translational modification necessary for the correct folding and structural stability of secretory and membrane proteins within the ER. Enzymes belonging to the protein disulfide isomerase (PDI) family facilitate the creation, isomerization, and reduction of these disulfide bonds, which are notably found in as much as 78 % of secretory glycoproteins [128, 129]. Oxidoreductases also form complexes with components involved in N-glycosylation to enhance the quality control and refolding of glycoproteins as well as play a crucial role in the decision-making process for either assisting refolding or degrading nascent glycoproteins that require disulfide bond formation. By cooperating with ER-mannosidase, these enzymes play a pivotal role in recognizing and targeting misfolded glycoproteins for ERAD [126]. Through the reduction of disulfides and irreversible trimming of N-linked glycans ($GlcNAc_2Man_9Glc_3$ to $GlcNAc_2Man_{5-7}$), they yield glycoproteins that are unable to re-engage with the ER chaperones CALR and CANX of the N-glycan-dependent system, thus preventing their return to the maturation-competent pool [126]. This process redirects the glycoproteins away from potential maturation and towards ERAD, underscoring the interconnected nature of N-glycan-dependent and disulfide bond-dependent quality control within the ER [125, 129]. Just as BIP plays a role in making misfolded proteins soluble again before their handover to ERAD, the process of disulfide reduction and the breaking of disulfide bonds ensures effective ERAD handover of substrates [114, 129]. This comprehensive integration of disulfide bond modulation with N-glycan processing and ERAD underscores the sophisticated level of coordination required to maintain natively folded proteins in the ER.

ER Chaperone Systems Converge on Proteolytic Systems

These three sophisticated chaperone systems actively monitor protein folding within the ER, specifically targeting anomalies such as exposed hydrophobic patches, improper N-glycosylation states, and incorrect disulfide bond formations. Upon the detection of irreparable protein misfolding or other defects, these systems coordinate the translocation of faulty ER proteins to the cytosolic degradation pathways. Given the inability of the ER to directly degrade and recycle polypeptides, the next section will detail how misfolded ER proteins cross membrane boundaries to access cytosolic mechanisms like the UPS and autophagy for degradation.

1.2.2.3 ER Proteolytic Systems

Two major degradation pathways have evolved to adapt the cytosolic UPS and autophagy to the ER. The UPS has been co-opted to the ER through the deployment of ER-associated E3 ubiquitin ligases (ER-E3). These ER-E3s cooperate with ER-associated VCP to recognize, retrotranslocate, and ubiquitinate misfolded proteins, leading to their degradation by the 26S proteasomes in the cytosol in a process called ER-associated degradation (ERAD; Figure 11). Autophagy, on the other hand, is co-opted to the ER through the deployment of ER-localized autophagy receptors, that direct ERAD-resistant and aggregation-prone proteins to autophagy in a process that is currently either called ER-phagy [112, 83] or ER-to-lysosome-associated degradation (ERLAD) [130, 115, 131]. Of note, both ERAD and ERLAD are Ub-dependent. ERAD is an ER-adapted arm of the UPS, where specialized ER-E3 ligases ubiquitinate target substrates directly. ERLAD, on the other hand, displays autophagic receptor ubiquitination and subsequent oligomerization, leading to increased autophagic flux and substrate degradation [132]. The pathway distinction between ERAD and ERLAD is therefore reminiscent of the decision-making process between the UPS and autophagy pathways in the cytosol (Figure 9) [132, 133]. In conclusion, by utilizing specialized ER-adapted E3 ligases and autophagy receptors, the cytosolic UPS and autophagy pathways effectively extend protein quality and quantity control across the ER membrane boundaries.

1.2.2.4 ER-Associated Protein Degradation

ERAD serves two principal physiological roles. The first role is the protection against the accumulation of defective, slow-folding, or misfolding proteins. These proteins might otherwise display dominant negative effects and impede secretory flux (quality control) [134]. The second role is the regulation of the abundance of key enzymes or proteins. These ER-resident enzymes or proteins can be conditionally destabilized in response to various metabolic ligands or cellular stimuli (quantity control) [135]. ERAD embodies a variety of protein degradation routes within the ER, accommodating a broad spectrum of substrates. As expected, to manage this extensive array of client substrates, specialized ER-E3s serve as platforms for interaction with the ER chaperon systems and resemble distinct ERAD disposal routes [114]. Unicellular eukaryotes, like yeast, utilize three ERAD pathways, while multicellular eukaryotes can employ up to 20 pathways that incorporate a diverse range of co-factors. [136]. The defining characteristic of ERAD is the participation of these ER-E3s, which distinguishes it from other proteolytic systems such as ER-phagy

and ERLAD. The best-studied and most prevalent pathway for ER luminal proteins is facilitated by the ER-E3 HRD1/SEL-11 (Figure 11). Upon ① recognition of erroneous folding or maturation, the chaperon system initiates interaction with ERAD adaptor proteins like OS9 and SEL1L. This interaction leads to the handover of the substrate to the E3 ligase HRD1 and its cofactors DERL2 and HERP. Following this, ② retrotranslocation and subsequent ③ ubiquitination of the substrate occur. VCP, in conjunction with several cofactors, mediates the ④ extraction and ⑤ Ub remodeling of the substrate. Next, the now cytosolic and ubiquitinated substrate is finally ⑥ degraded by the 26S proteasome. The initial stages ①-③ of each ERAD pathway are carried out by specialized complexes consisting of ER-E3s and ER chaperones and are influenced by the unique characteristics of substrates and their topologies. The later stages of ERAD ④-⑥ employ broader machinery like VCP and the 26S proteasome, a common trait with other quality control routes such as RQC.

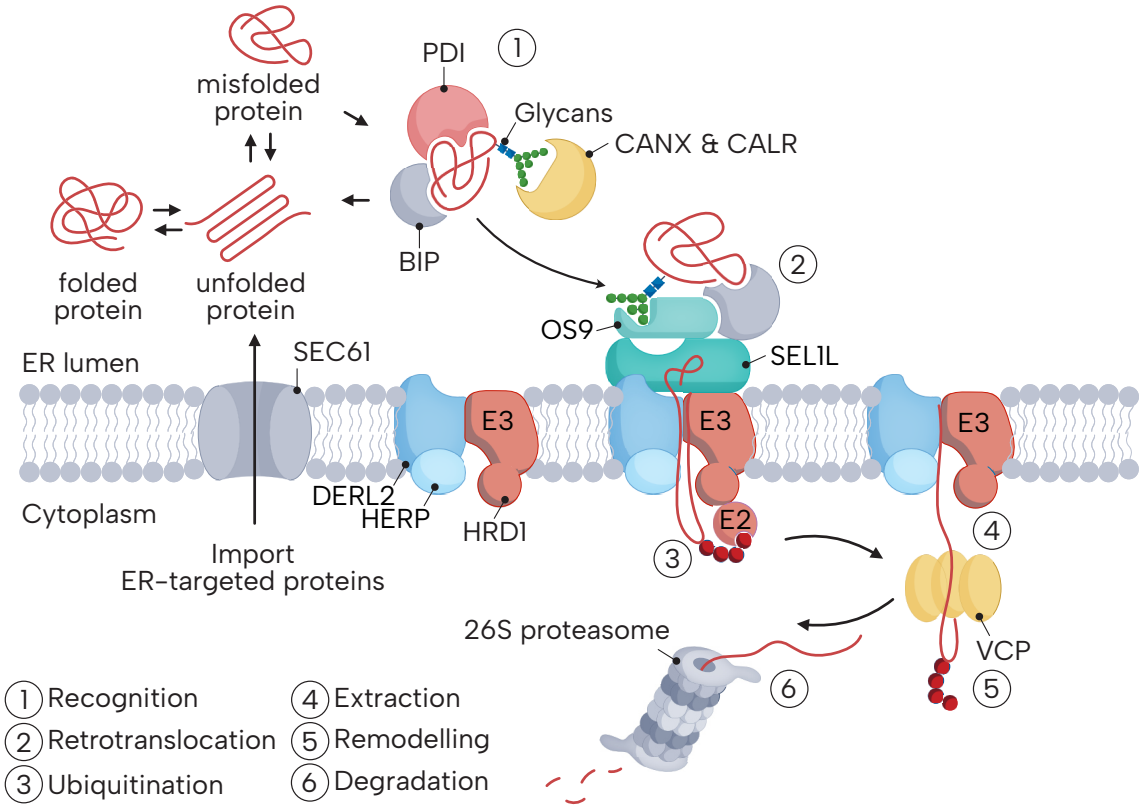

Figure 11: **ER-associated degradation**. This figure shows the most prevalent route for ER luminal proteins, which is facilitated by the ER-E3 HRD1/SEL-11. PDI: Protein disulfide isomerase, BIP: Binding-immunoglobulin protein, CANX: Calnexin, CALR; Calreticulin, SEC61: Secretory 61, OS9: Osteosarcoma amplified 9, SEL1L: Adaptor subunit of ERAD E3 Ub ligase, DERL2: Derlin 2, HERP: Homocysteine-inducible, ER stress-inducible, Ub-Like Domain, VCP: Valosin containing protein. Figure adapted and significantly modified from [114].

Conversely, the degradation route for polytopic membranous or tail-anchored proteins is not as thoroughly examined and may engage MARCHF6/MARC6, also recognized as Doa10 in yeast, along with a host of other factors [116, 114, 137]. Despite traditionally not being classified as an ER-E3, LTN1, which plays a vital role as an E3 ligase in RQC, has been independently demonstrated to effectively exhibit ERAD by directing ER-associated hard-to-fold membrane, nonstop or inefficiently translated proteins towards proteosomal degradation [56, 116, 58, 138] (see 1.2.2.1). While different ERAD routes efficiently handle a vast array of soluble and misfolded proteins within the ER, certain aberrant and aggregation-prone proteins prove ERAD-resistant. These protein species necessitate an alternative mechanism for degradation to prevent cellular stress and maintain ER homeostasis. The following section briefly introduces ERLAD/ER-Phagy, a proteolytic system that complements ERAD by targeting and disposing of aggregation-prone proteins through autophagic degradation.

1.2.2.5 ER-to-Lysosome-Associated Degradation | ER-Phagy

ERLAD or ER-phagy (hereafter ERLAD) is less well studied than ERAD [83, 130]. ERLAD operates in parallel with ERAD by recognizing misfolded and aggregated ERAD-resistant proteins and delivering these proteins for autophagic degradation in lysosomes. It utilizes ER-localized autophagy receptors, like FAM134B, which recognize and segregate misfolded and aggregated proteins into ER subdomains [133]. Subsequently, these are transported to lysosomes for autophagic degradation, successfully circumventing the inherent constraints of ERAD in the retrotranslocation process of only soluble proteins. The ERAD-resistant mutant form of alpha-1 antitrypsin (ATT), known as ATZ (further details in 2.1.3.1), resembles one ERLAD substrate [131, 115]. Although ERAD can degrade misfolded and aggregation-prone ATZ to some extent, a significant proportion of ATZ polymers resist ERAD and are instead degraded through ERLAD, involving key downstream autophagy components for successful lysosomal targeting [131]. Similarly to ERAD, the effectiveness of ERLAD is critically dependent on its collaboration with ER chaperone systems. Specifically, substrate N-glycosylation and CANX recruitment are essential for efficient interaction with the autophagy receptor FAM134B and the ERLAD-mediated degradation of ATZ. Disruption of the N-glycan system leads to a loss of CANX association, prompting engagement with the hydrophobic system via BIP. This transition results in resistance to ERLAD and accumulation of ATZ in insoluble fractions in the ER.

In essence, both ERAD and ERLAD serve as effective endomembrane adaptations of the UPS and the autophagy pathway, respectively, playing crucial roles in regulating the quality and quantity of nearly one-third of the proteome that is targeted to the endomembrane system.

1.2.3 Cytoprotective Stress Responses of the ER

1.2.3.1 The Unfolded Protein Response of the ER

Effective protein folding in the ER requires precise regulation of gene expression fidelity of ER-targeted gene products. This involves controlling both the quantity and quality of ER-targeted mRNAs and their resultant proteins. The unfolded protein response of the ER (UPR^{ER}) plays a key role in this process. It is activated when unfolded proteins accumulate and coordinate a comprehensive response aimed at maintaining ER protein quality control (ERQC), defined by the partition of proteins between the ER protein folding and degradation pathways [139]. To guarantee proper ERQC in accordance with imminent cell demands, UPR^{ER} increases the ER protein-folding and degradation capabilities while simultaneously reducing the ER protein-folding burden.

At the core of the UPR^{ER} are three main sensors that recognize ER stress: ATF6, IRE1, and PERK, which are transmembrane proteins located in the ER membrane (Figure 12). Under conditions of low levels of unfolded proteins, the luminal ER domains of ATF6, IRE1, and PERK readily interact with the chaperone BIP/HSP-4 and remain dormant. However, under the conditions of compromised ERQC, accumulating unfolded protein species require the folding assistance of the chaperon BIP and therefore displace the BIP from the luminal domains of ATF6, IRE1, and PERK, leading to the induction of UPR^{ER} signaling [140, 141]. Once BIP dissociates from IRE1 and PERK, these signal transducers homodimerize or oligomerize and induce auto-phosphorylation steps. In contrast, displacement of BIP from ATF6 leads to the dissociation of ATF6 oligomers into monomers, revealing a trafficking signal on ATF6 and marking it for vesicular transport to the Golgi apparatus [142, 141]. Once translocated to the Golgi apparatus, ATF6 is cleaved to form the active transcription factor ATF6N, which primarily increases the expression of ERQC factors, including molecular chaperones such as BIP and components of the ERAD system [139]. Activated IRE1 uses its endoribonuclease activity to splice *xbp1* mRNA at the endomotif consensus sequence (CUG/CAG). It removes a 26 nucleotide intronic stem-loop from *xbp1* mRNA to produce *xbp1s* [143], which translates into a transcription factor that more broadly upregulates ERQC supporting genes [141]. Lastly, activated PERK phosphorylates the eukaryotic initiation factor 2α (eIF2α), lead-

ing to a general reduction in cellular protein synthesis, and therefore also to a decrease in protein load on the ER. However, eIF2α phosphorylation permits the selective translation of mRNAs encoding stress response proteins, including the transcription factor ATF4 and CHOP, which regulate redox regulation, amino acid synthesis, and apoptosis (Figure 12).

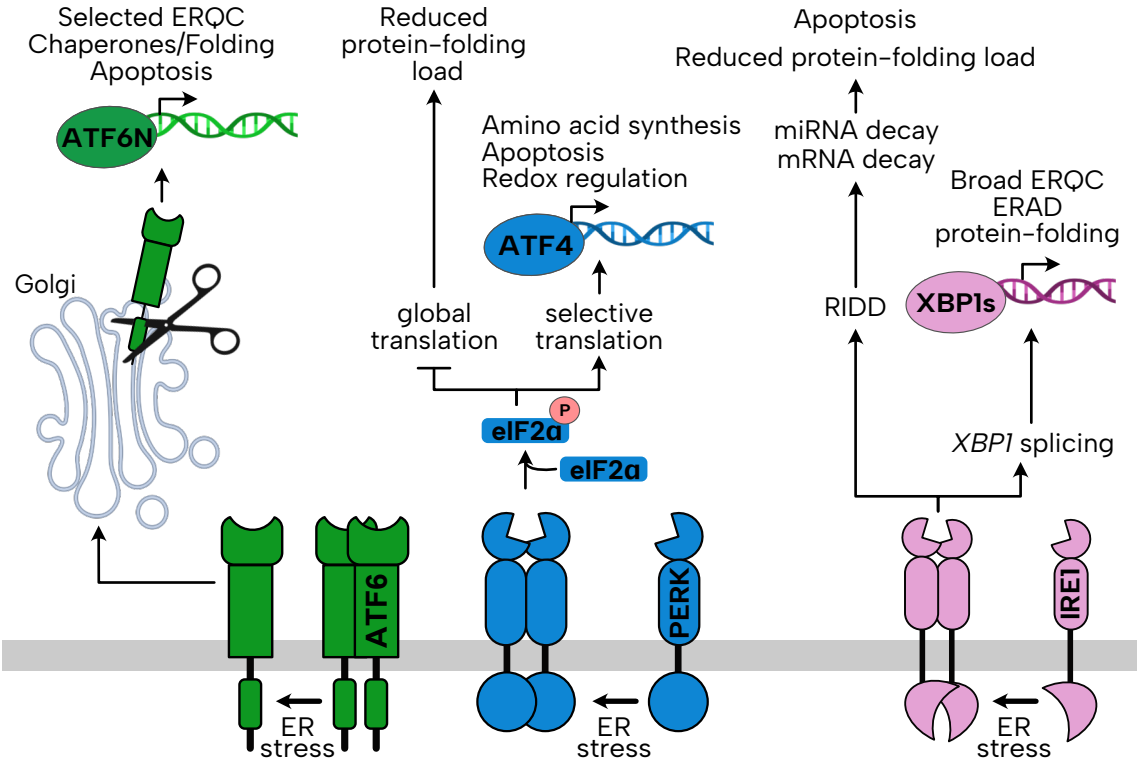

Figure 12: **The unfolded protein response of the ER**. ATF6: Activating transcription factor 6, IRE1: Inositol-requiring protein 1, PERK: Protein kinase RNA-activated (PKR)-like ER kinase, ATF4: Activating transcription factor 4, eIF2α: Eukaryotic translation initiation factor 2, subunit 1 alpha. The figure is adapted and modified from [19]

In general, UPR^{ER} orchestrates a response to ER stress that aims to promptly restore ERQC in the short term and induce apoptosis in prolonged and non-salvageable ERQC impairment.

1.2.3.2 The Integrated Stress Response

The ISR is a broader and evolutionary conserved signaling pathway that responds to a variety of stress conditions beyond ER stress. It aims to reduce global cellular translation while selectively enabling the translation of cytoprotective factors. While the eIF2α kinase PERK is triggered by unfolded proteins in the ER, other kinases such as GCN2, PKR, and HRI also contribute to ISR activation, each responding to distinct cellular stresses. For example, GCN2 is activated under amino acid deprivation, PKR responds to double-stranded RNA typically during viral infections, and HRI is regulated by heme deficiency.

These kinases converge on the phosphorylation of eIF2α, which in turn leads to a general reduction in cap-dependent translation while selectively allowing the translation of mRNAs that contain uORFs, such as the transcription factor ATF4. This selective translation leads to altered gene expression patterns, aiming to restore cellular balance and protect against chronic stress (Figure 12). Similarly to UPR^{ER}, chronic activation of the ISR leads to apoptosis. Thus, while overlapping with the UPR^{ER} through PERK, the ISR extends its influence beyond ER stress, integrating a multitude of signals to maintain cellular health and function [144, 145].

1.3 Molecular Tools to Study ER Homeostasis in *C.elegans*

1.3.1 *C. elegans* as Model Organism to Study ER Homeostasis

The study of ERQC processes in multicellular organisms is crucial to understanding intracellular implications, as well as tissue-specific and organismal consequences [146, 147]. The nematode *C. elegans* serves as a well-controlled and genetically tractable model, allowing a detailed exploration of these dynamics and providing insights into the conserved mechanisms of ERQC and the regulation of ER homeostasis.

ERQC Reporters

To investigate modifiers of ERQC in multicellular organisms, Miedel et al. engineered two transgenic strains of *C. elegans* that expressed ERQC reporter substrates under an intestinal promotor *Pnhx-2* with the co-injection marker *Pmyo-2::mCherry*. The engineered strains produce either the ER-targeted translational fusion protein with the native sequence of ① CPL-1^{W32,Y35}::YFP (CPL-1^{WT}) or its mutated version ② CPL-1^{A32,A35}::YFP (CPL-1*) [148]. The latter entails two mutations in the amino acids W32A, and Y35A within the pre-pro domain, which causes misfolding and strong degradation of CPL-1* through ERAD, resulting in a reduced level of detectable YFP under functional ERQC conditions. In contrast, CPL-1^{WT} is not targeted by ERAD and is directed to its canonical subcellular location, the lysosome, leading to readily detectable YFP. As a result, the knockdown of ERQC elements such as the ERAD factors SEL-11, SEL-1, or CDC-48, results in a selective elevation of CPL-1* protein levels, without causing changes in the levels of CPL-1^{WT}. Furthermore, the breakdown of CPL-1* does not depend on autophagy-related processes, clearly indicating a proteolytic pathway preference of CPL-1* in favor of ERAD and UPS, and against ERLAD and autophagy [148].

Taken together, the created CPL-1* and CPL-1^{WT} reporters facilitate the study of both known and yet unknown ERQC modifiers, that modulate levels

of the mutated CPL-1* variant without regulating CPL-1^{WT} substrate levels. In addition to the investigation of the ER-targeted reporter substrate level, the detection of disturbances in ER homeostasis, as indicated by UPR^{ER} and ISR activation in *C. elegans*, provides additional information on the occurrence of cellular stress responses and their influence on components of ERQC such as ERAD.

UPR^{ER} and ISR Reporters

Recent studies by Statzer et al. explored the selective translation mechanism of the mammalian ISR transcription factor ATF4 in *C. elegans* and identified ATF-5 as an orthologue [149]. In mammals, two to three small uORFs within the *atf4* 5′ UTR typically occupy the translation machinery under normal conditions, inhibiting the translation of the downstream *atf4* coding region. However, in conditions where translation initiation is impeded by eIF2α phosphorylation during ISR, the translation machinery bypasses the final uORF, facilitating preferential translation of *atf4* mRNA into the ATF4 transcription factor. Translated ATF4 is translocated to the nucleus and induces the expression of downstream effectors of ISR (Figure 12). Statzer et al. developed a *Patf-5(uORF)::GFP* transcriptional fusion reporter, hereafter referred to as ③ *Patf-5::gfp*, which incorporates both uORFs from the native 5′ UTR of the *atf-5* gene in *C. elegans*. This ISR reporter strain has been effectively employed in recent publications to evaluate ISR activation [150, 151, 149]. Previous work has referred to the gene as *atf-5* in *C. elegans*. To ensure alignment with this established literature, this dissertation will continue to use the term *atf-5*, despite its recent renaming to *atf-4*.

Similarly, Calfon et al. developed an UPR^{ER} reporter strain by fusing the 5′ upstream region of the native *C. elegans hsp-4* gene, with the *gfp* coding region. This effectively created the transcriptional fusion ④ *Phsp-4::gfp*, where GFP expression is driven by the *hsp-4* promoter and is therefore indicative for UPR^{ER} activation (Figure 12) [152].

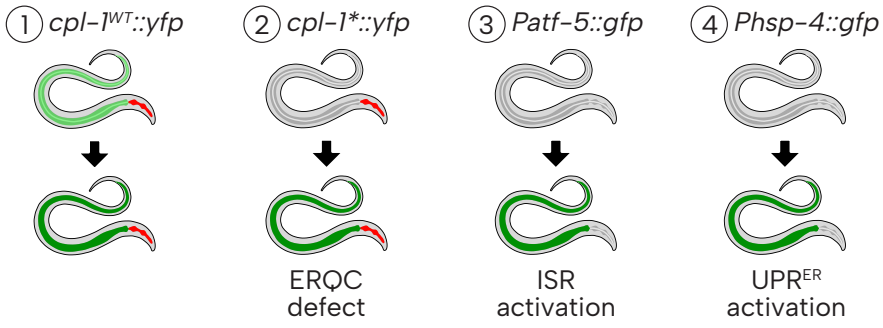

Figure 13: **ERQC and ER homeostasis reporter strains in *C. elegans***.

1.3.2 COPAS Large Particle Flow Cytometry for *C. elegans*

The Complex Object Parametric Analyzer and Sorter (COPAS) platform is based on flow cytometry principles, yet distinguishes itself from traditional flow cytometers with three notable modifications. First, it expands the upper size limit to 1500 µm, accommodating larger specimens, like *C. elegans*. Second, the COPAS system functions at reduced flow rates and pressures, which mitigates shear forces on the larger specimens. Finally, a specialized pneumatic sorting mechanism is utilized for the differentiation and sorting of objects. COPAS is capable of analyzing and sorting a range of objects including induced pluripotent stem cells (iPSCs), *C. elegans*, *Drosophila melanogaster*, and zebrafish embryos and larvae with speed rates up to 100 objects/s [153]. As objects like *C. elegans* traverse through the sensors in the flow cell, the COPAS platform measures multiple parameters (Figure 14). These include optical density (Extinction), the axial length of the object (Time-of-flight), and fluorescence in three different wavelengths: green (500–520 nm), yellow (535–555 nm), and red (600–620 nm) [154]. The time-of-flight (TOF) parameter provides a measure of the size by calculating the duration an object takes to pass through the laser beam. Fluorescence is measured both as peak intensity and width and as a complete value combined over the size of the individual object (Figure 14).

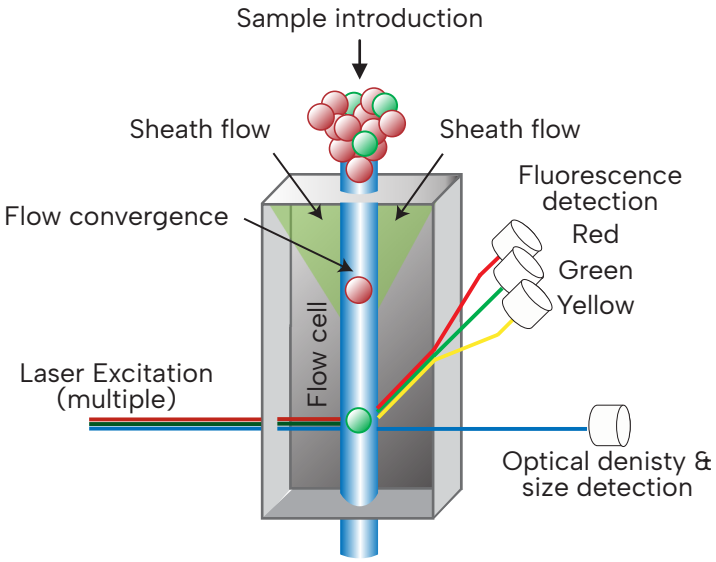

Figure 14: **Schematic Overview of the COPAS Flow Cell**. The flow cell is the central component of the COPAS system, designed for the precise introduction and alignment of samples within a laminar sheath flow. It incorporates multiple laser excitation sources to trigger fluorescence in the red, green, and yellow spectra, allowing for comprehensive fluorescence detection alongside optical density and size deduction. This arrangement allows for high-throughput characterization of each object as it passes through the flow cell. This depiction intentionally omits the sorting capabilities of the COPAS platform. Figure adapted and modified from a similar figure presented in Union Biometrica's COPAS brochure and based on concepts originally depicted in [153].

Each sample processed by the COPAS platform results in a comprehensive data file, capturing the values of each parameter for every object passed through the flow cell. These comprehensive datasets enable an extensive range of retrospective analyses. For instance, after isolating specific subpopulations to represent day 1 adult (D1A) *C. elegans* individuals using gating techniques, all remaining parameters not utilized in gating can serve as quantitative readouts. This includes the measurement of various fluorescence intensities, such as yellow, green, or red, which can be analyzed and compared across different experimental conditions. For example, the CPL-1* or CPL-1^{WT} expressing strains, co-express the *Pmyo-2::mCherry* and therefore display robust red fluorescence signals in their pharynx (Figure 13). Similar strains have been successfully used to leverage red fluorescence signals for gating, with extinction or TOF values serving as a read-out for measuring growth arrest or developmental delays in *C. elegans* [108].

The use of *C. elegans* reporter strains for UPR^{ER}, ISR, and CPL1* and $CPL1^{WT}$ as ERQC reporters (see 1.3.1), combined with the COPAS platform, greatly enhances the potential for high-throughput quantitative analysis. This combination allows for precise, automated measurements of key physiological changes in *C.elegans*, facilitating rapid and robust assessment of stress response and protein homeostasis pathways in large populations of nematodes.

1.4 Objectives of the Dissertation

Disruption of the coordination of ER-associated RNA and protein degradation pathways leads to chronic ER stress, proteostasis collapse, and ultimately cell death. This pathophysiological cascade is implicated in numerous diseases, including Alzheimer's disease, Creutzfeldt-Jakob disease, Huntington's disease, cardiovascular disease, and even the aging process itself. [155, 156, 157, 158, 159]. While significant progress has been made in understanding ER-associated degradation mechanisms (see 1.2), critical gaps remain in our knowledge regarding the specific factors and pathways cells utilize to recognize and target erroneous RNAs and proteins destined for the ER.

Thirteen years ago, Aljona Gutschmidt set the stage for this research by identifying novel ERQC factors through a forward genetic screen in *C. elegans*, highlighting RNA silencing factors as potential regulators of ERQC (Dissertation: [160]). Four years later, Lena-Sophie Schütter expanded upon this foundation, identifying potential mRNA targets of RNA silencing in both *C. elegans* and mammalian cell cultures, and exploring their interactions with viral infections and ERQC (Dissertation: [161]).

Building on these foundational studies, which for the first time convincingly linked the somatic RNA silencing pathway with ERQC, this dissertation aims to address the significant gaps in understanding the detailed mechanisms and physiological implications of this connection. The enclosed publications and accompanying data seek to elucidate the mechanisms of ER-associated RNA Silencing (ERAS) within the context of ERQC. Specifically, this dissertation aims to achieve the following objectives:

① Demonstrate post-transcriptional decay of ER-targeted mRNAs by ERAS

② Investigate the regulation of ERAS under ER stress conditions.

③ Elucidate the collaborative functions of ERAS and ERAD in ERQC.

④ Review established ER-associated RNA decay pathways.

⑤ Explore genetic interactions between ERAS and established ERQC factors.

2 Results

2.1 Publication A: ER-Associated RNA Silencing Promotes ER Quality Control

2.1.1 Summary Publication A

In this study [21], we discovered a physiologically relevant role of RDE-1/AGO2 in ERQC. Utilizing forward genetic screening in *C. elegans* expressing the ERAD model substrate CPL-1*, our research unexpectedly identified several genes within the somatic RNA silencing pathway (*rde-1*, *drh-1*, and *rrf-1*) as modulators of ERQC. Subsequent protein and RNA chase assays with cycloheximide (CHX) and α-amanitine revealed that the ERAD component SEL-11 and the ERAS component RDE-1 degrade the model substrate at the protein and mRNA level, respectively. Our results showed that ERAS activation is an ER stress response triggered by genetic, pharmacological, or viral factors. Further, we demonstrated that ERAS function is conserved in mouse embryonic fibroblasts, where AGO2 contributes to ER stress resistance by degrading numerous endogenous ER-targeted mRNAs. This study is the first to describe how RDE-1/AGO2 directly degrades multiple endogenous ER-targeted mRNAs through a process we have termed ER-associated RNA silencing, abbreviated as ERAS, highlighting its collaborative role with ERAD in maintaining ER homeostasis.

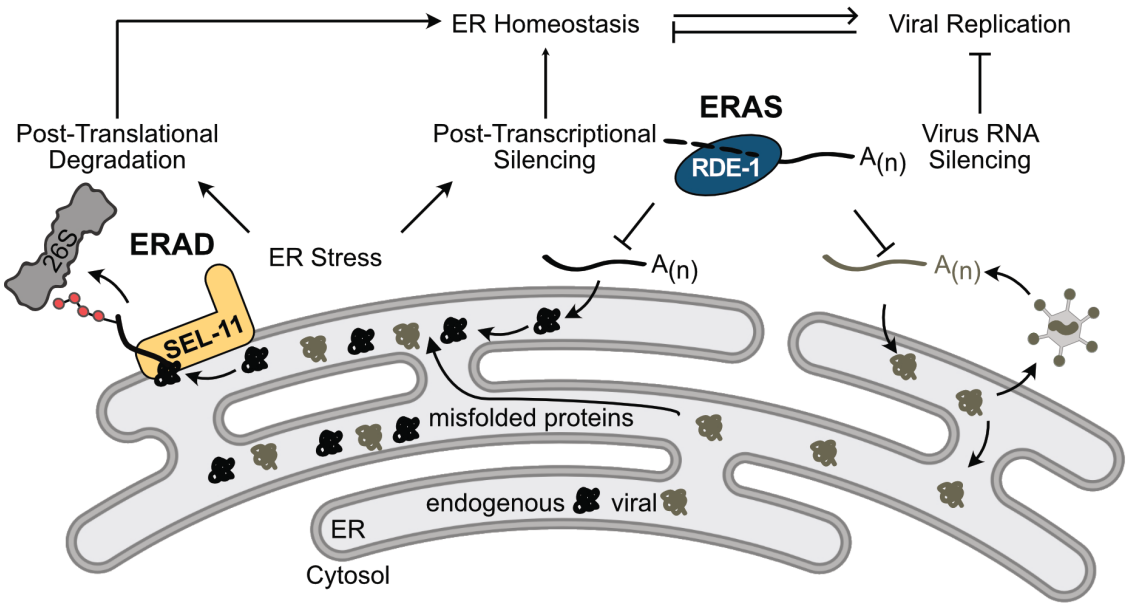

Figure 15: **ERAS and ERAD maintain ERQC.** The ERAD machinery detects misfolded proteins in the ER and retro-translocates them into the cytosol for polyubiquitylation by HRD1/SEL-11 and proteasomal turnover (Figure 11). The ERAS machinery mediates the degradation of ER-associated mRNAs and viral RNAs by AGO2/RDE-1 (Figure 3). ERAD and ERAS are needed upon genetic/pharmaceutical ER stress or viral replication and their complementary functions contribute to maintaining ER homeostasis, viral defense, and organismal health. The figure is adapted and modified from [21].

This research therefore elucidates how an ancient antiviral RNA silencing pathway has evolved to function as an ER-adapted RNA decay system, thereby playing a critical role in maintaining ERQC. This perspective opens new avenues for understanding both the cellular mechanisms that govern ER homeostasis and their impact on viral replication. It is well established that viruses utilize the endomembrane system for cell entry, replication, and assembly, and ER stress pretreatment triggers a strong antiviral state across various species from worms to mice and humans [162, 163, 164, 165, 166, 21, 167]. Our observation of an ERAS-dependent decrease in viral RNAs after ER stress pretreatment in *C. elegans* further supports this notion [21], providing an intriguing glimpse into cellular defense strategies that have evolved to combat viral infections while maintaining cellular protein homeostasis.

2.1.2 Contribution to Publication A

Sotirios Efstathiou (S.E.), Franziska Ottens (F.O.), and Lena-Sophie Schütter (L.-S.S.), as listed in this order, are shared co-first authors of the publication. S.E., F.O., and L.-S.S. designed, performed, and analyzed the experiments. L.-S.S. performed and analyzed the RNA-sequencing data together with Jorge Boucas (J.B.), S.E., and Sonia Ravanelli (S.R.). L.-S.S. performed viral infection and microsomal fractionation experiments. Aljona Gutschmidt (A.G.) performed the EMS screen and identified relevant genomic alleles. S.E. and Nikos Charmpilas (N.C.) performed the CHX chase assays. S.E. developed alpha-amanitin chase assays in *C. elegans* with improved time resolution. S.E. established the experimental setup and developed the R code for fluorescence quantification in *C. elegans* via COPAS in the manuscript. S.E. performed the CLIP-RT-qPCR assays with the technical help of Gabriella Stellbrink (G.S.). F.O. performed α-amanitin chase assays and ER stress resistance assays in MEFs. F.O. performed the northern blot assays. F.O. performed the smurf assay and confocal microscopy. Thorsten Hoppe (T.H.) supervised the experimental design and data interpretation. S.E., F.O., L.-S.S., and T.H. wrote the manuscript. S.E., F.O., and T.H. handled the submission and peer-review process.

My contributions in publication A as described above are marked with red asterisks $*$ on specific datasets in the attached publication in A.2

2.1.3 Follow-up of publication A

2.1.3.1 ERAS and ERAD regulate human alpha-1-antitrypsin in *C. elegans*

The insights gained from Publication A set the stage for further exploration into the specific criteria that define an ERAS target. To this end, we examined human α-1-antitrypsin (ATT) wildtype and disease variants expressed in *C. elegans*, investigating whether ERAS targets these reporter substrates similarly to CPL-1* and CPL-1^{WT}. This approach aimed to deepen our understanding of how ERAS recognizes and degrades specific substrates, particularly under conditions that simulate human pathological states.

Alpha-1-antitrypsin deficiency
Human AAT deficiency is a disease caused by impaired liver secretion of ATT protein, leading to reduced serum levels of ATT. Secreted ATT is required for inhibition of extracellular proteases such as neutrophile elastase, to prevent long-term tissue degradation (loss-of-function mechanism) [168, 169]. Furthermore, ATT disease variants that cause intracellular accumulation and aggregation of ATT in the ER of liver cells cause liver fibrosis, cirrhosis, or hepatocellular carcinoma (gain-of-function mechanism) [170, 171]. ATT deficiency is associated with more than 90 different mutations, with the Z allele being the most common pathological variant, leading to severely reduced ATT serum levels and aggregation of Z mutated ATT (*ATZ*) [170]. *ATZ* contributes to ATT deficiency due to its dominant negative gain-of-function (*GOF*) effect in liver cells and its loss-of-function (*LOF*) effect in other tissues from non-inhibited proteases that degrade the extracellular matrix [171].

A *C. elegans* model of alpha-1-antitrypsin deficiency
To investigate factors that modify ATT deficiency in multicellular organisms, a model of human ATT deficiency was developed in *C. elegans* by the Stephen C. Paks laboratory. They constructed quadripartite transgenes containing: ① the nhx-2 promoter (*Pnhx-2*), ② an N-terminal signal peptide linked to GFP (*sGFP*), ③ the human *ATM* or *ATZ* cDNA containing four synthetic introns, and ④ the 3' UTR and polyadenylation signal from *C. elegans unc-54*. The *ATM* and *ATZ* trangenic *C. elegans* strains were generated by microinjection with the co-marker *Pmyo-2::mCherry* and the transgenes were integrated into the genome by gamma irradiation [168, 172]. While *ATM* expressing nematodes appeared inconspicuous and *ATM* was successfully produced and excreted, the nematodes expressing *ATZ* showed intracellular aggregates within the ER and abnormal phenotypes such as reduced progeny and lifespan [168]. We obtained both the wild-type *ATM* and mutant *ATZ* versions of ATT from the

Stephen C. Pak laboratory and set out to determine whether ERAS plays a role in regulating the levels of these ER-targeted reporter substrates.

Expanding the range of ERAS targets: *ATM* and *ATZ*

In publication A we demonstrated that the mRNA of the misfolded substrate CPL-1* is an obligate target of ERAS. The mRNA of its properly folded counterpart CPL-1^{WT}, however, is not readily degraded by ERAS under baseline conditions and only becomes a target after ER stress induction. Both, CPL-1* and CPL-1^{WT} are soluble proteins in the ER without a propensity to aggregate or to be degraded by autophagy [21, 148]. To increase the repertoire of potential ERAS targets and potentially investigate ERAS substrate specificity, the *ATM* and *ATZ* reporter substrates were crossed with *rde-1(ne219)* to perform *LOF* studies. Fluorescent quantification of GFP in D1A worms was performed using the COPAS large particle flow cytometry platform (Figure 16).

Protein levels of *ATM* and *ATZ* are regulated by ERAS and ERAD

Indeed, crossing *rde-1(ne219)* into *ATM* expressing worms led to starkly higher levels of the non-aggregating substrate (Figure 16a). Furthermore, *ATM* protein levels were increased upon either *sel-11* or *rde-1* knockdown, indicating *ATM* regulation by both ERAD and ERAS (Figure 16c). The concurrent knockdown of *rde-1* and *sel-11* resulted in an additive accumulation (Figure 16c), suggesting that both ERAS and ERAD independently control *ATM* levels, which is highly analogous to our findings for CPL-1* in publication A. Similar experiments with *ATZ* expressing worms revealed milder effects of *rde-1 LOF* either in the knockout (Figure 16b) or knockdown (Figure 16d) experiments. Interestingly, it was solely the combined knockdown of *sel-11* and *rde-1* that resulted in a substantial rise in *ATZ* protein levels, once again suggesting a collaborative role of ERAD and ERAS, even in the case of the aggregation-susceptible *ATZ* variant (Figure 16d). Next, we investigated whether ERAS directly degrades *ATM* and *ATZ* mRNA, aiming to extend the findings from Publication A regarding the degradation of CPL-1* and CPL-1^{WT} mRNA.

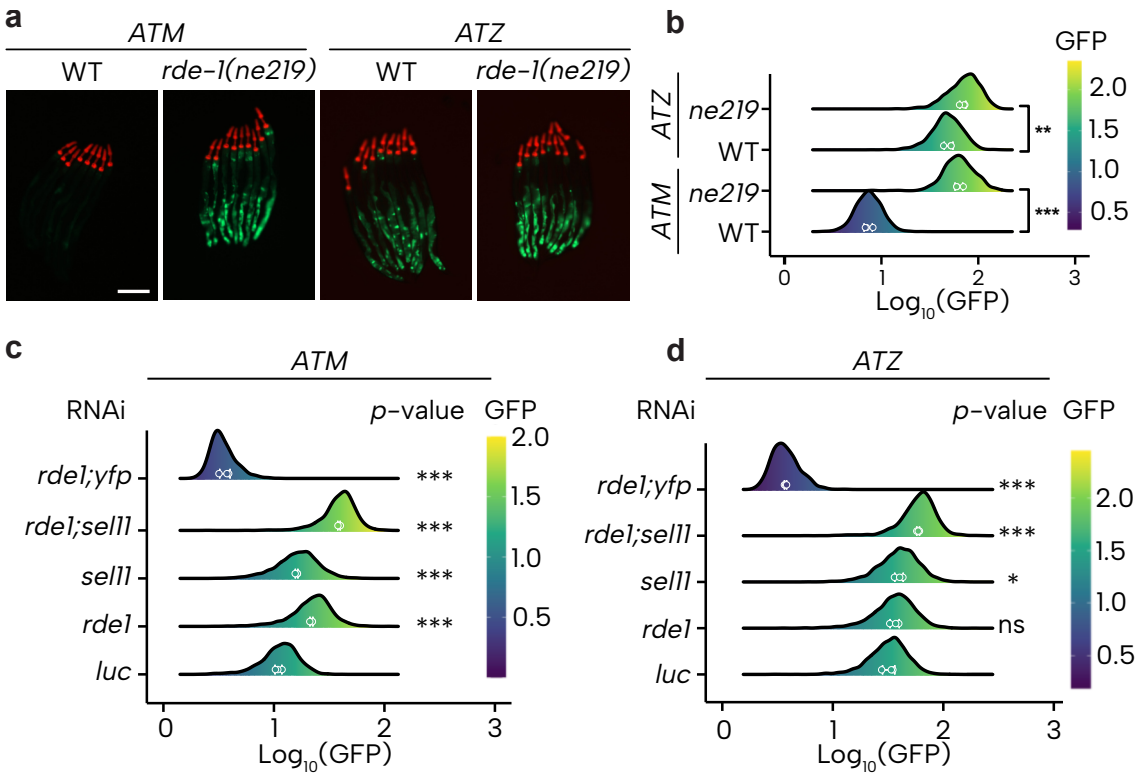

Figure 16: **ERAS and ERAD reduce *ATM* and *ATZ* protein levels. a**, fluorescence images of WT or *rde-1(ne219)* worms expressing *ATM* or *ATZ* (Scale bar, 200 µm). **b**, COPAS GFP fluorescence quantification of worms shown in a. **c** and **d** show GFP fluorescence levels of *ATM* and *ATZ* under ERAS and ERAD knockdowns. **b–d** were analyzed with a pairwise t-test on three biological replicates of >200 worms per replicate using the Holmes test. Significance: * p<0.05, ** p<0.01, *** p<0.001, ns p>0.05. To ensure accurate quantification, a gating procedure is crucial for distinguishing D1A worms from other entities (eggs, hatched L1 larvae, or OP50 bacteria). This procedure involves identifying TOF and extinction signals characteristic of D1A worms, which are then used to exclude observations not matching these TOF and extinction values (parameters are described in publication A [21]).

ATM and *ATZ* mRNAs are degraded by ERAS

To investigate whether ERAS degrades the mRNA of the *ATM* and *ATZ* variants similarly to CPL-1* mRNA, RT-qPCR measurements were performed in worms expressing *ATM* or *ATZ* in the *rde-1(ne219)* or WT background (Figure 17). The *rde-1(ne219)* mutation significantly elevated *ATM* (Figure 17a) and *hsp-4* mRNA levels (Figure 17b). These findings indicate that RDE-1 constantly degrades *ATM* mRNA and thus prevents ER stress. Indeed, α-amanitin chase assay experiments showed a strong destabilization of *ATM* mRNA by RDE-1 (Figure 17c). In summary, ERAS strongly targets *ATM*, leading to reduced protein and mRNA levels, decreased *ATM* mRNA stability, and thereby reduced ER stress. In contrast, *ATZ* protein and mRNA levels only slightly increase in *rde-1(ne219)* mutants (Figure 17a), with no *hsp-4* induction (Figure 17b), suggesting a smaller effect of ERAS on the aggregating variant. Similarly, α-amanitin chase assays show RDE-1 degrades *ATZ* less than the non-aggregating *ATM* variant (Figure 17c,d).

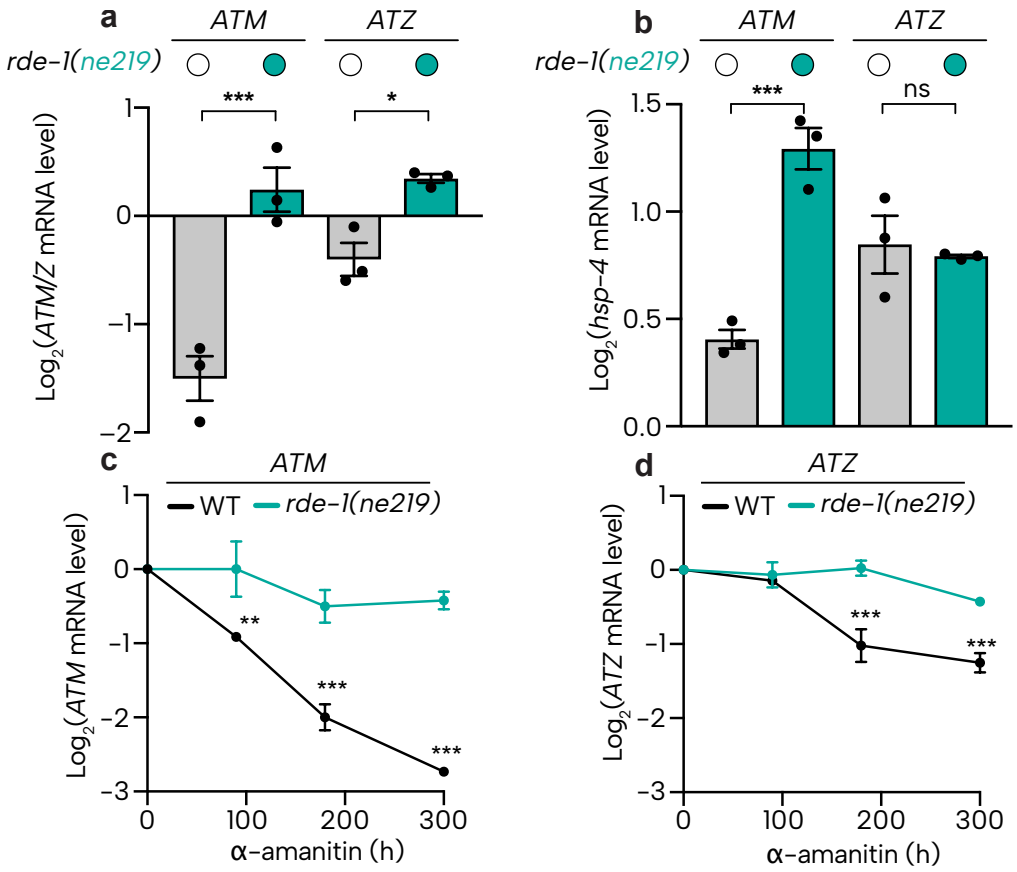

Figure 17: **ERAS degrades the mRNA of *ATM* and *ATZ*.** **a**, *ATM* and *ATZ* mRNA levels and **b** *hsp-4* mRNA levels measured by qRT-PCR in *ATM* and *ATZ* expressing worms with *rde-1(ne219)* mutation. **c** and **d** α-Amanitin chase assays and qRT–PCR against *ATM* and *ATZ* mRNA in *rde-1(ne219)* mutants expressing *ATM* or *ATZ*. **a–d**, were measured in n = 3 biological replicates. **a** and **b** were analyzed by one-way ANOVA with Sidak's multiple comparison test. **c** and **d**, were analyzed by two-way ANOVA with Dunnett's multiple comparison test. * $p<0.05$, ** $p<0.01$, *** $p<0.001$, ns $p>0.05$

Here, we were able to show that the reporter substrates *ATM* and *ATZ* can be utilized as additional tools for investigating ERAS and ERQC in *C. elegans*. Expanding upon the findings of publication A, this section demonstrated that ERAS predominantly targets the mRNA of the soluble *ATM* variant, while it only modestly targets the mRNA of the aggregation-prone *ATZ* variant. This observation holds despite higher baseline ER stress levels in the *ATZ* variant (Figure 17b), raising the question of whether the solubility/folding state of the ERAS target is more important than its impact on general ER homeostasis (discussed in 3.1.1).

In the next section we exploited the newly acquired *ATM* and *ATZ* strains, along with CPL-1^{WT} and CPL-1*, to verify or refute recent findings in yeast suggesting SEL-11 (yeast Hrd1) auto-ubiquitination to be crucial for effective ERAD [173, 174, 175].

2.1.3.2 SEL-11 auto-ubiquitination does not impact ERAD function

In collaboration with the John Christianson laboratory, we aimed to study the consequences of SEL-11 auto-ubiquitination on ERAD function in the multicellular context of *C. elegans*. Although, recent findings in yeast proposed the mechanism of repeated SEL-11 auto-ubiquitination and de-ubiquitination reactions to be important for the retro-translocation of ER luminal proteins [173, 174, 175], the John Christianson laboratory could not reproduce this mechanism in mammalian cell culture systems (unpublished data, not shown). In a collaborative effort, we exploited the ERAD reporter strains in *C.elegans* to investigate whether SEL-11 auto-ubiquitination is involved in ① the degradation of any of the ERAD reporter substrates or ② in maintaining ER homeostasis.

Generation of *sel-11(K306R)* mutant

As described in section 1.2.2.4, the E3 ligase HRD1/SEL-11, known in yeast as Hrd1, serves as the principal channel for the retro-translocation of ER luminal misfolded proteins during ERAD. In this context, SEL-11 collaborates with SEL1L/SEL-1 (yeast Hrd3), forming a protein complex (Figure 11). Notably, in the absence of SEL-1, SEL-11 undergoes significant auto-ubiquitination, leading to its rapid degradation [176]. The reported critical auto-ubiquitination of SEL-11 occurs on lysine residues within its RING finger domain and it has been proposed that mutation of key lysine residues in the RING domain disrupts retro-translocation in vitro and disrupts ERAD of ER luminal proteins in yeast [173, 174]. Sequence alignment between *S. cerevisiae*, *Homo sapienes* (*H. sapiens*), *Mus musculus* (*M. musculus*) and *C. elegans* reveals that *C. elegans* encodes for one highly conserved lysine residue (K306) on its cytosolic RING domain, which could be subjected to SEL-11 auto-ubiquitination (Figure 18).

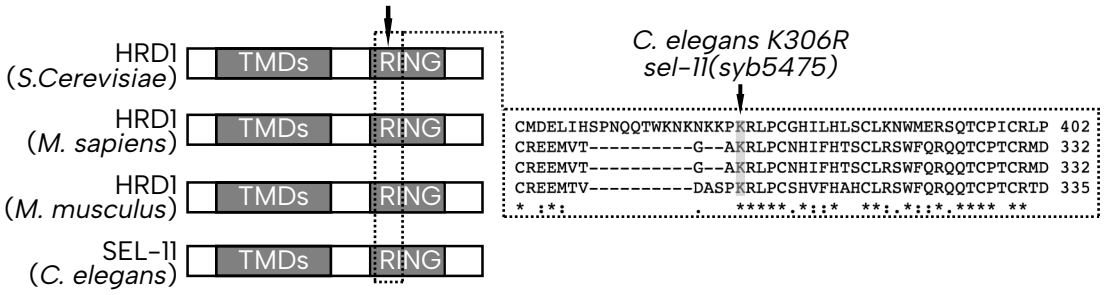

Figure 18: **Sequence alignment of SEL-11 reveals a single conserved lysine in the RING domain.** Schematic illustration of transmembrane domains (TMDs) and RING domain in the E3 ligase HRD1/SEL-11 in *S. cerevisiae*, *H. sapiens*, *M. musculus* and *C. elegans*, showing the cross-species conservation of K306 in the RING domain of SEL-11. (*): conserved residues. (:): conservation between residues of strongly similar properties. (.): conservation between residues of weakly similar properties. The alignment was performed by Clustal-Omega [177, 178].

Therefore we aimed to exchange the nucleotides 932, 933, and 934 from the AAA codon (K306) to a CGT codon (R306), which is the optimized codon usage for arginine in *C. elegans* [179]. Further, the new mutated codon to arginine displayed a novel restriction site for SalI, which would allow for robust restriction genotyping. SunyBiotech performed the mutagenesis of the amino acid exchange in N2 animals via CRISPR-Cas9. We confirmed the nucleotide exchange by two independent methods using tetra ARMS PCR [180, 181] and SalI restriction genotyping, verifying the successful introduction of the *K306R* mutation (AAA to CGT at positions 932-934; Figure 18). The strain was then outcrossed four times with N2 *C.elegans*. After successful outcrossing, the *sel-11(K306R)* strain was crossed into the following ERAD reporter strains: ① CPL-1^{WT}, ② CPL-1*, ③ *ATM* and ④ *ATZ*. To determine whether the *K306R* mutation in SEL-11 results in *LOF*, we used the known *LOF* allele *sel-11(nDf59)* [21] as a positive control.

Assessing *sel-11(K306R)* effect on ERAD model substrates

As noted in Figure 16, a gating procedure is essential to enable accurate fluorescence quantification of D1A worms using the COPAS large particle flow cytometry platform. Building on the gating techniques used in publication A, which applied only lower thresholds of TOF and extinction to separate D1A adults from smaller, more translucent particles such as eggs, hatched L1 larvae, and bacteria, this study also incorporates upper limits for TOF and extinction (Figure 19b,c). By excluding worm doublets and other contaminants—characterized by a higher TOF and increased opaqueness compared to D1A adults— we enhanced the accuracy of D1A gating and fluorescence quantification. This methodological improvement is explained in more detail in Figure 24 and was used for the following COPAS experiments.

As expected, the SEL-11 *LOF* allele *nDf59* led to significant accumulation of the ERAD substrates CPL-1* and *ATM*, while it did not cause accumulation of the properly folded substrate CPL-1^{WT} and only resulted in non-significant accumulation of the partial ERAD substrate *ATZ*. Interestingly, the *sel-11(K306R)* mutation did not result in the accumulation of any tested reporter substrates, suggesting that SEL-11 auto-ubiquitination at K306 may not have an obvious functional role in ERAD of those substrates (Figure 19d-g).

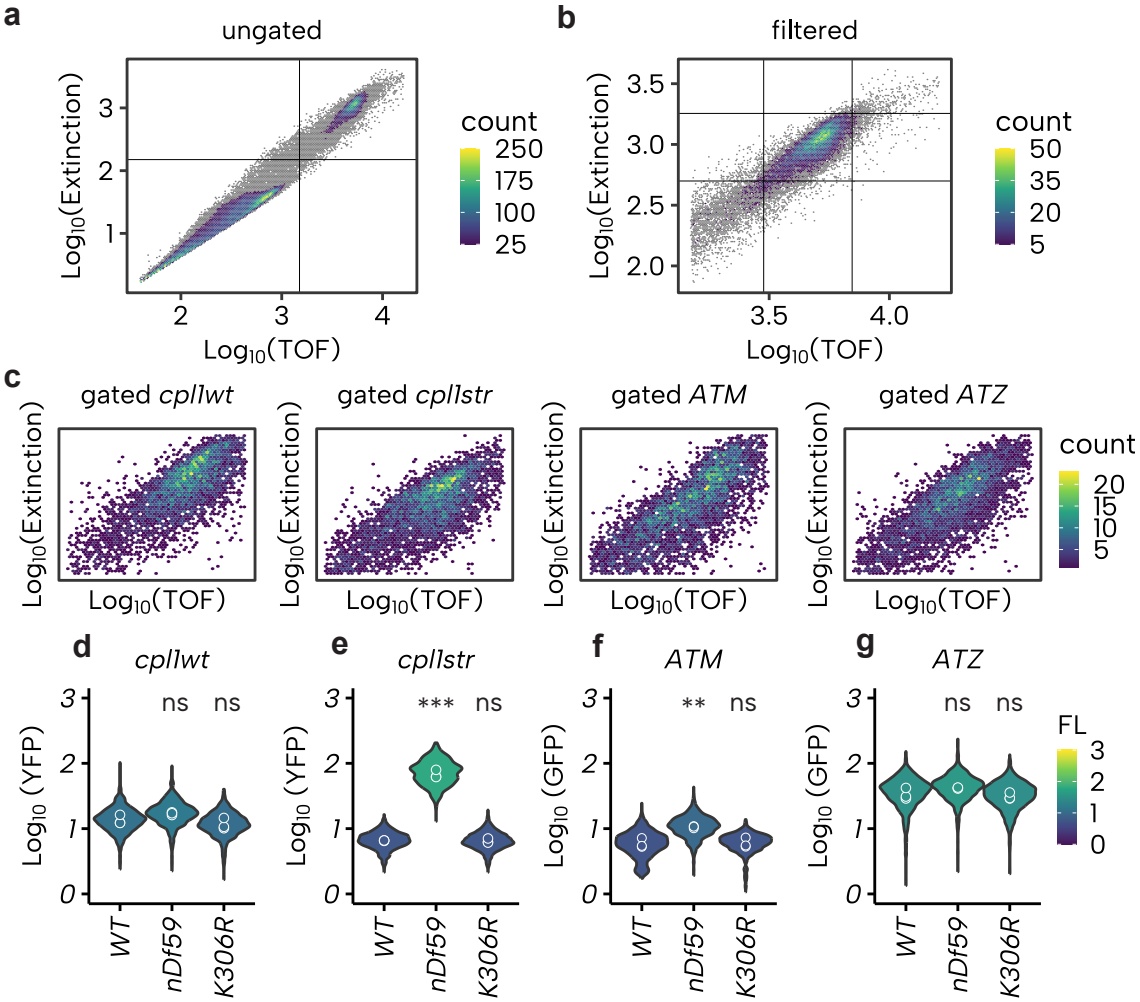

Figure 19: ***sel-11(K306R)* mutation does not lead to impaired ERAD. a,ungated** 2D density hexbin plot (150 bins) of over 100,000 observations across three *sel-11* alleles (WT, *nDf59*, *K306R*) and four reporter strains: CPL-1^{WT} (*cpl1wt*), CPL-1*(*cpl1str*), *ATM*, and *ATZ*. Initial filtering separates D1A worms from smaller particles like eggs, L1 larvae, and OP50 bacteria using extinction = 150 and TOF = 1500. **b**, **filtered** 2D density hexbin plot (150 bins) where refined extinction = 500–1800 and TOF = 3000–7000 thresholds are applied to isolate D1A worms. **c**, **gated** 2D density hexbin plot (50 bins) displaying D1A representing observations by individual strains. **d–g**, **gated** quantification of YFP or GFP fluorescence in *cpl1wt*, *cpl1str*, *ATM*, and *ATZ* expressing worms with alleles WT, *nDf59*, and *K306R*, measured in n = 3 biological replicates with >200 worms each and analyzed via pairwise t-tests and Holmes multiple comparison test. Significance levels: * p<0.05, ** p<0.01, *** p<0.001, ns p>0.05.

Assessing *sel-11(K306R)* effect on ER homeostasis

As described in 1.2.3.1, UPR^{ER} induction stimulates ERAD components such as SEL-1. We used western blotting to examine if the *K306R* mutation in SEL-11 triggers ER stress, indicated by increased SEL-1 levels. As anticipated, the *nDf59 LOF* allele significantly elevated SEL-1 protein levels, implying UPR^{ER} activation. However, the *K306R* allele did not affect SEL-1 protein levels (Figure 20a,b).

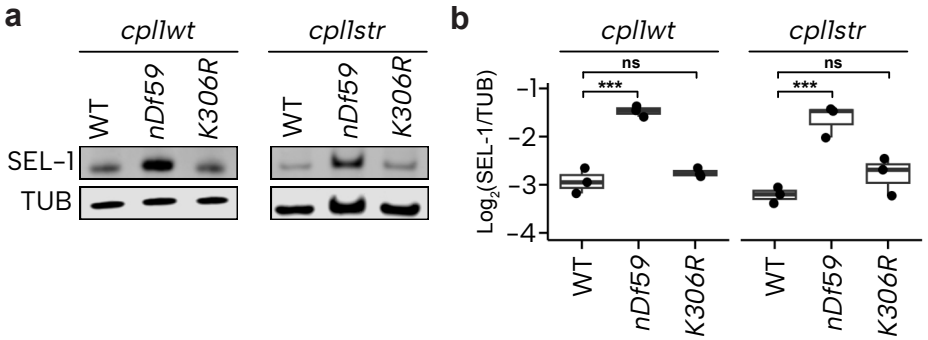

Figure 20: ***sel-11(K306R)* does not trigger UPR^{ER} a**, representative Western Blot examination of SEL-1 and tubulin (TUB) in CPL-1^{WT} (*cpl1wt*), CPL-1*(*cpl1str*) expressing worms with WT, *nDf59*, or *K306R sel-11* alleles. **b**, quantification of SEL-1/TUB intensity from three western blots. **b** was analyzed with a pairwise t-test and Holmes multiple comparison test. * p<0.05, ** p<0.01, *** p<0.001, ns p>0.05

Moreover, the *K306R* allele did not mimic the *nDf59* allele in terms of resistance to tunicamycin during larval growth stages (data not shown), nor did it affect the UPR^{ER} induction levels under tunicamycin exposure in D1A worms (data not shown). In light of our findings, altering the sole conserved cytosolic lysine residue in the RING domain of SEL-11 in *C. elegans* does not appear to influence the regulation of the examined ERAD model substrates, nor does it activate UPR^{ER} or alter susceptibility to tunicamycin. Considering that auto-ubiquitination on SEL-11 has also been shown to induce rapid degradation of SEL-11 via the UPS [176], the *K306R* mutation could have contributed to an increase in SEL-11 protein levels. Unfortunately, we were unable to explore if the lack of auto-ubiquitination on SEL-11 results in an increase in SEL-11 protein levels. An antibody against SEL-11, created by the Jarosch laboratory, did not exhibit a specific immune reaction with SEL-11 in the western blot experiments (data not shown).

In a manner consistent with the outcomes from the work of our collaborator in mammalian cell culture (see 2.1.3.2), we consequently challenge recent discoveries that describe a significant role of repeated SEL-11 auto-ubiquitination and de-ubiquitination cycles in the retro-translocation and ERAD of ER luminal proteins [173, 174, 175].

2.2 Publication B: Cutting through the Stress: RNA Decay Pathways at the Endoplasmic Reticulum

Publication A in this dissertation primarily focused on the discovery of the ERAS pathway, which in collaboration with the known ERAD pathway maintains ERQC (2.1.1). In addition, it encompassed the identification of the wild-type *ATM* and the mutant *ATZ* variants of human ATT as targets of ERAS in *C. elegans* (2.1.3.1), and the finding that the only conserved cytosolic lysine in SEL-11 does not affect ERAD function nor contributes to ER homeostasis (2.1.3.2). However, several simultaneous ER-related RNA and protein decay pathways work in unison to ensure RNA/protein quality control and degradation and to robustly respond to various challenges related to ER homeostasis and viral insults.

In the second part of this dissertation, our review article as publication B offers a summary of the most recent insights into the intricate interactions of the dominant ER-associated RNA decay pathways. Additionally, we underline the gaps in knowledge, especially concerning RNA target selectivity, interactions between RNA degradation machinery, and the physiological significance of ER-associated RNA decay pathways. Finally, as a follow-up to publication B, we conducted a small-scale epistasis knockdown screen. This aimed to investigate genetic interactions between ERAS and the reviewed ERQC factors, with the aim of integrating the newfound function of ERAS into the existing framework of known ERQC factors.

2.2.1 Summary publication B

In this publication, we review several ER-associated RNA decay pathways critical for maintaining ER homeostasis. These include RIDD, RIDD lacking endomotif (RIDDLE), ER-associated NMD (ER-NMD), and three AGO2-dependent processes: Regulation of Aberrant Protein Production (RAPP), RQC (AGO-RQC) and ERAS. These pathways, localized at the ER, are pivotal in controlling the endonucleolytic cleavage of mRNAs targeted to this organelle. We review the fundamental mechanisms of these pathways, particularly how they achieve ER-localization and substrate specificity. We further explore the interplay between these RNA decay pathways and cytoprotective stress responses such as the UPR^{ER} and the ISR. We highlight the central role of AGO2 in RNA decay within the ERAS, RAPP, and AGO-RQC pathways, and discuss how these pathways are integrated with protein degradation processes involving key factors like IRE1α, LTN1, HRD1, and VCP. This work presents an integrative model of an ER-associated RQC (ER-RQC) and ERQC system, establishing a critical link between ER-associated RNA degradation and protein degradation processes.

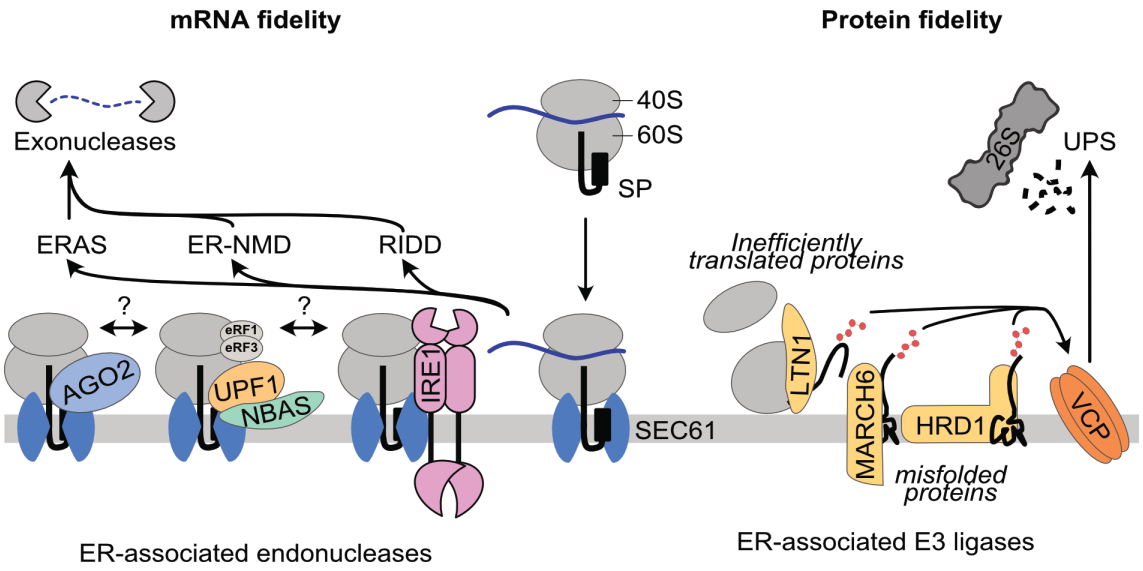

Figure 21: **Model of ER-associated RNA decay pathways and their ERQC integration.** RIDD, RIDDLE, ERAS, RAPP, and ER-NMD contribute to ERQC via endonucleolytic mRNA cleavage. Cytosolic exonucleases perform downstream mRNA degradation. Protein substrate specificity is ensured by ER-localized quality control factors and E3 ligases (LTN1, MARCH6, HRD1). Polypeptides, once unfolded, retro-translocated, and ubiquitinated, are degraded by the UPS. This figure depicts a possible integration of these pathways in a shared ER-RQC system, suggesting a potential link between translation efficiency, polypeptide folding, and activation of ER-associated RNA decay pathways. 40S: small ribosomal subunit, 60S: large ribosomal subunit, SP: signal peptide. Figure adapted and modified from [19].

2.2.2 Contribution to publication B

Sotirios Efstathiou (S.E.), Franziska Ottens (F.O.), and Thorsten Hoppe (T.H.) wrote the review article. F.O focused on the sections "The unfolded protein response at the ER", "Regulated IRE1α-dependent mRNA decay in ER homeostasis", "Nonsense-mediated mRNA decay" and "Intertwined dynamics of NMD and UPR". S.E. focused on the sections "somatic RNA silencing", "ER homeostasis, viral defense, and potential synergies", "Emerging AGO2-centered ERQC", "Quality control of ER-targeted polypeptides", "ERAS supports ER homeostasis and organismal health". S.E., F.O., and T.H. handled the submission and peer-review process. F.O. and S.E. contributed equally.

2.2.3 Follow-up of publication B

2.2.3.1 Epistasis knockdown screen of ERAS and ERQC factors

In publication B we reviewed a multitude of factors that contribute to the coordination of ER-associated mRNA and protein degradation. As a follow-up, we aimed to explore how ERAS interacts with recognized ERQC pathways (Figure 22). Therefore, we conducted a biased and small-scale knockdown screening against known ERQC pathways, in conjunction with the knockdown of *rde-1*, to discover potential epistatic interactions. Particularly we focused on factors functioning in miRNA silencing (see 1.1.1.2), ER-NMD (see 1.1.1.3), UFMylation (see 1.2.2.1), signal peptide complex (see 1.2.1), and ER-E3s (see 1.2.2.4).

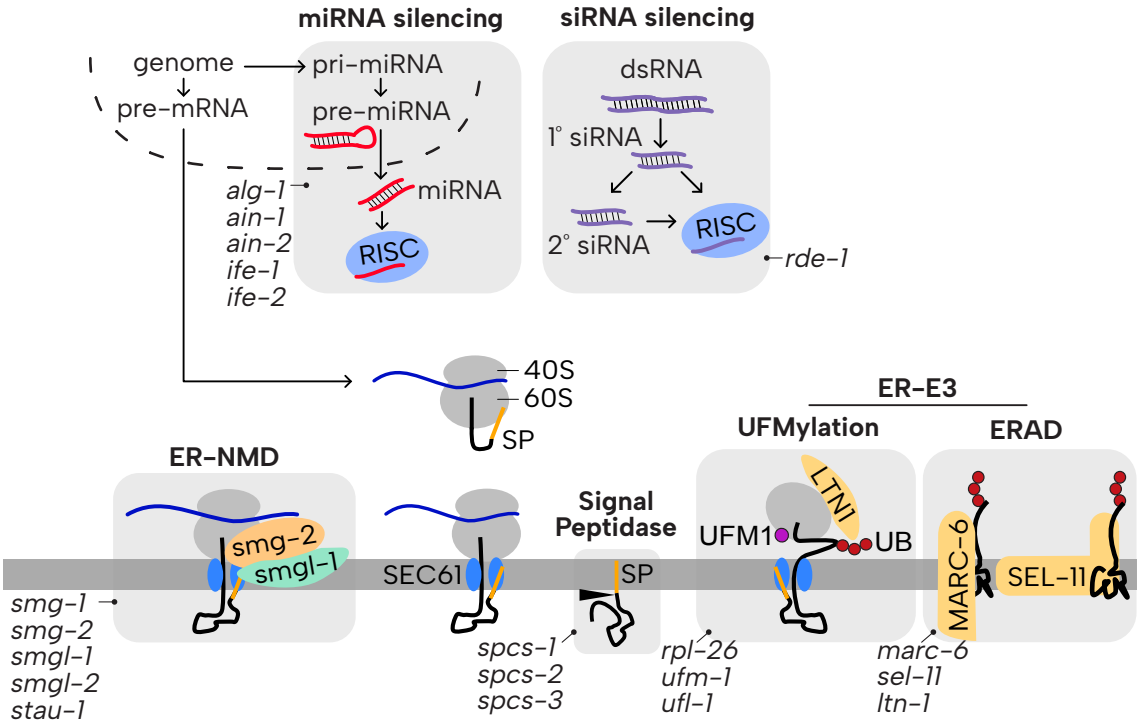

Figure 22: **Examining the interplay between ER-associated RNA and protein degradation machinery with ERAS**. Considering the review in publication B of this dissertation, we selected several genes for a knockdown study, with the objective of identifying an epistatic link between ERAS function and other ER-associated RNA and protein degradation pathways. All factors assessed in the knockdown screen are cataloged with their respective *C. elegans* gene names, displayed adjacent to the corresponding boxes. For information about the human orthologues of these tested factors, refer to the List of Gene Orthologues on page X (Roman numbering). The UFMylation pathway depiction was adapted and modified from [58]; the ER-NMD depiction was adapted and modified from [67]; the ER-E3 depiction was adapted and modified from [19].

To conduct the epistasis knockdown screen on the ERQC factors of interest (Figure 22), we created a library of knockdown constructs for both single and double knockdowns of the gene-of-interest (*GOI*) in conjunction with *rde-1*. Subsequently, we investigated the interaction of these elements with ERAS, in the context of ① model substrates regulation (CPL-1^{WT} and CPL-1*), ② UPR^{ER} activation (*Phsp-4::gfp*), ③ ISR activation (*Patf-5::gfp*) and finally ④ developmental delay of worms.

Generation of knockdown library against ERQC factors and *rde-1*

To enhance the knockdown efficiency of the two target genes (*rde-1* & *GOI*), we utilized an improved double knockdown method (Figure 23). In this approach, both target genes are incorporated into a single vector, significantly increasing the knockdown effectiveness against both targets [182]. The *rde-1* and *GOI* sequences were amplified from N2 *C. elegans* cDNA libraries, verified through sequencing, assembled into double knockdown vectors, and bidirectionally expressed in *E.coli* using an inducible T7 system. The RNAi feeding technique was used to induce robust knockdown against the *GOI* in *C. elegans*.

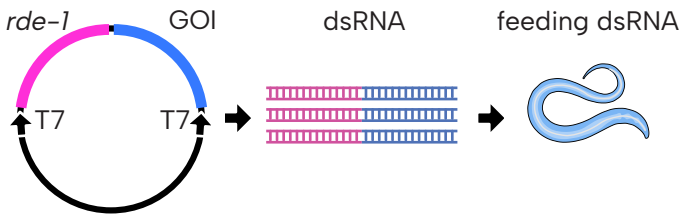

Figure 23: **Generation of ERQC knockdown library in conjunction with *rde-1*.** Library generation for the screening included the generation of double knockdown vectors entailing 1 kb of *rde-1* and 1 kb of *GOI* sequence, respectively.

Establishing the quantification of fluorescence and developmental delay

After the generation of the vector library for the knockdowns of interest, we aimed to explore the interaction of the *GOI* with ERAS in the context of ER homeostasis and the model substrate regulation. We utilized COPAS large particle flow cytometry to measure YFP and GFP fluorescence levels in D1A worms. In a similar manner to Figure 19, we employed bidirectional gating to enhance the accuracy of the quantification (Figure 24a-c) and achieved the clearest fluorescence quantification in the gated observations representing D1A worms (Figure 24d-f; ungated: $p=4x10^{-3}$, filtered: $p=4x10^{-6}$, gated: $p=4x10^{-12}$). Additionally, and as already exploited in a recent publication [108], the constitutive pharyngeal expression of *Pmyo-2::mCherry* can be used as sole gating parameter to separate worms from other observation and then quantify their extinction value as a readout for developmental delay, given that worms with developmental delay and smaller size demonstrate lower extinction val-

ues. In this dissertation, we similarly leveraged the *Pmyo-2::mCherry* expression in the strains (CPL-1^{WT} and CPL-1*) to quantify the developmental delay in the knockdown conditions in the ERQC screen. Therefore, we recapitulated successful gating of *Pmyo-2::mCherry* expressing worms (Figure 25a-c) and demonstrated successful extinction quantification as a read-out for developmental delay (Figure 25d-g).

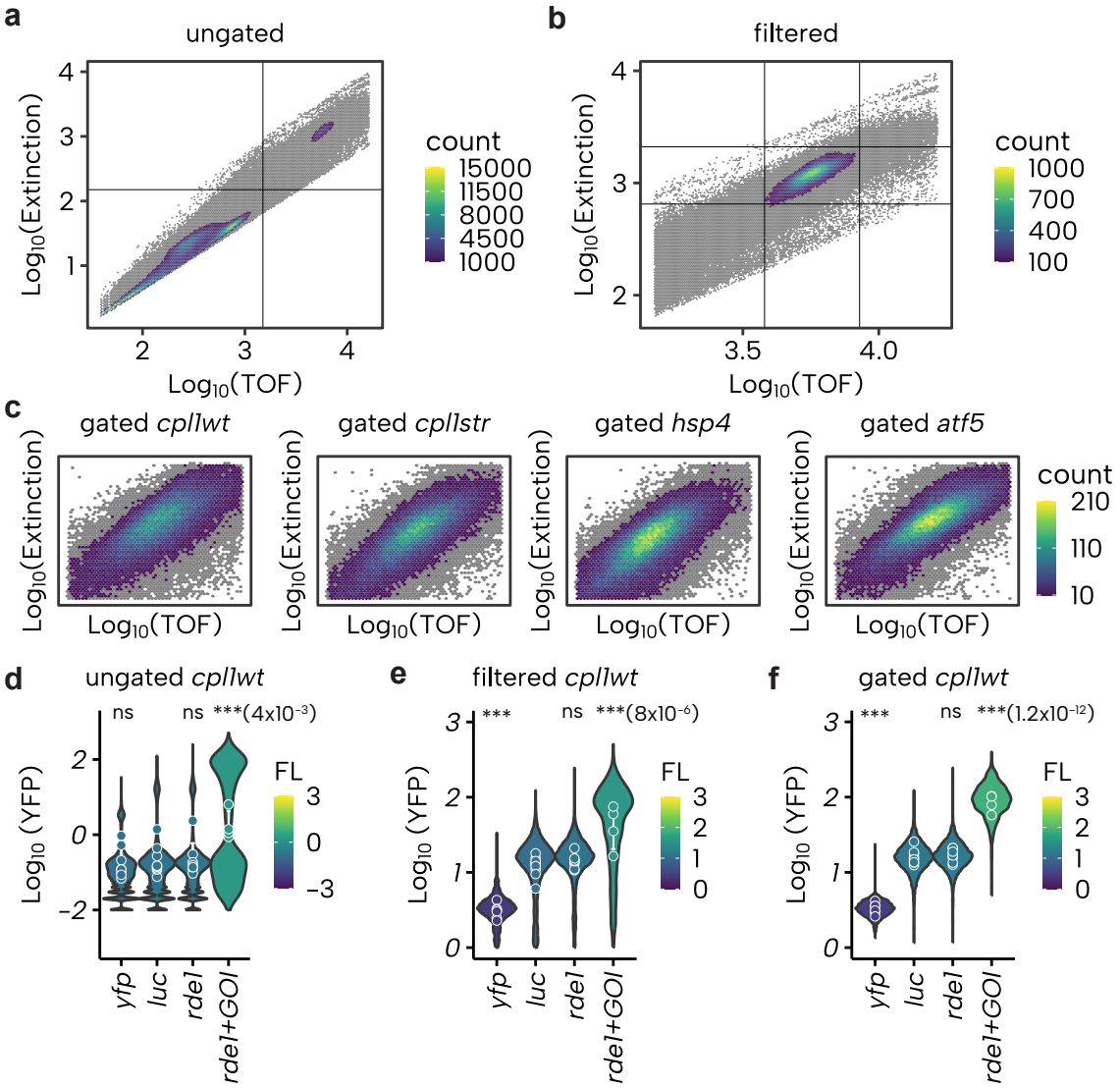

Figure 24: **Fluorescence quantification strategy with COPAS**. **a**, **ungated** 2D density hexbin plot (150 bins) representing over 4 million ungated observations across 42 knockdown conditions for reporter lines: CPL-1^{WT} (*cpl1wt*), CPL-1* (*cpl1str*), *Phsp-4::gfp* (*hsp4*), and *Patf-5::gfp* (*atf5*). Initial filtering differentiates D1A worms from smaller particles (e.g., eggs, L1 larvae, OP50 bacteria) using cutoffs at extinction = 150 and TOF = 1500 (see lines in plot). **b**, **filtered** 2D density hexbin plot (150 bins) for all strains, further refined by extinction = 650-2100 and TOF = 3800-8500 thresholds to finalize D1A worm gating (see lines in plot). **c**, **gated** 2D density hexbin plot (50 bins) for gated D1A observations that separate data by reporter strain. **d-f**, representative YFP fluorescence (FL) quantification of **d** ungated, **e** filtered and **f** gated observations in *cpl1wt* expressing worms and knockdowns conditions (*yfp*, *luc*, *rde-1*, *rde1+GOI*) double knockdowns, where *GOI* represents a knockdown condition of increased *cpl1wt* accumulation.

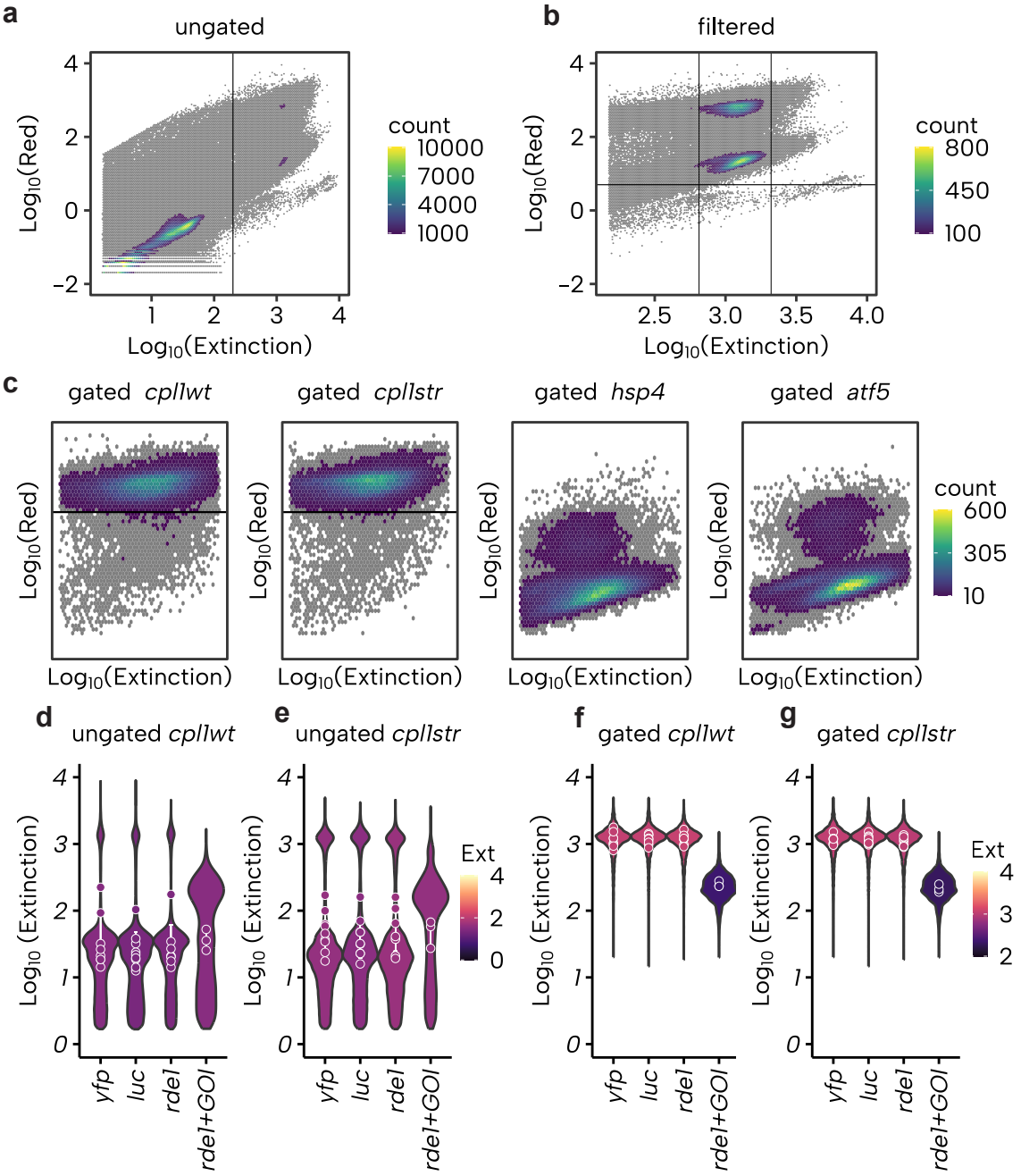

Figure 25: **Extinction quantification strategy with COPAS. a**, **ungated** 2D density hexbin plot (150 bins) from over 4 million observations from 42 knockdown conditions visualized for extinction and Red fluorescence values of all four reporter strains: CPL-1^{WT} (*cpl1wt*), CPL-1* (*cpl1str*), *Phsp-4::gfp* (*hsp4*), and *Patf-5::gfp* (*atf5*). Initial filtering separates D1A worms from smaller particles (e.g., eggs, L1 larvae, OP50 bacteria) at extinction = 150. **b**, **filtered** observations reveal two sub-populations representing red-negative (*hsp4*, *atf5*) and red-positive (*cpl1wt*, *cpl1str*) worms, corresponding to the expression of mCherry in the pharynx of *cpl1wt* and *cpl1str* worms. Further filtering extinction = 650–2100, Red = 5 allows for strain-specific information in c to confirm red-positive vs. red-negative strains and to identify a gating threshold for red signal. **c**, **gated** 2D density hexbin plot (50 bins) for gated D1A worms, establishing final gating criteria for red-positive worms (Red = 250; black horizontal line). **d–g** Extinction quantification of **d & e** ungated and **f & g** gated red-positive worms in control and double knockdowns (*yfp*, *luc*, *rde-1*, *rde1+GOI*), demonstrating a successful red-positive gating and extinction quantification strategy.

ERQC RNAi screening: interaction of examined genes with ERAS

After establishing the strategies for quantifying fluorescence (Figure 24) and developmental delay (Figure 25), the impact of single and double knockdown on fluorescence and developmental delay was examined (Figure 26).

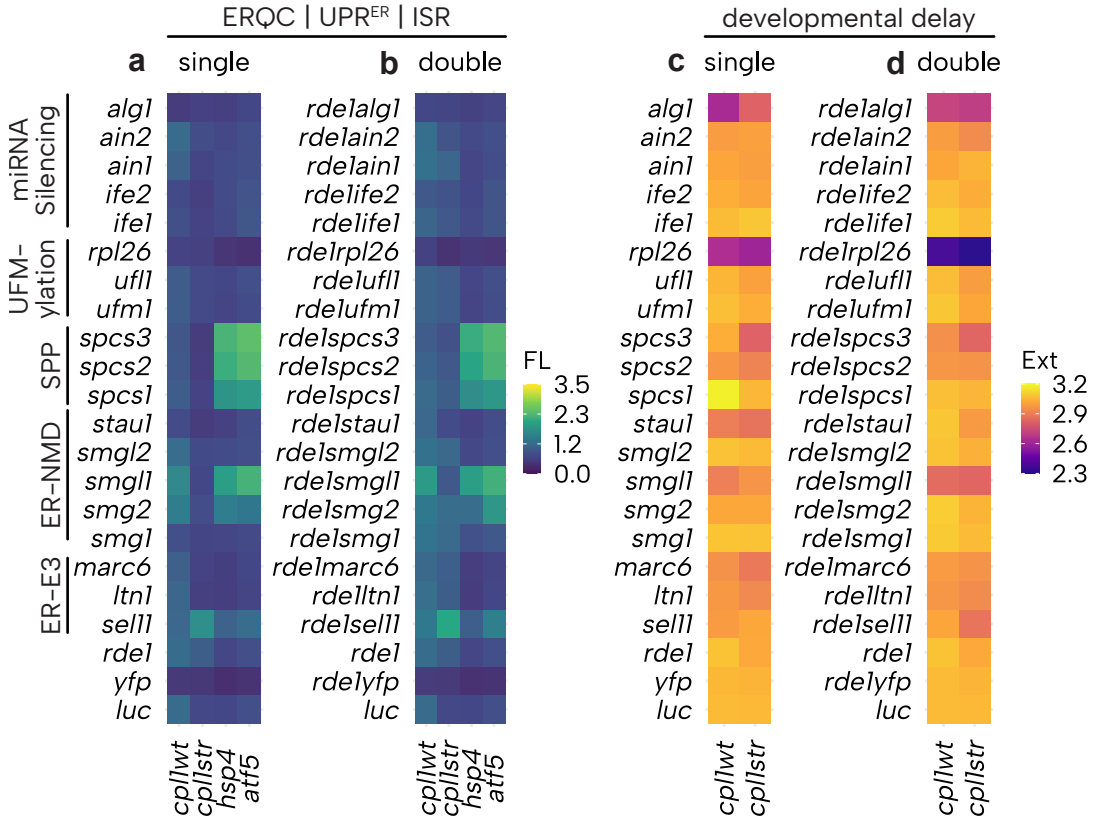

Figure 26: **ERQC RNAi screen: reporter activation and developmental delay**. **a** and **b** illustrate the fluorescence (FL) values of YFP and GFP. **c** and **d** developmental delay quantification measured by extinction (Ext) values of the strains expressing the pharyngeal mCherry marker in the same knockdown conditions. **a** and **c** show results of single knockdown experiments, with normalized values to luciferase (*luc*). **b** and **d**, depict outcomes from double knockdown experiments, with values normalized against *rde-1* (*rde1*)

ERAS and ERAD are the main CPL-1* regulating factors in the screen

Apart from the ERAS and ERAD factors *sel-11* and *rde-1*, none of the other knockdown conditions tested resulted in a substantial accumulation of the misfolded CPL-1* substrate (Figure 26a,b). This suggests that miRNA silencing, UFMylation, the SPP, and ER-NMD do not play a significant role in the regulation of CPL-1*. The known epistatic interaction between ERAS and ERAD was confirmed in this screen, since double knockdown of *rde-1* and *sel-11* shows significant additive CPL-1* accumulation (Figure 29b & A. 1d) and ISR activation (Figure A. 1f). The two additional ER-E3 ligases under investigation, *marc-6* and *ltn-1*, exhibited no influence on the control of the ER-targeted model substrates (Figure A. 1c,d), ER homeostasis (Figure A. 1e,f), or developmental delay (Figure A. 1b).

ER-NMD regulates CPL-1^{WT} levels

This screen revealed a novel genetic interaction between the ER-NMD factor *smgl-1* and *rde-1*. The knockdown of *smgl-1* alone leads to a significant increase in CPL-1^{WT} levels, which are further elevated with concurrent *rde-1* knockdown, although single *rde-1* knockdown does not affect CPL-1^{WT} levels (Figure 29b & Figure A. 2c). In addition, the double *smgl-1* and *rde-1* knockdown leads to developmental delay ($p<0.001$; ***), while the single *smgl-1* ($p=0.09$; ns) and *rde-1* ($p=1.0$; ns) knockdowns do not induce developmental delay (Figure A. 2b). Apart from *smgl-1*, a substantial decrease in CPL-1^{WT} levels was triggered in the individual knockdown of either of the two ER-NMD factors, *smg1* ($p<0.001$; ***) and *stau-1* ($p<0.001$; ***). This reduction was not observed anymore in the *rde-1* double knockdown conditions, suggesting that RDE-1 might mediate the reduction of CPL-1^{WT} in these cases (Figure A. 2c). Interestingly, *stau-1* single knockdown leads to developmental delay ($p<0.004$; **), while the double knockdown with *rde-1* rescues the developmental delay ($p=1$; ns)(Figure A. 2b). Taken together, ER-NMD factors seem to have differential effects on CPL-1^{WT} substrate levels, which is not reflected in the CPL-1* misfolded version (Figure 29b & Figure A. 2c,d) and to cause developmental delay that is either aggravated (*smgl-1*) by or rescued (*stau-1*) by simultaneous *rde-1* knockdown (Figure 29b). While the mechanism of the genetic interaction between ER-NMD and ERAS could not be determined in this epistasis screen, the identification of a genetic interaction between ER-NMD and ERAS in CPL-1^{WT} regulation paves the way for mechanistic studies.

ER stress regulates CPL-1^{WT} levels

In publication A we showed that the induction of genetic ER stress in the CPL-1^{WT} expressing worms resulted in the instability of the mRNA of the model substrate. Here, this RNAi screen allowed us to investigate if various ER stress-triggering knockdowns could similarly lead to a decrease in CPL-1^{WT} levels. In fact, by including conditions that induce ER stress (knockdown of *sel-11*, *spcs-1*, *spcs-2*, *spcs-3*) and excluding ER-NMD factors that might independently regulate CPL-1^{WT} levels, we observed a correlation between the induction of *Phsp4::gfp* and CPL-1^{WT} levels. Notably, we observed a strong negative correlation ($r = -1$, ***), indicating that an increase in ER stress levels leads to a decrease in CPL-1^{WT} levels (Figure 27a). When the double knockdown conditions with *rde-1* were additionally considered, the destabilization of CPL-1^{WT} is partially mitigated ($r = -0.81$, ***), leading to a general increase in CPL-1^{WT} levels. This observation suggests that RDE-1 plays a role in the degradation of CPL-1^{WT} under the considered ER stress conditions (Figure 27b).

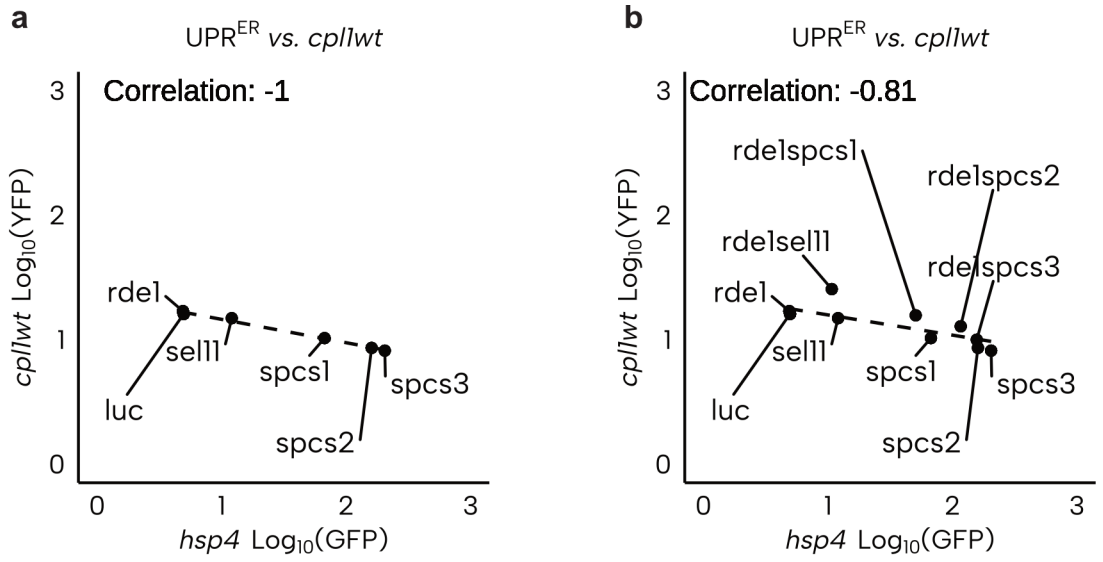

Figure 27: **ERQC RNAi screen: correlation between UPR^{ER} and CPL-1^{WT} levels**. **a**, CPL-1^{WT} (*cpl1wt*) levels are negatively correlated with *Phsp-4::gfp* (*hsp4*) induction (r = -1, ***) . ER stress-inducing knockdown conditions together with *luc* and *rde-1* (n = 6) are used for the correlative analysis. **b**, in addition to the knockdown conditions in a, the double knockdown conditions with *rde-1* are included (n = 10). The negative correlation between *cpl1wt* and *hsp4* is changed by the inclusion of the double knockdown conditions (r = -0.81, ***). The significance of the correlation was tested with Pearson's product-moment correlation. *** p <0.001.

Half of the single knockdown conditions achieved a significant reduction of CPL-1^{WT} levels: *sel-11* (p = 1; ns), *spcs-1* (p = 0.36; ns), *spcs-2* (p = 0.008; **) and *spcs-3* (p = 0.01; *). However, none of the *rde-1* double knockdown conditions demonstrated a significant decrease in CPL-1^{WT} levels, indicating that RDE-1 is involved in the ER stress-dependent degradation of CPL-1^{WT}(Figure 28).

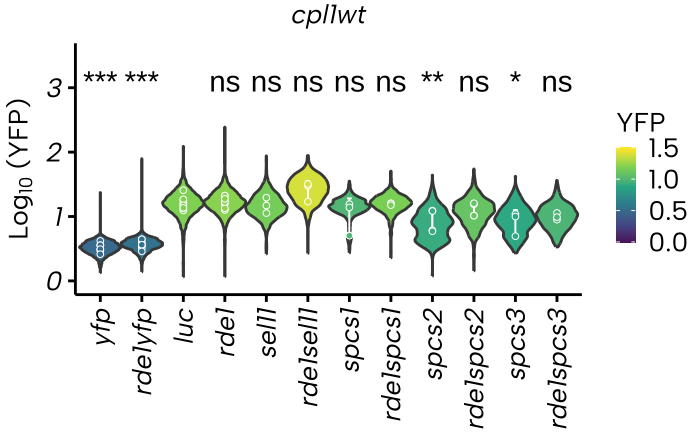

Figure 28: **ERQC RNAi screen: CPL-1^{WT} levels under ER stress-inducing knockdowns**. YFP quantification in CPL-1^{WT} (*cpl1wt*) in ER stress-inducing single and double knockdown conditions. Data was analyzed by pairwise t-test with Holmes multiple comparison test. Single knockdown conditions were compared to luc and double knockdown conditions were compared to *rde1*. * p<0.05, ** p<0.01, *** p<0.001, ns p>0.05. The efficiency of the double knockdown in *rde-1* was evaluated through *rde-1* and *yfp* double knockdown (p<0.001; ***), where a successful *yfp* reduction signifies a high efficiency, even with simultaneous *rde-1* knockdown

RNAi against *spcs-1,2,3*, *smgl-1* and *smg-2* activates UPR^{ER} and ISR.
Several knockdown conditions appear to trigger the UPR^{ER} and ISR reporter strains, with the signal peptidase complex (*spcs-1,2,3*) demonstrating the most robust activation levels, followed by the ER-NMD factors *smgl-1*, *smg-2* and the ERAD factor *sel-11*. Strinkingly, a correlation study of all knockdown conditions (n = 42) in the activation of UPR^{ER} and ISR reporter strains reveals a correlation coefficient of r = 0.99 (p<0.001 ***)(Figure 29a). Interestingly, the combined knockdown of *sel-11* and *rde-1* resulted in a significantly higher induction of *Patf5::gfp* compared to *rde-1* (p<0.001; ***) or *sel-11* (p=0.001; **) single knockdown condition (Figure A. 1f). This confirms the notion that the concurrent suppression of ERAS and ERAD triggers cellular stress responses [21].

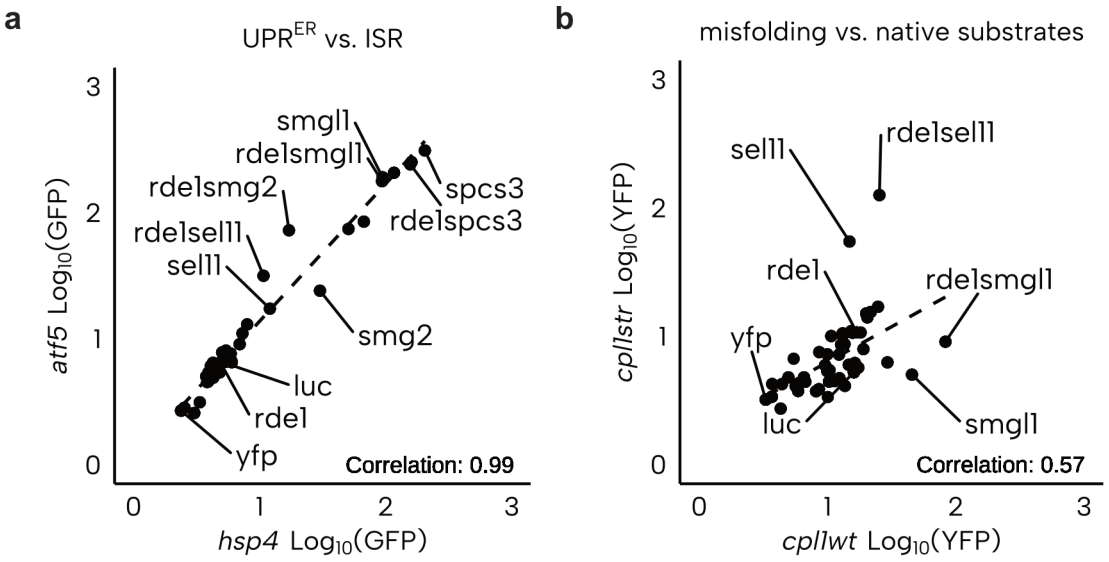

Figure 29: **ERQC RNAi screen: correlation analysis between UPR^{ER}, ISR and ERQC**. **a**, the UPR^{ER} and ISR are highly co-regulated. All knockdown conditions (n = 42) in this screen demonstrate a tightly correlative regulation (r = 0.99, ***) between the UPR^{ER} and ISR based on the *Phsp-4::gfp* (*hsp4*) and *Patf-5::gfp* (*atf5*) reporter strains. **b**, the ERQC reporter strains CPL-1* (*cpl1str*) and CPL-1^{WT} (*cpl1wt*) show less correlation (r = 0.57, ***) due to the specific effects of knockdowns on either the misfolding or native substrate. *sel-11* knockdown displayed specific *cpl1str* and *smgl-1* knockdown specific *cpl1wt* accumulation. The significance of the correlation was tested with Pearson's product-moment correlation. *** p <0.001.

RDE-1 knockdown aggravates developmental delay phenotypes
As shown in Figure 26, several conditions in the ERQC knockdown screen caused a developmental delay in the red-positive gated CPL-1^{WT} and CPL-1* strains. A correlational study of the extinction values for these strains reveals that most knockdown conditions result in a strain-independent decrease in extinction, represented by a high correlation of r = 0.9 (p<0.001, ***) (Figure 31). For example, knockdowns such as *rpl-26* and *rde-1;rpl-26* caused developmental delay independent of the strain. Conversely, other knockdown

scenarios, for instance *spcs-3*, *rde-1;spcs-3* and *rde-1;sel-11*, lead to a strain-specific developmental delay in CPL-1* and not in CPL-1^{WT}, indicating that the expression of the misfolded CPL-1* substrate together with these knockdowns causes developmental delay (Figure 30). Single *alg-1* knockdown on the other hand seems to cause stronger developmental delay in CPL-1^{WT} (p=2.8x10^{-7}; ***) than in CPL-1* (p=3.6x10^{-4}; ***) (Figure 30).

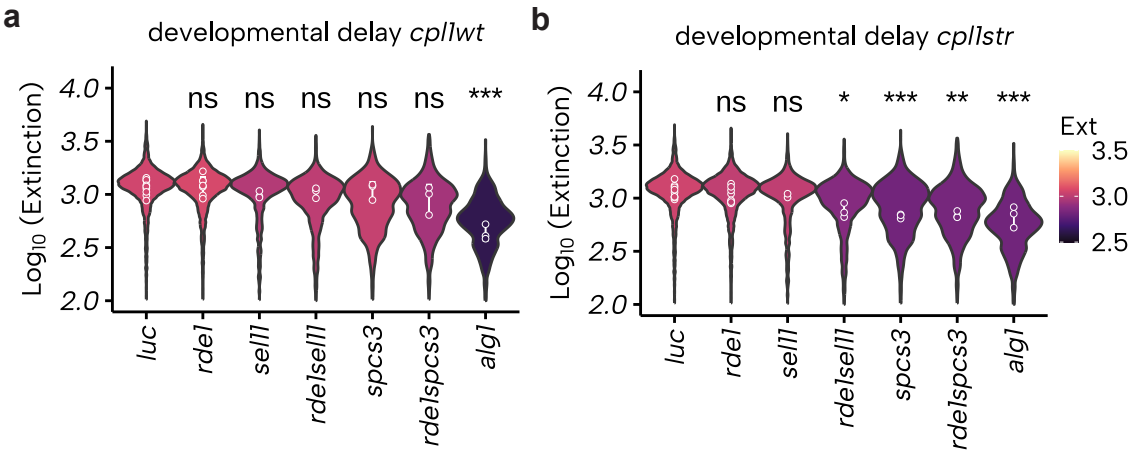

Figure 30: **ERQC RNAi screen: strain-specific developmental delay**. Extinction quantification in **a** CPL-1^{WT} (*cpl1wt*) and **b** CPL-1* (*cpl1str*) under strain-specific developmental delay knockdown conditions. **a–b** pairwise t-test with Holmes multiple comparison test was performed. Single knockdown conditions were compared to luc and double knockdown conditions were compared to *rde1*. * p<0.05, ** p<0.01, *** p<0.001, ns p>0.05.

Interestingly, several conditions demonstrate that additional *rde-1* knockdown on top of the *GOI* can aggravate developmental delay, as it is the case for *rpl-26*, *alg-1* and *smgl-1*, *spcs-3*. (Figure 31, A. 2b, A. 3b, A. 4b). The finding that RDE-1 *LOF* can exacerbate physiological impairments when other ERQC components such as SEL-11 are already compromised, was also noted in publication A [21], and indicates a compensatory role for RDE-1 in maintaining organismal health in case of ERQC dysfunction. Interestingly, *rde-1* knockdown extensively aggravates the developmental delay phenotype of *rpl-26* knockdown, a ribosomal subunit that is the principal target for ER-associated UFMylation (see 1.2.2.1). In independent experiments, we observed that crossing *rde-1(ne219)* into an *rpl-29::gfp* strain (GFP tagged RPL-29 protein in an *rpl-29(tm3555)* null mutant background) [183], led to a robust *rde-1*-dependent dumpy phenotype (data not shown). The observed genetic interaction between *rpl-26*, *rpl-29*, and *rde-1*, alongside the established role of AGO2 — the functional mammalian orthologue of RDE-1 — in competitively binding with the SRP on the translating ribosome [59], supports a co-translational, AGO2-dependent mechanism for regulating ER-targeted gene products [56] (discussed in 3.1.4).

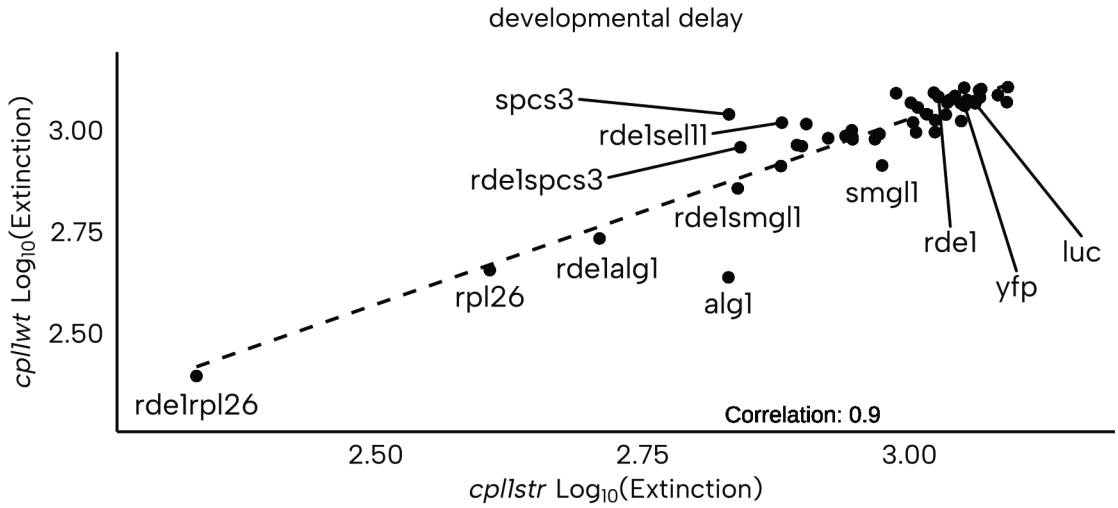

Figure 31: **ERQC RNAi screen: extinction correlation analysis between CPL-1* and CPL-1^{WT}.** Scatter plot demonstrating a strong correlation (r = 0.90, ***) in extinction levels between the red-positive gated worms CPL-1* (*cpl1str*) and CPL-1^{WT} (*cpl1wt*), effectively differentiating developmental delay induced in different knockdown conditions (n = 42). The significance of the correlation was tested with Pearson's product-moment correlation. *** p <0.001.

Synopsis of ERQC RNAi screen and future screening capabilities

In essence, the latter half of this thesis has shed light on the intertwined nature of ER-associated RNA and protein degradation pathways. As outlined in publication B, these pathways demonstrate a substantial level of interconnectedness and possess the ability to compensate for the *LOF* of other ERQC pathways. As one example, the conducted small-scale epistasis screen (2.2.3.1), revealed a novel genetic interplay between ER-NMD and ERAS in controlling the native folded and ER-targeted CPL-1^{WT} substrate, while not controlling the misfolded CPL-1* substrate, necessitating additional exploration. From a methodological perspective, this small-scale and non-automated screening process showcased the potential and efficiency of using the COPAS platform to carry out screenings in a variety of reporter strains and knockdown conditions, with multiple readout parameters such as fluorescence (Red, Green, Yellow), TOF and extinction. This facilitates the analysis of multiple physiological outcomes (e.g. reporter activation or the developmental delay observed in this study) and the correlative comparison of these results across various reporter strains (Figure 27, 29, 31). When combined with automated sample screening, this method offers considerable potential for carrying out comprehensive RNAi screens to assess cytoprotective stress responses such as UPR^{ER} and ISR and to comprehend the influence of genetic factors on these pathways (Figure 29). The latest COPAS platform significantly enhances these capabilities by providing brightfield microscopy images of sufficient resolution to evaluate tissue-specific fluorescence measurements to anatomical features in *C. elegans*, such as the head, intestine, or tail region.

3 Discussion

3.1 What makes an ERAS target?

This work demonstrates that the somatic RNA silencing pathway regulates ER-localized gene expression by degrading various ER-targeted endogenous and transgenic mRNAs in an ER stress-dependent manner. This ERAS function can be triggered by conditions such as transgenic expression of CPL-1* and *ATM*, treatment with ER stress agents like tunicamycin or thapsigargin, or viral infections. The activation of ERAS is evidenced by the observed degradation of the respective reporter substrate mRNAs, endogenous mRNAs, or viral RNAs. However, the defining characteristics of ERAS activation remain elusive [21]. This section focuses on the known targets of ERAS, examining their properties at the mRNA and protein levels and exploring how these characteristics might provide insights into the mechanism of ERAS activation and target selectivity.

To better understand the potential mechanism of ERAS action, two models of ERAS activation are proposed as a conceptual framework (Figure 32). The cis-acting and trans-acting models describe two distinct mechanisms of ERAS activation. In the cis-acting model, similar to mRNA surveillance and quality control mechanisms, ERAS targets mRNAs either due to errors in their sequences or when their associated protein species exhibit inefficient translation, processing, or folding within the ER. Conversely, in the trans-acting model, akin to a stress response, ERAS targets mRNAs regardless of the translation, processing, or folding efficiency of their encoded proteins. Instead, it is activated by general ER stress, such as the accumulation of misfolded proteins within the ER (Figure 32).

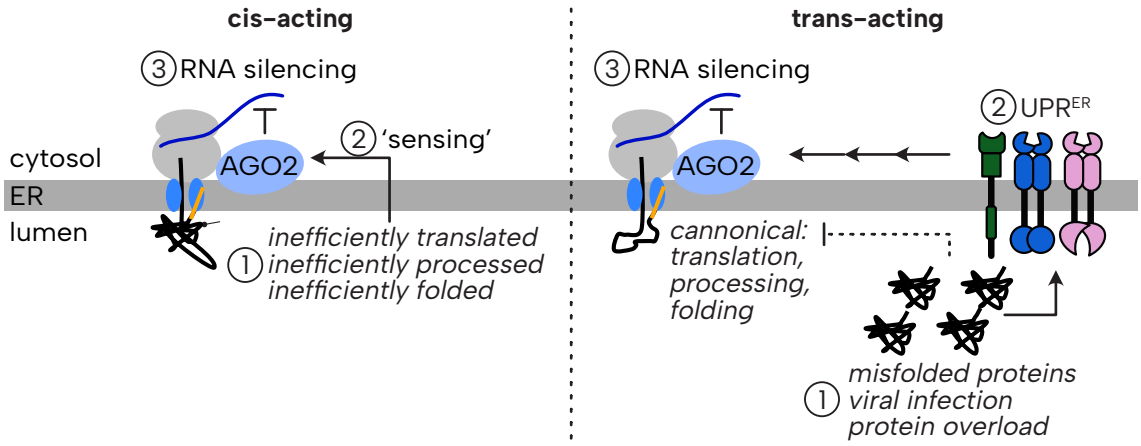

Figure 32: **Two models of ERAS activation.** In the cis-acting model, ① proteins that are inefficiently translated, processed, or folded are ② sensed and ③ subsequently silenced by ERAS. In the trans-acting model, ① general ER stress, mediated by various factors, ② activates ERAS potentially through the UPR^{ER}, ③ leading to the silencing of mRNAs regardless of their translation, processing, or folding status. The dashed line interaction in the trans-acting model highlights the methodological challenge of discerning between the two models

Mechanistically, these two models of ERAS activation are mutually exclusive, offering distinct insights into the cellular function and target identification process of ERAS (Figure 32). Experimentally, however, separating these models presents significant challenges. For example, transgenic overexpression of an inefficiently folding reporter substrate can induce ER stress, as required for the trans-acting model, but it may also sequester essential chaperones and quality control factors from endogenous protein species. This depletion can thereby inadvertently trigger the cis-acting mechanism for those endogenous protein species.

In publication A, for example, we demonstrated that transgenic expression of the misfolding CPL-1* substrate leads to RDE-1-dependent degradation of many endogenous mRNAs, and that expression of the ERAD substrate *ATM* results in RDE-1-dependent degradation of the endogenous *cpl-1* transcript [21], implying a trans-acting ERAS function. In addition, we demonstrated that introducing ER stress through an ERAD *LOF* mutation led to the RDE-1-dependent degradation of the CPL-1^{WT} transcript [21]. However, these findings neither exclude the possibility of a cis-acting mechanism nor prove a trans-acting mechanism. The expression of CPL-1* [21] and *ATM* (data not shown; personal communication with Stephen C. Pak) cause ER stress, potentially resulting in suboptimal translation, processing, and folding of the protein species, whose cognate mRNAs we identified as ERAS targets. It is therefore unclear whether overall ER stress led to the degradation of the endogenous mRNA transcripts (trans-acting) or the inefficient translation, processing, or folding of their encoded peptides (cis-acting).

3.1.1 Reevaluating ER stress as a primary trigger for ERAS activation

The data in this dissertation demonstrate, that ERAS can be triggered by ER stress induced by expression of the ERAD substrates CPL-1* and *ATM*, treatment with tunicamycin/thapsigargin, or viral infection ([21]; Figure 16, Figure 17). However, the presented data cannot conclusively prove a general trans-acting mechanism mediated solely by ER stress. Further, some data in this dissertation indicate that ER stress is neither the sole nor the direct cause of RDE-1-dependent degradation of target mRNAs: For example, while the aggregation-prone *ATZ* reporter substrate exhibits higher baseline ER stress levels compared with *ATM* (Figure 17b), ERAS-mediated degradation of *ATZ* is less pronounced than that of *ATM* (Figure 17c-d).

CPL-1^{WT} represents a particularly interesting ERAS target, as it acts as a facultative target, since ER stress, induced by factors such as the *sel-11(nDf59)* allele or knockdown of the SPP complex, is necessary for observing an ERAS-dependent reduction in CPL-1^{WT} levels (Figure 27, 28). However, repeated attempts to induce CPL-1^{WT} degradation with the ER stress agent tunicamycin—employing western blotting and RNA chase experiments across various concentrations, exposure times, and treatments in L4 or D1A worms—consistently failed to demonstrate RDE-1-dependent effects, regardless of the experimenter ([184]; data not shown). In addition, although CPL-1^{WT} levels can be reduced in ER stress-causing knockdown conditions in an RDE-1-dependent manner, there are also knockdown conditions that ER stress independently regulate CPL-1^{WT} levels in an RDE-1-dependent manner (*ufm-1*, *ufl-1*, *stau-1*, *smg-1* and *smgl-1* (Figure A. 2, A. 4). The novel genetic interaction between ER-NMD and ERAS in regulating CPL-1^{WT} levels, suggests an ER stress-independent mechanism for CPL-1^{WT} regulation through ERAS (Figure A. 2, Figure 26). This phenomenon warrants further scrutiny and may provide the necessary insights regarding the activation mechanisms of ERAS. Another line of evidence that ER stress is not the sole cause for ERAS activation is the observation that the ER-targeted transgene mCherry::HEDL used in publication A is neither degraded by ERAS under baseline conditions nor in the SEL-11 *LOF* background. This line of evidence prompts new questions about why certain ER-targeted substrates are not affected by ERAS, whereas CPL-1*, CPL-1^{WT}, *ATM*, and *ATZ* are.

3.1.2 Could the transgene composition influence ERAS target specificity?

The four reporter strains ① CPL-1*, ② CPL-1^{WT}, ③ *ATM*, and ④ *ATZ* were conceptually conceived by two close laboratories and display an extremely similar transgene composition [168, 148], while the ⑤ mCherry::HEDL transgene was generated by an independent laboratory [185]:

① *Pnhx-2::CPL-1^{W32Y35}::YFP::unc-54(3'UTR); Pmyo-2::mCherry* (CPL-1^{WT})

② *Pnhx-2::CPL-1^{A32A35}::YFP::unc-54(3'UTR); Pmyo-2::mCherry* (CPL-1*)

③ *Pnhx-2::sGFP::ATM::unc-54(3'UTR); Pmyo-2::mCherry* (*ATM*)

④ *Pnhx-2::sGFP::ATZ::unc-54(3'UTR); Pmyo-2::mCherry* (*ATZ*)

⑤ *Pvha-6::SEL-1(1-79)::mCherry::HEDL::let-858(3'UTR)* (mCherry::HEDL)

Although these strains employ different promoters (indicated in beige), specifically *Pvha-6* and *Pnhx-2*, which are both intestinal promoters in *C. elegans* [186, 187], our data demonstrate that ERAS regulates its targets directly at the post-transcriptional level. This suggests that the use of two different intestinal promoters is unlikely to account for the observed differences between the mCherry::HEDL and the other reporters.

Another distinction among the tested reporter substrates lies in the use of the transgenic marker *Pmyo-2::mCherry*, which is co-expressed in the pharynx of worms expressing intestinal CPL-1*, CPL-1^{WT}, *ATM*, and *ATZ* (indicated in red). This marker is not present in worms expressing mCherry::HEDL. The presence of *Pmyo-2::mCherry* might impact the intestinal ERQC substrates through potential cell-non-autonomous regulation of the somatic RNA silencing pathway [188]. Such regulation would depend on the inter-tissue transfer of small guide RNA species. For example, guide RNAs from the pharyngeal muscle could potentially target the CDS or 3'UTR of CPL-1*, CPL-1^{WT}, *ATM*, and *ATZ*. The activity of these guide RNAs would likely hinge on their ER stress-inducibility and the presence of the Pmyo2::mCherry::HEDL expression. However, such a cell-non-autonomous regulation seems unlikely as the protein folding status of the reporter substrates CPL-1* and CPL-1^{WT} and its downstream consequences in the intestine is sufficient to activate ERAS. Nevertheless, the data in this dissertation do not conclusively rule out the possibility that this effect is independent of Pmyo2::mCherry::HEDL co-expression.

A notable difference between the reporters is the sequence of their 3'UTR (highlighted in blue). This variation may be critical in the context of ERAS regulation, given that miRNA-driven RISCs predominantly target the 3'UTR regions of mRNAs (Figure 5). Notably, RDE-1 is capable of binding miRNAs and pull-down experiments demonstrate that >80 % of identified small RNAs on RDE-1 are miRNAs [189]. The deployed *unc-54* 3'UTR in CPL-^{WT}, CPL-1*, *ATM*, and *ATZ* for example has *mir-60*, *mir-71*, *mir-85*, *mir-230*, *mir-249*, *mir-2953*, etc. as predicted binding miRNAs while *let-858* 3'UTR in Cherry::HEDL has a starkly different profile of predicted binding miRNAs: *mir-85*, *mir-71*, *mir-70*, *mir-792*, etc (TargetScan; [190]). These miRNAs could be differentially regulated through the activation of UPR^{ER} or ISR, as it has already been shown for many other miRNAs to be heavily regulated upon ER stress [16]. Such a regulation would resemble a trans-acting mechanism of ERAS activation and would be in line with the current understanding of how miRNAs can reshape gene expression profiles of cells under stress conditions [15] (Figure 33).

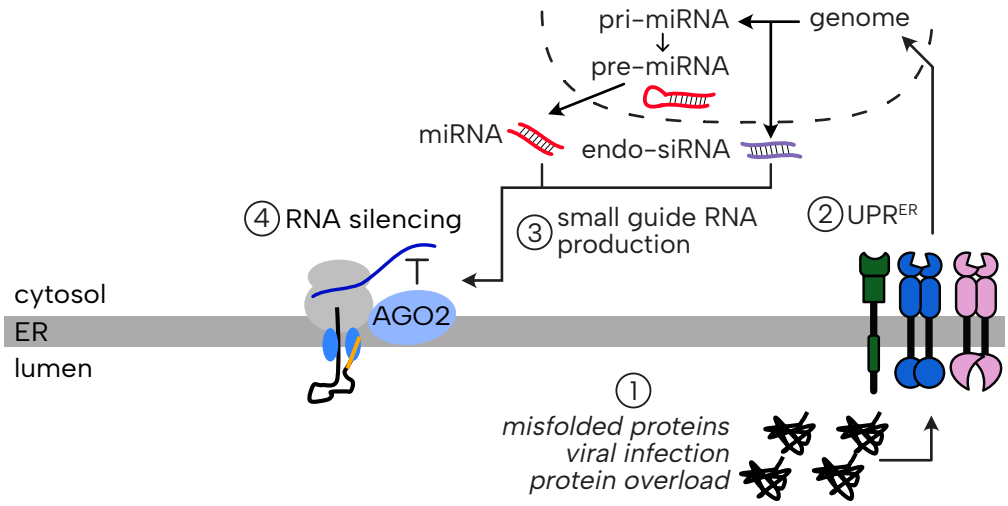

Figure 33: **Model of trans-acting ERAS activation by miRNAs or endo-siRNAs**. General ER stress, ① triggered by events such as the accumulation of misfolded proteins, viral protein production, or an overload of proteins in the ER, activates ② UPR^{ER}. This response transcriptionally upregulates ③ the production of small guide RNAs, including miRNAs and endo-siRNAs, which are employed for ④ RNA silencing.

In the case of the tested reporter substrates in this dissertation, the miRNA profile of the *unc-54* 3'UTR may be modulated by general ER stress, affecting the stability of the CPL-1*, CPL-1^{WT}, *ATM*, and *ATZ* mRNA via ERAS, while the miRNA profile of the *let-858* 3'UTR might not be modulated by ER stress, thereby rendering mCherry::HEDL mRNA stability independent of ER stress (Figure 33).

However, several indications in this study contradict a trans-acting and miRNA-driven ERAS activation. First, several knockdown experiments demonstrated that miRNA silencing components such as ALG-1, AIN-1, AIN-2, or components in miRNA biogenesis like PASH-1 and DRSH-1 are not important for the RDE-1-dependent reduction of *ATM* and CPL-1* (Figure A. 5, [21]). Second, while the knockdown of miRNA silencing and biogenesis components does not mimic the knockdown of RDE-1, the knockdown of DICER results in a complete phenocopy of the RDE-1 knockdown. Further knocking down DICER and RDE-1 simultaneously, does not show an additive effect in CPL-1* levels, indicating that the miRNA pathway is specifically not required, while, DICER, a shared factor between the miRNA and siRNA pathways, is necessary for the ERAS response (publication A). Finally, the differential regulation of CPL-1^{WT}, CPL-1*, *ATM*, and *ATZ* that responds to changes in ERQC suggests that it is implausible for the same set of miRNAs acting on identical 3'UTRs to achieve such varied regulation. Collectively, the evidence presented in this dissertation suggests that the ERAS-dependent regulation of these substrates in *C. elegans* is unlikely to be mediated by miRNA-driven silencing. Another con-

sideration is the role of endo-siRNAs, increasingly recognized for their ability to regulate endogenous mRNAs in worms, flies, and vertebrates [191, 192] (Figure 33). Operating independently of miRNA biogenesis and the miRNA-driven RISC, endo-siRNAs align with the findings presented in this dissertation as well as the finding from two independent laboratories that identified the only slicing active Argonaute in mammals, AGO2, to be important for RAPP [59] and AGO-RQC [57, 56] (see publication B). Unlike miRNAs, which predominantly bind to the 3'UTR, endo-siRNAs can also target the CDS region of mRNA transcripts. Therefore, they represent a viable option for a trans-acting ERAS activation mechanism that does not conflict with any data presented throughout this dissertation (Figure 33).

The last and most significant difference among the studied transgenes lies in the CDS region (highlighted in black). Changes in the mRNA sequence in this region can have a threefold impact: ① they can affect mRNA stability by engaging or disengaging sequence-specific endonucleases like IRE1 and AGO2 [19], ② they can alter translational efficiency through suboptimal codon usage thereby engaging or disengaging RQC [12], ③ and they can modify the stability of the encoded protein through amino acid substitutions, leading to engagement or disengagement of ERQC [114]. This dissertation does not present data that conclusively support or strongly refute a cis-acting ERAS mechanism based on ① changes in mRNA sequences or ② differences in translation efficiency between the CPL-1*/^{WT} and ATM/Z substrate reporter pairs. However, it primarily supports ③ ERAS activation in response to protein folding challenges caused by amino acid exchanges. Our datasets suggest that changes in mRNA sequence may not directly trigger ERAS, given that endogenous *cpl-1*, CPL-1^{WT}, and *ATZ* can become facultative targets without alterations in mRNA sequences. Additionally, we cannot discount the potential influence of slowed translation due to altered codon usage in CPL-1* or *ATM* substrates on ERAS activation. Therefore, inefficiencies in translation and changes in protein stability emerge as the most viable hypotheses for ERAS activation, with changes in mRNA sequences being a plausible but less supported hypothesis. Given that minor changes in mRNA sequence, such as in CPL-1^{WT} vs. CPL-1* or *ATM* vs *ATZ*, can affect each of these three levels by engaging distinct quality control and degradation machinery, well-controlled experimental setups will be required to investigate the mechanisms of action of ERAS (see 3.3). The final section of 'What makes an ERAS target' will discuss why ERAS activation by altered protein stability of the substrates is the most supported hypothesis for ERAS activation.

3.1.3 Is ERAD participation a more accurate indicator of ERAS activation?

By ranking the propensity of each reporter substrate to be degraded by ERAS or ERAD, it becomes apparent that CPL-1* is the strongest target of both pathways, followed by *ATM*, which is also an obligate target for ERAS and ERAD (publication A, Figure 16, 17). *ATZ* emerges as a significant yet milder ERAS target, evidenced by mild but significant RNA destabilization observed in RNA chase experiments (Figure 17d), leading to a corresponding increase in *ATZ* protein levels (Figure 16b). This milder targeting by ERAS is mirrored in its degradation by ERAD: compared to *ATM* (p=***), *ATZ* (p=*) shows less pronounced accumulation upon knockdown of *sel-11*, an effect also noted in the literature where *ATZ* is described as ERAD-resistant compared to the properly folding *ATM* variant [131]. The double knockdown of *rde-1* and *sel-11* indicates that *ATZ* might become more degraded by ERAS upon ERAD *LOF*, since the double knockdown leads to a more-than-additive *ATZ* accumulation (Figure 16c-d) (*rde-1*:+4 % ns, *sel-11*:+6 % *, *rde-1;sel-11*:+18 % ***). A more-than-additive effect in protein accumulation is also observed for the facultative ERAS target CPL-1^{WT} (Figure A. 1), where individual knockdowns of *rde-1*(+2 %, ns) and *sel-11* (-3 %, ns) show minimal changes, but their combined knockdown results in a considerable accumulation (+17 %, ns). Unlike *ATZ*, CPL-1^{WT} remains stable under baseline conditions and only becomes destabilized upon *LOF* of *sel-11*, indicating a lesser propensity for ERAS-mediated degradation compared to *ATZ*. This absence of ERAS-mediated degradation in CPL-1^{WT} corresponds to its weak propensity to be a bona fide ERAD target. Of note, a more-than-additive effect as observed for *ATZ* and CPL-1^{WT} is less prominent or absent for the obligate ERAS and ERAD targets CPL-1* (*rde-1*:+43 % ***, *sel-11*:+142 % ***, *rde-1;sel-11*:+192 % ***) and *ATM* (*rde-1*:+29 % ***, *sel-11*:+16 % ***, *rde-1;sel-11*:+52 % ***). Finally, mCherry::HEDL is neither a target of ERAS nor ERAD nor does it become a target upon *sel-11* LOF [21], displaying the weakest propensity for ERAD and ERAS activation among all reporter substrates studied. Taken together, all tested reporter substrates in this study demonstrate a surprisingly similar propensity of being targeted by ERAS and ERAD simultaneously or not at all. For targets that are not strong bona fide ERAD targets like *ATZ* and CPL-1^{WT}, concurrent ERAD and ERAS *LOF* shows a more-than-additive substrate accumulation effect, indicating that upon ERAD *LOF*, ERAS might be needed to reduce the protein folding burden at the ER (Figure 34).

	ERAS target	ERAD target	additive effect	additive (+)effect
CPL-1*	yes	yes	yes	no
ATM	yes	yes	yes	no
ATZ	mild	mild	yes	yes
CPL-1^{WT}	no/yes	no/yes	yes*	yes
mCherry::HEDL	no	no	no	no

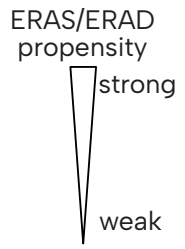

Figure 34: **Comparison of ER-targeted reporter substrates.** The reporter strains in this figure are ranked based on their relative propensity to be targeted by ERAS and ERAD. *: the additive effect is observable but not significant in the shown dataset. (+): more-than-additive effect.

3.1.4 Emerging AGO-dependent and ER-associated RNA and protein degradation pathway

AGO2 has been consistently shown to be localized at the rough ER membrane [193, 194, 195] and to interact with ribosomal subunits and RNA [59, 196, 197] and SRP [59]. Ribosome-dependent unfolding of mRNA structures can enhance AGO2-target interactions, establishing a direct, causal link between mRNA translation and AGO2-target binding [198]. This finding aligns with data showing that ER-targeted proteins are initially transported via the SRP system to the ER, where translation resumes before AGO2 can perform silencing [193]. A recent study of mammalian AGO2 and *D. melanogaster* Argonautes has indicated that slicing-active Argonautes co-localize with LTN1 at the ER membrane, supporting a co-translational ER-adapted RQC that degrades ER-targeted proteins, coupling PTGS with RQC [57, 56]. Altogether, these studies place AGO2 very close to the co-translational translocation process at the ER. This dissertation indicates cooperation between ERAD and ERAS and the potential linking of PTGS with protein degradation and proposes a model that integrates the observations published previously with those found in this dissertation (Figure 35). In this model, AGO2 potentially interacts with ER-E3s such as LTN1 from RQC and HRD1 from ERAD, leading to the simultaneous degradation of target mRNAs and their cognate proteins via AGO2 and the ER-E3s, respectively (Figure 35). Such an adapted ER-QC mechanism has been recently postulated [55] and would significantly contribute to the understanding of the coordination of ER-associated RNA and protein degradation pathways (publication B).

Distinguishing between cis-acting and trans-acting activation mechanisms may clarify the chronological sequence of events: In a cis-acting mechanism, the primary trigger arises from ① inefficient translation, processing, or folding of the encoded protein, leading to ② RQC or ERAD activation and subsequently ③ AGO2 involvement. Conversely, in a trans-acting mechanism, the ① small guide RNA-loaded AGO2 protein ② identifies target mRNAs, ③ interferes with canonical translation, and ultimately leads to ④ the activation of RQC or ERAD. The missing link in the cis-acting mechanism is how RQC or ERAD activation directs AGO2 to degrade the corresponding mRNA and how small guide RNAs are involved. In the trans-acting mechanism, the key questions are how mRNA targets are selected and how the small guide RNA biogenesis is regulated (Figure 33).

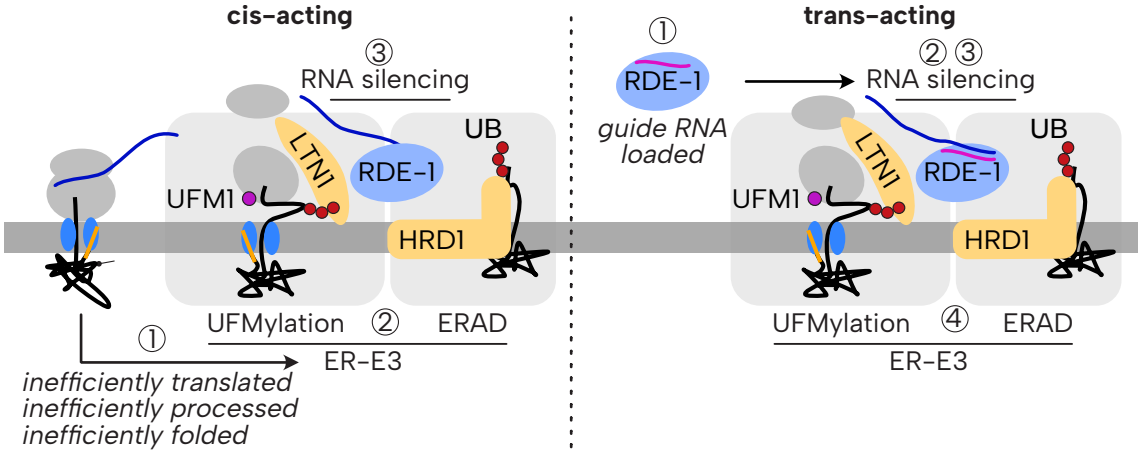

Figure 35: **Model of ER-RQC, ERAD, and RNA silencing cooperation.** Based on the data presented in this dissertation and published data, this study proposes a model of how ER-RQC, ERAD, and RNA silencing could cooperate in coordinating ER-associated RNA and protein degradation.

Both of these mechanisms critically depend on understanding how the AGO protein is programmed to degrade target mRNAs. Since AGO proteins are known to exert silencing through small guide RNA species, another important question concerns the source of such guide RNA species.

3.2 What is the source of the small guide RNA species in ERAS?

This dissertation did not provide evidence regarding the source of the guide RNA species involved in ERAS, and will therefore only briefly discuss potential mechanisms: As suggested in Figure 33, a trans-acting mechanism for ERAS activation aligns with the current understanding of how miRNAs or potentially endo-siRNAs can regulate ER-associated gene expression fidelity in response to ER stress. These nuclear-encoded small guide RNA species are the most promising candidates for reprogramming AGO proteins to degrade

ER-targeted mRNAs. Their expression is likely inducible through ER stress-dependent transcriptional activation and targets a pre-defined set of mRNA sequences. An illustrative example is *mir-708*, a UPR^{ER}-inducible miRNA that regulates rhodopsin—a protein abundantly produced in the ER and crucial for retina development. Through AGO2-dependent downregulation of rhodopsin in response to ER stress, *mir-708* helps prevent the accumulation of misfolded rhodopsin within the ER [199]. A similar trans-acting activation of endo-siRNA expression and silencing of ER-targets mRNAs is therefore in line with the presented data in this dissertation (see 3.1.2). Experimental approaches to study such a trans-acting activation mechanism of ERAS are proposed in 3.3.

Currently, a cis-acting mechanism that generates sequence-specific small guide RNA species targeting the erroneous mRNAs encoding proteins that are inefficiently translated, processed, or folded is unknown in mammals and other animals. Such a mechanism has been observed in plants, where significant cross-talk between RNA quality control and RNA silencing occurs. This interaction allows erroneous mRNAs to trigger RdRPs to generate endo-siRNAs targeting these mRNAs [200, 201], allowing for a cis-acting mechanism. *C. elegans* expresses the functional RdRP, RRF-1, and this dissertation demonstrated that RRF-1 is conducive to, but not essential for, ERAS (publication A). However, mammals completely lack a functional RdRP, precluding the existence of such a mechanism [40]. Overall, a cis-acting mechanism of ERAS activation driven by canonical small guide RNA species thus appears unlikely.

Recent studies have also uncovered several AGO-dependent small RNA pathways initiated by single-strand (ssRNA) precursors, which lack recognizable dsRNA or hairpin structures [202]. Particularly under conditions where these highly unstable ssRNAs are stabilized through chemical modifications or *LOF* of cellular RNases that degrade them [203], these findings demonstrate the feasibility of ssRNA-guided AGO silencing. For example, a study using a human Ago2 protein purified from insect cells revealed an unexpectedly broad range of guide molecules including even a 73 nt non-structured ssRNA [204]. Such structured or unstructured ssRNA species could resemble mRNA degradation products after endonucleolytic cleavage, such as RIDD or RIDDLE degradation products. In a speculative model, the ER-associated and ER stress-activated ① RIDD or ② RIDDLE pathways could provide ssRNA or stem-loop containing RNA fragments of ER-targeted mRNAs that could be ③ loaded into AGOs and lead to RNA ④ of cognate ER-associated RNAs (Figure 36).

RIDD generates ssRNA fragments that lack both 5′ caps and 3′ polyA tails, typically recognized by the dsRNA sensor RIG-I, the orthologue of DRH-1 in mammals [205]. This might suggest a potential for AGO2 recognition, given its capacity to bind unstable ssRNAs [204] and its proximity to IRE1 a the ER membrane. Consequently, AGO2 may engage with ssRNA fragments produced by RIDD during ER stress, contributing to a novel regulatory mechanism of mRNA under stress conditions (Figure 36).

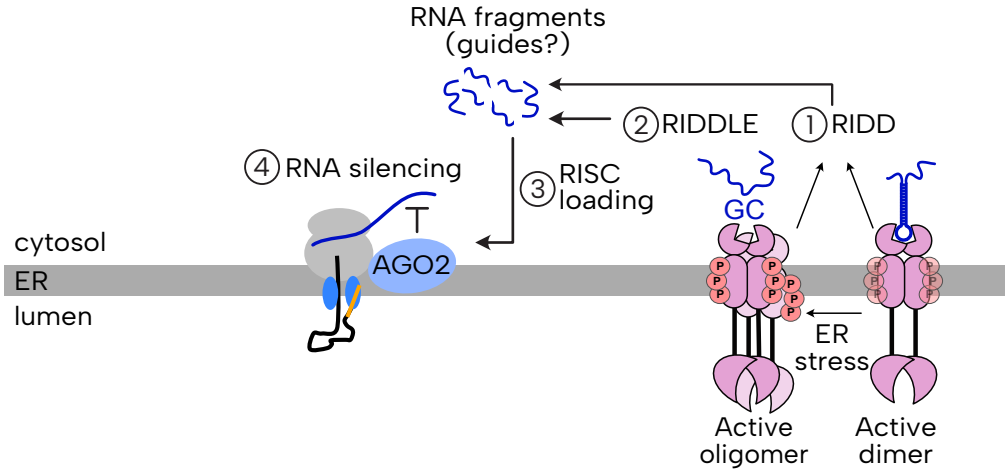

Figure 36: **Speculative model of RIDD(LE)-mediated generation of RNA Fragments for RNA silencing**. In this speculative model, RIDD and RIDDLE might produce ssRNA or stem-loop containing RNA fragments that might be suitable for AGO loading and subsequent RNA silencing of ER-targeted RNAs.

3.3 Conclusion and outlook

In summary, the coordination of ER-associated RNA and protein degradation pathways is a complex and multilayered process, involving the surveillance of mRNAs and proteins as well as the capability to respond to perturbations through ER-localized stress responses. The identification of ERAS as a key player in this coordination—through its role in degrading ER-targeted mRNAs and its activation upon ER stress—has raised numerous questions about the criteria for defining an ERAS target and how ERAS interacts with established quality control and ERAD factors. Combining our data with recently published findings, we hypothesize an ER-associated and AGO-dependent RNA and protein degradation pathway, which will require further investigation for comprehensive understanding. This dissertation presents a conceptual framework for understanding ERAS mechanisms through cis-acting or trans-acting modes of action, and it highlights the methodological challenges in distinguishing between these mutually exclusive mechanisms.

To investigate a trans-acting ERAS activation mechanism, the following experiments will be pivotal:

① Perform small RNA sequencing under ERAS-activating and non-stressed conditions (e.g. CPL-1* vs. CPL-1^{WT} expression).

② Conduct α-amanitin RNA chase assays under the same conditions and combine with RNA sequencing to identify a list of true ERAS targets.

③ Analyze the small guide RNAs and the identified ERAS mRNA targets to determine if the predicted targets of the small guide RNAs coincide with the observed ERAS mRNA targets.

To investigate the observed compensatory interaction between ERAS and ERAD, the following experiments will be pivotal:

① Perform CHX protein chase assays under the same conditions from above (e.g. CPL-1* vs. CPL-1^{WT} expression).

② Analyze the identified ERAD protein targets alongside the list of ERAS mRNA targets to determine if there is a significant overlap between ERAD and ERAS targets for the same gene products.

To investigate a cis-acting ERAS activation mechanism, the following experiments will be pivotal:

① Perform CPL-1* and CPL-1^{WT} mRNA pulldowns and investigate which co-immunoprecipitated protein factors are enriched on CPL-1* compared with CPL-1^{WT} mRNA.

② Conduct single-gene insertion with low expression levels of CPL-1* and *ATM* to circumvent sequestering of important ERQC machinery of endogenous protein species.

③ Investigate whether low levels of CPL-1* or ATM expression still lead to a trans-acting mechanism, where endogenous mRNAs are ERAS-dependently degraded.

④ Utilize α-amanitin RNA chase assays to examine whether the genetic interaction between ER-NMD and ERAS in regulating CPL-1^{WT} levels occurs at the mRNA level.

4 Material and Methods

This dissertation incorporates, updates, and expands upon methodologies initially reported in my Master's thesis, entitled 'Involvement of the exogenous RNAi pathway in mRNA turnover and ER homeostasis,' which I completed at the University of Cologne in 2019 [184].

4.1 Consumables and Instruments

Consumables and instruments used in this study were purchased from the companies AppliChem (Darmstadt), Applied Biosystems(Carlsbad), BD Biosciences (Heidelberg), Bio-Rad (Hercules), Carl Zeiss Microscopy GmbH (Jena), Clontech (Mountain View), Eppendorf (Hamburg), Fermentas (Waltham), GE Healthcare (Chicago), Invitrogen (Carlsberg), Leica Camera (Wetzlar), Merck (Darmstadt), Metabion (Steinkirchen), Millipore (Burlington), Nerpe plus (Winsen), New England Biolabs (Ipswich), Peqlab (Darmstadt), Qiagen (Hilden), Roche (Basel), Roth (Karlsruhe), SERVA (Heidelberg), Sigma (Deisenhoff), Sarstedt (Nümbrecht) and VWR (Darmstadt). Union Biometric (Boston).

4.2 Software and Resources

For this dissertation the following software packages were used: Affinity Designer v1.10.8 and Affinity Publisher v1.10.8 (Serif Europe Ltd.) for generating illustrations and compiling data sets into figures, Bio-Rad CFX Manger for RT-qPCR Analysis (Bio-Rad Laboratories Inc.), GraphPad Prism 7 for data visualization (GraphPad Software), ImageStudioLite v5.2.5 for the analysis of Western Blots (LI-COR Biosciences), Microsoft Office 365™ ProPlus package v16.80 with Word, Excel and PowerPoint (Microsoft Corporation), Leica Application Suite v.3.3.0 for acquisition and evaluation of fluorescence microscopy pictures (Leica fluorescence microscope), Zen 2.3 Pro (Carl Zeiss Microscopy). Mendeley 2.107.0 for the citation of relevant literature (Mendeley Ltd.). *C. elegans* specific resources regarding techniques and nematode biology were obtained from WormBook (www.wormbook.org). WormBase (www.wormbase.org) was used as an additional resource for genetic information of *C. elegans*. The bioinformatic resource portal ExPASy (www.expasy.org) and UniProt (www.uniprot.org) was used for access to data of *C. elegans and M. musculus* proteins. The website of the National Center for Biotechnology Information NCBI (www.ncbi.nlm.nih.gov) together with Google Scholar (scholar.google.de) were used for literature research. Overleaf Premium (Digital Science UK Limited) was employed for compiling and formatting the dissertation in LaTeX . GPT-4 (OpenAI) was used for translating the "Zusammen-

fassung" into German and enhancing overall sentence readability in the dissertation. R Studio (Posit Software, PBC) v.2023.12.0 was used to analyze and visualize COPAS data.

4.3 Antibodies

To specifically stain or immunoprecipitate proteins of interest, the following primary and secondary antibodies were used in this study (Table 1).

Table 1: List of primary and secondary antibodies used in this study.

Antibody	Origin	Dilution	Source	Use	Identifier	#
α-Tubulin	Mouse	1:5000	Sigma	WB[a]	T6074	Ab192
α-GFP/YFP	Mouse	1:5000	Clontech	WB[a]	632380	Ab15
α-SEL-1	Rabbit	1:8000	Jarosch Lab	WB[a]	Hoppe Lab	Ab177
α-CDC-48	Rabbit	1:50000	Biogenes	WB[a]	Hoppe Lab	Ab161
α-AGO-2	Rabbit	1:1000	Cell Signalling	WB[a]	2897	N/A
α-AGO-2	Mouse	20 µl[c]	Fujifilm	CLIP[b]	014-22023	N/A
α-Mouse680	Donkey	1:10000	LI-COR	WB[a]	926-68072	Ab183
α-Mouse800	Donkey	1:10000	LI-COR	WB[a]	962-32222	Ab185
α-Rabbit800	Donkey	1:10000	LI-COR	WB[a]	926-32213	Ab184

[a] WB: western blotting
[b] CLIP: UV cross-linking immunoprecipitation
[c] per CLIP reaction

4.4 Microbiology

4.4.1 Media and Solutions

The following media and solutions were used in microbiological experiments in this study (Table 2). All media and solutions were sterilized by autoclavation.

Table 2: List of media and solutions used in this study.

Solution/Media	Component
LB Agar	LB Broth, 1.5% (w/v) agar
LB Broth	1% (w/v) bacto-tryptone, 0.5% (w/v) yeast extract, 1% (w/v) NaCl, pH: 7.5

4.4.2 Antibiotics

The following antibiotics were used in LB broth or agar in this study (Table 3).

Table 3: List of antibiotics used in this study.

Antibiotic	Abbreviation	Concentration
Ampicillin	Amp	100 µg/ml
Tetracycline	Tet	12.5 µg/ml

4.4.3 Bacterial Strains

The following *E. coli* strains were used in this study (Table 4).

Table 4: List of *E. coli* strains used in this study.

Strain	Resistance	Use	Source
HT115(DE3)	Amp, Tet	*C. elegans* food source in RNAi[a]	CGC[b]
OP50	–	*C. elegans* food source	CGC[b]

[a] RNAi is described in 4.6.10
[b] Caenorhabditis Genetics Center

4.4.4 Cultivation of Bacteria

Bacterial cultures were grown in LB broth at 37 ºC with 180 rpm or on LB agar plates at 37 ºC. For short term storage, bacterial cultures were stored at 4 ºC. For long term storage, glycerol stocks were prepared by mixing the bacterial culture 1:1 with sterile 50 % glycerol in ddH2O and stored at – 80 ºC. To ensure the perpetuation of the transformed plasmid in the *HT155(DE3)* and to ensure a robust dsRNA expression for RNAi experiments, the *HT155* cultures were grown with the respective antibiotics (Table 3, 4). The density of the liquid bacterial culture was determined by measuring the absorbance at 600 nm using the Ultrospec 10 spectrophotometer (Amersahm Biosciences). For further details regarding the robust dsRNA expression for RNAi knockdown experiments, see section 4.6.10

4.5 Molecular Biology

4.5.1 Solutions

The following solutions were used in molecular biology experiments in this study (Table 5).

Table 5: List of solutions used for experiments in molecular biology in this study.

Solution/Media	Component
MES SDS running buffer	50 mM MES, 50 mM Tris, 0.1% SDS, 1 mM EDTA, pH: 7.3
NuPAGE® transfer buffer	25 mM bicine, 25 mM Bis-Tris, 1 mM EDTA, pH:7.2, 10% freshly added methanol
PBS	137 mM KCL, 8.1 mM Na_2HPO_4, 1.5 mM KH_2PO_4, pH: 7.4
PBST	PBS, 0.01% (v/v) Tween 20
SDS loading buffer (2x)	125 mM Tris, 4% (w/v) SDS, 10% glycerol, 0.03% (w/v) bromphenole blue, 0.04% (w/v) β-mercaptoethanol
TAE	40 mM Tris/HCl, 1 mM EDTA, 17.5% (v/v) acetic acid, pH: 8.3

4.5.2 Oligonucleotides

The following oligonucleotides were used for genotyping (Table 6) and RT-qPCR (Table 7) experiments in this study.

Table 6: List of oligonucleotides for genotyping experiments in this study

Primer	**Tm**	**Sequence**	**#**
ne219 I	53 °C	AGCAAAAGAATACGCTGTACCAAGGA	TH2344
ne219 II	53 °C	GGCTTCTCATGAACTTCAAGATGGTC	TH2345
ne219 III	53 °C	GACAGAGGAAGAAATGCAAAAAAGTACG	TH2346
ne219 IV	53 °C	TCTGAAGTTTGGAGCATAATCCAAATCT	TH2347
ok3495 I	53 °C	TCACCGATCCAGTTGCATTA	TH2352
ok3495 II	53 °C	AACCCAACAGTATCCCTCCA	TH2353
ok3495 III	53 °C	TAATGCTTGTTGCTCATCCG	TH2354
ok3495 IV	53 °C	ACACGCAACGCAGTTTTATT	TH2355
nDf59 I	53 °C	GATGCTGCTGCTAATGTGG	TH3038
nDf59 II	53 °C	GAGGGAATGGTCCAGGC	TH3039
nDf59 III	53 °C	GGAGTTTCCCACGACAGGC	TH3040
syb5475 I	68 °C	GTGAAGAAATGACTGTCGATGCTTCACTAC	TH4663
syb5475 II	68 °C	AACACATGGGAACATGGTAGTCGCTT	TH4664
syb5475 III	68 °C	CACAAAGCATTCCTCGACGTTATTCTTT	TH4665
syb5475 IV	68 °C	CCGCACCATTTCTTCCCTCTAAAAATTA	TH4666
tm3555 I	51 °C	CACGTTTTCGTCGTTTGG	TH3926
tm3555 II	51 °C	GGCCACAAGCTTTCGG	TH3927
tm3555 III	51 °C	GGCCTAAATTGTTGTTAATTCGG	TH3928
GFP I	56 °C	CTACCTGTTCCATGGGTAAG	TH930
GFP II	56 °C	CTTCCATCTTCAATGTTGTGTC	TH931
hh17 I	68 °C	TCGTGAAGAAATGACTGTCGATGCTTCACC	TH5185
hh17 II	68 °C	ACATTAGCAGCAGCATCAGCCGCATTTC	TH5186
hh17 III	68 °C	GTTCCATGCCCATTGTCTCCGCAGGTA	TH5187
hh17 IV	68 °C	AGTTGGACATGTTTGCTGTCTTTGGACCC	TH5188
dh785 I	–	TCACAATTGGAGTCACCAACACTGTAGG	TH2081
dh785 II	–	ATGAGATTCACGGCAAATGGATGCTT	TH2082
dh785 III	–	CTGTGGAACATCCTATCACTCTGCCATC	TH2083
dh785 IV	–	TGATCTCTTCACGTCTCTTAGCCATGGA	TH2084
n4749 I	53 °C	GCAACGGTCTAAAATGATGTG	TH2360
n4749 II	53 °C	CAACACCGCATTCCATTCC	TH2361
n4749 III	53 °C	CGACACAACCGCTACAG	TH2362
v33 I	–	CACTTCAGGCAACAAATGG	TH2469
v33 II	–	CCATTTGTTGCCTGAAGTG	TH2470
v33 III	–	GACTTTCACTCTAAGGCTG	TH2471

Table 7: List of oligonucleotides for RT-qPCR experiments used in this study

Primer	**Use**[a]	**Tm**	**Sequence**	**#**
hsp-4 fwd	w	55 °C	AACGGAATATTGCACGTAAGCGCC	TH2501
hsp-4 rev	w	55 °C	TGAGACGATTGTGGTCGTTGGTGA	TH2502
sqt-1 fwd	w	55 °C	TCGCCACTCTTATGGTATGCT	TH3671
sqt-1 rev	w	55 °C	TCCATTGGTAGATTGTCTGAACAC	TH3672
cpl-1 fwd	w	55 °C	GGCTCCATTCAATGTTCAGG	TH3724
cpl-1 rev	w	55 °C	TGGTTGTCACGAATGTACTC	TH3725
pmp-3 fwd	w	55 °C	GTTCCCCTGTTCATCACTCAT	TH2463
pmp-3 rev	w	55 °C	ACACCGTCGAGAAGCTGTAGA	TH2464
cdc-42 fwd	w	55 °C	CTGCTGGACAGGAAGATTACG	TH2462
cdc-42 rev	w	55 °C	CTCGGACATTCCTCGAATGAAG	TH2467
spliced xbp-1 fwd	w	55 °C	TGCCTTTGAATCAGCAGTGG	TH2494
spliced xbp-1 rev	w	55 °C	ACCGTCTGCTCCTTCCTCAATG	TH2493
asp-12 fwd	w	55 °C	GAGTATGATCCGAGCTTAAATCCA	TH4621
asp-12 rev	w	55 °C	CTAACTTTAAGAATGACGCTGCTG	TH4620
pas-7 fwd	w	55 °C	CAATGCAGGAACAATGATTGC	TH3679
pas-7 rev	w	55 °C	TCTTGGATTAGCGTTATCAGTG	TH3680
ATM/Z fwd	w	55 °C	ACTGTCAACTTCGGGGACACC	TH4606
ATM/Z rev	w	55 °C	TCATCAGCAGCACCCAGCTGG	TH4607
18sRNA fwd	m	55 °C	GAGACGGCTACCACATCTAAG	TH3689
18sRNA rev	m	55 °C	ATACGCTAGTGGAGCTGGA	TH3690
rpl-19 fwd	m	55 °C	CTGATCAAGGATGGGCTGAT	TH3691
rpl-19 rev	m	55 °C	GCCGCTATGTACAGACACGA	TH3692
nov fwd	m	55 °C	GCCCTTCCAGCCTATAGACC	TH3693
nov rev	m	55 °C	GGATTTCTTGGTGCGGAGAC	TH3694
c1rl fwd	m	55 °C	GGAGTTTGTATCTTCTGGTAGGAG	TH3695
c1rl rev	m	55 °C	GCTAAGTGTCCCTGTCTGGT	TH3696
mertk fwd	m	55 °C	CTGGGTGAAGGAGAGTTTGG	TH3697
mertk rev	m	55 °C	ACATTTGGGTGGTTGAAGTC	TH3698
18S rRNA fwd	m	55 °C	ACCCGTTGAACCCCATTCGTGA	TH4604
18S rRNA rev	m	55 °C	GCCTCACTAAACCATCCAATCGG	TH4605
28S rRNA fwd	m	55 °C	CCGTGCCTTGGAAAGCGTCGC	TH4600
28S rRNA rev	m	55 °C	CAGAGGCTGTTCACCTTGGA	TH4601
BiP fwd	m	55 °C	TCAGCATCAAGCAAGGATTG	TH3728
BiP rev	m	55 °C	AAGCCGTGGAGAAGATCTGA	TH3729

[a] w = *C. elegans*, m = *M. musculus*

4.5.3 Polymerase chain reactions (PCR)

To amplify DNA fragments of interest during genotyping the following 25 µl reaction mixture was used.

Table 8: Genotyping reaction mix components.

Volume	Component
12.5 µl	OneTaq® 2X Master Mix with standard buffer
0.5 µl	Genotyping primer mix (10 µM)
2.0 µl	Single worm lysate (see 4.6.5)
10 µl	ddH_2O

The reaction mixture was then introduced to the thermocycler to start the polymerase chain reaction (PCR) with the following standard protocol (Table 9). The annealing temperature (Table 6) and the elongation time were variably adjusted to the respective genotyping PCR. Steps 2 to 4 were repeated for 30 cycles.

Table 9: Standard protocol of the thermocycler for genotyping PCR.

Step	Temperature	Time
1. Initial denaturation of DNA	95 °C	2 min
2. Cyclic denaturation	95 °C	1 min
3. Cyclic primer annealing	50–55 °C	1 min
4. Cyclic extension	72 °C	1 min/kb
5. Final extension	72 °C	4 min
6. Storage	4 °C	hold

4.5.4 Agarose gel electrophoresis

To analyze DNA fragments of interest generated by genotyping PCR, agarose gel electrophoresis (AGE) was deployed. 2 % (w/v) agarose TAE gels containing the nucleic acid stainer GelRed™ (Biotium) were used for the separation and visualization of the DNA fragments of interest. GeneRuler 1kb Plus (Thermo Scientific™) was used as standard marker for fragment sizes. AGE was performed with voltage of 120–150 V for 20–60 min. Visualization of the fragments after AGE was conducted with the UV-Transilluminator (Wealtec).

4.5.5 Sodium-dodecyl sulfate polyacrylamid gel electrophoresis (SDS-PAGE)

For the separation of proteins of interest on account of their molecular weight, discontinuous sodium-dodecyl sulfate polyacrylamide gel electrophoresis (SDS- PAGE) was performed. Proteins were denatured by SDS (detergent) and β-mercaptoethanol (reducing disulfide bonds). NuPAGE® 4-12 % Bis-Tris SDS gels with the NuPAGE® MES SDS running buffer were used accordingly to the instructions of the manufacturer. The PageRuler™ Plus Prestained Protein Ladder, 10 to 250 kDA (Thermo Scientific™) was used as standard marker for protein size. Subsequent to SDS-PAGE the gel was stained unspecifically for all proteins with InstantBlue™ staining solution (Merck) and washed with ddH2O. The unspecific protein staining was used for the normalization of samples used in quantitative western blotting and was carried out with the software ImageStudioLite.

4.5.6 Quantitative Western Blotting

Following the SDS-PAGE, electroblotting and immunostaining for the proteins of interest were conducted (Western Blotting). First, the proteins in the SDS-PAGE gel were transferred onto a nitrocellulose membrane by electroblotting with the Trans-Blot Turbo Transfer System (Bio-Rad) according to the instructions of the manufacturer. The standard transfer was performed with NuPAGE® transfer buffer and a constant 25 V voltage for 30 min. In this process, the negatively charged, and denatured proteins migrate through the SDS polyacrylamide gel towards the anode (+) and therefore onto the nitrocellulose membrane. After the semi-dry electroblotting, the membrane was incubated on a shaker for 1 h at RT or overnight at 4 °C with the primary antibody solution containing 1x Roti®-Block solution. The membrane was further washed 3x with PBST for 10 min before further incubation with the fluorescently labeled secondary antibody solution for 1 h at RT. Before the visualization of the proteins of interest, the membrane was washed 3x with PBST for 10 min. Visualization was performed using the Odyssey scanner (LI-COR) and the software ImageStudioLite.

4.6 *C.elegans* Techniques

4.6.1 Buffer and Solutions

The following solutions and buffer were used in this study in experiments with *C. elegans* in (Table 10).

Table 10: List of solutions and buffers used for experiments with *C. elegans* in this study.

Solution/Buffer	Component
M9 buffer	20 mM KH_2PO_4, 40 mM Na_2HPO_4, 80 mM NaCl, 1 mM $MgSO_4$
NGM agar	0.25% (w/v) bacto-peptone, 0.3% (w/v) NaCl, 1.7% (w/v) Serva agar, 1 mM $CaCl_2$, 1 mM $MgSO_4$, 5 µg/ml cholesterol, 25 mM KPO_4, 25 units/ml Nystatin
Fractionation buffer	50 mM Tris pH: 7.5, 150 mM NaCl, 1 mM DTT, 1 mM PMSF, 1 x Protease Inhibitor Cocktail
Single worm lysis buffer	10 mM Tris pH: 8.3, 50 mM KCl, 2.5 mM $MgCl_2$, 0.45% (v/v) Tween 20, 0.01% gelatin, freshly added proteinase K (50 µg/ml)

4.6.2 Strains

The following *C. elegans* strains were used in experiments conducted in this study (Table 11).

Table 11: List of *C. elegans* strains in this study

#	Origin	Genotype
PP1	CGC	N2 (BR10)
PP135	David Ron	zcls4[hsp-4:: GFP]V
PP1065	CGC	rde-1(ne219)V
PP1238	CGC	sel-11(nDf59)V

Continued on next page

Table 11 – Continued from previous page

#	Origin	Genotype
PP1350	Aljona Gutschmid	N2; hhIs257[nhx-2p:: cpl-1:: YFP; myo-2p:: mCherry]III
PP1385	Aljona Gutschmid	N2; hhIs112[Pnhx-2:: cpl-1W32AY35A:: YFP; Pmyo-2:: mCherry]X
PP1386	Aljona Gutschmid	N2; hhIs113[Pnhx-2:: cpl-1W32AY35A:: YFP; Pmyo-2:: mCherry]I
PP2044	CGC	drh-1(ok3495)IV
PP2325	Aljona Gutschmid	N2; hhIs110[Pnhx-2:: cpl-1W32AY35A:: YFP; Pmyo-2:: mCherry]I; drh-1(ok3495)IV
PP2932	Andrew Chrisholm	juSi123 II; rpl-29(tm3555)IV
PP2968	Ho Yi Mak lab	hjSi158(vha-6p:: SEL-1(1-79):: mCherry:: HEDL:: let-858 3´UTR)
PP3080	Sotirios Efstathiou	rde-1(ne219)V; sel-11(nDf59)V
PP3081	Sotirios Efstathiou	hjSi158(vha-6p:: SEL-1(1-79):: mCherry:: HEDL:: let-858 3´UTR); sel-11(nDf59)V
PP3259	Sotirios Efstathiou	hjSi158(vha-6p:: SEL-1(1-79):: mCherry:: HEDL:: let-858 3´UTR); rde-1(ne219)V
PP3260	Sotirios Efstathiou	hjSi158(vha-6p:: SEL-1(1-79):: mCherry:: HEDL:: let-858 3´UTR); rde-1(ne219)V; sel-11(nDf59)V
PP3329	this study	juSi123 II; rpl-29(tm3555)IV; rde-1(ne219)V
PP3330	this study	juSi123 II; rpl-29(tm3555)IV; sel-11(nDf59)V
PP3331	this study	rde-1(ne219)V; sel-11(nDf59)V; juSi123 II; rpl-29(tm3555) IV

Continued on next page

Table 11 – Continued from previous page

#	Origin	Genotype
PP3441	this study	drSi2 [vha-6p:: 3XFLAG:: pgp-3/CFTR(wt):: mCherry:: unc-54 3'UTR]II; (drSi2 II; unc-119(ed3)III; rde-1(ne219)
PP3442	this study	drSi2 [vha-6p:: 3XFLAG:: pgp-3/CFTR(wt):: mCherry:: unc-54 3'UTR]II; (drSi2 II; unc-119(ed3) III; sel-11(nDf59)
PP3443	this study	drSi2 [vha-6p:: 3XFLAG:: pgp-3/CFTR(wt):: mCherry:: unc-54 3'UTR]II; (drSi2 II; unc-119(ed3) III; rde-1(ne219) sel-11(nDf59)
PP3444	this study	drSi4 [vha-6p:: 3XFLAG:: pgp-3/CFTR(delta F508):: mCherry:: unc-54 3'UTR] II; drSi4 II; unc-119(ed3) III; rde-1(ne219)
PP3445	this study	drSi4 [vha-6p:: 3XFLAG:: pgp-3/CFTR(delta F508):: mCherry:: unc-54 3'UTR]II; drSi4 II; unc-119(ed3) III; sel-11(nDf59)
PP3446	this study	drSi4 [vha-6p:: 3XFLAG:: pgp-3/CFTR(delta F508):: mCherry:: unc-54 3'UTR] II; drSi4 II; unc-119(ed3) III; rde-1(ne219) sel-11(nDf59)
PP3489	Stephen C Pak lab	vkIs689 [nhx-2p:: sGFP:: ATM + myo-2p:: mCherry]
PP3490	Stephen C Pak lab	vkIs694 [nhx-2p:: sGFP:: ATZ + myo-2p:: mCherry]
PP3493	this study	hhIs257[nhx-2p:: cpl-1:: YFP; myo-2p:: mCherry]III; rde-1(ne219) sel-11(nDf59)V
PP3499	this study	rde-1(ne219)V; ire-1(v33)II
PP3500	this study	hhIs113[Pnhx-2:: cpl-1W32AY35A:: YFP; Pmyo-2:: mCherry]I; rde-1(ne219)V; mir-243(n4759)IV

Continued on next page

Table 11 – Continued from previous page

#	Origin	Genotype
PP3667	this study	vkIs689 [nhx-2p:: sGFP:: ATM + myo-2p:: mCherry]; rde-1(ne219)V
PP3668	this study	vkIs694 [nhx-2p:: sGFP:: ATZ + myo-2p:: mCherry]; rde-1(ne219)V
PP3682	this study	sel-11(syb5475)V; 0 x outcrossed
PP3789	this study	N2; sel-11(syb5475)V; 2 x outcrossed
PP3795	this study	N2; sel-11(syb5475)V; 4 x outcrossed
PP3859	this study	vkIs694 [nhx-2p:: sGFP:: ATZ + myo-2p:: mCherry]; sel-11(nDf59)V
PP3860	this study	vkIs694 [nhx-2p:: sGFP:: ATZ + myo-2p:: mCherry], sel-11(syb5475)V
PP3861	this study	hhIs112[Pnhx-2:: cpl-1W32AY35A:: YFP; Pmyo-2:: mCherry]X; sel-11(nDf59)V
PP3862	this study	hhIs112[Pnhx-2:: cpl-1W32AY35A:: YFP; Pmyo-2:: mCherry]X; sel-11(syb5475)V
PP3863	this study	hhIs257[nhx-2p:: cpl-1:: YFP; myo-2p:: mCherry]III; sel-11(syb5475)V
PP3864	this study	vkIs689 [nhx-2p:: sGFP:: ATM + myo-2p:: mCherry]; sel-11(nDf59)V
PP3865	this study	vkIs689 [nhx-2p:: sGFP:: ATM + myo-2p:: mCherry]; sel-11(syb5475)V

4.6.3 Age synchronization of *C.elegans*

Age synchronization in this study was performed via the filtering method. Plates containing worms that were grown for 1 week at 20 ºC after transferring 10–20 worms onto the plate were washed with M9 buffer. The worms in the M9 buffer were then transferred onto a 10 µm NY11 filter (Millipore), which only allow trespassing of worms with the diameter of L1 larvae and blocking eggs as well as L2, L3 & L4 larvae. The synchronized L1 larvae were placed onto fresh NGM plates and were used for further experiments.

4.6.4 Preparation of protein lysates for Western Blotting

Synchronized worms in the young adult stage were washed of the NGM plates and washed twice with M9. The supernatant was removed from the pelleted worms and 2x SDS sample buffer was supplied. The samples were incubated for 5 min at 95ºC, sonicated (60 % amplitude, 2 x 30 s on ice) and sharply centrifuged at 13.000 rcf. An additional incubation for 5 min at 95 ºC was conducted before the samples were stored at -80 ºC. For quantitative western blotting the samples were normalized to each other with as described in sections 4.5.5 and 4.5.6

4.6.5 Single worm lysis

To identify alleles of interest in *C. elegans*, a single worm harboring the respective allele was added to 10 µl of single worm lysis buffer. The sample was incubated at 65 ºC for 1 h followed by a final lysis step at 95 ºC for 15 min. 3 µl of the obtained lysate was used for the genotyping PCR as described in section 4.5.3.

4.6.6 Generation of *C.elegans* males

To obtain males, 10–15 L4 larvae were placed on NGM plates and incubated at 32 ºC. After 5.5, 6.0 and 6.5 h the NGM plates were removed from 32 ºC and incubated at 20 ºC. The F1 generation was screened for males, that could be used in crossing experiments.

4.6.7 Crossing of *C.elegans* strains

Approximately 10–15 males were co-cultured with 2–3 L4 hermaphrodite larvae. Successful crossing was accompanied by occurring males in the F1 generation. From the F1 generation, several (12–20) L4 larvae were individually

cultured on small NGM plates and genotyped after egg laying. 15–30 L4 larvae of the F2 generation with shown heterozygosity for the gene of interest were singled again to individual plates. The aforementioned procedure was repeated until homozygosity for the gene of interest could be confirmed in all descendants from a single plate.

4.6.8 RNA isolation

RNA isolation was conducted with a Trizol-based purification protocol. Age-synchronized nematodes were collected and washed 2x with M9 buffer. After removal of the supernatant, 1 ml of Trizol was added before storage of the worms at -80 °C. For the RNA purification, the worms were thawed at 37 °C and were disrupted using zirconia beads and the Precellys 24 Dual cell homogenizer (Peq-Lab) for 2x 20 s at 5000 rpm. Subsequently, the samples were incubated for 15 min at RT and supplied with 100 µl 1-bromo-3-chloropropane before centrifugation for 15 min at 8000 rcf at 4 °C to separate the organic from the aqueous phase. The aqueous phase was transferred into a new tube and supplied with 1 µl glycogen (10 mg/ml) and 500 µl 100 % Isopropanol, inverted several times, and incubated for at least 1 h or OV at - 80 °C. The samples were then centrifuged for 45 min at 13000 rpm at 4 °C. The supernatant was completely removed, and the pellet was washed with 70 % ethanol diluted in nuclease-free water. The obtained pellet was air-dried and resuspended in 30–50 µl of nuclease-free water. The purity and concentration of the obtained RNA was spectrophotometrically measured by NanoDrop 8000 (Thermo Fisher Scientific).

4.6.9 cDNA synthesis and real time quantitative PCR (RT-qPCR)

cDNA synthesis was conducted with 1000–2000 ng total RNA and the High-Capacity cDNA Reverse Transcription Kit (Applied Biosystems) according to the instructions of the manufacturer. Quantitative real-time PCR was performed with Luna (New England Biolabs) and Bio-Rad CFX96 Real-Time PCR Detection System. For each sample, technical replicates were measured and were normalized to housekeeper genes like *18sRNA*, *cdc-42* and *pmp-3* for *C. elegans* or *rpl-19*, *18rRNA* and *28rRNA* for mammalian cell culture (Table 7).

4.6.10 RNA Interference (RNAi)

RNAi is a crucial tool for the transient knockdown of genes of interest in *C. elegans* [206]. In this study, nematodes were fed with RNase III deficient *E. coli* HT115 expressing dsRNA through the IPTG-inducible vector L4440 coding for the RNAi of interest [207]. The *C. elegans* RNAi collection from Ahringer and ORF were used. For RNAi experiments, overnight cultures of bacteria containing the RNAi construct of interest were started in LB medium with 100 µg/ml ampicillin. From this culture a new fresh culture was inoculated to an OD600 of 0.2 and grown until an OD600 of approximately 1.0. This culture was seeded on NGM agar plates containing 100 µg/ml ampicillin and 2 mM IPTG. The NGM plates were incubated overnight at 37 ºC and used for experiments shortly after. Age-synchronized L1 larval stage nematodes were transferred to the plates and grown for analysis.

4.6.11 Cellular microsomal fractionation assay

For the microsomal fractionation assay, age-synchronized nematodes were washed 3x with M9 buffer and were frozen at -80 ºC for further analysis. The samples were thawed on ice, sonicated for 20 s with 60 % amplitude and subsequently manually homogenized with 50 strokes in the Dounce Homogenizer with the tight morter. The lysates were then centrifuged 2x for 5 min at 2000 rcf and 4 ºC and the pellet was discarded. The supernatant was then centrifuged for 1:30 h at 20.000 rcf and 4 ºC. The pellet then contained the microsomal fraction and was resuspended in 150 µl fractionation buffer of which 30 µl were distributed into 5 new tubes each. Each tube was supplied with 3 µl of the following reagents: 5 M NaCl, 1 M Na_2CO_3, 10 % Triton X-100 and 1 % SDS, respectively. Afterward, the samples were incubated on ice for 1h and centrifuged for 1 h at 20000 rcf at 4 ºC. The obtained pellets and supernatant from the 5 fractions were analyzed by western blotting.

4.6.12 UV cross-link immunoprecipitation (CLIP)

The UV crosslinked mouse embryonic fibroblasts (MEF) were supplied by Gabriele Stellbrink. The samples were thawed on ice and supplied with 1 ml of lysis buffer (50 mM Tris-HCl, 100 mM NaCl, 1 % MP-40 (IGEPAL®), 0.1 % SDS, 0.5 % sodium deoxycholate, pH: 7.4) with freshly added protein inhibitor Cocktail and RNase inhibitor according to the instructions of the manufacturer. The samples were resuspended in the lysis buffer. The MEFs were lysed using a syringe with a 23g gauge and were incubated 15 min on ice. The samples were sonicated in the Bioruptor® for 10 min with 10 pulses á 30 s on and off.

2 µl of TurboDNaseTM were added and the samples were shaken for 5 min at 37 ºC and 12000 rpm and were subsequently centrifuged at max speed for 15 min at 4 ºC. After centrifugation, 2 % of the total volume of the SN were put aside for RNA extraction and WB analysis, respectively (input control). For the immunoprecipitation, Dynabeads (50 µl) were coupled with 20 µl AGO2 antibody from cell signaling (#2897) or FujiFilm (α-mouse, monoclonal) and rotated for 1 h at 4 ºC. The coupled magnetic Dynabeads were then added to the samples and rotated overnight at 4 ºC. The tubes were placed on the respective magnet tray to bind the magnet tubes at the side of the tube. 20 µl of the SN were put aside for RNA extraction and WB analysis, respectively (input control). The samples were washed 3x with cold wash buffer (20 mM Tris-HCl, 10 mM $MgCl_2$, 0.2 % Tween-20, pH: 7.4) and resuspended in 100 µl wash buffer afterward. 10 µl of each sample were put aside for WB analysis and 700 µl of Trizol were added to the samples. RNA extraction was conducted with glycogen followed by RT-qPCR against the targets *nov*, *mertk*, *c1rl* and *rpl19*.

4.6.13 COPAS quantification of fluorescence and extinction

The COPAS (Union Biometrica) with the FlowPilot-Pro software is a large-particle flow cytometer that allows for the quantification of fluorescence in three different channels 'Red', 'Yellow', 'Green' and parameters such as TOF and extinction. TOF, Red, and extinction measurements for each observation were used for gating of observations, which resembled day 1 adult worms expressing either *CPL-1**, CPL-1^{WT}, *ATM* or *ATZ* exhibiting pharyngeal expression of *Pmyo-2::mCherry* as a transgenic marker (Figure 16, 19, 24, 25). Unless stated otherwise the fluorescence values (YFP as yellow or GFP as green) of TOF/extinction gated worms (Figure 24) or the Extinction values of red-positive gated worms (Figure 25) was used for the analysis of reporter activation or developmental delay, respectively. At least 200 gated worms from three independent biological replicates were used to calculate mean ± standard deviation (s.d.) values and plot density ridgeline plots or violin plots (ggplot2 v.3.6.2 and ggridges v.3.6.2). A graphical illustration of each gating method is presented with a 2d density hexbin plot (hexbin v.1.28.2) in Figure 24 and Figure 25. For further information see 1.3.2

5 References

[1] Bruce Alberts. *Molecular biology of the cell*. Ed. by Garland Science. Sixth Edit. Vol. 53. 9. New York – NY, 2014, p. 1392. ISBN: 9780815344322.

[2] Antonios Papadakis, Akos Gyenis, Joris Pothof, Jan H. J. Hoeijmakers, Argyris Papantonis, and Andreas Beyer. "Age-associated transcriptional stress due to accelerated elongation and increased stalling of RNAPII". In: *Nature genetics* 55.12 (2023), pp. 2011–2012. ISSN: 1546-1718.

[3] Cédric Debès, Antonios Papadakis, Sebastian Grönke, Özlem Karalay, Luke S. Tain, Athanasia Mizi, Shuhei Nakamura, Oliver Hahn, Carina Weigelt, Natasa Josipovic, et al. "Ageing-associated changes in transcriptional elongation influence longevity". In: *Nature* 616.7958 (2023), pp. 814–821. ISSN: 1476-4687.

[4] Zhonghe Ke, Pramit Mallik, Adam B. Johnson, Facundo Luna, Eviatar Nevo, Zhengdong D. Zhang, Vadim N. Gladyshev, Andrei Seluanov, and Vera Gorbunova. "Translation fidelity coevolves with longevity". In: *Aging Cell* 16.5 (2017), p. 988. ISSN: 14749726.

[5] Victoria Eugenia Martinez-Miguel, Celia Lujan, Tristan Espie–Caullet, Daniel Martinez-Martinez, Saul Moore, Cassandra Backes, Suam Gonzalez, Evgeniy R. Galimov, André E.X. Brown, Mario Halic, et al. "Increased fidelity of protein synthesis extends lifespan". In: *Cell Metabolism* 33.11 (2021), pp. 2288–2300. ISSN: 1550-4131.

[6] Mark S. Hipp, Prasad Kasturi, and F. Ulrich Hartl. "The proteostasis network and its decline in ageing". In: *Nature Reviews Molecular Cell Biology 2019 20:7* 20.7 (2019), pp. 421–435. ISSN: 1471-0080.

[7] Mantu Santra, Ken A. Dill, and Adam M.R. De Graff. "Proteostasis collapse is a driver of cell aging and death". In: *Proceedings of the National Academy of Sciences of the United States of America* 116.44 (2019), pp. 22173–22178. ISSN: 10916490.

[8] Mathias Uhlén, Linn Fagerberg, Björ M. Hallström, Cecilia Lindskog, Per Oksvold, Adil Mardinoglu, Åsa Sivertsson, Caroline Kampf, Evelina Sjöstedt, Anna Asplund, et al. "Proteomics. Tissue-based map of the human proteome". In: *Science (New York, N.Y.)* 347.6220 (2015). ISSN: 1095-9203.

[9] Christopher J. Shoemaker and Rachel Green. "Translation drives mRNA quality control". In: *Nature structural & molecular biology* 19.6 (2012), p. 594. ISSN: 15459993.

[10] Adam M. Heck and Jeffrey Wilusz. “The Interplay between the RNA Decay and Translation Machinery in Eukaryotes”. In: *Cold Spring Harbor Perspectives in Biology* 10.5 (2018). ISSN: 19430264.

[11] Alex Charles Tuck, Aneliya Rankova, Alaaddin Bulak Arpat, Luz Angelica Liechti, Daniel Hess, Vytautas Iesmantavicius, Violeta Castelo-Szekely, David Gatfield, and Marc Bühler. “Mammalian RNA Decay Pathways Are Highly Specialized and Widely Linked to Translation”. In: *Molecular Cell* 77.6 (2020), p. 1222. ISSN: 10974164.

[12] Christelle Morris, David Cluet, and Emiliano P. Ricci. “Ribosome dynamics and mRNA turnover, a complex relationship under constant cellular scrutiny”. In: *Wiley Interdisciplinary Reviews: RNA* 12.6 (2021). ISSN: 17577012.

[13] Qiushuang Wu, Santiago Gerardo Medina, Gopal Kushawah, Michelle Lynn Devore, Luciana A. Castellano, Jacqelyn M. Hand, Matthew Wright, and Ariel Alejandro Bazzini. “Translation affects mRNA stability in a codon-dependent manner in human cells”. In: *eLife* 8 (2019). ISSN: 2050084X.

[14] Paulo Gaspar, Gabriela Moura, Manuel A.S. Santos, and José Luís Oliveira. “mRNA secondary structure optimization using a correlated stem–loop prediction”. In: *Nucleic Acids Research* 41.6 (2013), e73. ISSN: 13624962.

[15] Anthony K.L. Leung and Phillip A. Sharp. “MicroRNA Functions in Stress Responses”. In: *Molecular Cell* 40.2 (2010), pp. 205–215. ISSN: 10972765.

[16] Nilesh Chitnis, Dariusz Pytel, and J. Alan Diehl. “UPR-inducible miRNAs contribute to stressful situations”. In: *Trends in biochemical sciences* 38.9 (2013), pp. 447–452. ISSN: 0968-0004.

[17] René F. Ketting. “The Many Faces of RNAi”. In: *Developmental Cell* 20.2 (2011), pp. 148–161. ISSN: 1534-5807.

[18] Petr Svoboda. “Key Mechanistic Principles and Considerations Concerning RNA Interference”. In: *Frontiers in Plant Science* 11 (2020), p. 495350. ISSN: 1664462X.

[19] Franziska Ottens, Sotirios Efstathiou, and Thorsten Hoppe. “Cutting through the stress: RNA decay pathways at the endoplasmic reticulum”. In: *Trends in Cell Biology* (2023). ISSN: 0962-8924.

[20] Kotaro Nakanishi. “Anatomy of four human Argonaute proteins”. In: *Nucleic acids research* 50.12 (2022), pp. 6618–6638. ISSN: 1362-4962.

[21] Sotirios Efstathiou, Franziska Ottens, Lena Sophie Schütter, Sonia Ravanelli, Nikolaos Charmpilas, Aljona Gutschmidt, Jérémie Le Pen, Niels H. Gehring, Eric A. Miska, Jorge Bouças, et al. “ER-associated RNA silencing promotes ER quality control”. In: *Nature cell biology* 24.12 (2022), pp. 1714–1725. ISSN: 1476-4679.

[22] Sonomi Yamaguchi, Masahiro Naganuma, Tomohiro Nishizawa, Tsukasa Kusakizako, Yukihide Tomari, Hiroshi Nishimasu, and Osamu Nureki. “Structure of the Dicer-2-R2D2 heterodimer bound to a small RNA duplex”. In: *Nature* 607.7918 (2022), pp. 393–398. ISSN: 1476-4687.

[23] Nicole T. Schirle, Garth A. Kinberger, Heather F. Murray, Walt F. Lima, Thazha P. Prakash, and Ian J. MacRae. “Structural Analysis of Human Argonaute-2 Bound to a Modified siRNA Guide”. In: *Journal of the American Chemical Society* 138.28 (2016), pp. 8694–8697. ISSN: 1520-5126.

[24] Nicole T. Schirle, Jessica Sheu-Gruttadauria, and Ian J. MacRae. “Structural basis for microRNA targeting”. In: *Science (New York, N.Y.)* 346.6209 (2014), pp. 608–613. ISSN: 1095-9203.

[25] David S. Goodsell, Ludovic Autin, and Arthur J. Olson. “Illustrate: Software for Biomolecular Illustration”. In: *Structure (London, England : 1993)* 27.11 (2019), pp. 1716–1720. ISSN: 1878-4186.

[26] Darren J. Obbard, Karl H.J. Gordon, Amy H. Buck, and Francis M. Jiggins. “The evolution of RNAi as a defence against viruses and transposable elements”. In: *Philosophical Transactions of the Royal Society B: Biological Sciences* 364.1513 (2008), pp. 99–115. ISSN: 14712970.

[27] Svetlana A. Shabalina and Eugene V. Koonin. “Origins and evolution of eukaryotic RNA interference”. In: *Trends in Ecology & Evolution* 23.10 (2008), pp. 578–587. ISSN: 0169-5347.

[28] Deborah L. McEwan, Alexandra S. Weisman, and Craig P. Hunter. “Uptake of Extracellular Double-Stranded RNA by SID-2”. In: *Molecular Cell* 47.5 (2012), pp. 746–754. ISSN: 1097-2765.

[29] Hiroaki Tabara, Erbay Yigit, Haruhiko Siomi, and Craig C. Mello. “The dsRNA binding protein RDE-4 interacts with RDE-1, DCR-1, and a DExH-Box helicase to direct RNAi in C. elegans”. In: *Cell* 109.7 (2002), pp. 861–871. ISSN: 00928674.

[30] Julia Pak and Andrew Fire. “Distinct populations of primary and secondary effectors during RNAi in C. elegans”. In: *Science (New York, N.Y.)* 315.5809 (2007), pp. 241–244. ISSN: 1095-9203.

[31] Sylvia E.J. Fischer. “Small RNA-mediated gene silencing pathways in C. elegans”. In: *The International Journal of Biochemistry & Cell Biology* 42.8 (2010), pp. 1306–1315. ISSN: 1357-2725.

[32] Keita Yoshida, Yuji Suehiro, Katsufumi Dejima, Sawako Yoshina, and Shohei Mitani. “Distinct pathways for export of silencing RNA in Caenorhabditis elegans systemic RNAi”. In: *iScience* 26.10 (2023). ISSN: 2589-0042.

[33] Oded Rechavi and Itamar Lev. “Principles of Transgenerational Small RNA Inheritance in Caenorhabditis elegans”. In: *Current Biology* 27.14 (2017), R720–R730. ISSN: 0960-9822.

[34] Yusuke Shiromoto, Masayuki Sakurai, Helen Qu, Andrew V. Kossenkov, and Kazuko Nishikura. “Processing of Alu small RNAs by DICER/ADAR1 complexes and their RNAi targets”. In: *RNA (New York, N.Y.)* 26.12 (2020), pp. 1801–1814. ISSN: 1469-9001.

[35] Katsutomo Okamura and Eric C. Lai. “Endogenous small interfering RNAs in animals”. In: *Nature reviews. Molecular cell biology* 9.9 (2008), p. 673. ISSN: 14710072.

[36] Kristina L Schierhorn, Raul Y Sanchez□David, and Pierre V Maillard. “Mammalian antiviral RNAi is on the move”. In: *The EMBO Journal* 41.11 (2022). ISSN: 0261-4189.

[37] Yuqiang Zhang, Yunpeng Dai, Jiaxin Wang, Yan Xu, Zhe Li, Jinfeng Lu, Yongfen Xu, Jin Zhong, Shou□Wei Ding, and Yang Li. “Mouse circulating extracellular vesicles contain virus□derived siRNAs active in antiviral immunity”. In: *The EMBO Journal* 41.11 (2022). ISSN: 0261-4189.

[38] Yang Qiu, Yanpeng Xu, Yao Zhang, Ligang Wu, Cheng-Feng Qin, and Xi Zhou Correspondence. “Human Virus-Derived Small RNAs Can Confer Antiviral Immunity in Mammals”. In: *Immunity* 46 (2017), pp. 992–1004.

[39] Yang Li, Megha Basavappa, Jinfeng Lu, Shuwei Dong, D. Alexander Cronkite, John T. Prior, Hans Christian Reinecker, Paul Hertzog, Yanhong Han, Wan Xiang Li, et al. “Induction and suppression of antiviral RNA interference by influenza A virus in mammalian cells”. In: *Nature Microbiology 2016 2:3* 2.3 (2016), pp. 1–9. ISSN: 2058-5276.

[40] Natalia Pinzón, Stéphanie Bertrand, Lucie Subirana, Isabelle Busseau, Hector Escrivá, and Hervé Seitz. “Functional lability of RNA-dependent RNA polymerases in animals”. In: *PLoS Genetics* 15.2 (2019). ISSN: 15537404.

[41] Lea Duempelmann, Merle Skribbe, and Marc Bühler. “Small RNAs in the Transgenerational Inheritance of Epigenetic Information”. In: *Trends in Genetics* 36.3 (2020), pp. 203–214. ISSN: 13624555.

[42] Shuo Gu and John J. Rossi. “Uncoupling of RNAi from active translation in mammalian cells”. In: *RNA* 11.1 (2005), p. 38. ISSN: 13558382.

[43] Adriano Biasini, Baroj Abdulkarim, Stefano de Pretis, Jennifer Y Tan, Rajika Arora, Harry Wischnewski, Rene Dreos, Mattia Pelizzola, Constance Ciaudo, and Ana Claudia Marques. “Translation is required for miRNA□dependent decay of endogenous transcripts”. In: *The EMBO Journal* 40.3 (2021). ISSN: 0261-4189.

[44] Thomas F Duchaine and Marc R Fabian. “Hershey Additional Perspectives on Translation Mechanisms and Control available at Cite this article as”. In: *Cold Spring Harb Perspect Biol* 11 (2019), pp. 32771–32772.

[45] Vinay K Mayya, Mathieu N Flamand, Alice M Lambert, Seyed Mehdi Jafarnejad, James A Wohlschlegel, Nahum Sonenberg, and Thomas F Duchaine. “NAR Breakthrough Article microRNA-mediated translation repression through GYF-1 and IFE-4 in C. elegans development”. In: *Nucleic Acids Research* 49.9 (2021), pp. 4803–4815.

[46] Duygu Kuzuoğlu-Öztürk, Eric Huntzinger, Steffen Schmidt, and Elisa Izaurralde. “The Caenorhabditis elegans GW182 protein AIN-1 interacts with PAB-1 and subunits of the PAN2-PAN3 and CCR4-NOT deadenylase complexes”. In: *Nucleic acids research* 40.12 (2012), pp. 5651–5665. ISSN: 1362-4962.

[47] Mathieu N. Flamand, Edlyn Wu, Ajay Vashisht, Guillaume Jannot, Brett D. Keiper, Martin J. Simard, James Wohlschlegel, and Thomas F. Duchaine. “Poly(A)-binding proteins are required for microRNA-mediated silencing and to promote target deadenylation in C. elegans”. In: *Nucleic acids research* 44.12 (2016), pp. 5924–5935. ISSN: 1362-4962.

[48] Saibal Chatterjee and Helge Großhans. “Active turnover modulates mature microRNA activity in Caenorhabditis elegans”. In: *Nature 2009 461:7263* 461.7263 (2009), pp. 546–549. ISSN: 1476-4687.

[49] Liang Zhang, Lei Ding, Tom H. Cheung, Meng Qiu Dong, Jun Chen, Aileen K. Sewell, Xuedong Liu, John R. Yates, and Min Han. “Systematic Identification of C. elegans miRISC Proteins, miRNAs, and mRNA Targets by Their Interactions with GW182 Proteins AIN-1 and AIN-2”. In: *Molecular Cell* 28.4 (2007), pp. 598–613. ISSN: 10972765.

[50] Marianthi Kiriakidou, Grace S. Tan, Styliani Lamprinaki, Mariangels De Planell-Saguer, Peter T. Nelson, and Zissimos Mourelatos. “An mRNA m7G Cap Binding-like Motif within Human Ago2 Represses Translation”. In: *Cell* 129.6 (2007), pp. 1141–1151. ISSN: 00928674.

[51] Hayden P. Huggins, Jacob S. Subash, Hamilton Stoffel, Melissa A. Henderson, Jenna L. Hoffman, David S. Buckner, Madhu S. Sengupta, Peter R. Boag, Myon Hee Lee, and Brett D. Keiper. “Distinct roles of two eIF4E isoforms in the germline of Caenorhabditis elegans”. In: *Journal of Cell Science* 133.6 (2020). ISSN: 14779137.

[52] Mennatallah M.Y. Albarqi and Sean P. Ryder. “The role of RNA-binding proteins in orchestrating germline development in Caenorhabditis elegans”. In: *Frontiers in Cell and Developmental Biology* 10 (2023), p. 1094295. ISSN: 2296634X.

[53] Richard J. Jackson, Christopher U.T. Hellen, and Tatyana V. Pestova. “The mechanism of eukaryotic translation initiation and principles of its regulation”. In: *Nature Reviews Molecular Cell Biology 2010 11:2* 11.2 (2010), pp. 113–127. ISSN: 1471-0080.

[54] Tom Joshua Eisenack and Débora Broch Trentini. “Ending a bad start: Triggers and mechanisms of co-translational protein degradation”. In: *Frontiers in Molecular Biosciences* 9 (2022). ISSN: 2296889X.

[55] Ben P. Phillips and Elizabeth A. Miller. “Ribosome-associated quality control of membrane proteins at the endoplasmic reticulum”. In: *Journal of cell science* 133.22 (2020). ISSN: 1477-9137.

[56] Yajie Gao, Yuanxiang Zhu, Hailong Wang, Ying Cheng, Dongbo Zhao, Qinmiao Sun, and Dahua Chen. “Lipid-mediated phase separation of AGO proteins on the ER controls nascent-peptide ubiquitination”. In: *Molecular cell* 82.7 (2022), pp. 1313–1328. ISSN: 1097-4164.

[57] Yajie Gao, Yuanxiang Zhu, Qinmiao Sun, and Dahua Chen. “Argonaute-dependent ribosome-associated protein quality control”. In: *Trends in Cell Biology* 33.3 (2023), pp. 260–272. ISSN: 0962-8924.

[58] Francesco Scavone, Samantha C. Gumbin, Paul A. Da Rosa, and Ron R. Kopito. “RPL26/uL24 UFMylation is essential for ribosome-associated quality control at the endoplasmic reticulum”. In: *Proceedings of the National Academy of Sciences of the United States of America* 120.16 (2023). ISSN: 1091-6490.

[59] Andrey L. Karamyshev, Anna E. Patrick, Zemfira N. Karamysheva, Dustin S. Griesemer, Henry Hudson, Sandra Tjon-Kon-Sang, Ingmarie Nilsson, Hendrik Otto, Qinghua Liu, Sabine Rospert, et al. “Inefficient SRP Interaction with a Nascent Chain Triggers a mRNA Quality Control Pathway”. In: *Cell* 156.1-2 (2014), pp. 146–157. ISSN: 0092-8674.

[60] Yoon K.I. Kim and Lynne E. Maquat. “UPFront and center in RNA decay: UPF1 in nonsense-mediated mRNA decay and beyond”. In: *RNA (New York, N.Y.)* 25.4 (2019), pp. 407–422. ISSN: 1469-9001.

[61] Søren Lykke-Andersen and Torben Heick Jensen. “Nonsense-mediated mRNA decay: an intricate machinery that shapes transcriptomes”. In: *Nature Reviews Molecular Cell Biology 2015 16:11* 16.11 (2015), pp. 665–677. ISSN: 1471-0080.

[62] Tatsuaki Kurosaki, Wencheng Li, Mainul Hoque, Maximilian W.L. Popp, Dmitri N. Ermolenko, Bin Tian, and Lynne E. Maquat. “A post-translational regulatory switch on UPF1 controls targeted mRNA degradation”. In: *Genes & development* 28.17 (2014), pp. 1900–1916. ISSN: 1549-5477.

[63] Jessica A. Hurt, Alex D. Robertson, and Christopher B. Burge. “Global analyses of UPF1 binding and function reveal expanded scope of nonsense-mediated mRNA decay”. In: *Genome research* 23.10 (2013), pp. 1636–1650. ISSN: 1549-5469.

[64] Joachim Weischenfeldt, Johannes Waage, Geng Tian, Jing Zhao, Inge Damgaard, Janus S. Jakobsen, Karsten Kristiansen, Anders Krogh, Jun Wang, and Bo T. Porse. “Mammalian tissues defective in nonsense-mediated mRNA decay display highly aberrant splicing patterns”. In: *Genome biology* 13.5 (2012). ISSN: 1474-760X.

[65] Megan Peccarelli and Bessie W. Kebaara. “Regulation of natural mRNAs by the nonsense-mediated mRNA decay pathway”. In: *Eukaryotic Cell* 13.9 (2014), pp. 1126–1135. ISSN: 15359778.

[66] Lulu Huang and Miles F. Wilkinson. “Regulation of nonsense-mediated mRNA decay”. In: *Wiley Interdisciplinary Reviews: RNA* 3.6 (2012), pp. 807–828. ISSN: 1757-7012.

[67] Dasa Longman, Kathryn A. Jackson-Jones, Magdalena M. Maslon, Laura C. Murphy, Robert S. Young, Jack J. Stoddart, Nele Hug, Martin S. Taylor, Dimitrios K. Papadopoulos, and Javier F. Cáceres. “Identification of a localized nonsense-mediated decay pathway at the endoplasmic reticulum”. In: *Genes & Development* 34.15-16 (2020), pp. 1075–1088. ISSN: 0890-9369.

[68] Virginia S. Muir, Audrey P. Gasch, and Philip Anderson. “The substrates of nonsense-mediated mRNA decay in Caenorhabditis elegans”. In: *G3: Genes, Genomes, Genetics* 8.1 (2018), pp. 195–205. ISSN: 21601836.

[69] Akio Yamashita, Tetsuo Ohnishi, Isao Kashima, Yoichi Taya, and Shigeo Ohno. “Human SMG-1, a novel phosphatidylinositol 3-kinase-related protein kinase, associates with components of the mRNA surveillance complex and is involved in the regulation of nonsense-mediated mRNA decay”. In: *Genes & development* 15.17 (2001), pp. 2215–2228. ISSN: 0890-9369.

[70] Andrew Grimson, Sean O’Connor, Carrie Loushin Newman, and Philip Anderson. “SMG-1 is a phosphatidylinositol kinase-related protein kinase required for nonsense-mediated mRNA Decay in Caenorhabditis elegans”. In: *Molecular and cellular biology* 24.17 (2004), pp. 7483–7490. ISSN: 0270-7306.

[71] Lisa Johns, Andrew Grimson, Sherry L. Kuchma, Carrie Loushin Newman, and Philip Anderson. “Caenorhabditis elegans SMG-2 Selectively Marks mRNAs Containing Premature Translation Termination Codons”. In: *Molecular and Cellular Biology* 27.16 (2007), pp. 5630–5638. ISSN: 02707306.

[72] Dasa Longman, Ronald H.A. Plasterk, Iain L. Johnstone, and Javier F. Cáceres. “Mechanistic insights and identification of two novel factors in the C. elegans NMD pathway”. In: *Genes & Development* 21.9 (2007), p. 1075. ISSN: 08909369.

[73] Eonyoung Park and Lynne E. Maquat. “Staufen-mediated mRNA decay”. In: *Wiley interdisciplinary reviews. RNA* 4.4 (2013), pp. 423–435. ISSN: 1757-7012.

[74] Yoon Ki Kim, Luc Furic, Marc Parisien, François Major, Luc DesGroseillers, and Lynne E. Maquat. “Staufen1 regulates diverse classes of mammalian transcripts”. In: *The EMBO Journal* 26.11 (2007), p. 2670. ISSN: 02614189.

[75] Louise Wickham, Thomas Duchaîne, Ming Luo, Ivan R. Nabi, and Luc DesGroseillers. “Mammalian staufen is a double-stranded-RNA- and tubulin-binding protein which localizes to the rough endoplasmic reticulum”. In: *Molecular and cellular biology* 19.3 (1999), pp. 2220–2230. ISSN: 0270-7306.

[76] Yoontae Lee, Inha Hur, Seong Yeon Park, Young Kook Kim, Ra Suh Mi, and V. Narry Kim. “The role of PACT in the RNA silencing pathway”. In: *EMBO Journal* 25.3 (2006), pp. 522–532. ISSN: 02614189.

[77] Jacqueline Baca LeGendre, Zachary T. Campbell, Peggy Kroll-Conner, Phil Anderson, Judith Kimble, and Marvin Wickens. “RNA targets and specificity of Staufen, a double-stranded RNA-binding protein in Caenorhabditis elegans”. In: *The Journal of biological chemistry* 288.4 (2013), pp. 2532–2545. ISSN: 1083-351X.

[78] Zhiji Ren, Isana Veksler-Lublinsky, David Morrissey, and Victor Ambros. “Staufen negatively modulates microRNA activity in Caenorhabditis elegans”. In: *G3: Genes, Genomes, Genetics* 6.5 (2016), pp. 1227–1237. ISSN: 21601836.

[79] Maruf M.U. Ali, Tina Bagratuni, Emma L. Davenport, Piotr R. Nowak, M. Cris Silva-Santisteban, Anthea Hardcastle, Craig McAndrews, Martin G. Rowlands, Gareth J. Morgan, Wynne Aherne, et al. “Structure of the Ire1 autophosphorylation complex and implications for the

unfolded protein response". In: *The EMBO journal* 30.5 (2011), pp. 894–905. ISSN: 1460-2075.

[80] Julie Hollien, Jonathan H. Lin, Han Li, Nicole Stevens, Peter Walter, and Jonathan S. Weissman. "Regulated Ire1-dependent decay of messenger RNAs in mammalian cells". In: *Journal of Cell Biology* 186.3 (2009), pp. 323–331. ISSN: 0021-9525.

[81] Adrien Le Thomas, Elena Ferri, Scot Marsters, Jonathan M. Harnoss, David A. Lawrence, Iratxe Zuazo-Gaztelu, Zora Modrusan, Sara Chan, Margaret Solon, Cécile Chalouni, et al. "Decoding non-canonical mRNA decay by the endoplasmic-reticulum stress sensor IRE1α". In: *Nature communications* 12.1 (2021). ISSN: 2041-1723.

[82] John Paul Upton, Likun Wang, Dan Han, Eric S. Wang, Noelle E. Huskey, Lionel Lim, Morgan Truitt, Michael T. McManus, Davide Ruggero, Andrei Goga, et al. "IRE1α cleaves select microRNAs during ER stress to derepress translation of proapoptotic Caspase-2". In: *Science (New York, N.Y.)* 338.6108 (2012), pp. 818–822. ISSN: 1095-9203.

[83] Christian Pohl and Ivan Dikic. "Cellular quality control by the ubiquitin-proteasome system and autophagy". In: *Science* 366.6467 (2019), pp. 818–822. ISSN: 10959203.

[84] Cecile M. Pickart and Michael J. Eddins. "Ubiquitin: structures, functions, mechanisms". In: *Biochimica et Biophysica Acta (BBA) - Molecular Cell Research* 1695.1-3 (2004), pp. 55–72. ISSN: 0167-4889.

[85] Mikaela D. Stewart, Tobias Ritterhoff, Rachel E. Klevit, and Peter S. Brzovic. "E2 enzymes: more than just middle men". In: *Cell research* 26.4 (2016), pp. 423–440. ISSN: 1748-7838.

[86] David Komander, Michael J. Clague, and Sylvie Urbé. "Breaking the chains: structure and function of the deubiquitinases". In: *Nature Reviews Molecular Cell Biology 2009 10:8* 10.8 (2009), pp. 550–563. ISSN: 1471-0080.

[87] Mary E. Matyskiela, Monica C. Rodrigo-Brenni, and David O. Morgan. "Mechanisms of ubiquitin transfer by the anaphase-promoting complex". In: *Journal of Biology* 8.10 (2009), pp. 1–10. ISSN: 14754924.

[88] David Komander and Michael Rape. "The ubiquitin code". In: *Annual Review of Biochemistry* 81.Volume 81, 2012 (2012), pp. 203–229. ISSN: 00664154.

[89] Anna Dósa and Tamás Csizmadia. “The role of K63-linked polyubiquitin in several types of autophagy”. In: *Biologia Futura* 73.2 (2022), pp. 137–148. ISSN: 26768607.

[90] W. Li and Y. Ye. “Polyubiquitin chains: functions, structures, and mechanisms”. In: *Cellular and molecular life sciences : CMLS* 65.15 (2008), pp. 2397–2406. ISSN: 1420-682X.

[91] Sadek Fournane, Ksenia Krupina, Charlotte Kleiss, and Izabela Sumara. “Decoding ubiquitin for mitosis”. In: *Genes and Cancer* 3.11-12 (2012), pp. 697–711. ISSN: 19476027.

[92] Kefeng Lu, Fabian Den Brave, and Stefan Jentsch. “Receptor oligomerization guides pathway choice between proteasomal and autophagic degradation”. In: *Nature cell biology* 19.6 (2017), pp. 732–739. ISSN: 1476-4679.

[93] Bettina Wurzer, Gabriele Zaffagnini, Dorotea Fracchiolla, Eleonora Turco, Christine Abert, Julia Romanov, and Sascha Martens. “Oligomerization of p62 allows for selection of ubiquitinated cargo and isolation membrane during selective autophagy”. In: *eLife* 4.September 2015 (2015). ISSN: 2050084X.

[94] Karole N D’Orazio, Colin Chih-Chien Wu, Niladri Sinha, Raphael Loll-Krippleber, Grant W Brown, and Rachel Green. “The endonuclease Cue2 cleaves mRNAs at stalled ribosomes during No Go Decay”. In: *eLife* 8 (2019).

[95] Claudio A.P. Joazeiro. “Mechanisms and functions of ribosome-associated protein quality control”. In: *Nature Reviews Molecular Cell Biology 2019 20:6* 20.6 (2019), pp. 368–383. ISSN: 1471-0080.

[96] Karole N D’orazio and Rachel Green. “Ribosome states signal RNA quality control”. In: *Molecular Cell* 81 (2021), pp. 1372–1383.

[97] Marissa L. Glover, A. Max Burroughs, Parissa C. Monem, Thea A. Egelhofer, Makena N. Pule, L. Aravind, and Joshua A. Arribere. “NONU-1 Encodes a Conserved Endonuclease Required for mRNA Translation Surveillance”. In: *Cell reports* 30.13 (2020), p. 4321. ISSN: 22111247.

[98] Martin R. Pool. “Targeting of Proteins for Translocation at the Endoplasmic Reticulum”. In: *International Journal of Molecular Sciences 2022, Vol. 23, Page 3773* 23.7 (2022), p. 3773. ISSN: 1422-0067.

[99] A. Manuel Liaci and Friedrich Förster. “Take Me Home, Protein Roads: Structural Insights into Signal Peptide Interactions during ER Translocation”. In: *International Journal of Molecular Sciences 2021, Vol. 22, Page 11871* 22.21 (2021), p. 11871. ISSN: 1422-0067.

[100] Vladimir Denic, Volker Dötsch, and Irmgard Sinning. “Endoplasmic Reticulum Targeting and Insertion of Tail-Anchored Membrane Proteins by the GET Pathway”. In: *Cold Spring Harbor Perspectives in Biology* 5.8 (2013). ISSN: 19430264.

[101] Martin Gamerdinger, Marie Anne Hanebuth, Tancred Frickey, and Elke Deuerling. “The principle of antagonism ensures protein targeting specificity at the endoplasmic reticulum”. In: *Science* 348.6231 (2015), pp. 201–207. ISSN: 10959203.

[102] Martin Gamerdinger, Kan Kobayashi, Annalena Wallisch, Stefan G. Kreft, Carolin Sailer, Renate Schlömer, Nadine Sachs, Ahmad Jomaa, Florian Stengel, Nenad Ban, et al. “Early Scanning of Nascent Polypeptides inside the Ribosomal Tunnel by NAC”. In: *Molecular Cell* 75.5 (2019), pp. 996–1006. ISSN: 1097-2765.

[103] Ahmad Jomaa, Martin Gamerdinger, Hao Hsuan Hsieh, Annalena Wallisch, Viswanathan Chandrasekaran, Zeynel Ulusoy, Alain Scaiola, Ramanujan S. Hegde, Shu Ou Shan, Nenad Ban, et al. “Mechanism of signal sequence handover from NAC to SRP on ribosomes during ER-protein targeting”. In: *Science* 375.6583 (2022), pp. 839–844. ISSN: 10959203.

[104] P. Walter and G. Blobel. “Translocation of proteins across the endoplasmic reticulum III. Signal recognition protein (SRP) causes signal sequence-dependent and site-specific arrest of chain elongation that is released by microsomal membranes.” In: *Journal of Cell Biology* 91.2 (1981), pp. 557–561. ISSN: 0021-9525.

[105] Walther Mothes, Berit Jungnickel, Josef Brunner, and Tom A. Rapoport. “Signal Sequence Recognition in Cotranslational Translocation by Protein Components of the Endoplasmic Reticulum Membrane”. In: *The Journal of Cell Biology* 142.2 (1998), p. 355. ISSN: 00219525.

[106] Sichen Shao. “Protein biosynthesis at the ER: finding the right accessories”. In: *Molecular Biology of the Cell* 34.1 (2023). ISSN: 19394586.

[107] Arunkumar Sundaram, Melvin Yamsek, Frank Zhong, Yogesh Hooda, Ramanujan S Hegde, and Robert J Keenan. “Substrate-driven assembly of a translocon for multipass membrane proteins”. In: *Nature* / 611 (2022).

[108] Mateusz Jaskolowski, Ahmad Jomaa, Martin Gamerdinger, Sandeep Shrestha, Marc Leibundgut, Elke Deuerling, and Nenad Ban. “Molecular basis of the TRAP complex function in ER protein biogenesis”. In: *Nature Structural & Molecular Biology 2023 30:6* 30.6 (2023), pp. 770–777. ISSN: 1545-9985.

[109] Patrick J. Chitwood, Szymon Juszkiewicz, Alina Guna, Sichen Shao, and Ramanujan S. Hegde. “EMC Is Required to Initiate Accurate Membrane Protein Topogenesis”. In: *Cell* 175.6 (2018), p. 1507. ISSN: 10974172.

[110] Ineke Braakman and Neil J. Bulleid. “Protein folding and modification in the mammalian endoplasmic reticulum”. In: *Annual review of biochemistry* 80 (2011), pp. 71–99. ISSN: 1545-4509.

[111] Ineke Braakman and Daniel N. Hebert. “Protein folding in the endoplasmic reticulum”. In: *Cold Spring Harbor perspectives in biology* 5.5 (2013). ISSN: 1943-0264.

[112] Haruka Chino and Noboru Mizushima. “ER-Phagy: Quality and Quantity Control of the Endoplasmic Reticulum by Autophagy”. In: *Cold Spring Harbor perspectives in biology* 15.1 (2023). ISSN: 1943-0264.

[113] Ramanujan S. Hegde and Hidde L. Ploegh. “Quality and quantity control at the endoplasmic reticulum”. In: *Current Opinion in Cell Biology* 22.4 (2010), pp. 437–446. ISSN: 0955-0674.

[114] John C. Christianson, Ernst Jarosch, and Thomas Sommer. “Mechanisms of substrate processing during ER-associated protein degradation”. In: *Nature Reviews Molecular Cell Biology 2023 24:11* 24.11 (2023), pp. 777–796. ISSN: 1471-0080.

[115] Ilaria Fregno, Elisa Fasana, Timothy J Bergmann, Andrea Raimondi, Marisa Loi, Tatiana Soldà, Carmela Galli, Rocco D’Antuono, Diego Morone, Alberto Danieli, et al. “ER-to-lysosome-associated degradation of proteasome-resistant ATZ polymers occurs via receptor-mediated vesicular transport”. In: *The EMBO journal* 37.17 (2018). ISSN: 1460-2075.

[116] Justin J. Crowder, Marco Geigges, Ryan T. Gibson, Eric S. Fults, Bryce W. Buchanan, Nadine Sachs, Andrea Schink, Stefan G. Kreft, and Eric M. Rubenstein. “Rkr1/Ltn1 ubiquitin ligase-mediated degradation of translationally stalled endoplasmic reticulum proteins”. In: *Journal of Biological Chemistry* 290.30 (2015), pp. 18454–18466. ISSN: 1083351X.

[117] Karina Von Der Malsburg, Sichen Shao, and Ramanujan S. Hegde. “The ribosome quality control pathway can access nascent polypeptides stalled at the Sec61 translocon”. In: *Molecular Biology of the Cell* 26.12 (2015), pp. 2168–2180. ISSN: 19394586.

[118] Christopher P. Walczak, Dara E. Leto, Lichao Zhang, Celeste Riepe, Ryan Y. Muller, Paul A. DaRosa, Nicholas T. Ingolia, Joshua E. Elias, and Ron R. Kopito. “Ribosomal protein RPL26 is the principal target of UFMylation”. In: *Proceedings of the National Academy of Sciences of the United States of America* 116.4 (2019), pp. 1299–1308. ISSN: 1091-6490.

[119] Lihui Wang, Yue Xu, Heather Rogers, Layla Saidi, Constance Tom Noguchi, Honglin Li, Jonathan Wilson Yewdell, Nicholas Raymond Guydosh, and Yihong Ye. “UFMylation of RPL26 links translocation-associated quality control to endoplasmic reticulum protein homeostasis”. In: *Cell research* 30.1 (2020), pp. 5–20. ISSN: 1748-7838.

[120] Linda Makhlouf, Joshua J. Peter, Helge M. Magnussen, Rohan Thakur, David Millrine, Thomas C. Minshull, Grace Harrison, Joby Varghese, Frederic Lamoliatte, Martina Foglizzo, et al. “The UFM1 E3 ligase recognizes and releases 60S ribosomes from ER translocons”. In: *Nature 2024 627:8003* 627.8003 (2024), pp. 437–444. ISSN: 1476-4687.

[121] Jiang Liu, Ying Wang, Lizhi Song, Linghua Zeng, Weiwei Yi, Ting Liu, Huanzhen Chen, Miao Wang, Zhenyu Ju, and Yu Sheng Cong. “A critical role of DDRGK1 in endoplasmic reticulum homoeostasis via regulation of IRE1α stability”. In: *Nature communications* 8 (2017). ISSN: 2041-1723.

[122] Yinghua Zhang, Mingsheng Zhang, Jianchun Wu, Guohua Lei, and Honglin Li. “Transcriptional regulation of the Ufm1 conjugation system in response to disturbance of the endoplasmic reticulum homeostasis and inhibition of vesicle trafficking”. In: *PloS one* 7.11 (2012). ISSN: 1932-6203.

[123] Jie Wang, Jessica Lee, David Liem, and Peipei Ping. “HSPA5 Gene encoding Hsp70 chaperone BiP in the endoplasmic reticulum”. In: *Gene* 618 (2017), pp. 14–23. ISSN: 0378-1119.

[124] Alexandra Stolz and Dieter H. Wolf. “Endoplasmic reticulum associated protein degradation: a chaperone assisted journey to hell”. In: *Biochimica et biophysica acta* 1803.6 (2010), pp. 694–705. ISSN: 0006-3002.

[125] Tadashi Satoh, Takumi Yamaguchi, and Koichi Kato. “Emerging structural insights into glycoprotein quality control coupled with N-glycan processing in the endoplasmic reticulum”. In: *Molecules (Basel, Switzerland)* 20.2 (2015), pp. 2475–2491. ISSN: 1420-3049.

[126] Sheng Tao Li, Tian Tian Lu, Xin Xin Xu, Yi Ding, Zijie Li, Toshihiko Kitajima, Neta Dean, Ning Wang, and Xiao Dong Gao. “Reconstitution of the lipid-linked oligosaccharide pathway for assembly of high-mannose N-glycans”. In: *Nature Communications 2019 10:1* 10.1 (2019), pp. 1–11. ISSN: 2041-1723.

[127] Chengchao Xu and Davis T.W. Ng. “Glycosylation-directed quality control of protein folding”. In: *Nature reviews. Molecular cell biology* 16.12 (2015), pp. 742–752. ISSN: 1471-0080.

[128] I. Bošnjak, V. Bojović, T. S. Šegvić-Bubić, and A. Bielen. “Occurrence of protein disulfide bonds in different domains of life: a comparison of proteins from the Protein Data Bank”. In: *Protein engineering, design & selection : PEDS* 27.3 (2014), pp. 65–72. ISSN: 1741-0134.

[129] Chaitanya Patel, Haddas Saad, Marina Shenkman, and Gerardo Z. Lederkremer. “Oxidoreductases in Glycoprotein Glycosylation, Folding, and ERAD”. In: *Cells* 9.9 (2020), pp. 1–17. ISSN: 20734409.

[130] Ilaria Fregno and Maurizio Molinari. “Proteasomal and lysosomal clearance of faulty secretory proteins: ER-associated degradation (ERAD) and ER-to-lysosome-associated degradation (ERLAD) pathways”. In: *Critical Reviews in Biochemistry and Molecular Biology* 54.2 (2019), pp. 153–163. ISSN: 15497798.

[131] Ilaria Fregno, Elisa Fasana, Tatiana Soldà, Carmela Galli, and Maurizio Molinari. “N-glycan processing selects ERAD-resistant misfolded proteins for ER-to-lysosome-associated degradation”. In: *The EMBO journal* 40.15 (2021). ISSN: 1460-2075.

[132] Alexis González, Adriana Covarrubias-Pinto, Ramachandra M. Bhaskara, Marius Glogger, Santosh K. Kuncha, Audrey Xavier, Eric Seemann, Mohit Misra, Marina E. Hoffmann, Bastian Bräuning, et al. "Ubiquitination regulates ER-phagy and remodelling of endoplasmic reticulum". In: *Nature 2023 618:7964* 618.7964 (2023), pp. 394–401. ISSN: 1476-4687.

[133] Rayene Berkane, Hung Ho-Xuan, Marius Glogger, Pablo Sanz-Martinez, Lorène Brunello, Tristan Glaesner, Santosh Kumar Kuncha, Katharina Holzhüter, Sara Cano-Franco, Viviana Buonomo, et al. "The function of ER-phagy receptors is regulated through phosphorylation-dependent ubiquitination pathways". In: *Nature Communications 2023 14:1* 14.1 (2023), pp. 1–17. ISSN: 2041-1723.

[134] Julian Stevenson, Edmond Y. Huang, and James A. Olzmann. "Endoplasmic Reticulum-Associated Degradation and Lipid Homeostasis". In: *Annual review of nutrition* 36 (2016), pp. 511–542. ISSN: 1545-4312.

[135] Deepa Kumari and Jeffrey L. Brodsky. "The Targeting of Native Proteins to the Endoplasmic Reticulum-Associated Degradation (ERAD) Pathway: An Expanding Repertoire of Regulated Substrates". In: *Biomolecules* 11.8 (2021). ISSN: 2218-273X.

[136] Emma J. Fenech, Federica Lari, Philip D. Charles, Roman Fischer, Marie Laétitia-Thézénas, Katrin Bagola, Adrienne W. Paton, James C. Paton, Mads Gyrd-Hansen, Benedikt M. Kessler, et al. "Interaction mapping of endoplasmic reticulum ubiquitin ligases identifies modulators of innate immune signalling". In: *eLife* 9 (2020), pp. 1–29. ISSN: 2050-084X.

[137] Sandra Stefanovic□Barrett, Anna S Dickson, Stephen P Burr, James C Williamson, Ian T Lobb, Dick JH van den Boomen, Paul J Lehner, and James A Nathan. "MARCH6 and TRC8 facilitate the quality control of cytosolic and tail-anchored proteins". In: *EMBO reports* 19.5 (2018). ISSN: 1469-3178.

[138] Débora Broch Trentini, Matteo Pecoraro, Shivani Tiwary, Jürgen Cox, Matthias Mann, Mark S. Hipp, and F. Ulrich Hartl. "Role for ribosome-associated quality control in sampling proteins for MHC class I-mediated antigen presentation". In: *Proceedings of the National Academy of Sciences of the United States of America* 117.8 (2020), pp. 4099–4108. ISSN: 10916490.

[139] R. Luke Wiseman, Jaleh S. Mesgarzadeh, and Linda M. Hendershot. “Reshaping endoplasmic reticulum quality control through the unfolded protein response”. In: *Molecular Cell* 82.8 (2022), pp. 1477–1491. ISSN: 1097-2765.

[140] Peter Walter and David Ron. “The unfolded protein response: from stress pathway to homeostatic regulation”. In: *Science (New York, N.Y.)* 334.6059 (2011), pp. 1081–1086. ISSN: 1095-9203.

[141] Claudio Hetz, Kezhong Zhang, and Randal J. Kaufman. “Mechanisms, regulation and functions of the unfolded protein response”. In: *Nature reviews. Molecular cell biology* 21.8 (2020), pp. 421–438. ISSN: 1471-0080.

[142] Brooke M. Gardner, David Pincus, Katja Gotthardt, Ciara M. Gallagher, and Peter Walter. “Endoplasmic reticulum stress sensing in the unfolded protein response”. In: *Cold Spring Harbor perspectives in biology* 5.3 (2013). ISSN: 1943-0264.

[143] Jirka Peschek, Diego Acosta□Alvear, Aaron S Mendez, and Peter Walter. “ A conformational RNA zipper promotes intron ejection during non□conventional XBP 1 mRNA splicing ”. In: *EMBO reports* 16.12 (2015), pp. 1688–1698. ISSN: 1469-221X.

[144] Mauro Costa-Mattioli and Peter Walter. “The integrated stress response: From mechanism to disease”. In: *Science (New York, N.Y.)* 368.6489 (2020). ISSN: 10959203.

[145] Karolina Pakos□Zebrucka, Izabela Koryga, Katarzyna Mnich, Mila Ljujic, Afshin Samali, and Adrienne M Gorman. “The integrated stress response”. In: *EMBO reports* 17.10 (2016), pp. 1374–1395. ISSN: 1469-221X.

[146] Hillary A. Miller, Elizabeth S. Dean, Scott D. Pletcher, and Scott F. Leiser. “Cell non-autonomous regulation of health and longevity”. In: *eLife* 9 (2020), pp. 1–28. ISSN: 2050084X.

[147] Janine Kirstein-Miles and Richard I. Morimoto. “Caenorhabditis Elegans as a Model System to Study Intercompartmental Proteostasis: Interrelation of Mitochondrial Function, Longevity, and Neurodegenerative Diseases”. In: *Developmental Dynamics* 239.5 (2010), p. 1529. ISSN: 10588388.

[148] Mark T. Miedel, Nathan J. Graf, Kate E. Stephen, Olivia S. Long, Stephen C. Pak, David H. Perlmutter, Gary A. Silverman, and Cliff J. Luke. “A Pro-Cathepsin L Mutant Is a Luminal Substrate for Endoplasmic-Reticulum-Associated Degradation in C. elegans”. In: *PLOS ONE* 7.7 (2012), e40145. ISSN: 1932-6203.

[149] Cyril Statzer, Jin Meng, Richard Venz, Monet Bland, Stacey Robida-Stubbs, Krina Patel, Dunja Petrovic, Raffaella Emsley, Pengpeng Liu, Ianessa Morantte, et al. “ATF-4 and hydrogen sulfide signalling mediate longevity in response to inhibition of translation or mTORC1”. In: *Nature Communications 2022 13:1* 13.1 (2022), pp. 1–15. ISSN: 2041-1723.

[150] Moritz Horn, Sarah I. Denzel, Balaji Srinivasan, Kira Allmeroth, Isabelle Schiffer, Vignesh Karthikaisamy, Stephan Miethe, Peter Breuer, Adam Antebi, and Martin S. Denzel. “Hexosamine Pathway Activation Improves Protein Homeostasis through the Integrated Stress Response”. In: *iScience* 23.3 (2020), p. 100887. ISSN: 2589-0042.

[151] Maxime J. Derisbourg, Laura E. Wester, Ruth Baddi, and Martin S. Denzel. “Mutagenesis screen uncovers lifespan extension through integrated stress response inhibition without reduced mRNA translation”. In: *Nature Communications 2021 12:1* 12.1 (2021), pp. 1–14. ISSN: 2041-1723.

[152] Marcella Calfon, Huiqing Zeng, Fumihiko Urano, Jeffery H. Till, Stevan R. Hubbard, Heather P. Harding, Scott G. Clark, and David Ron. “IRE1 couples endoplasmic reticulum load to secretory capacity by processing the XBP-1 mRNA”. In: *Nature 2002 415:6867* 415.6867 (2002), pp. 92–96. ISSN: 1476-4687.

[153] Rock Pulak. “Techniques for analysis, sorting, and dispensing of C. elegans on the COPAS flow-sorting system.” In: *Methods in molecular biology (Clifton, N.J.)* 351 (2006), pp. 275–286. ISSN: 10643745.

[154] Abolfazl Hajihassani and Louise Marie Dandurand. “An improved technique for sorting developmental stages and assessing egg viability of globodera pallida using high-throughput complex object parametric analyzer and sorter”. In: *Plant Disease* 102.10 (2018), pp. 2001–2008. ISSN: 19437692.

[155] Rose Ghemrawi and Mostafa Khair. “Endoplasmic Reticulum Stress and Unfolded Protein Response in Neurodegenerative Diseases”. In: *International Journal of Molecular Sciences* 21.17 (2020), pp. 1–25. ISSN: 14220067.

[156] Angela Schipanski, Sascha Lange, Alexandra Segref, Aljona Gutschmidt, David A. Lomas, Elena Miranda, Michaela Schweizer, Thorsten Hoppe, and Markus Glatzel. “A novel interaction between aging and ER overload in a protein conformational dementia”. In: *Genetics* 193.3 (2013), pp. 865–876. ISSN: 1943-2631.

[157] Jun Ren, Yaguang Bi, James R. Sowers, Claudio Hetz, and Yingmei Zhang. “Endoplasmic reticulum stress and unfolded protein response in cardiovascular diseases”. In: *Nature Reviews Cardiology 2021 18:7* 18.7 (2021), pp. 499–521. ISSN: 1759-5010.

[158] Md Sahab Uddin, Wing Shan Yu, and Lee Wei Lim. “Exploring ER stress response in cellular aging and neuroinflammation in Alzheimer’s disease”. In: *Ageing research reviews* 70 (2021). ISSN: 1872-9649.

[159] Tarah Satterfield, Jessica Pritchett, Sarah Cruz, and Kyeorda Kemp. “Prion disease and endoplasmic reticulum stress pathway correlations and treatment pursuits”. In: *Cell Pathology* 4.1 (2017), pp. 27–36. ISSN: 2300-4266.

[160] Aljona Gutschmidt. *Regulation der ER-Homöostase in Caenorhabditis elegans*. Tech. rep. University of Cologne, 2015, pp. 1–132.

[161] Lena-Sophie Schütter. *The Antiviral RNAi Pathway Maintains ER Homeostasis by Degrading mRNAs of Secretory Proteins*. Tech. rep. University of Cologne, 2020, pp. 1–119.

[162] Tea Carletti, Mohammad Khalid Zakaria, Valentina Faoro, Laura Reale, Yvette Kazungu, Danilo Licastro, and Alessandro Marcello. “Viral priming of cell intrinsic innate antiviral signaling by the unfolded protein response”. In: *Nature Communications 2019 10:1* 10.1 (2019), pp. 1–9. ISSN: 2041-1723.

[163] Leah V. Goulding, Jiayun Yang, Zhimin Jiang, Hongyu Zhang, Daniel Lea, Richard D. Emes, Tania Dottorini, Juan Pu, Jinhua Liu, and Kin Chow Chang. “Thapsigargin at Non-Cytotoxic Levels Induces a Potent Host Antiviral Response that Blocks Influenza A Virus Replication”. In: *Viruses* 12.10 (2020). ISSN: 1999-4915.

[164] Sarah Al-Beltagi, Cristian Alexandru Preda, Leah V. Goulding, Joe James, Juan Pu, Paul Skinner, Zhimin Jiang, Belinda Lei Wang, Jiayun Yang, Ashley C. Banyard, et al. “Thapsigargin Is a Broad-Spectrum Inhibitor of Major Human Respiratory Viruses: Coronavirus, Respiratory Syncytial Virus and Influenza A Virus”. In: *Viruses* 13.2 (2021), p. 234. ISSN: 19994915.

[165] Sarah Al-Beltagi, Leah V. Goulding, Daniel K.E. Chang, Kenneth H. Mellits, Christopher J. Hayes, Pavel Gershkovich, Christopher M. Coleman, and Kin Chow Chang. “Emergent SARS-CoV-2 variants: comparative replication dynamics and high sensitivity to thapsigargin”. In: *Virulence* 12.1 (2021), pp. 2946–2956. ISSN: 2150-5608.

[166] Mohammed Samer Shaban, Christin Mayr-Buro, Johanna Meier-Soelch, Benadict Vincent Albert, M. Lienhard Schmitz, John Ziebuhr, and Michael Kracht. “Thapsigargin: key to new host-directed coronavirus antivirals?” In: *Trends in pharmacological sciences* 43.7 (2022), pp. 557–568. ISSN: 1873-3735.

[167] Mohammed Samer Shaban, Christin Müller, Christin Mayr-Buro, Hendrik Weiser, Johanna Meier-Soelch, Benadict Vincent Albert, Axel Weber, Uwe Linne, Torsten Hain, Ilya Babayev, et al. “Multi-level inhibition of coronavirus replication by chemical ER stress”. In: *Nature Communications 2021 12:1* 12.1 (2021), pp. 1–20. ISSN: 2041-1723.

[168] Olivia S. Long, Joshua A. Benson, Joon H.yeok Kwak, Cliff J. Luke, Sager J. Gosai, Linda P. O’Reilly, Yan Wang, Jie Li, Anne C. Vetica, Mark T. Miedel, et al. “A C. elegans model of human α1-antitrypsin deficiency links components of the RNAi pathway to misfolded protein turnover”. In: *Human Molecular Genetics* 23.19 (2014), pp. 5109–5122. ISSN: 0964-6906.

[169] M. Luisetti and N. Seersholm. “Alpha1-antitrypsin deficiency. 1: epidemiology of alpha1-antitrypsin deficiency”. In: *Thorax* 59.2 (2004), pp. 164–169. ISSN: 0040-6376.

[170] David A. Rudnick and David H. Perlmutter. “Alpha-1-antitrypsin deficiency: a new paradigm for hepatocellular carcinoma in genetic liver disease”. In: *Hepatology (Baltimore, Md.)* 42.3 (2005), pp. 514–521. ISSN: 0270-9139.

[171] David H. Perlmutter and Gary A. Silverman. “Hepatic Fibrosis and Carcinogenesis in α1-Antitrypsin Deficiency: A Prototype for Chronic Tissue Damage in Gain-of-Function Disorders”. In: *Cold Spring Harbor Perspectives in Biology* 3.3 (2011), a005801. ISSN: 19430264.

[172] Sager J. Gosai, Joon Hyeok Kwak, Cliff J. Luke, Olivia S. Long, Dale E. King, Kevin J. Kovatch, Paul A. Johnston, Tong Ying Shun, John S. Lazo, David H. Perlmutter, et al. “Automated high-content live animal drug screening using C. elegans expressing the aggregation prone serpin α1-antitrypsin Z”. In: *PloS one* 5.11 (2010). ISSN: 1932-6203.

[173] Ryan D. Baldridge and Tom A. Rapoport. “Autoubiquitination of the Hrd1 Ligase Triggers Protein Retrotranslocation in ERAD”. In: *Cell* 166.2 (2016), pp. 394–407. ISSN: 10974172.

[174] Brian G. Peterson, Morgan L. Glaser, Tom A. Rapoport, and Ryan D. Baldridge. “Cycles of autoubiquitination and deubiquitination regulate the erad ubiquitin ligase hrd1”. In: *eLife* 8 (2019). ISSN: 2050084X.

[175] Vedran Vasic, Niels Denkert, Claudia C. Schmidt, Dietmar Riedel, Alexander Stein, and Michael Meinecke. “Hrd1 forms the retrotranslocation pore regulated by auto-ubiquitination and binding of misfolded proteins”. In: *Nature cell biology* 22.3 (2020), pp. 274–281. ISSN: 1476-4679.

[176] Richard G. Gardner, Gwendolyn M. Swarbrick, Nathan W. Bays, Stephen R. Cronin, Sharon Wilhovsky, Linda Seelig, Christine Kim, and Randolph Y. Hampton. “Endoplasmic Reticulum Degradation Requires Lumen to Cytosol SignalingTransmembrane Control of Hrd1p by Hrd3p”. In: *Journal of Cell Biology* 151.1 (2000), pp. 69–82. ISSN: 0021-9525.

[177] Fábio Madeira, Matt Pearce, Adrian R.N. Tivey, Prasad Basutkar, Joon Lee, Ossama Edbali, Nandana Madhusoodanan, Anton Kolesnikov, and Rodrigo Lopez. “Search and sequence analysis tools services from EMBL-EBI in 2022.” In: *Nucleic Acids Research* 50.W1 (2022), W276–W279. ISSN: 0305-1048.

[178] Fabian Sievers and Desmond G. Higgins. “The Clustal Omega Multiple Alignment Package.” In: *Methods in Molecular Biology (Clifton, N.J.)* 2231 (2021), pp. 3–16. ISSN: 1064-3745.

[179] Paul M Sharp and Keith R Bradnam. “Appendix 3 Codon Usage in C. elegans”. In: (1997).

[180] Andrew Collins and Xiayi Ke. “Primer1: Primer Design Web Service for Tetra-Primer ARMS-PCR”. In: *The Open Bioinformatics Journal* 6.1 (2012), pp. 55–58. ISSN: 1875-0362.

[181] Ruan Felipe Vieira Medrano and Camila Andréa De Oliveira. “Guidelines for the tetra-primer ARMS-PCR technique development”. In: *Molecular biotechnology* 56.7 (2014), pp. 599–608. ISSN: 1559-0305.

[182] Kyoengwoo Min, Junsu Kang, and Junho Lee. “A modified feeding RNAi method for simultaneous knock-down of more than one gene in Caenorhabditis elegans”. In: *BioTechniques* 48.3 (2010), pp. 229–232. ISSN: 1940-9818.

[183] Kentaro Noma, Alexandr Goncharov, Mark H. Ellisman, and Yishi Jin. “Microtubule-dependent ribosome localization in C. elegans neurons”. In: *eLife* 6 (2017). ISSN: 2050084X.

[184] Sotirios Efstathiou. *Involvement of the exogenous RNAi pathway in mRNA turnover and ER homeostasis*. Tech. rep. Cologne: University of Cologne, 2019, pp. 1–63.

[185] Zhe Cao, Yan Hao, Chun Wing Fung, Yiu Yiu Lee, Pengfei Wang, Xuesong Li, Kang Xie, Wen Jiun Lam, Yifei Qiu, Ben Zhong Tang, et al. “Dietary fatty acids promote lipid droplet diversity through seipin enrichment in an ER subdomain”. In: *Nature Communications* 10.1 (2019). ISSN: 20411723.

[186] Frauke Adamla and Zoya Ignatova. “Somatic expression of unc-54 and vha-6 mRNAs declines but not pan-neuronal rgef-1 and unc-119 expression in aging Caenorhabditis elegans”. In: *Scientific Reports* 5 (2015). ISSN: 20452322.

[187] Keith Nehrke and James E. Melvin. “The NHX Family of Na+-H+ Exchangers in Caenorhabditis elegans”. In: *Journal of Biological Chemistry* 277.32 (2002), pp. 29036–29044. ISSN: 0021-9258.

[188] Olivier Voinnet. “Non-cell autonomous RNA silencing”. In: *FEBS Letters* 579.26 (2005), pp. 5858–5871. ISSN: 0014-5793.

[189] Régis L. Corrêa, Florian A. Steiner, Eugene Berezikov, and René F. Ketting. “MicroRNA–Directed siRNA Biogenesis in Caenorhabditis elegans”. In: *PLoS Genetics* 6.4 (2010), p. 1000903. ISSN: 15537390.

[190] Sean E. McGeary, Kathy S. Lin, Charlie Y. Shi, Thy M. Pham, Namita Bisaria, Gina M. Kelley, and David P. Bartel. “The biochemical basis of microRNA targeting efficacy”. In: *Science (New York, N.Y.)* 366.6472 (2019). ISSN: 1095-9203.

[191] Moran Cohen-Berkman, Reut Dudkevich, Shani Ben-Hamo, Alla Fishman, Yehuda Salzberg, Hiba Waldman Ben-Asher, Ayelet T. Lamm, and Sivan Henis-Korenblit. “Endogenous siRNAs promote proteostasis and longevity in germlineless c .Elegans”. In: *eLife* 9 (2020). ISSN: 2050084X.

[192] Monica J. Piatek and Andreas Werner. “Endogenous siRNAs, regulators of internal affairs”. In: *Biochemical Society transactions* 42.4 (2014), p. 1174. ISSN: 14708752.

[193] Bahnisikha Barman and Suvendra N. Bhattacharyya. “mRNA targeting to endoplasmic reticulum precedes ago protein interaction and MicroRNA (miRNA)-mediated translation repression in mammalian cells”. In: *Journal of Biological Chemistry* 290.41 (2015), pp. 24650–24656. ISSN: 1083351X.

[194] Lukas Stalder, Wolf Heusermann, Lena Sokol, Dominic Trojer, Joel Wirz, Justin Hean, Anja Fritzsche, Florian Aeschimann, Vera Pfanzagl, Pascal Basselet, et al. “The rough endoplasmatic reticulum is a central nucleation site of siRNA-mediated RNA silencing”. In: *The EMBO Journal* 32.8 (2013), p. 1115. ISSN: 02614189.

[195] Sunita Shankar, Sethuramasundaram Pitchiaya, Rohit Malik, Vishal Kothari, Yasuyuki Hosono, Anastasia K. Yocum, Harika Gundlapalli, Yasmine White, Ari Firestone, Xuhong Cao, et al. “KRAS Engages AGO2 to Enhance Cellular Transformation”. In: *Cell Reports* 14.6 (2016), pp. 1448–1461. ISSN: 2211-1247.

[196] Anne Frohn, H. Christian Eberl, Julia Stöhr, Elke Glasmacher, Sabine Rüdel, Vigo Heissmeyer, Matthias Mann, and Gunter Meister. “Dicer-dependent and -independent Argonaute2 Protein Interaction Networks in Mammalian Cells”. In: *Molecular & Cellular Proteomics : MCP* 11.11 (2012), p. 1442. ISSN: 15359476.

[197] Blake L. Atwood, Jessica L. Woolnough, Gaelle M. Lefevre, Mariana Saint Just Ribeiro, Gary Felsenfeld, and Keith E. Giles. “Human Argonaute 2 Is Tethered to Ribosomal RNA through MicroRNA Interactions”. In: *The Journal of biological chemistry* 291.34 (2016), pp. 17919–17928. ISSN: 1083-351X.

[198] Suzan Ruijtenberg, Stijn Sonneveld, Tao Ju Cui, Ive Logister, Dion de Steenwinkel, Yao Xiao, Ian J. MacRae, Chirlmin Joo, and Marvin E. Tanenbaum. “mRNA structural dynamics shape Argonaute-target interactions”. In: *Nature structural & molecular biology* 27.9 (2020), p. 790. ISSN: 15459985.

[199] Shannon Behrman, Diego Acosta-Alvear, and Peter Walter. “A CHOP-regulated microRNA controls rhodopsin expression”. In: *Journal of Cell Biology* 192.6 (2011), pp. 919–927. ISSN: 0021-9525.

[200] Yun Ju Kim. “Crosstalk between RNA silencing and RNA quality control in plants”. In: *BMB Reports* 56.6 (2023), p. 321. ISSN: 1976670X.

[201] Lin Liu and Xuemei Chen. “RNA Quality Control as a Key to Suppressing RNA Silencing of Endogenous Genes in Plants”. In: *Molecular plant* 9.6 (2016), p. 826. ISSN: 17529867.

[202] Li Ling Chak and Katsutomo Okamura. “Argonaute-dependent small RNAs derived from single-stranded, non-structured precursors”. In: *Frontiers in Genetics* 5.JUN (2014), p. 91949. ISSN: 16648021.

[203] Eling Goh and Katsutomo Okamura. “Hidden sequence specificity in loading of single-stranded RNAs onto Drosophila Argonautes”. In: *Nucleic Acids Research* 47.6 (2019), p. 3101. ISSN: 13624962.

[204] Grace S. Tan, Barry G. Garchow, Xuhang Liu, Jennifer Yeung, John P. Morris IV, Trinna L. Cuellar, Michael T. McManus, and Marianthi Kiriakidou. “Expanded RNA-binding activities of mammalian Argonaute 2”. In: *Nucleic acids research* 37.22 (2009), pp. 7533–7545. ISSN: 1362-4962.

[205] Wayne I. Lencer, Heidi DeLuca, Michael J. Grey, and Jin Ah Cho. “Innate immunity at mucosal surfaces: the IRE1-RIDD-RIG-I pathway”. In: *Trends in Immunology* 36.7 (2015), pp. 401–409. ISSN: 1471-4906.

[206] Darryl Conte, Lesley T. MacNei, Albertha J.M. Walhout, and Craig C. Mello. “RNA Interference in Caenorhabditis elegans”. In: *Current protocols in molecular biology* 109 (2015), pp. 1–26. ISSN: 1934-3647.

[207] Lisa Timmons, Donald L. Court, and Andrew Fire. “Ingestion of bacterially expressed dsRNAs can produce specific and potent genetic interference in Caenorhabditis elegans”. In: *Gene* 263.1-2 (2001), pp. 103–112. ISSN: 03781119.

6 Erklärung zur Dissertation

”Hiermit versichere ich an Eides statt, dass ich die vorliegende Dissertation selbstständig und ohne die Benutzung anderer als der angegebenen Hilfsmittel und Literatur angefertigt habe. Alle Stellen, die wörtlich oder sinngemäß aus veröffentlichten und nicht veröffentlichten Werken dem Wortlaut oder dem Sinn nach entnommen wurden, sind als solche kenntlich gemacht. Ich versichere an Eides statt, dass diese Dissertation noch keiner anderen Fakultät oder Universität zur Prüfung vorgelegen hat; dass sie – abgesehen von unten angegebenen Teilpublikationen und eingebundenen Artikeln und Manuskripten – noch nicht veröffentlicht worden ist sowie, dass ich eine Veröffentlichung der Dissertation vor Abschluss der Promotion nicht ohne Genehmigung des Promotionsausschusses vornehmen werde. Die Bestimmungen dieser Ordnung sind mir bekannt. Darüber hinaus erkläre ich hiermit, dass ich die Ordnung zur Sicherung guter wissenschaftlicher Praxis und zum Umgang mit wissenschaftlichem Fehlverhalten der Universität zu Köln gelesen und sie bei der Durchführung der Dissertation zugrundeliegenden Arbeiten und der schriftlich verfassten Dissertation beachtet habe und verpflichte mich hiermit, die dort genannten Vorgaben bei allen wissenschaftlichen Tätigkeiten zu beachten und umzusetzen. Ich versichere, dass die eingereichte elektronische Fassung der eingereichten Druckfassung vollständig entspricht.”

Teilpublikationen

(I) **Efstathiou, S***., Ottens, F.*, Schütter*, L. S., Ravanelli, S., Charmpilas, N., Gutschmidt, A., le Pen, J., Gehring, N. H., Miska, E. A., Bouças, J., & Hoppe, T. (2022). ER-associated RNA silencing promotes ER quality control. *Nature Cell Biology*, 24(12), 1714–1725. `https://doi.org/10.1038/S41556-022-01025-4`

(II) Ottens, F.*, **Efstathiou, S***., & Hoppe, T. (2023). Cutting through the stress: RNA decay pathways at the endoplasmic reticulum. In *Trends in Cell Biology*. Elsevier Ltd. `https://doi.org/10.1016/j.tcb.2023.11.003`

* Diese Autoren waren gleichermaßen beteiligt

Sotirios Efstathiou
Köln, Freitag 30 August, 2024.

7 Curriculum Vitae

SOTIRIOS EFSTATHIOU

B.Sc. Biology and M.Sc. Biochemistry

Sotirios.Efstathiou@gmail.com

Sotirios Efstathiou

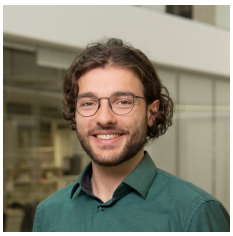

PERSONAL INFORMATION

Address:
Weyertal 20, 50937 Köln

Date of Birth:
20.09.1994

Nationality:
German, Greek

EDUCATION

since 10/2019 — **Ph.D. Candidate**
Thesis: Coordination of ER-Associated RNA and Protein Degradation Pathways
Cologne Excellence Cluster on Cellular Stress Responses in Aging-Associated Diseases (**CECAD**),
Cologne Graduate School of Aging Research (**CGA**),
EIT Health Aging PhD School **(EIT Health)**

04/2017 - 09/2019 — **M.Sc. Biochemistry (grade: 1.1)**
Thesis: Involvement of the exogenous RNAi pathway in mRNA turnover and ER homeostasis
University of Cologne, CECAD

10/2013 - 09/2016 — **B.Sc. Biology (grade: 1.3)**
Thesis: Identification & characterization of posttranslational modifications in murine sulfite oxidase
University of Cologne, Institute of Biochemistry

PROJECTS

as of 2019 — **Coordination of ER-Associated RNA and Protein Degradation Pathways** — **Hoppe Lab**
CECAD

eleven-months 2019 — **Involvement of the exo-RNAi pathway in ER homeostasis** — **Hoppe Lab**
CECAD

four-months 2018 — **Impact of GDF15 on muscle metabolism & systemic fat accumulation, M. musculus** — **Klaus Lab**
German Institute for Human Nutrition Potsdam-Rehbrücke (DIfE)

four-months 2017 — **Enzyme purification & characterization from native tissues, M. musculus & S. domesticus** — **Schwarz Lab**
Institute for Biochemistry, University of Cologne

three-months 2016 — **Recombinant expression of HIV/SIV vaccines, L. Plantarum** — **Scherbak Lab**
School of Science and Technology, Örebro University, Sweden

four-months 2016 — **Enzyme purification & characterization from native tissues, M. musculus & S. domesticus** — **Schwarz Lab**
Institute for Biochemistry, University of Cologne

six-weeks 2016 — **Stem cell homeostasis - hair follicle stem cells, M. musculus & cell culture** — **Wickström Lab**
Max Planck Institute for Biology of Ageing

four-weeks 2015 — **Cell signaling - shade avoidance response, A. thaliana** — **Höcker Lab**
Institute for Plant Sciences, University of Cologne & CEPLAS

PUBLICATIONS

I — **Efstathiou, S**[*]., Ottens, F.[*], Schütter, L. S.[*], Ravanelli, S., Charmpilas, N., Gutschmidt, A., le Pen, J., Gehring, N. H., Miska, E. A., Bouças, J., & Hoppe, T. (2022). ER-associated RNA silencing promotes ER quality control. *Nature Cell Biology*, *24*(12), 1714–1725. `https://doi.org/10.1038/S41556-022-01025-4`

II — Ottens, F.[*], **Efstathiou, S**[*]., & Hoppe, T. (2023). Cutting through the stress: RNA decay pathways at the endoplasmic reticulum. In *Trends in Cell Biology*. Elsevier Ltd. `https://doi.org/10.1016/j.tcb.2023.11.003`

III — Ost, M., Gil, C. I., Coleman, V., Keipert, **S., Efstathiou**, S., Vidic, V., Weyers, M., & Klaus, S. (2020). Muscle-derived GDF15 drives diurnal anorexia and systemic metabolic remodeling during mitochondrial stress. *EMBO Reports*, 21(3). `https://doi.org/10.15252/EMBR.201948804`

[*] Authors contributed equally.

A Appendix

A.1 Epistasis knockdown screen of ERQC and ERAS factors

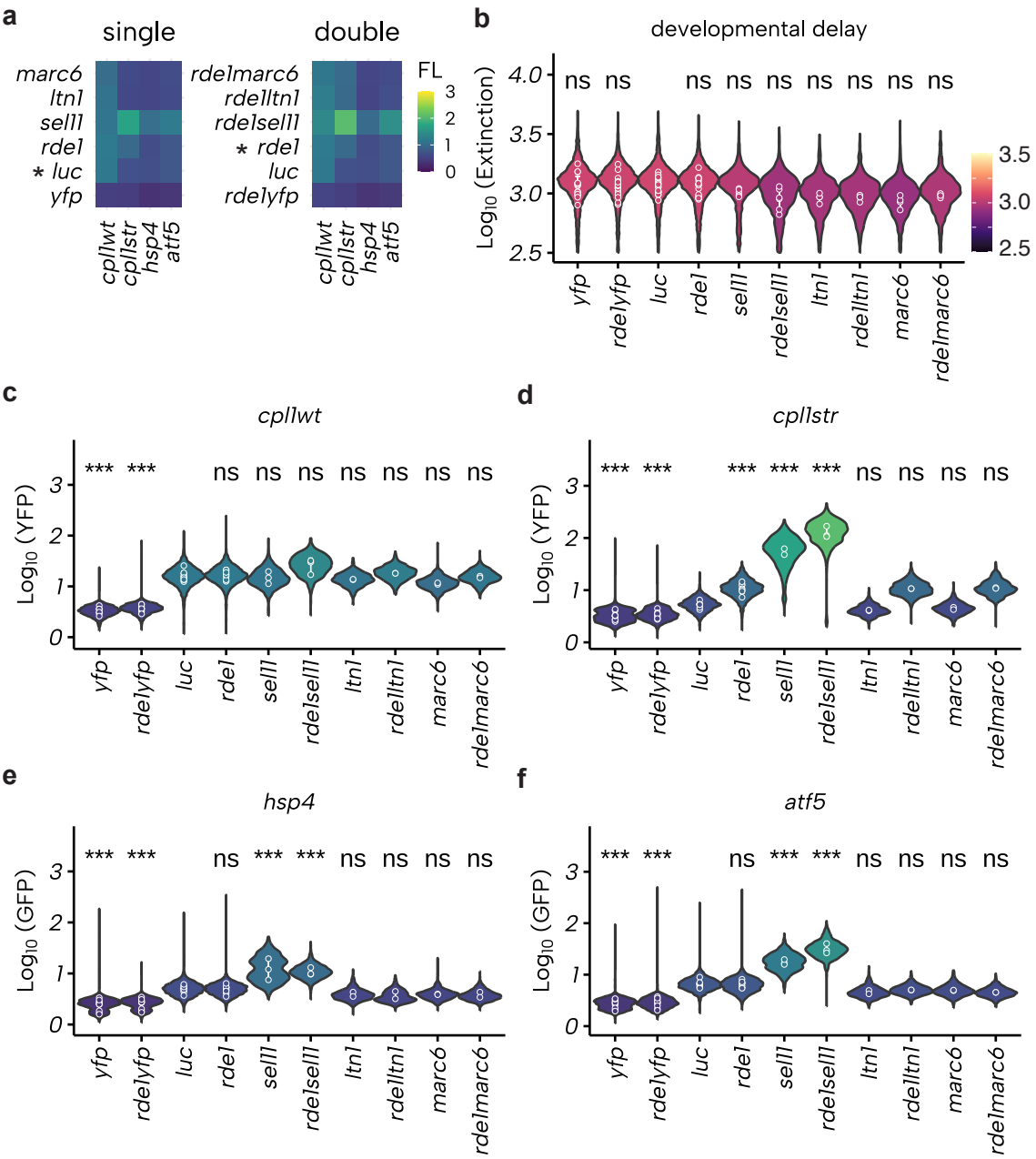

Figure A. 1: **Knockdown screen: ER-associated E3 ligases. a**, heatmaps display YFP and GFP fluorescence levels (FL) in reporter strains under RNAi conditions targeting *rde-1* (*rde1*) and ER-associated E3 ligases (ER-E3). Single knockdowns are normalized to luciferase (*luc*), and double knockdowns are normalized against *rde1* (asterisks indicate normalization condition). **b**, Quantification of developmental delay via extinction in red-positive strains as in figure 25 (*cpl1wt* and *cpl1str*) under RNAi conditions targeting ER-E3s.**c–f** Quantification of YFP and GFP fluorescence levels in all four reporter strains (*cpl1wt*: **c**, *cpl1str*: **d**, *hsp4*: **e** and *atf5*: **f**) under RNAi conditions targeting ER-E3s. **c–f**, were analyzed by pairwise t-test with Holmes multiple comparison test. Single knockdown conditions were compared to *luc* and double knockdown conditions were compared to *rde1*. * p<0.05, ** p<0.01, *** p<0.001, ns p>0.05

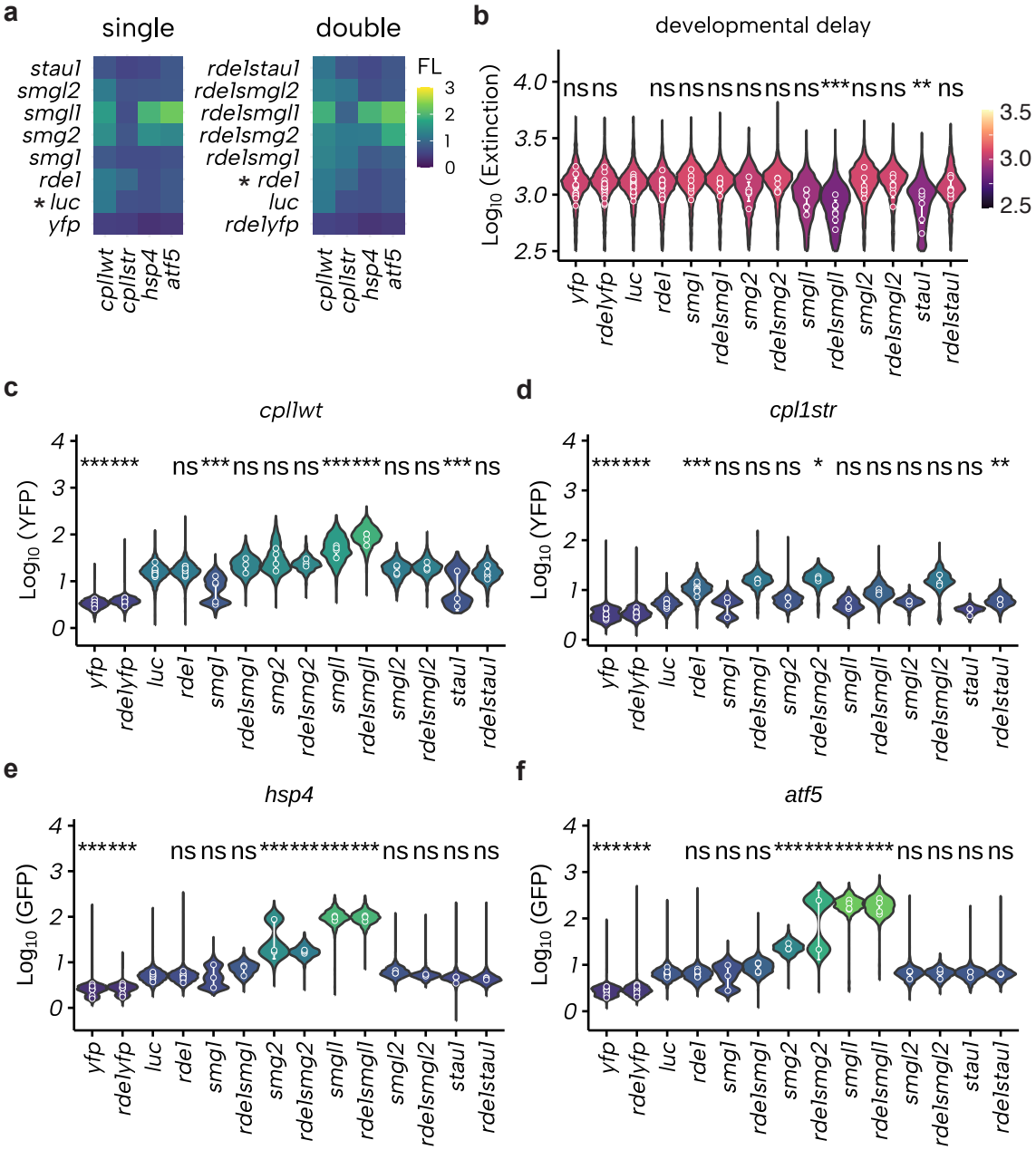

Figure A. 2: **Knockdown screen: ER-associated NMD. a**, heatmaps display YFP and GFP fluorescence levels (FL) in reporter strains under RNAi conditions targeting *rde-1* (*rde1*) and ER-associated NMD (ER-NMD). Single knockdowns are normalized to luciferase (*luc*), and double knockdowns are normalized against *rde1* (asterisks indicate normalization condition). **b**, Quantification of developmental delay via extinction in red-positive strains as in figure 25 (*cpl1wt* and *cpl1str*) under RNAi conditions targeting ER-NMD. **c–f** Quantification of YFP and GFP fluorescence levels in all four reporter strains (*cpl1wt*: **c**, *cpl1str*: **d**, *hsp4*: **e** and *atf5*: **f**) under RNAi conditions targeting ER-NMD. **c–f**, were analyzed by pairwise t-test with Holmes multiple comparison test. Single knockdown conditions were compared to *luc* and double knockdown conditions were compared to *rde1*. * $p<0.05$, ** $p<0.01$, *** $p<0.001$, ns $p>0.05$

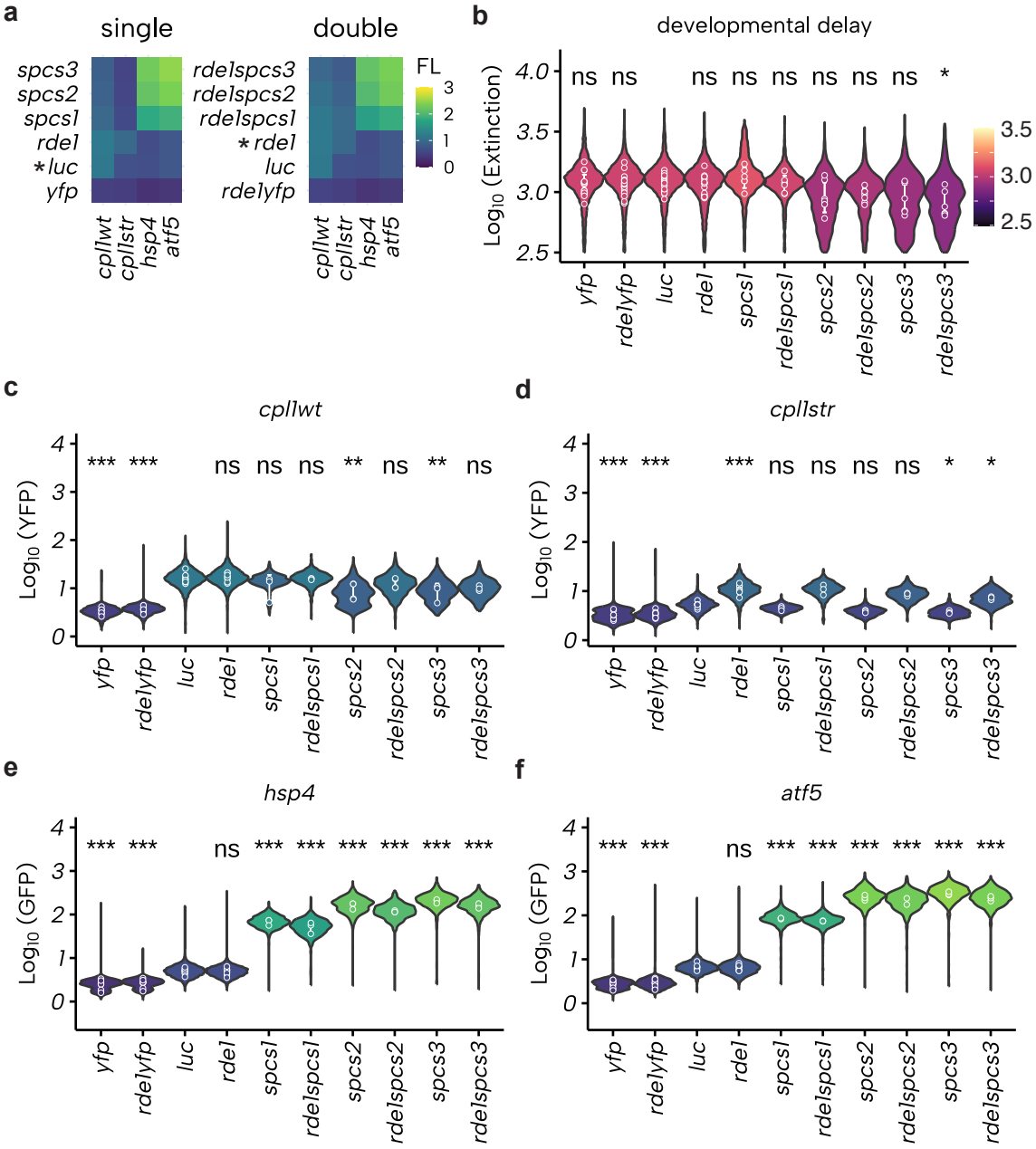

Figure A. 3: **Knockdown screen: ER-resident signal peptidase complex.** **a**, heatmaps display YFP and GFP fluorescence levels (FL) in reporter strains under RNAi conditions targeting *rde-1* (*rde1*) and ER-resident signal peptidase complex (SPP). Single knockdowns are normalized to luciferase (*luc*), and double knockdowns are normalized against *rde1* (asterisks indicate normalization condition). **b**, Quantification of developmental delay via extinction in red-positive strains as in figure 25 (*cpl1wt* and *cpl1str*) under RNAi conditions targeting SPP. **c–f** Quantification of YFP and GFP fluorescence levels in all four reporter strains (*cpl1wt*: **c**, *cpl1str*: **d**, *hsp4*: **e** and *atf5*: **f**) under RNAi conditions targeting SPP. **c–f**, were analyzed by pairwise t-test with Holmes multiple comparison test. Single knockdown conditions were compared to *luc* and double knockdown conditions were compared to *rde1*. * p<0.05, ** p<0.01, *** p<0.001, ns p>0.05

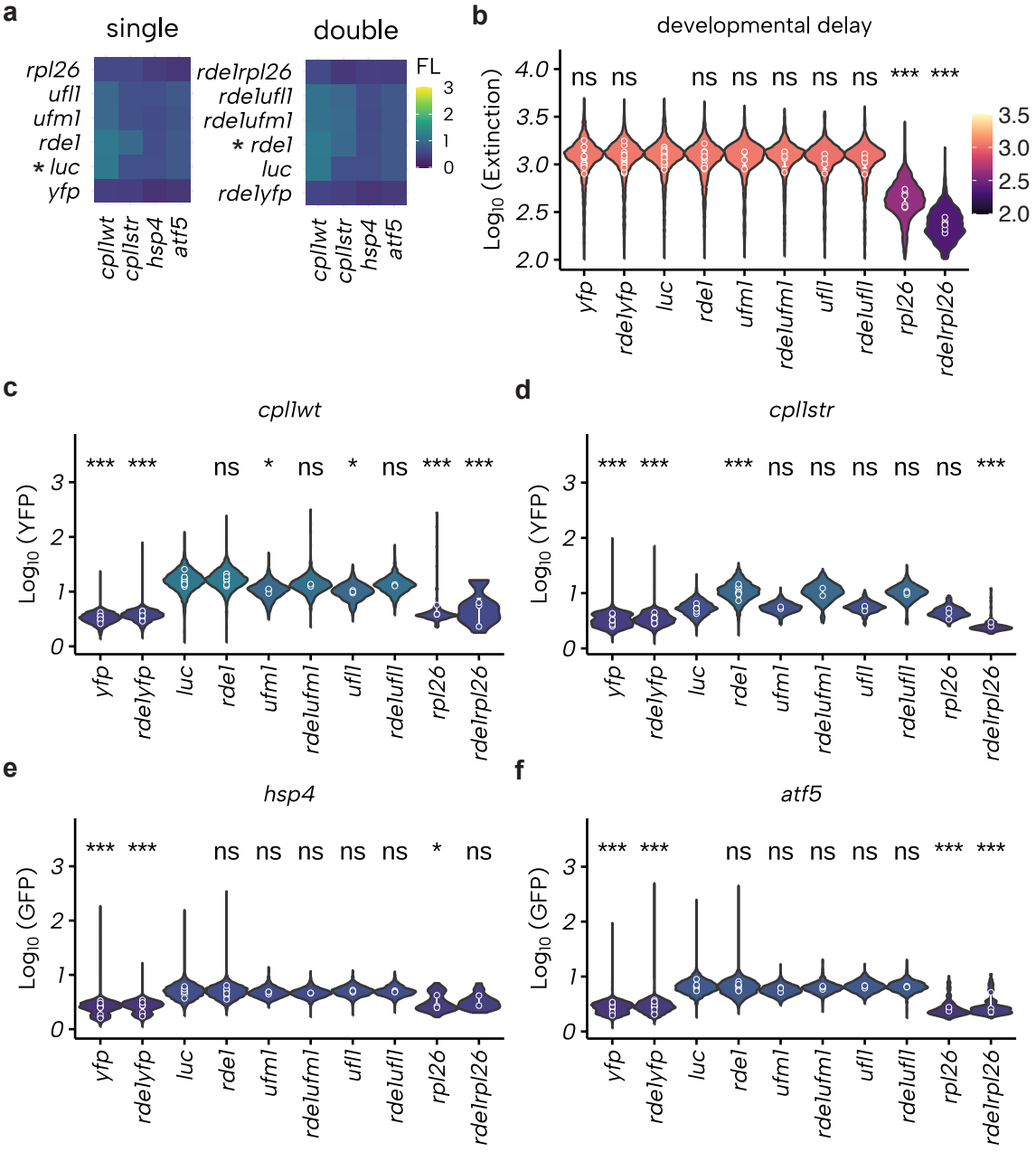

Figure A. 4: **Knockdown screen: UFMylation machinery.** **a**, heatmaps display YFP and GFP fluorescence (FL) in the reporter strains under RNAi conditions targeting *rde-1* (*rde1*) and the UFMylation machinery. Single knockdowns are normalized to luciferase (*luc*), and double knockdowns are normalized against *rde1* (asterisks indicate normalization condition). **b**, Quantification of developmental delay via extinction in red-positive strains as in figure 25 (*cpl1wt* and *cpl1str*) under RNAi conditions targeting the UFMylation machinery. **c–f** Quantification of YFP and GFP fluorescence levels in all four reporter strains (*cpl1wt*: **c**, *cpl1str*: **d**, *hsp4*: **e** and *atf5*: **f**) under RNAi conditions targeting the UFMylation machinery. **c–f**, were analyzed by pairwise t-test with Holmes multiple comparison test. Single knockdown conditions were compared to *luc* and double knockdown conditions were compared to *rde1*. * p<0.05, ** p<0.01, *** p<0.001, ns p>0.05

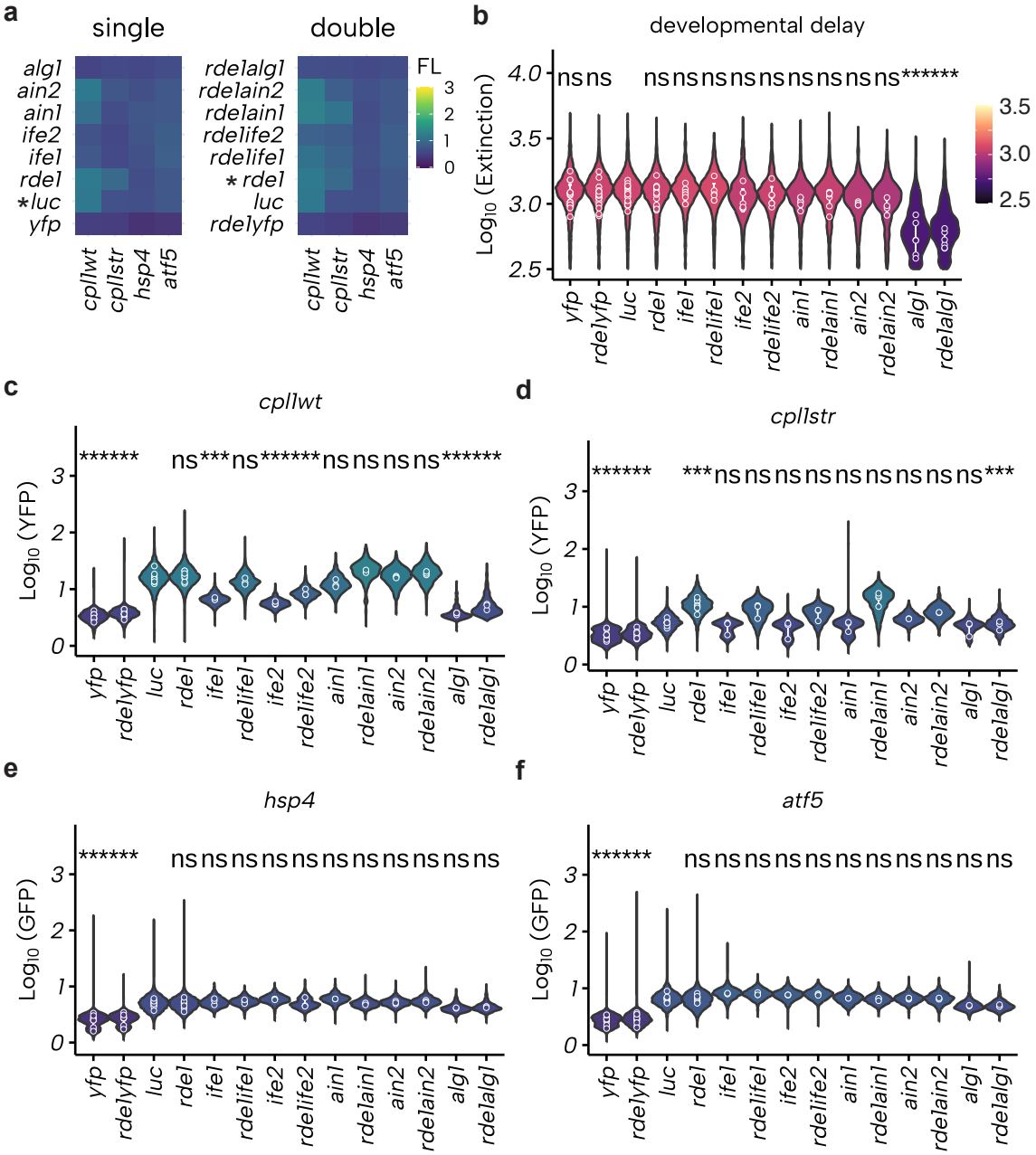

Figure A. 5: **Knockdown screen: miRNA silencing.** **a**, heatmaps display YFP and GFP fluorescence levels (FL) in reporter strains under RNAi conditions targeting *rde-1* (*rde1*) and the miRNA silencing machinery. Single knockdowns are normalized to luciferase (*luc*), and double knockdowns are normalized against *rde1* (asterisks indicate normalization condition). **b**, Quantification of developmental delay via extinction in red-positive strains as in figure 25 (*cpl1wt* and *cpl1str*) under RNAi conditions targeting the miRNA silencing machinery. **c–f** Quantification of YFP and GFP fluorescence levels in all four reporter strains (*cpl1wt*: **c**, *cpl1str*: **d**, *hsp4*: **e** and *atf5*: **f**) under RNAi conditions targeting the miRNA silencing machinery. **c–f**, were analyzed by pairwise t-test with Holmes multiple comparison test. Single knockdown conditions were compared to *luc* and double knockdown conditions were compared to *rde1*. * p<0.05, ** p<0.01, *** p<0.001, ns p>0.05

A.2 Publication A: ER-associated RNA silencing promotes ER quality control

(I) **Efstathiou, S***., Ottens, F.*, Schütter*, L. S., Ravanelli, S., Charmpilas, N., Gutschmidt, A., le Pen, J., Gehring, N. H., Miska, E. A., Bouças, J., & Hoppe, T. (2022). ER-associated RNA silencing promotes ER quality control. *Nature Cell Biology*, 24(12), 1714–1725. https://doi.org/10.1038/S41556-022-01025-4

* These authors contributed equally

nature cell biology

Article

https://doi.org/10.1038/s41556-022-01025-4

ER-associated RNA silencing promotes ER quality control

Received: 18 June 2021

Accepted: 14 October 2022

Published online: 5 December 2022

Check for updates

Sotirios Efstathiou[1,2,10], Franziska Ottens[1,2,10], Lena-Sophie Schütter[1,2,10], Sonia Ravanelli[1,2], Nikolaos Charmpilas[1,2], Aljona Gutschmidt[1,2,9], Jérémie Le Pen[3,4,5], Niels H. Gehring[1,6], Eric A. Miska[4,5,7], Jorge Bouças[8] & Thorsten Hoppe[1,2,6]

The endoplasmic reticulum (ER) coordinates mRNA translation and processing of secreted and endomembrane proteins. ER-associated degradation (ERAD) prevents the accumulation of misfolded proteins in the ER, but the physiological regulation of this process remains poorly characterized. Here, in a genetic screen using an ERAD model substrate in *Caenorhabditis elegans*, we identified an anti-viral RNA interference pathway, referred to as ER-associated RNA silencing (ERAS), which acts together with ERAD to preserve ER homeostasis and function. Induced by ER stress, ERAS is mediated by the Argonaute protein RDE-1/AGO2, is conserved in mammals and promotes ER-associated RNA turnover. ERAS and ERAD are complementary, as simultaneous inactivation of both quality-control pathways leads to increased ER stress, reduced protein quality control and impaired intestinal integrity. Collectively, our findings indicate that ER homeostasis and organismal health are protected by synergistic functions of ERAS and ERAD.

The endoplasmic reticulum (ER) coordinates translation, folding and maturation of luminal, secreted and transmembrane proteins within the endomembrane system. Challenging the protein folding capacity of the ER by increased protein import or drug-induced dysfunction results in ER stress, which activates a series of conserved protein quality-control pathways that together constitute the unfolded protein response of the ER (UPR^{ER})[1,2]. ER stress signalling is essential for organismal development and has been associated with many pathological states, including metabolic, neurologic and inflammatory diseases[3,4].

Upon ER stress, the inositol-requiring enzyme (IRE1), a transmembrane protein kinase and endoribonuclease, promotes the unconventional splicing of the XBP1-encoding messenger RNA precursor, leading to the translation of the transcription factor XBP1s (refs. [5–7]). One of the molecular mechanisms controlled by XBP1s is the ER-associated protein degradation (ERAD) pathway. ERAD targets ER-resident proteins for selective degradation by the ubiquitin/proteasome system[8]. Under stress conditions, ERAD prevents the accumulation of misfolded proteins through the luminal ER chaperone BiP and glycoprotein-binding lectins, which cooperate with the Sel1L–Hrd1 protein complex. Sel1L is an obligatory co-factor for the ER membrane spanning E3 ligase Hrd1, which ubiquitylates retro-translocated proteins for proteasomal turnover in the cytosol. In mammalian cells, IRE1 overexpression initiates the cleavage of particular mRNAs in a process termed regulated IRE1-dependent mRNA decay[9,10]. However, the functional relevance of this mechanism remains largely unclear, since mRNA levels of most regulated

[1]Institute for Genetics, University of Cologne, Cologne, Germany. [2]Cologne Excellence Cluster on Cellular Stress Responses in Aging-Associated Diseases (CECAD), University of Cologne, Cologne, Germany. [3]Laboratory of Virology and Infectious Disease, The Rockefeller University, New York, NY, USA. [4]Wellcome Trust/Cancer Research UK Gurdon Institute, University of Cambridge, Cambridge, UK. [5]Department of Genetics, University of Cambridge, Cambridge, UK. [6]Center for Molecular Medicine Cologne (CMMC), Faculty of Medicine and University Hospital of Cologne, Cologne, Germany. [7]Wellcome Sanger Institute, Wellcome Trust Genome Campus, Cambridge, UK. [8]Bioinformatics Core Facility, Max Planck Institute for Biology of Aging, Cologne, Germany. [9]Present address: BioNTech SE, Mainz, Germany. [10]These authors contributed equally: Sotirios Efstathiou, Franziska Ottens, Lena-Sophie Schütter. e-mail: thorsten.hoppe@uni-koeln.de

IRE1-dependent mRNA decay targets do not notably change even under ER stress conditions[11].

In this Article, we investigated the physiological regulation of ERAD and discovered an mRNA silencing mechanism that ensures ER homeostasis and function. In response to ER stress, the conserved Argonaute protein RDE-1/AGO2 mediates the bulk degradation of ER-associated mRNAs to ameliorate ER overload. This protective mechanism that we named ER-associated RNA silencing (ERAS) acts together with ERAD to maintain ER homeostasis and tissue integrity. Our work shows that ER-targeted mRNAs and proteins need to be actively degraded to allow the ER to cope with stress and maintain the essential function of this organelle as the cellular sorting centre.

Results

The exo-RNAi pathway is linked to ERQC

To investigate physiological ER quality control (ERQC) mechanisms, we examined the ERAD substrate protein CPL-1*::YFP (CPL-1*) in *Caenorhabditis elegans*. CPL-1*, a misfolding mutant form of the lysosomal cathepsin L-like peptidase, accumulates in the ER lumen when ERAD is impaired (Fig. 1a and Extended Data Fig. 1a)[12,13]. We stably expressed CPL-1* in intestinal cells, which are enriched in rough ER and secretory vesicles (Extended Data Fig. 1b)[13]. Knockdown of the E3 ligase SEL-11 (Hrd1 orthologue), its adaptor protein SEL-1 (Sel1L orthologue), the lectin C47E12.3 (EDEM1 orthologue) or the chaperone CDC-48 resulted in increased YFP levels, validating CPL-1* as a bona fide ERAD substrate (Extended Data Fig. 1c,d). In contrast, depletion of the autophagy regulators LGG-1 (LC3 orthologue) or BEC-1 (Beclin-1 orthologue) did not change CPL-1* protein levels (Extended Data Fig. 1e,f).

We performed a forward genetic screen using ethyl methane sulfonate (EMS)-induced mutagenesis and isolated YFP-positive mutants with increased CPL-1* levels (Fig. 1a and Extended Data Fig. 1a,b). Whole-genome sequencing and genetic mapping of selected mutants identified known components of ERAD, including *sel-11* (Fig. 1b,c and Extended Data Fig. 1g)[14]. The screen also revealed that *rde-1(hh26)*, *rde-1(ne219)*, *drh-1(hh18)*, *drh-1(hh20)*, *drh-1(ok3495)* and *rrf-1(hh22)* loss-of-function (LOF) mutants (Extended Data Fig. 2b), or their RNA interference (RNAi) depletion, robustly increased CPL-1* protein levels, as seen in *sel-11(hh17)* (Fig. 1d,e and Extended Data Fig. 2c,d). CPL-1* co-fractionated with SEL-1 in ER-derived microsomes of *rde-1(ne219)* worms (Fig. 1f), indicating that the CPL-1* protein accumulated in the ER fraction. Intestinal expression of *rde-1* rescued the accumulation of CPL-1* in the *rde-1(ne219)* mutant (Fig. 1g and Extended Data Fig. 2e). Thus, our identification of *rde-1, drh-1* and *rrf-1* as factors in CPL-1* accumulation suggested an involvement in ERQC.

RNAi defective (RDE-1), dicer-related helicase (DRH-1) and RNA-dependent RNA polymerase (RRF-1) are all components of the exogenous RNAi (exo-RNAi) pathway that mediates the degradation of viral RNAs (Extended Data Fig. 2a)[15]. Many viruses use the ER for their replication and also manipulate factors localized in the ER, such as ERAD, to their advantage[16]. We wanted to know whether Orsay virus, which infects *C. elegans* and is targeted by exo-RNAi[17,18], also has ER association. To this end, we used a viral infection transcriptional reporter[19] that allowed us to enrich worms infected with Orsay virus (Extended Data Fig. 2f). Like the CPL-1* protein, cellular fractionation assays showed that Orsay virus RNA1 and its capsid protein α are enriched in the ER fraction, suggesting that virus replication and exo-RNAi function at the ER membrane (Extended Data Fig. 2g,h).

Exo-RNAi degrades CPL-1* substrate-encoding mRNA

To examine the role of the exo-RNAi machinery in ERQC we monitored CPL-1* protein turnover over a period of 9 h after blocking translation with cycloheximide (CHX). While CPL-1* degradation was significantly impaired in the ERAD-defective mutant *sel-11(nDf59)*, the *rde-1(ne219)* and *drh-1(ok3495)* mutants were not impaired in substrate protein degradation (Fig. 2a,b), indicating that its accumulation in *rde-1* and *drh-1* (Fig. 1d,e) was not linked to ERAD-mediated post-translational control. RDE-1 belongs to the Argonaute protein family[20] and contains a PIWI/Argonaute/Zwille (PAZ) domain and a PIWI domain with endonucleolytic activity[21], which is required for RNAi[22]. Given that RDE-1 and the DRH-1 RNA helicase form part of the RNA-induced silencing complex, which participates in target RNA degradation (Extended Data Fig. 2a), we wondered if they directly targeted the transgenic *cpl-1* mRNA. The *rde-1(ne219)* LOF lesion converts a conserved glutamate to lysine within the PAZ domain, which binds the 3′ end of small interfering RNAs (siRNAs)[22], abrogating its RNA silencing function (Extended Data Fig. 2b). Thus, we reasoned that the exo-RNAi pathway might affect CPL-1* protein levels via post-transcriptional regulation of transgenic *cpl-1** mRNA turnover. To test this idea, we blocked transcription using α-amanitin and measured *cpl-1** mRNA levels over 10 h. We observed rapid mRNA turnover in wild-type (WT) animals, but increased stability in *rde-1(ne219)* and *drh-1(ok3495)* mutant worms (Fig. 2c,d). Intriguingly, we found decreased *cpl-1** mRNA baseline levels in the ERAD-defective *sel-11* and *sel-1* mutants (Extended Data Fig. 3a), suggesting a link between ERQC and mRNA turnover. To further investigate the interplay between ERAD and post-transcriptional regulation of mRNA turnover by exo-RNAi, we analysed *cpl-1* mRNA levels in worms expressing the natively folded wild-type CPL-1 (CPL-1^{WT}) protein. In contrast to the rapid degradation of the *cpl-1** transcript, *cpl-1^{WT}* mRNA remained unchanged in the absence of functional RDE-1 or DRH-1 (Fig. 2e,f), suggesting that the exo-RNAi pathway predominantly targets the *cpl-1** mRNA.

As both CPL-1 and viral components are localized at the ER (Fig. 1f and Extended Data Fig. 2f–h), we examined the effects of ER homeostasis on Orsay virus infection in *C. elegans*. Consistent with the known anti-viral function of exo-RNAi[17,18], *rde-1* and *drh-1* mutants showed increased levels of viral RNA1 upon infection with Orsay virus (Fig. 2g), which was rescued by intestinal *rde-1* expression (Extended Data Fig. 3b)[18,23–26]. Viral infection induced expression of the ER-resident chaperone *hsp-4* (BiP orthologue) and triggered splicing of *xbp-1* (Extended Data Fig. 3c). In addition, we found that viral RNA1 levels decreased sharply in worms pre-treated with the ER stressor tunicamycin before virus infection, indicating increased viral RNA turnover upon ER stress (Fig. 2h). The ERAD *sel-11* mutant also exhibited decreased RNA1 levels (Fig. 2g), as did the *atf-6*, *pek-1* and *ire-1* mutants, which have defects in UPR^{ER} regulation (Fig. 2i), suggesting a functional link between ER fidelity and viral RNA degradation. Our results suggest that ER stress triggers the degradation of ER-associated mRNAs and viral RNAs via the exo-RNAi machinery.

mRNA turnover is linked to ER stress

To investigate the signalling mechanism that activates exo-RNAi, we analysed the transcriptional landscape of worms expressing *cpl-1** and compared them with *cpl-1^{WT}* and wild-type worms by RNA sequencing. Gene Ontology (GO) term enrichment analysis of the significantly upregulated transcripts identified genes involved in UPR^{ER}, response to ER stress, and innate immunity (Fig. 3a,b), suggesting that overexpression and misfolding of CPL-1* increased protein folding load and ERQC requirements of the ER and induced ER stress[13,27,28].

We hypothesized that increased ER stress caused by *cpl-1** expression or *sel-11* deficiency determines substrate mRNA stability (Fig. 3a,b and Extended Data Fig. 3a), which could also explain the previously observed degradation of *cpl-1** but not *cpl-1^{WT}* mRNA (Fig. 2c–f). To understand the relationship between ER stress and post-transcriptional regulation of mRNA turnover by exo-RNAi, we directly compared *cpl-1* mRNA levels in worms expressing either wild-type CPL-1 (CPL-1^{WT}) or the misfolding CPL-1* substrate protein. Quantitative real-time polymerase chain reaction qRT–PCR showed that *cpl-1^{WT}* mRNA levels were stable for 10 h, whereas *cpl-1** mRNA decreased rapidly (Fig. 3c). In *rde-1* mutant worms, the rapid decay of *cpl-1** mRNA was suppressed (Fig. 3c), whereas the stability of *cpl-1^{WT}* mRNA was unchanged in the absence of functional RDE-1 (Fig. 3d). Strikingly, RDE-1-mediated degradation

https://doi.org/10.1038/s41556-022-01025-4

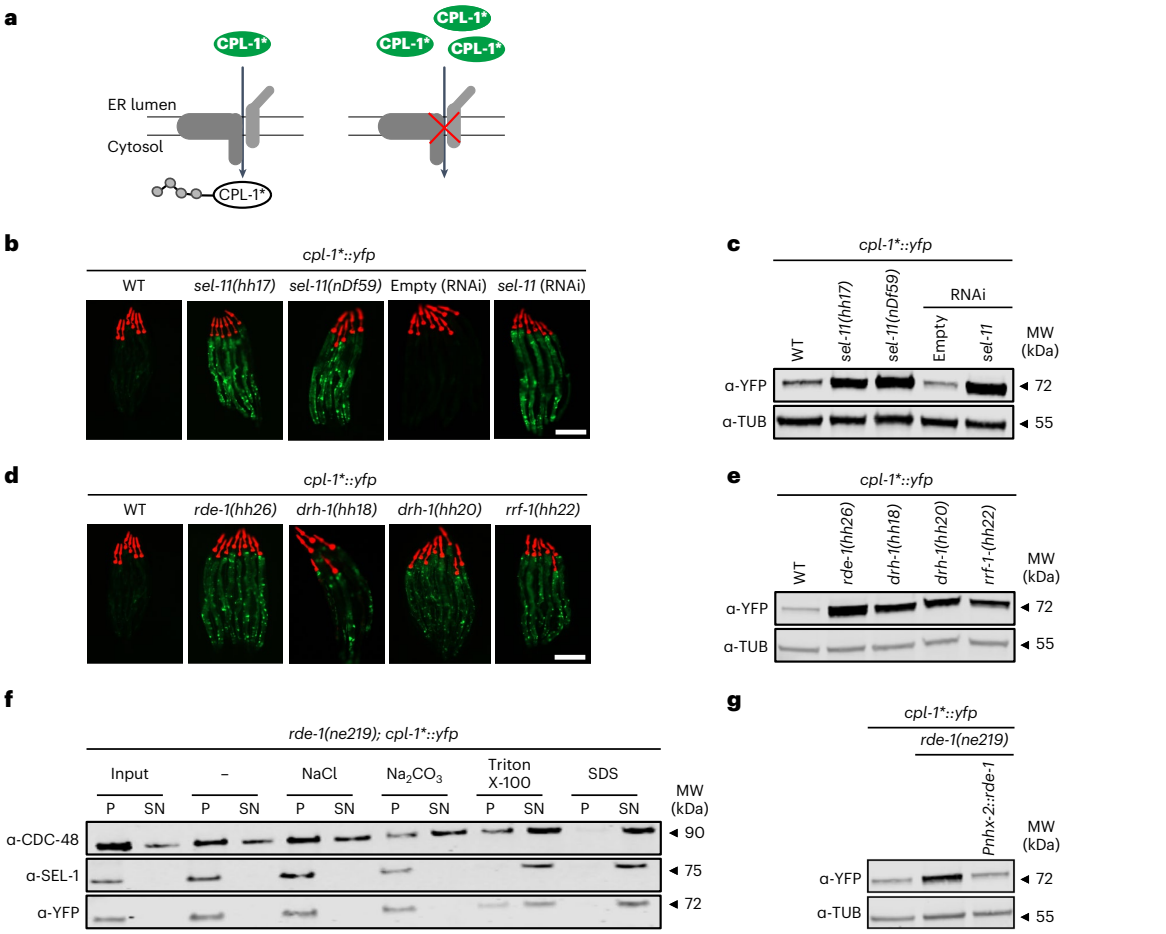

Fig. 1 | A role for exo-RNAi in ER homeostasis. a, Turnover of the model substrate CPL-1* via ERAD. **b**, Fluorescence images of worms expressing *cpl-1** with the indicated mutations and RNAi (empty control (Empty)) for the ERAD factor *sel-11*. **c**, Western blot of worm lysates corresponding to images shown in **b**, detecting CPL-1* (YFP) and tubulin (TUB). **d**, Fluorescence images of worms expressing *cpl-1** with mutations in the exo-RNAi pathway. **e**, Western blot of worm lysates corresponding to the samples in **d**, detecting CPL-1* (YFP) and tubulin (TUB). **f**, Cellular fractionation of microsomes. Western blot detecting CPL-1* (YFP), CDC-48 (CDC-48) and SEL-1 (SEL-1). Pellet (P) and supernatant (SN) fractions of *rde-1(ne219); cpl-1** worm lysates treated with the indicated chemicals after subcellular fractionation. **g**, Western blot of worm lysates detecting CPL-1* (YFP) and tubulin (TUB) in *rde-1(ne219)* worms and animals with intestinal *Pnhx-2::rde-1* rescue. In **b** and **d**, pharyngeal expression of *Pmyo-2::mCherry* serves as transgenic marker. Scale bar, 200 µm. MW, molecular weight. Unprocessed blots are available in the source data.

of *cpl-1*^{WT} transcripts can be triggered in the ERAD-defective *sel-11* mutant which shows increased ER stress, as observed by *hsp-4* expression levels (Fig. 3d,e). These data suggest that induction of ER stress makes *cpl-1*^{WT} mRNA an optional target of the exo-RNAi pathway. Thus, RDE-1-dependent mRNA turnover is coupled to ER homeostasis.

RDE-1 regulates the turnover of ER-associated mRNAs

To investigate whether other potential ERAD reporter substrates are also targeted by exo-RNAi components, we tested the *sGFP::ATM* (ATM) transgene, a signal peptide-GFP fused to human serpin that has previously been shown to reside in the ER[29]. Like the *cpl-1** reporter, the ATM protein accumulates upon depletion of *rde-1* or *sel-11* (Fig. 4a,b and Extended Data Figs. 2c,d and 4a–c,f), which is enhanced upon double depletion of both factors (Extended Data Fig. 4a,d). In addition, the *ATM* transcript was strongly degraded by RDE-1 (Fig. 4c). Taken together, these data indicate continuous turnover of ATM protein and mRNA by SEL-11 and RDE-1, respectively.

Following the identification of exo-RNAi components as ER stress-dependent ERQC factors, we sought to characterize in vivo targets of the exo-RNAi machinery. To this end, we performed RNA sequencing and searched for upregulated mRNAs in *rde-1(ne219)* mutants in the context of exo-RNAi activation in *cpl-1** expressing worms (Fig. 4d). We identified 485 mRNAs that were significantly upregulated and therefore represent potential exo-RNAi targets. By applying BUSCA analysis of subcellular localization[30] we found that 73% of these candidates were associated with GO terms related to the endomembrane and secretory system, 11% to the nucleus and 2% to mitochondria (Fig. 4e and Supplementary Table 4). In addition, GO enrichment analysis for cellular components revealed significant positive enrichment for mRNAs encoding proteins with endomembrane involvement, such as collagen trimers and components of the extracellular space processed by the ER. In contrast, mRNAs encoding cytoplasmic, mitochondrial or nuclear factors showed significant negative enrichment (Fig. 4f and Supplementary Table 4).

As collagens are highly abundant throughout the animal kingdom and rely on ER import and proper ER homeostasis, we focused our analysis on the collagen trimer-encoding mRNAs *rol-6* and *sqt-1*. In addition, we tested *asp-12*, which encodes a lysosomal endopeptidase

https://doi.org/10.1038/s41556-022-01025-4

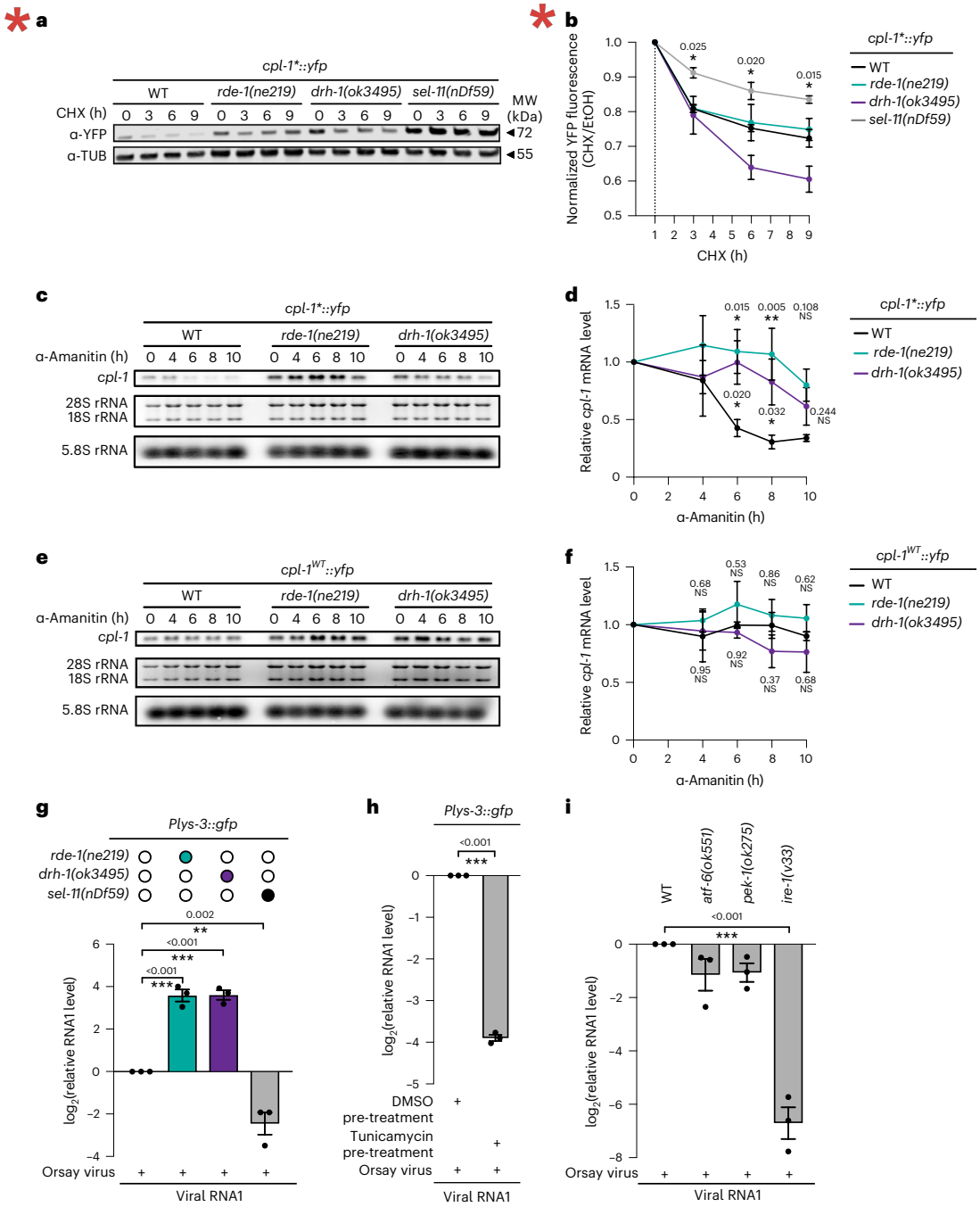

Fig. 2 | Post-transcriptional regulation of ERAD substrate and viral RNA level. **a**,**b**, CHX chase assay to assess CPL-1* protein stability: western blot of lysates from *cpl-1** expressing worms with indicated mutations detecting CPL-1* (YFP) and tubulin (TUB) over 9 h of CHX treatment (**a**); BioSorter quantification of YFP fluorescence in vehicle (EtOH)- and CHX-treated *cpl-1**-expressing worms (**b**). CHX/EtOH ratios were normalized to the 1 h timepoint of the respective genotype. **c**, α-Amanitin chase assay to monitor *cpl-1* mRNA level in *rde-1(ne219)* and *drh-1(ok3495)* mutant worms expressing *cpl-1**. Northern blot of purified RNA from animals expressing *cpl-1**, detecting *cpl-1* mRNA and 5.8S rRNA. 28S and 18S rRNA served as agarose gel loading control. **d**, Quantification of *cpl-1* mRNA level corresponding to the data shown in **c**, relative to 5.8 S rRNA. **e**, α-Amanitin chase assay to monitor *cpl-1* mRNA level in *rde-1(ne219)* and *drh-1(ok3495)* mutant worms expressing *cpl-1*^{WT}. Northern blot of purified RNA from animals expressing *cpl-1*^{WT}, detecting *cpl-1* mRNA and 5.8 S rRNA. 28S and 18S rRNA served as agarose gel loading control. **f**, Quantification of *cpl-1* mRNA level corresponding to the data shown in **e**, relative to 5.8S rRNA. **g**, Viral RNA1 level measured by qRT–PCR in worms infected with the Orsay virus. **h**, Viral RNA1 level measured by qRT–PCR in worms pre-treated with vehicle (DMSO) or tunicamycin before viral infection. Data are relative to 18S rRNA. **i**, Viral RNA1 level measured by qRT–PCR in worms, defective for the UPR^{ER} pathway. In **b**, **d** and **f**–**i**, Values are depicted as mean ± standard error of the mean (s.e.m.) generated from $n = 3$ independent experiments, $^{*}P < 0.05$; $^{**}P < 0.01$; $^{***}P < 0.001$; NS, $P > 0.05$. Data were analysed by two-way ANOVA with Sidak's multiple comparison test. Source numerical data and unprocessed blots are available in source data.

https://doi.org/10.1038/s41556-022-01025-4

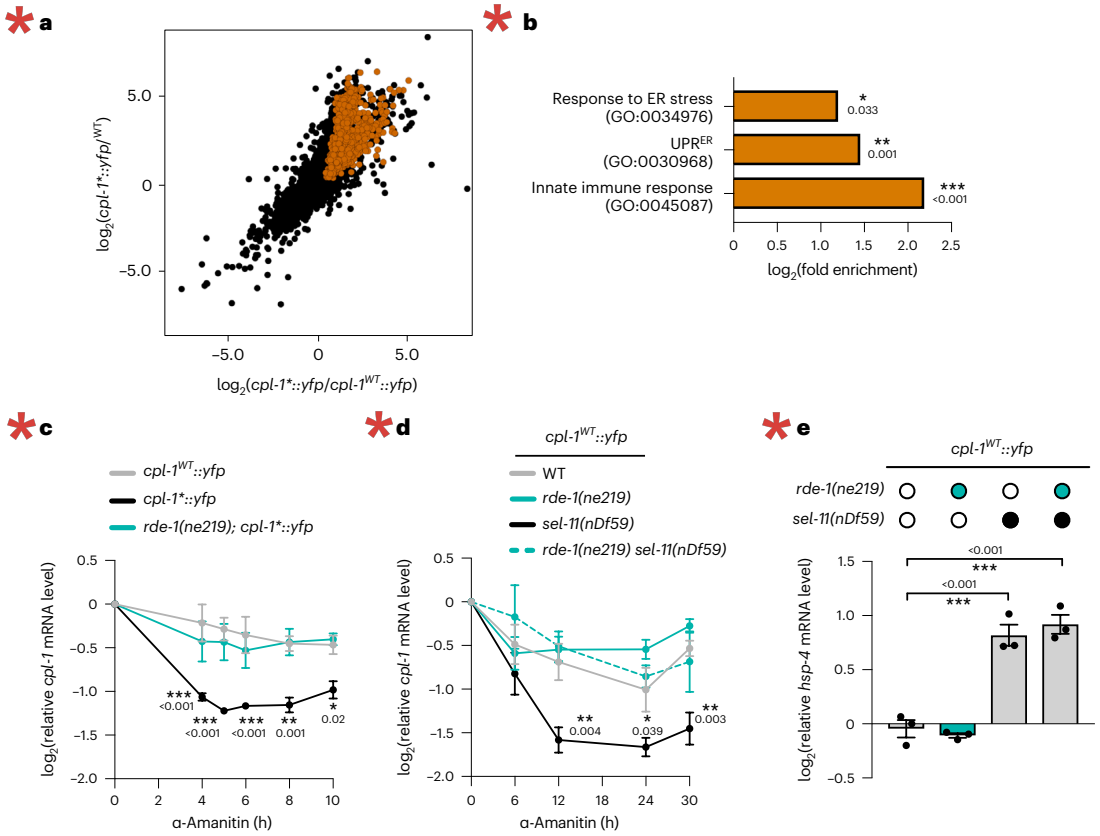

Fig. 3 | RDE-1-dependent RNA turnover is affected by ER stress. a, RNA sequencing results of *cpl-1** expressing worms compared with WT and *cpl-1*^{WT} expressing worms, respectively. The cut-off for filtering of upregulated constructs was performed with $P \leq 0.05$ (brown spheres). **b**, GO term enrichment for biological processes of the transcripts identified in **a** (brown). Only transcripts that were upregulated in both datasets shown in **a** were selected for analysis, resulting in 996 upregulated transcripts. **c**,**d**, α-Amanitin chase assays for *cpl-1*^{WT} and *cpl-1** mRNA from mutant animals for ERAD and/or ERAS expressing *cpl-1*^{WT} or *cpl-1** mRNA measured by qRT–PCR. Data relative to 18S rRNA, *cdc-42* and *pmp-3* mRNA. **e**, *hsp-4* mRNA level measured by qRT-PCR at the 0 h timepoint corresponding to the samples shown in **d**. Data relative to *cdc-42* and *pmp-3* mRNA. In **c** and **d**, data were analysed by two-way ANOVA with Dunnett's multiple comparison test. In **e**, data were analysed by one-way ANOVA with Sidak's multiple comparison test. In **c**–**e**, values are depicted as mean ± s.e.m. generated from $n = 3$ independent experiments, $^*P < 0.05$; $^{**}P < 0.01$; $^{***}P < 0.001$; NS, $P > 0.05$. In **b**, raw P values were corrected for FDR. *FDR <0.05; **FDR <0.01; ***FDR <0.001; NS, FDR >0.05. Source numerical data are available in source data.

that, like the model substrate *cpl-1*, is highly expressed in the intestine. We found that all three exo-RNAi target candidates undergo RDE-1-dependent turnover in worms expressing the *cpl-1** transgene (Fig. 4g–i). In contrast, mRNA of the proteasomal subunit *pas-7*, which was not upregulated in *rde-1(ne219)*, was not degraded by RDE-1 (Fig. 4d,j). Furthermore, we tested ER stress-dependent regulation of *rol-6* and *sqt-1* mRNAs by treatment with tunicamycin, which resulted in a strong decrease in *rol-6* and *sqt-1* transcript levels in WT and *sel-11* mutants but not in *rde-1* and *drh-1* mutants (Fig. 4k). In contrast, *pas-7* mRNA was also not regulated by RDE-1 in tunicamycin-treated worms (Fig. 4l). Taken together, our data suggest a previously unknown ER-associated RNA silencing mechanism regulated by ER folding capacity that contributes to ERQC. We termed this mechanism ERAS.

DCR-1 is essential and RRF-1 conducive to ERAS

Argonaute proteins such as RDE-1 are controlled by DCR-1-processed double-stranded RNA (dsRNA) to regulate target RNAs (for example, mRNAs or viral RNAs). DCR-1, in turn, has a variety of substrates associated with endogenous mRNAs, including many collagens and, intriguingly, *cpl-1* (ref. [31]). RDE-1 is heavily loaded with microRNAs (miRNA) and siRNA species, so the transcriptome may be examined for homology with DCR-1-processed dsRNA species[32]. Indeed, DCR-1 proved to be indispensable for ERAS, as depletion of DCR-1 phenotypically copies the loss of RDE-1 in terms of CPL-1* substrate stabilization (Extended Data Fig. 4d). Moreover, double depletion of *rde-1* and *dcr-1* did not further increase substrate levels (Extended Data Fig. 4e). Remarkably, we identified endogenous *cpl-1* mRNA as an RDE-1 target in animals expressing the ER-directed *ATM* substrate (Fig. 4m), demonstrating the natural potential of *C. elegans* to undergo an RNA silencing reaction against *cpl-1*. In contrast to DCR-1, the canonical miRNA biogenesis pathway mediated by DRSH-1 and PASH-1 was not required for the degradation of CPL-1* (Extended Data Fig. 4d,e). Furthermore, we tested whether RNA-dependent RNA polymerases (*rrf-1*, *rrf-3* and *ego-1*) contribute to substrate stabilization and confirmed the involvement of RRF-1, as knockdown of *rrf-1* leads to protein stabilization of the ATM substrate, albeit to a lesser extent than knockdown of *rde-1* (Extended Data Fig. 4g). These results recapitulate the effect of the *rrf-1(hh22)* mutant on CPL-1* (Fig. 1d,e). However, double depletion of *rrf-1* and *rde-1* showed an additive effect on protein substrate stabilization (Extended Data Fig. 4g,h), suggesting that RRF-1 and secondary siRNAs support RDE-1 even if they are not essential for its function in ERQC. We further investigated a possible role of *mir-243* in ER homeostasis, as *mir-243* was

https://doi.org/10.1038/s41556-022-01025-4

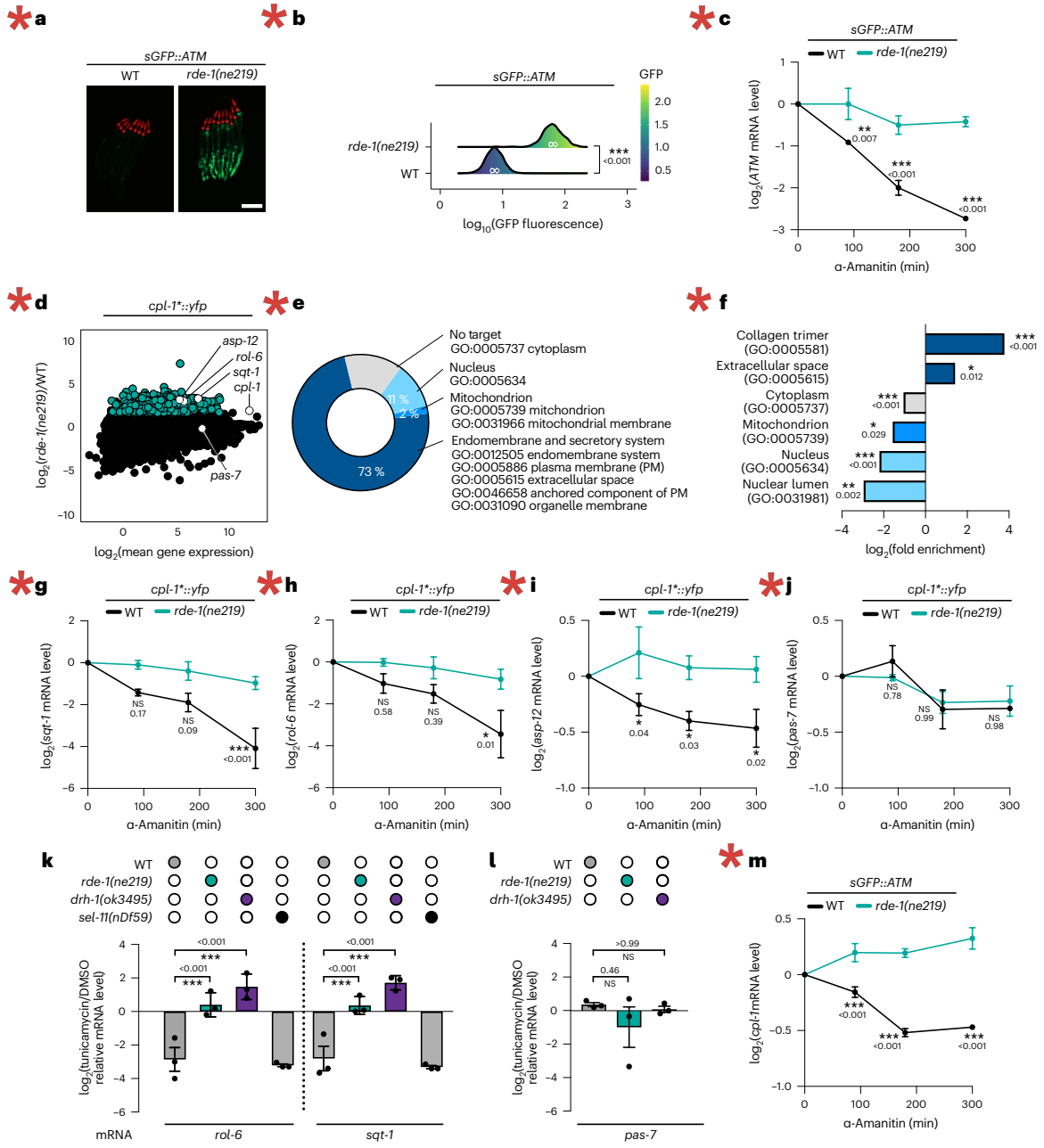

Fig. 4 | Endogenous mRNAs regulated by RDE-1. a, Fluorescence images of mutant worms for the exo-RNAi pathway expressing *ATM*. Pharyngeal expression of *Pmyo-2::mCherry* serves as transgenic marker. Scale bar, 200 µm. **b**, Quantification of GFP fluorescence intensity of *ATM* expressing worms together with *rde-1(ne219)* mutation. Measurements were carried out with the BioSorter using at least 200 animals per replicate, which were merged and displayed in ridgeline density plots. **c**, α-Amanitin chase assays for *ATM* mRNA from *rde-1(ne219)* mutants expressing *ATM*. mRNA measured by qRT–PCR. **d**, RNA sequencing results of *cpl-1**-expressing worms bearing the *rde-1(ne219)* mutation or the WT allele. Cut-off for upregulated constructs: $P \leq 0.05$. **e**, A total of 485 transcripts identified in **d** were subjected to BUSCA subcellular localization analysis. **f**, Subcellular component GO term enrichment for the genes identified in **d** and **e**. **g**–**j**, α-Amanitin chase assays for indicated endogenous mRNAs identified in **d** from *rde-1(ne219)* mutants and WT animals expressing *cpl-1**. mRNA measured by qRT–PCR. **k**,**l**, Endogenous *rol-6*, *sqt-1* (**k**) and *pas-7* (**l**) mRNA level measured by qRT–PCR in vehicle (DMSO)- versus tunicamycin-treated WT worms. Data relative to 18S rRNA. **m**, α-Amanitin chase assays for endogenous *cpl-1* mRNA from *ATM* expressing animals with the *rde-1(ne219)* mutation or WT allele. mRNA measured by qRT–PCR. In c, g–j and m, data are relative to *cdc-42* and *pmp-3* mRNA. In **b**, data were analysed by pairwise *t*-test with Holmes multiple comparison test. In **k** and **l**, data were analysed by one-way ANOVA with Sidak's multiple comparison test. In **c**, **g**–**j** and **m**, data were analysed by two-way ANOVA with Dunnett's multiple comparison test. Values are depicted as mean ± s.e.m or, in **c** and **g**–**m**, as mean (white circles) ± standard deviation (s.d.) (white error bars). Data in **b** are generated from $n = 3$ independent experiments. *$P < 0.05$; **$P < 0.01$; ***$P < 0.001$; NS, $P > 0.05$. In **f**, raw *P* values were corrected for FDR. *FDR <0.05; **FDR <0.01; *** FDR <0.001; NS, FDR >0.05. Source numerical data are available in source data.

https://doi.org/10.1038/s41556-022-01025-4

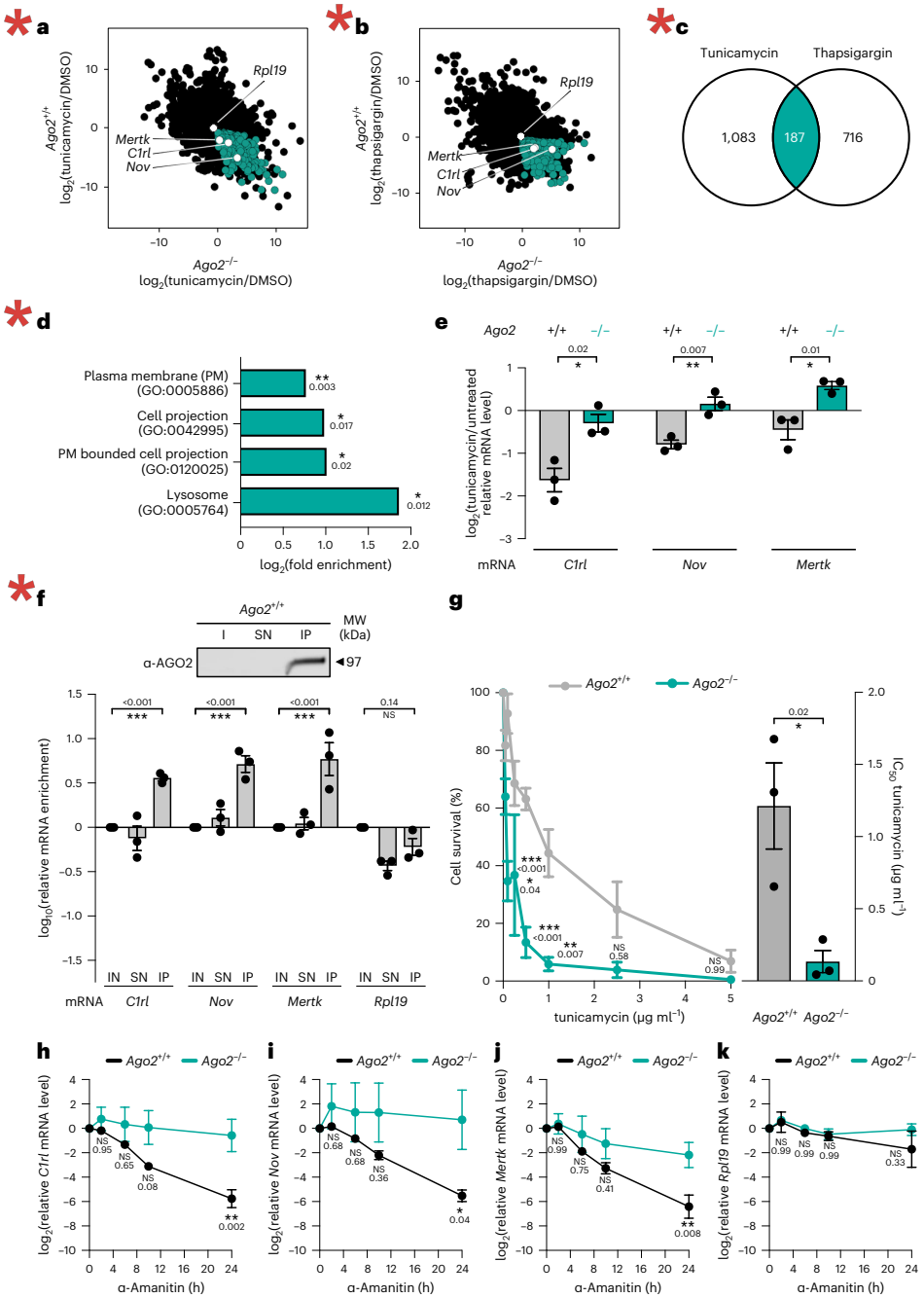

Fig. 5 | ERAS is conserved in mammalian cells. a,**b**, RNA sequencing results of tunicamycin/DMSO-treated (**a**) thapsigargin/DMSO-treated (**b**) *Ago2*$^{+/+}$ and *Ago2*$^{-/-}$ MEF cells. Ago2-specific targets were selected by filtering ($P \leq 0.05$) transcripts that were downregulated in *Ago2*$^{+/+}$ and upregulated in *Ago2*$^{-/-}$ cells (cyan). **c**, Venn diagram showing the number of transcripts regulated by AGO2 upon ER stress induction. Only transcripts that were identified in both ER stress conditions (**a** and **b**) were further investigated (cyan). **d**, Cellular component GO term enrichment of the genes identified in **a** and **b**. **e**, Expression levels of endogenous *Nov*, *Mertk* and *C1rl* mRNA in tunicamycin-treated MEFs measured by qRT–PCR. Data relative to 18S rRNA. **f**, UV CLIP of tunicamycin-treated MEF cells using AGO2 as bait and subsequent qRT–PCR of target mRNAs in the input (IN), supernatant (SN) and immunoprecipitation (IP) fractions. Data normalized to input fraction. Top shows western blot against AGO2 for the performed CLIP experiment. **g**, Dose-dependent cell survival after tunicamycin treatment calculated from the colony formation assay shown in Extended Data Fig. 5f. Bar graph showing the IC_{50} values for tunicamycin between *Ago2*$^{+/+}$ and *Ago2*$^{-/-}$ MEF cells. **h**–**k**, α-Amanitin chase assays for indicated endogenous mRNAs identified in **a** and **b** from *Ago2*$^{+/+}$ and *Ago2*$^{-/-}$ MEF cells pre-treated with tunicamycin. mRNA measured by qRT–PCR. Data relative to 18S and 28S rRNA. Data in **e** were analysed by unpaired two-tailed t-tests. Data in **f** were analysed by a two-way ANOVA with Dunnett's multiple comparison test. The bar graph in **g** was analysed by paired two-tailed *t*-test. In **g**–**k**, data were analysed by two-way ANOVA with Sidak´s multiple comparison test. In **e**-**k** values are depicted as mean ± s.e.m. generated from $n = 3$ independent experiments, $^{*}P < 0.05$; $^{**}P < 0.01$; $^{***}P < 0.001$; NS, $P > 0.05$. In **d**, raw *P* values were corrected for FDR. *FDR <0.05; ** FDR <0.01; *** FDR <0.001; NS, FDR >0.05. Source numerical data and unprocessed blots are available in source data.

previously shown to physically interact with RDE-1, induce biogenesis of cognate siRNAs, and ultimately regulate its target transcript Y47H10A.5 (ref. [32]). Accordingly, *mir-243(n4759)* LOF mutants were not shown to directly alter *cpl-1** substrate stabilization at the protein or mRNA level (Extended Data Fig. 4i,j) because the *cpl-1** transcript is not directly targeted by *mir-243*. However, *rde-1; mir-243* double mutants showed dramatically increased CPL-1* protein levels and strongly induced *hsp-4* mRNA expression (Extended Data Fig. 4i,k). GO enrichment analysis of published microarray data in *mir-243(n4759)* LOF mutants[32] reveals an overrepresentation of the 'unfolded protein response at the ER' (false discovery rate (FDR) <0.01; Supplementary Table 4) in the upregulated gene group. Taken together, these data suggest that RDE-1-associated miRNAs such as *mir-243* are involved in the maintenance of ER homeostasis and confirm the role of ERAS in ERQC.

AGO2 controls turnover of ER-associated mRNAs

To investigate a possible role of ERAS in mammalian cells, we examined AGO2, which has high sequence similarity to RDE-1 in *C. elegans* and is functionally orthologous for siRNA-mediated RNA silencing in mammals[33]. AGO2 shares the same PAZ–PIWI domains and is conserved for the glutamate residue mutated in the *rde-1(ne219)* E414K allele (Extended Data Fig. 5a)[22,34]. We treated AGO2-deficient ($Ago2^{-/-}$) mouse embryonic fibroblasts (MEFs)[20] with the ER stressors tunicamycin or thapsigargin. To identify ERAS targets, we filtered for mRNAs that were upregulated in $Ago2^{-/-}$ cells and downregulated in wild-type ($Ago2^{+/+}$) control cells for both ER stressors (Fig. 5a,b). BUSCA analysis of subcellular localization revealed that of the 187 candidates (Fig. 5c) 42% had GO terms associated with the endomembrane and secretory system, 18% with mitochondria and 5% with the nucleus (Extended Data Fig. 5b)[30]. GO term analysis showed significant enrichment of mRNAs associated with cell projection, plasma membrane (PM), PM bounded cell projection and lysosomes (Fig. 5d).

We selected three mRNAs from candidate genes representing ER luminal (*C1rl*), PM (*Mertk*) and secreted (*Nov*) proteins and confirmed AGO2-dependent regulation for all three mRNAs upon tunicamycin-induced ER stress (Fig. 5e and Extended Data Fig. 5c). UV-crosslinking immunoprecipitation (CLIP) for AGO2 combined with qRT–PCR revealed direct protein–RNA binding between AGO2 and the mRNAs *C1rl*, *Nov* and *Mertk* (Fig. 5f). We were able to enrich the *C1rl*, *Nov* and *Mertk* transcripts in $Ago2^{+/+}$ cells but not in $Ago2^{-/-}$ cells or negative UV-crosslinking controls, demonstrating the specificity of the assay (Fig. 5f and Extended Data Fig. 5d,e). In contrast, the housekeeping mRNA *Rpl19*, which encodes the 60S ribosomal protein L19 and whose expression did not change significantly in the RNA-sequencing assay (Fig. 5a,b), was not enriched in AGO2 CLIP-qRT-PCR (Fig. 5f). We also tested the ability of single $Ago2^{-/-}$ cells to form a colony after tunicamycin treatment. Compared with $Ago2^{+/+}$ controls, $Ago2^{-/-}$ cells showed reduced survival with increasing tunicamycin dose, suggesting a cytoprotective ERQC function of ERAS in mammals (Fig. 5g, and Extended Data Fig. 5f). Strikingly, the endogenous mRNAs bound by AGO2 in the CLIP qRT–PCR assay (Fig. 5f) were indeed degraded in an AGO2-dependent manner upon ER stress exerted by tunicamycin pre-treatment (Fig. 5h–j), whereas *Rpl19* mRNA showed no AGO2-mediated turnover (Fig. 5k). Thus, downregulation of ER-associated RNAs by the Argonaute proteins RDE-1/AGO2 upon ER stress is conserved from worms to mammals.

ERAS and ERAD work together to maintain ER homeostasis

To understand the regulatory relationship between post-transcriptional and post-translational ERQC, we combined ERAS and ERAD mutants and tracked changes in CPL-1* protein levels. ERAS-defective *drh-1* mutants combined with *sel-1* or *sel-11* depletion showed enhanced CPL-1* accumulation compared with *sel-1* and *sel-11* single mutants (Fig. 6a,b), recapitulating the effects of double depletion of *rde-1* and *sel-11* on CPL-1* and ATM protein (Extended Data Fig. 4a,d). Whereas knockdown of *sel-11* slightly induced expression of the ER stress reporter *Phsp-4::gfp*, this was significantly increased by the additional depletion of *rde-1*, highlighting the role of ERAS in ERQC, especially when ERAD is impaired (Fig. 6c). To distinguish the mechanism of RNA silencing from that of protein degradation in ERAS and ERAD, respectively, we used glutamine fructose 6-phosphate aminotransferase (*gfat-1*) gain-of-function (GOF) mutants, which exhibit enhanced glycosylation and ER protein folding and thus enhanced glycan-dependent ERAD[27]. We found that *gfat-1* (GOF) mutants were able to fully suppress ERAS-mediated but not ERAD-mediated CPL-1* substrate accumulation, confirming a role for GFAT-1 in enhancing ERAD (Fig. 6d). In contrast, simultaneous inhibition of ERAS and ERAD in *gfat-1* (GOF) mutants showed an additive effect, indicating that *gfat-1* (GOF) was no longer able to suppress ERAS-mediated CPL-1* substrate accumulation in the presence of dysfunctional ERAD (Fig. 6d). Moreover, *gfat-1* (GOF) had no effect on the correctly folded and ERAD-independent $CPL\text{-}1^{WT}$ protein (Extended Data Fig. 6a). Finally, we found that *gfat-1* (GOF) had no effect on ERAS activity at the mRNA level of the *cpl-1** substrate (Extended Data Fig. 6b), which is in line with the observation that baseline *hsp-4* expression remains constant in *gfat-1* (GOF) mutants[27] (Extended Data Fig. 6c). Overall, our data show that ERAS and ERAD work together to maintain ER homeostasis by reducing the protein folding load of the ER.

To investigate the physiological consequences of simultaneous impairment of ERAS and ERAD, we monitored ER protein folding capacity and intestinal integrity, representing changes at the cellular and organismal level. The mCherry-HDEL fusion protein, which is targeted to the ER lumen by a SEL-1 signal sequence[35,36], requires functional protein quality control in the ER for correct folding. Confocal imaging revealed focal accumulations of mCherry-HDEL protein with concomitant impairment of ERAS and ERAD (Fig. 6e,f). To exclude the possibility that the observed effects were due to altered transgene expression in the different mutant backgrounds, we monitored mCherry-HDEL protein level, which remained unchanged in ERAS and ERAD mutants (Extended Data Fig. 6d). These findings further underline a cooperation between ERAS and ERAD in maintaining ER homeostasis.

ER stress has been associated with loss of intestinal homeostasis, including the development of inflammatory bowel disease and loss of epithelial barrier integrity[37,38]. To assess intestinal integrity of *rde-1 sel-11* double mutants, we tested intestinal barrier function in *C. elegans*[39]. Animals were fed a blue food dye, and leakage of the dye from the intestine into the body cavity (Smurf phenotype) was observed microscopically. While single mutants were able to retain the dye in the intestine, *rde-1 sel-11* double mutants showed severely compromised intestinal barrier integrity (Fig. 6g,h and Extended Data Fig. 6e). Taken together, our results identify ERAS as an RNA surveillance mechanism that regulates the turnover of ER-associated RNAs and viral RNAs to maintain ER homeostasis and organism functionality (Fig. 6i).

Discussion

ER homeostasis is disrupted by the accumulation of misfolded luminal proteins, which are generally degraded via ERAD[8]. Here we identified a conserved post-transcriptional pathway with a complementary function to ERAD in ERQC, which we termed ERAS. ERAS consists of the exo-RNAi machinery in worms and focuses on RDE-1/AGO2, a member of the Argonaute protein family that exists in plants, *Drosophila* and vertebrates[22]. DCR-1, DRH-1 and RRF-1 are also involved in the turnover of ER-targeted mRNAs during ER stress (Figs. 1d,e and 2c,d and Extended Data Figs. 2a and 4e–h). Here we show that the ERAS machinery targets a variety of endogenous mRNAs encoding proteins of the endomembrane and secretion system (Fig. 4e and Extended Data Fig. 5b). Although ERAS and ERAD work together to maintain ER protein homeostasis, their mechanisms of action are distinct. ERAS works through the cellular RNA silencing machinery for

https://doi.org/10.1038/s41556-022-01025-4

mRNA degradation, whereas ERAD uses the ubiquitin/proteasome system for protein degradation (Figs. 2a–d and 6d and Extended Data Figs. 4 c,f,g–i and 6a,b). We show that ERAS is triggered by ER stress induced by expression of the ERAD substrates CPL-1* and ATM, treatment with tunicamycin/thapsigargin, or viral infection (Figs. 2c,d,g,i, 3a–c, 4c,k and 5 and Extended Data Figs. 2g and 3c). Similarly, defects in the ERAD

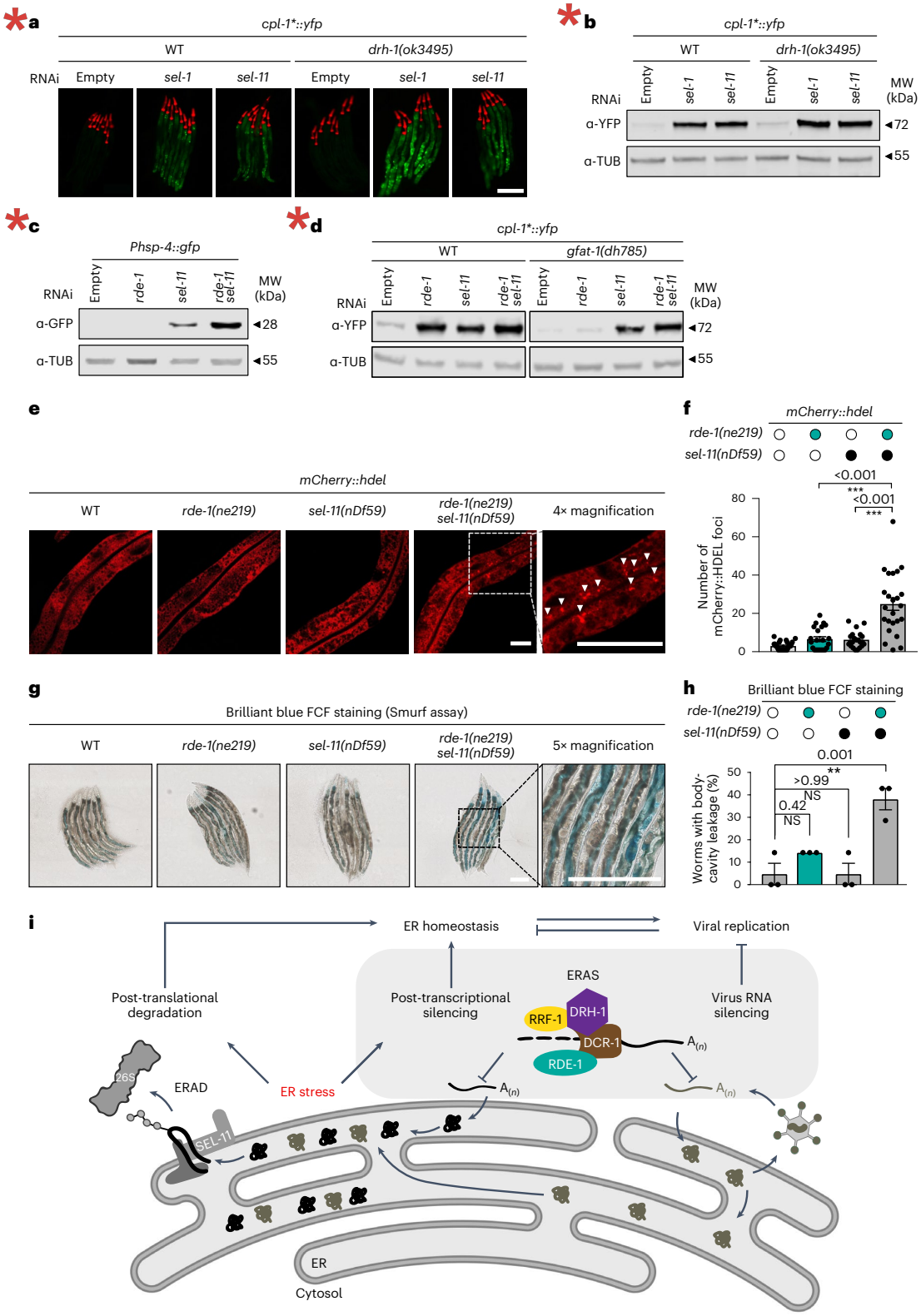

Fig. 6 | ERAS and ERAD execute complementary functions in ERQC. Fluorescence images of worms expressing *cpl-1**. Pharyngeal expression of *Pmyo-2::mCherry* serves as transgenic marker. Scale bar, 200 µm. Images were taken with lower exposure time to prevent YFP overexposure for animals with defects in both, the ERAS and ERAD pathway. **b**, Western blot of worm lysates corresponding to the samples in **a**, detecting CPL-1* (YFP) and tubulin (TUB). **c**, Western blot of worm lysates with the indicated RNAi treatment, detecting GFP (GFP) and tubulin (TUB). **d**, Western blot of worm lysates from worms depleted for ERAS and/or ERAD components expressing *cpl-1** in the WT or *gfat-1* GOF background detecting CPL-1* (YFP) and tubulin (TUB). **e**, Confocal microscopy images showing worms expressing the ER marker *mCherry::hdel* (red). Focal accumulation of mCherry highlighted by arrow heads. Scale bars, 20 µm. **f**, Quantification of mCherry-HDEL foci shown in **e**, $n = 28$, 22, 21 and 24 animals (left to right). **g**, Intestinal barrier (Smurf) assay. Representative images of day 5 adult worms soaked in blue food dye (Brilliant Blue FCF). Blue dye leaking from the intestinal lumen into the body cavity gives rise to the Smurf phenotype. Scale bars, 200 µm. **h**, Quantification of body-cavity leakage in animals shown in **g**, $n = 7$ individual animals/$n = 3$ replicates. In **f** and **h**, data were analysed by one-way ANOVA with Bonferroni's multiple comparison test and values are depicted as mean ± s.e.m. generated from $n = 3$ independent experiments, $^{**}P < 0.01$; $^{***}P < 0.001$; NS, $P > 0.05$. **i**, The ERAD machinery detects misfolded proteins and retro-translocates them into the cytosol for polyubiquitylation by SEL-11 and proteasomal turnover. The ERAS machinery mediates silencing of ER-associated mRNAs and viral RNA. ERAD and ERAS are required upon ER stress caused by misfolded proteins and virus replication and their complementary functions contribute to maintain ER homeostasis and organismal functionality. Source numerical data and unprocessed blots are available in source data.

or UPR^{ER} pathways triggered stress that significantly reduced the levels of ERAS-targeted RNAs, as shown in *sel-1*, *sel-11*, *atf-6*, *pek-1* and *ire-1* LOF mutants (Figs. 2i and 3d,e and Extended Data Fig. 3a), indicating the interdependence of ERAD, UPR^{ER} and ERAS in mediating ERQC and viral defence. The cooperation of ERAS and ERAD is crucial, as shown by the enhanced upregulation of UPR^{ER}, reduced protein quality control and impaired intestinal integrity when both ERAD and ERAS are defective (Fig. 6c,e–h). In addition to anti-viral defence, the exo-RNAi pathway may also play a role in silencing extrachromosomal transgenes, which has not yet been fully elucidated[40,41]. Our data rule out ERAS being affected by indirect transgene silencing effects, on the basis of its causal relationship with ER homeostasis (Figs. 2g, 3a–d, 4a–c, 5a–g and 6d and Extended Data Figs. 3a, 4c,f and 6a,b), constitutive degradation of *cpl-1** but only facultative turnover of *cpl-1*^{WT} (Fig. 3a,b and Extended Data Fig. 3a,b), the identification of endogenous ERAS-targets in worms and MEFs (Figs. 4g–m and 5a–f,h–k), and finally the specific regulation of *cpl-1**, *cpl-1*^{WT} and *ATM* compared with other transgenes used in this study (Figs. 3c,d, and 6c,d and Extended Data Fig. 6a,c). RDE-1 mediates RNA silencing by binding to the 3′ end of Dicer-processed dsRNAs via its conserved PAZ domain[22]. As regulation of ER-targeted RNAs is abolished in *rde-1(ne219)* worms with a single point mutation in the PAZ domain (Figs. 2c,d,g, 3c and 4c,d,g–m and Extended Data Figs. 2b, 3b and 4c,f), we propose a comparable mechanistic function of RDE-1 in ERAS. This conclusion is supported by the fact that AGO2 specifically binds and degrades mRNA targets that accumulate in *Ago2*$^{-/-}$ cells under ER stress conditions (Fig. 5f,h–k and Extended Data Fig. 5d,e). However, the precise mechanisms by which ER stress triggers RDE-1/AGO2-mediated mRNA silencing remain unclear. Recent evidence suggests that the ER membrane is a central hub for RNA silencing. Membrane fractionation and immunostaining experiments have shown that siRNA-loaded AGO2 binds to the cytosolic side of the rough ER membrane along with Dicer and that induction of ER stress by thapsigargin treatment repels AGO2-bound mRNAs from the ER[42,43]. Given that *Ago2*$^{-/-}$ cells are sensitive to tunicamycin treatment (Fig. 5g and Extended Data Fig. 5f), these data suggest a conserved role for *Ago2*-mediated RNA silencing in ER homeostasis. Interestingly, several UPR^{ER}-inducible miRNAs were found to regulate the cellular survival response by directly targeting components of the UPR^{ER} such as CHOP, Xbp-1 or Caspase-2 (ref. [44]). The UPR^{ER}-inducible miRNA *miR-708* regulates rhodopsin, which is produced in large amounts in the ER and is an important component of the developing retina. Through *Ago2*-dependent downregulation of rhodopsin upon ER stress, *miR-708* prevents the accumulation of misfolded rhodopsin in the ER, highlighting the physiological importance of ERAS[44,45]. The description of an miRNA-directed siRNA biogenesis pathway, as demonstrated for *mir-243* (ref. [32]), together with our results, suggests a highly adaptive RNA regulatory capacity of ERAS and may provide an exciting avenue for further studies to elucidate tissue-specific small RNA regulatory circuits that regulate ERQC. Conceptually, any DCR-1 processed small RNA species could be involved in ERAS. A recent publication also found that AGOs localized at the ER promote ubiquitylation of nascent polypeptide chains by the E3 ligase Ltn1 (ref. [46]). This raises the intriguing idea that AGO proteins represent interaction nodes for coupling post-transcriptional gene silencing and protein quality control at the ER. However, our results suggest that ERAS does not specifically degrade the mRNA of an unstable protein species, but that multiple ER stress-inducing factors such as *cpl-1**, *ATM*, tunicamycin, thapsigargin, *sel-11* LOF and viral infection act on ERAS to mediate ERQC, independent of the protein fold status of the gene product (Figs. 2g–i, 3c,d, 4g–m and 5 and Extended Data Fig. 3).

Many viruses use the endomembrane system for cell entry, replication and assembly. However, the causal relationship between anti-viral defence by RNA silencing and ER homeostasis has been underestimated. We cannot completely exclude the possibility that the decreased viral RNA level in response to ER stress is due to decreased viral replication rather than ERAS-mediated RNA degradation (Fig. 2g–i). However, the reduction of viral RNAs upon pre-treatment with ER stress is conserved in mammals[47,48]; for example, non-cytotoxic pre-treatment with thapsigargin effectively protected mice from otherwise lethal doses of influenza A[48], and cells pre-treated with thapsigargin showed a dramatic reduction in viral RNA levels in cells infected with severe acute respiratory syndrome coronavirus 2 (ref. [47]). These two RNA viruses use the ER and endomembrane system for their replication[49–51]. From an evolutionary perspective, we speculate that ERAS has co-opted an ancient anti-viral pathway into a general RNA surveillance mechanism that regulates ERQC. Our results may therefore integrate these phenomena into a coherent model of how ERAS mediates ERQC and viral defence (Fig. 6i).

Online content

Any methods, additional references, Nature Portfolio reporting summaries, source data, extended data, supplementary information, acknowledgements, peer review information; details of author contributions and competing interests; and statements of data and code availability are available at https://doi.org/10.1038/s41556-022-01025-4.

References

1. Hetz, C. & Papa, F. R. The unfolded protein response and cell fate control. *Mol. Cell* **69**, 169–181 (2018).
2. Walter, P. & Ron, D. The unfolded protein response: from stress pathway to homeostatic regulation. *Science* **334**, 1081–1086 (2011).
3. Koksal, A. R., Verne, G. N. & Zhou, Q. Endoplasmic reticulum stress in biological processing and disease. *J. Investig. Med.* **69**, 309–315 (2021).
4. Hetz, C., Zhang, K. & Kaufman, R. J. Mechanisms, regulation and functions of the unfolded protein response. *Nat. Rev. Mol. Cell Biol.* **21**, 421–438 (2020).
5. Calfon, M. et al. IRE1 couples endoplasmic reticulum load to secretory capacity by processing the XBP-1 mRNA. *Nature* **415**, 92–96 (2002).

6. Lee, K. et al. IRE1-mediated unconventional mRNA splicing and S2P-mediated ATF6 cleavage merge to regulate XBP1 in signaling the unfolded protein response. *Genes Dev.* **16**, 452–466 (2002).
7. Yoshida, H., Matsui, T., Yamamoto, A., Okada, T. & Mori, K. XBP1 mRNA is induced by ATF6 and spliced by IRE1 in response to ER stress to produce a highly active transcription factor. *Cell* **107**, 881–891 (2001).
8. Smith, M. H., Ploegh, H. L. & Weissman, J. S. Road to ruin: targeting proteins for degradation in the endoplasmic reticulum. *Science* **334**, 1086–1090 (2011).
9. Hollien, J. & Weissman, J. S. Decay of endoplasmic reticulum-localized mRNAs during the unfolded protein response. *Science* **313**, 104–107 (2006).
10. Hollien, J. et al. Regulated Ire1-dependent decay of messenger RNAs in mammalian cells. *J. Cell Biol.* **186**, 323–331 (2009).
11. Moore, K. & Hollien, J. Ire1-mediated decay in mammalian cells relies on mRNA sequence, structure, and translational status. *Mol. Biol. Cell* **26**, 2873–2884 (2015).
12. Finger, F. et al. Olfaction regulates organismal proteostasis and longevity via microRNA-dependent signalling. *Nat. Metab.* **1**, 350–359 (2019).
13. Miedel, M. T. et al. A Pro-Cathepsin L mutant is a luminal substrate for endoplasmic-reticulum-associated degradation in *C. elegans*. *PLoS ONE* **7**, e40145 (2012).
14. Bigelow, H., Doitsidou, M., Sarin, S. & Hobert, O. MAQGene: software to facilitate *C. elegans* mutant genome sequence analysis. *Nat. Methods* **6**, 549 (2009).
15. Fire, A. et al. Potent and specific genetic interference by double-stranded RNA in *Caenorhabditis elegans*. *Nature* **391**, 806–811 (1998).
16. Byun, H., Gou, Y., Zook, A., Lozano, M. M. & Dudley, J. P. ERAD and how viruses exploit it. *Front. Microbiol.* **5**, 330 (2014).
17. Sarkies, P. & Miska, E. A. RNAi pathways in the recognition of foreign RNA: antiviral responses and host–parasite interactions in nematodes. *Biochem. Soc. Trans.* **41**, 876–880 (2013).
18. Ashe, A. et al. A deletion polymorphism in the *Caenorhabditis elegans* RIG-I homolog disables viral RNA dicing and antiviral immunity. *eLife* **2**, e00994 (2013).
19. Le Pen, J. et al. Terminal uridylyltransferases target RNA viruses as part of the innate immune system. *Nat. Struct. Mol. Biol.* **25**, 778–786 (2018).
20. Carmell, M. A., Xuan, Z., Zhang, M. Q. & Hannon, G. J. The Argonaute family: tentacles that reach into RNAi, developmental control, stem cell maintenance, and tumorigenesis. *Genes Dev.* **16**, 2733–2742 (2002).
21. Boland, A., Tritschler, F., Heimstädt, S., Izaurralde, E. & Weichenrieder, O. Crystal structure and ligand binding of the MID domain of a eukaryotic Argonaute protein. *EMBO Rep.* **11**, 522–527 (2010).
22. Tabara, H. et al. The rde-1 gene, RNA interference, and transposon silencing in *C. elegans*. *Cell* **99**, 123–132 (1999).
23. Franz, C. J. et al. Orsay, Santeuil and Le Blanc viruses primarily infect intestinal cells in *Caenorhabditis* nematodes. *Virology* **448**, 255–264 (2014).
24. Yuan, W., Zhou, Y., Fan, Y., Tao, Y. J. & Zhong, W. Orsay δ protein is required for nonlytic viral egress. *J. Virol.* **92**, 1–13 (2018).
25. Félix, M.-A. et al. Natural and experimental infection of caenorhabditis nematodes by novel viruses related to nodaviruses. *PLoS Biol.* **9**, e1000586 (2011).
26. Jiang, H. et al. Orsay virus utilizes ribosomal frameshifting to express a novel protein that is incorporated into virions. *Virology* **450–451**, 213–221 (2014).
27. Denzel, M. S. et al. Hexosamine pathway metabolites enhance protein quality control and prolong life. *Cell* **156**, 1167–1178 (2014).
28. Hou, N. S. et al. Activation of the endoplasmic reticulum unfolded protein response by lipid disequilibrium without disturbed proteostasis in vivo. *Proc. Natl Acad. Sci. USA* **111**, E2271–E2280 (2014).
29. Long, O. S. et al. A *C. elegans* model of human α1-antitrypsin deficiency links components of the RNAi pathway to misfolded protein turnover. *Hum. Mol. Genet.* **23**, 5109–5122 (2014).
30. Savojardo, C., Martelli, P. L., Fariselli, P., Profiti, G. & Casadio, R. BUSCA: an integrative web server to predict subcellular localization of proteins. *Nucleic Acids Res.* **46**, W459–W466 (2018).
31. Rybak-Wolf, A. et al. A variety of dicer substrates in human and *C. elegans*. *Cell* **159**, 1153–1167 (2014).
32. Corrêa, R. L., Steiner, F. A., Berezikov, E. & Ketting, R. F. MicroRNA-directed siRNA biogenesis in *Caenorhabditis elegans*. *PLoS Genet.* **6**, e1000903 (2010).
33. Meister, G. et al. Human Argonaute2 mediates RNA cleavage targeted by miRNAs and siRNAs. *Mol. Cell* **15**, 185–197 (2004).
34. Soding, J. Protein homology detection by HMM–HMM comparison. *Bioinformatics* **21**, 951–960 (2005).
35. Klemm, R. W. et al. A conserved role for atlastin GTPases in regulating lipid droplet size. *Cell Rep.* **3**, 1465–1475 (2013).
36. Daniele, J. R. et al. UPRER promotes lipophagy independent of chaperones to extend life span. *Sci. Adv.* **6**, eaaz1441 (2020).
37. Luo, K. & Cao, S. S. Endoplasmic reticulum stress in intestinal epithelial cell function and inflammatory bowel disease. *Gastroenterol. Res. Pract.* **2015**, 1–6 (2015).
38. Coleman, O. I. & Haller, D. ER Stress and the UPR in shaping intestinal tissue homeostasis and immunity. *Front. Immunol.* **10**, 2825 (2019).
39. Gelino, S. et al. Intestinal autophagy improves healthspan and longevity in *C. elegans* during dietary restriction. *PLoS Genet.* **12**, e1006135 (2016).
40. Grishok, A. Transcriptional silencing of a transgene by RNAi in the soma of *C. elegans*. *Genes Dev.* **19**, 683–696 (2005).
41. Yang, H. et al. The RDE-10/RDE-11 complex triggers RNAi-induced mRNA degradation by association with target mRNA in *C. elegans*. *Genes Dev.* **26**, 846–856 (2012).
42. Stalder, L. et al. The rough endoplasmatic reticulum is a central nucleation site of siRNA-mediated RNA silencing. *EMBO J.* **32**, 1115–1127 (2013).
43. Barman, B. & Bhattacharyya, S. N. mRNA targeting to endoplasmic reticulum precedes Ago protein interaction and microRNA (miRNA)-mediated translation repression in mammalian cells. *J. Biol. Chem.* **290**, 24650–24656 (2015).
44. Chitnis, N., Pytel, D. & Diehl, J. A. UPR-inducible miRNAs contribute to stressful situations. *Trends Biochem. Sci.* **38**, 447–452 (2013).
45. Behrman, S., Acosta-Alvear, D. & Walter, P. A CHOP-regulated microRNA controls rhodopsin expression. *J. Cell Biol.* **192**, 919–927 (2011).
46. Gao, Y. et al. Lipid-mediated phase separation of AGO proteins on the ER controls nascent-peptide ubiquitination. *Mol. Cell* **82**, 1313–1328.e8 (2022).
47. Al-Beltagi, S. et al. Thapsigargin is a broad-spectrum inhibitor of major human respiratory viruses: coronavirus, respiratory syncytial virus and influenza A virus. *Viruses* **13**, 234 (2021).
48. Goulding, L. V. et al. Thapsigargin at non-cytotoxic levels induces a potent host antiviral response that blocks influenza a virus replication. *Viruses* **12**, 1093 (2020).

49. de Castro Martin, I. F. et al. Influenza virus genome reaches the plasma membrane via a modified endoplasmic reticulum and Rab11-dependent vesicles. *Nat. Commun.* **8**, 1396 (2017).
50. Alenquer, M. et al. Influenza A virus ribonucleoproteins form liquid organelles at endoplasmic reticulum exit sites. *Nat. Commun.* **10**, 1629 (2019).
51. Boson, B. et al. The SARS-CoV-2 envelope and membrane proteins modulate maturation and retention of the spike protein, allowing assembly of virus-like particles. *J. Biol. Chem.* **296**, 100111–100112 (2021).

Publisher's note Springer Nature remains neutral with regard to jurisdictional claims in published maps and institutional affiliations.

Open Access This article is licensed under a Creative Commons Attribution 4.0 International License, which permits use, sharing, adaptation, distribution and reproduction in any medium or format, as long as you give appropriate credit to the original author(s) and the source, provide a link to the Creative Commons license, and indicate if changes were made. The images or other third party material in this article are included in the article's Creative Commons license, unless indicated otherwise in a credit line to the material. If material is not included in the article's Creative Commons license and your intended use is not permitted by statutory regulation or exceeds the permitted use, you will need to obtain permission directly from the copyright holder. To view a copy of this license, visit http://creativecommons.org/licenses/by/4.0/.

© The Author(s) 2022

Methods

C. elegans maintenance and transgenic lines

Nematodes were grown at 20 °C (unless stated otherwise) on nematode growth medium (NGM) plates seeded with the bacterial *Escherichia coli* strain OP50 as a food source according to standard protocols and methods[52,53]. The N2 Bristol strain served as wild-type. If not stated otherwise, all experiments were performed at day 1 of adulthood, and the examined worms were all hermaphrodites. Integration of the extrachromosomal arrays of the *cpl-1^{WT}::yfp* and *cpl-1*::yfp* strains obtained from Gary Silverman[13] was conducted by UV-induced DNA double-strand breaks. Synchronized L4 larvae were irradiated with 30 Gy UV light and cultured for 2 h at room temperature (RT). Eight worms per plate were picked onto 20 NGM plates (100 mm) and were grown until the F2 generation (approximately 5 days at 20 °C). Five-hundred worms of the obtained progeny were isolated on NGM plates (35 mm). The F3 generation was screened for 100% penetrance for the transgenic markers. If not stated otherwise, ER stress in worms was induced by treatment with 5 µg ml^{-1} tunicamycin (Sigma-Aldrich) for 8 h. Dimethyl sulfoxide (DMSO) (v/v) served as solvent control. All worm and bacterial strains that were used in this study are listed in Supplementary Table 1.

Mammalian cell lines

Ago2$^{-/-}$ MEF and *Ago2*$^{+/+}$ MEF cells were a kind gift from Gunter Meister (University of Regensburg). Cells were grown at 37 °C and 5% CO_2 in Dulbecco's modified Eagle medium GlutaMAX (Gibco) supplemented with 10% foetal calf serum and 1% penicillin–streptomycin. Cells were passaged every 3–4 days (at ~80% confluency) by trypsinization with 0.5% trypsin–EDTA. If not stated otherwise, ER stress in cells was induced by treatment with 3 µg ml^{-1} tunicamycin (Sigma-Aldrich) for 4 h. DMSO (v/v) served as solvent control.

Western blotting

For the preparation of whole worm lysates, animals were collected in M9 buffer and washed twice. Worm pellets were stored at −80 °C or used immediately for downstream applications. Worm pellets were resuspended in cooled RIPA buffer (150 mM NaCl, 1% Triton X-100, 0.5% sodium deoxycholate, 0.1% sodium dodecyl sulfate (SDS) and 50 mM Tris (pH 8.0)). Subsequently, samples were boiled at 95 °C for 5 min, sonicated (30 s at 60% amplitude, Bandelin Sonoplus with MS 1.5 sonotrode) and boiled again at 95°C for 5 min. Lysates were cleared by centrifugation (5 min, 21,000 relative centrifugal force (RCF), 4°C) and the protein concentration was determined with the Pierce BCA Protein Assay Kit (Thermo Fisher Scientific). Samples were then mixed with 2× SDS loading buffer. For analysis and size separation of proteins, SDS gel electrophoresis was performed (PAGE)[54]. NuPAGE 4–12% Bis-Tris SDS gels were used with the respective NuPAGE MES SDS running buffer (Thermo Fisher Scientific; settings according to the manufacturer's instructions). For the transfer of proteins to a nitrocellulose membrane (Amersham, Protran 0.2 µm), a semi-dry blotting system (Bio-Rad, Trans-Blot Turbo) was used. Standard transfer was performed with 25 V (constant) for 30 min using NuPAGE transfer buffer, supplemented with 10% methanol. After blotting, the membrane was directly incubated with the respective primary antibody, diluted in 1× Roti-Block (Carl Roth) overnight at 4 °C while constantly shaking. For detection of AGO2, the T22 Mighty Small wet transfer system (Hoefer; 11 V, overnight at 4 °C) with wet transfer buffer (25 mM Tris, 192 mM glycine, 0.01% SDS and 20% methanol) was used. The membrane was blocked with 5% milk powder (Carl Roth) in phosphate-buffered saline (PBS)–Tween (137 mM KCl, 8.1 mM Na_2HPO_4, 1.5 mM KH_2PO_4 and 0.1% (v/v) Tween-20, pH 7.4) for 1 h at RT, before incubation with primary antibodies (in 5% milk powder (Carl Roth) in PBS–Tween) overnight at 4 °C. Subsequently, the membrane was washed three times with PBS–Tween for approximately 10 min. The membrane was further incubated with the respective fluorescently labelled secondary antibody (LI-COR Biosciences) for 1 h at RT and subsequently washed again three times with PBS–Tween for approximately 10 min. Final visualization was performed using the Odyssey scanner (LI-COR Biosciences) and respective software (Image Studio Software v4.0 or v5.0, LI-COR Biosciences). Western blots were quantified using the Image Studio Software v4.0 or 5.0 (LI-COR Biosciences). The antibodies that were used in this study were as follows (see also Supplementary Table 2): mouse monoclonal anti-α-tubulin (B-5-1-2) (Sigma, catalogue number T6074, 1:5,000); mouse monoclonal anti Living Colors (JL-8, anti-GFP) (Clontech Laboratories, catalogue number 632380, 1:5,000); mouse monoclonal anti Living Colors, DsRed (anti-mCherry) (Clontech Laboratories, catalogue number 632393, 1:5,000); anti-CDC-48.1 (Hoppe-lab/Biogenes Berlin, custom antibody, 1:50,000); anti-SEL-1, (Sommer-lab, Berlin, custom antibody, 1:8,000); anti-Ago2 monoclonal (C34C6) (Cell Signaling catalogue number 2897, 1:10,000; anti-α (orsay virus) (Wang-lab, Washington, custom antibody, 1:2,000); IRDye 800CW donkey anti-mouse IgG (H + L) (LI-COR Biosciences, catalogue number 926-32212, 1:10,000); IRDye 800CW donkey anti-rabbit IgG (H + L) (LI-COR Biosciences, catalogue number 926-32213, 1:10,000); IRDye 680 donkey anti-mouse IgG (H + L) (LI-COR Biosciences, catalogue number 962-32222, 1:10,000); IRDye 680 donkey anti-rabbit IgG (H + L) (LI-COR Biosciences, catalogue number 962-32223, 1:10,000).

EMS mutagenesis

A total of 10,000 synchronized L4 larvae (*Pnhx-2::cpl-1^{Y32A,W35A}::yfp*) were washed three times with M9 buffer (20 mM KH_2PO_4, 40 mM Na_2HPO_4, 80 mM NaCl and 1 mM $MgSO_4$) and subsequently incubated with 50 mM EMS while shaking for 4 h at RT. Further, the worms were washed three times with M9 buffer and incubated for 24 h at 20 °C on NGM plates. The microscopy-based selection process for elevated CPL-1* level was performed at the F_2 generation using the Leica M80 fluorescent microscope. Selected worms were outcrossed twice with wild-type N2.

CHX chase assay

Cycloheximide (CHX) interferes with the ribosomal translocation step during protein synthesis and thereby blocks eukaryotic protein translation, which makes it a valuable tool to monitor time-dependent protein degradation rates. NGM plates (90 mm) were coated with 200 µl CHX (50 mg ml^{-1} in ethanol, Sigma-Aldrich) or with 200 µl ethanol and incubated for 30 min at RT. Subsequently the plates were seeded with 1,000 µl *E. coli* OP50 and incubated over night at 37 °C. A total of 400–600 worms each were distributed on each plate and incubated at 20 °C for 0 h, 1 h, 3 h, 6 h and 9 h, respectively. After the incubation time, worms were collected and analysed via western blot and BioSorter. For each timepoint, the treated/untreated (CHX/EtOH) ratio was calculated and normalized by dividing by the 1 h timepoint ratio.

BioSorter quantification of fluorescence

The BioSorter (Union Biometrica) with the FlowPilot-Pro software is a large-particle flow cytometer that allows for the quantification of fluorescence in three different channels 'Red', 'Yellow', 'Green' and parameters such as time-of-flight (TOF) and extinction. TOF, Red and extinction were used for gating of observations, which resembled day 1 adult worms expressing either *cpl-1** or *ATM* exhibiting pharyngeal expression of *Pmyo-2::mCherry* as transgenic marker (Figs. 1b,d and 4a). Unless stated otherwise, after gating (TOF >1,500, Red >300 and extinction >800), the fluorescence values (YFP yellow or GFP green) of at least 200 gated worms from three independent biological replicates were used to calculate mean ± standard deviation (s.d.) values and plot density ridgeline plots (ggplot2 v.3.6.2 and ggridges v.3.6.2). Experiments with smaller *sel-11(nDf59)* mutant worms (Fig. 2b) were gated with (TOF >1200, Red >300 and extinction >600). A graphical illustration of the gating method is presented with a 2d density hexbin plot (hexbin v.1.28.2) in Extended Data Fig. 4a,b.

RNA extraction

Isolation of total RNA was performed using TRIzol (Invitrogen). Age-synchronized worms were collected and washed twice with M9 buffer. Finally, 1 ml of TRIzol was added and worms were frozen at −80 °C for at least 1 h. Subsequently, worms were thawed at 37 °C. Disruption of worms and RNA release was achieved by using silica beads and the Precellys 24-Dual cell homogenizer (Peq-Lab) twice for 20 s at 5,000 rpm. Samples were incubated for 15 min at RT. For RNA extraction from mammalian cells, the growth medium was removed and cells were washed once with PBS. Subsequently, cells were scratched from the culture dish, collected in PBS and pelleted by centrifugation (5 min, 500 RCF, RT). The supernatant was removed, the pellet resuspended in 1 ml TRIzol and samples frozen at −80 °C for at least 1 h. Next, 100 µl 1-bromo-3-chloropropane was added to the cell culture or *C. elegans* samples and centrifuged for 15 min at 8,000 RCF at 4 °C to separate aqueous and organic phase. The aqueous phase was used to isolate total RNA with the RNeasy Mini Kit (Qiagen) following the manufacturer's instructions or by isopropanol–glycogen precipitation. In brief, 1 µl glycogen (10 mg ml^{-1}) and 500 µl of isopropanol was added. The samples were subsequently incubated for 1 h at −80 °C. The samples were further centrifuged for 45 min at 16,000 RCF at 4 °C. The supernatant was removed, and the pellet was washed with 70% ethanol. Then the RNA was air dried and resuspended in nuclease-free water. Quality and concentration of the isolated RNA was measured using the NanoDrop 8000 spectrophotometer (Thermo Fisher Scientific).

cDNA synthesis and qRT–PCR

A total of 1,000–2,000 ng of total RNA was used for cDNA synthesis with the High-Capacity cDNA Reverse Transcription kit (Applied Biosystems) following the manufacturer's instructions. Measurement of cDNA level was performed with Luna Universal qPCR Master Mix (New England Biolabs) and the Bio-Rad CFX96 Real-Time PCR Detection System. Three technical replicates were analysed per sample. As reference for normalization, 18S ribosomal RNA (rRNA) *cdc-42* and *pmp-3* mRNA (*C. elegans*) or *Rpl19* mRNA, 18S rRNA and 28S rRNA (MEF cells) were used. All oligonucleotides that were used in this study are listed in Supplementary Table 3.

α-Amanitin chase assay

Worms of the respective genotypes were L1 synchronized on NGM plates by filtering and exposed at day 1 of adulthood to α-Amanitin (50 µg ml^{-1}, Sigma-Aldrich) in liquid culture (M9 with OP50 bacteria as food source (t = 0 h). For monitoring mRNA degradation for shorter time periods (up to 300 min), 0.1% Triton X-100 was added to the reaction to improve α-Amanitin uptake. Samples were collected in TRIzol after the respective timepoints of the transcriptional block, purified by RNA extraction and cDNA synthesis, and analysed by qRT–PCR for the constructs of interest as described above. For α-Amanitin chase assays in mammalian cells, 160,000 MEF cells were seeded in six-well plates. Two days later, ER stress was induced with 3 µg ml^{-1} tunicamycin (Sigma-Aldrich) for 4 h. Adding only DMSO (v/v) served as solvent control. Next, tunicamycin was removed, α-Amanitin (35 µg ml^{-1}) was added and cells were collected at 0 h, 2 h, 6 h, 10 h and 24 h after treatment in TRIzol, followed by RNA extraction, cDNA synthesis and qRT–PCR.

RNAi

To achieve transient gene depletion, the RNAi feeding method was used[55,56]. Clones encoding the respective gene of interest were either taken from the *C. elegans* RNAi Collection (Ahringer) or the *C. elegans* ORF-RNAi Resource (Vidal)[57], both distributed by Source BioScience. All clones were confirmed to contain the right gene by sequencing. All double knockdowns were performed with a single RNAi vector for high efficiency. In general, overnight cultures of transformed HT115 *E. coli* in LB medium with 100 µg ml^{-1} ampicillin were used as starting culture. A fresh culture was grown until an OD_{600} of approximately 0.8 and subsequently seeded on NGM agar plates containing 100 µg ml^{-1} ampicillin and 2 mM IPTG. Plates were incubated overnight at 37 °C and used for experiments. Age-synchronized worms were transferred to RNAi plates at L1 larval stage.

Viral infection

Five adult worms were placed on an NGM plate. On the following day, worms were removed and hatched eggs were infected with 30 µl of Orsay viral lysate. Orsay lysate was obtained as previously described[25]. On the first day of adulthood, worms were either collected for western blotting of RNA extraction or worms were sorted for infection with the COPAS BioSorter (Union Biometrica) by using the viral reporter *Plys-3*::*gfp*[19]. To study the influence of ER stress on viral infection worms were pre-treated with either 5 µg ml^{-1} tunicamycin or DMSO (solvent control) for 8 h before viral infection.

Cellular fractionation

For cellular fractionation, age-synchronized worms were washed three times with M9 buffer and stored in fractionation buffer (5 M NaCl, 1 M Na_2CO_3, 10% Triton X-100 or 1% SDS) at −80 °C. While proteins associated to ER-derived microsomes are solubilized by sodium chloride (NaCl) or sodium carbonate (Na_2CO_3), resident proteins inside the microsomes are released only by dissolving the ER membrane with detergents such as Triton X-100 or SDS. Samples were thawed on ice and sonicated for 20 s (60% amplitude) and homogenized using a Dounce homogenizer 50 times. Cell lysates were centrifuged two times for 5 min at 2,000 RCF at 4 °C. The supernatant was again centrifuged for 90 min at 20,000 RCF at 4 °C. The pellet was resuspended in 150 µl fractionation buffer, and 30 µl of the sample was supplemented with 3 µl fractionation buffer, respectively. Samples were incubated on ice for 1 h and subsequently centrifuged for 1 h at 20,000 RCF at 4 °C. Pellets and supernatants were separated and analysed via western blotting. Cellular fractionation using sequential detergent fractionation was performed as previously described[58]. Worm lysates were treated with the permeabilization buffer (110 mM KCl, 25 mM K-HEPES, pH 7.4, 1 mM $MgCl_2$, 0.015% digitonin (Calbiochem), 0.1 mM EDTA, 40 units ml^{-1} RNAseOUT (Invitrogen) and 1 mM dithiothreitol) to release the cytosolic content. To release the ER fraction, worm lysates were further washed with ER fractionation buffer (2% dodecyl-maltoside, 200 mM KCl, 25 mM K-HEPES, pH 7.4, 10 mM $MgCl_2$, 40 units ml^{-1} RNAseOUT and 2 mM dithiothreitol). Subsequently, samples were subjected to RNA extraction followed by qRT–PCR.

Northern blotting

Denaturing RNA gel electrophoresis was performed using a 1% agarose gel (supplemented with 4% formaldehyde and 5% 20× TT (0.6 M tricine and 0.6 M triethanolamine). Total RNA was added to 16 µl of northern sample buffer (100 µl 20× TT, 4 µl 0.5 M EDTA, pH 8.0, 70 µl de-ionized formamide, 70 µl non-acidic formaldehyde (37%), 5 µl 0.07% ethidium bromide), heated for 15 min at 65 °C and immediately chilled on ice for 2 min. Before loading, 2 µl of RNA loading dye (1 mM EDTA, 50% glycerol and 0.25% bromophenol blue) was added to each sample. The gel was run at 150 V in 1× TT buffer for 3–4 h on ice. After RNA gel electrophoresis, 18S and 28S rRNA was imaged as gel loading control. Then, the separated RNA molecules were blotted on a neutral nylon membrane. After brief washing with H_2O, the capillary transfer was set up for at least 4 h using 10× saline-sodium citrate (SSC) (1.5 M NaCl and 150 mM trisodium citrate, pH 7.0) as a transfer medium. Subsequently, the RNA was UV-crosslinked to the membrane at 254 nm (120 mJ cm^{-2}, on both sides), followed by membrane pre-hybridization in Church buffer (0.5 M Na_2HPO_4, 1 mM EDTA and 7% SDS, pH 7.2) at 65 °C for 1 h. Further, the Church buffer was exchanged to 25 ml Church buffer supplemented with 25 µl ^{32}P-labelled

RNA probes directed against the corresponding sequences of the *cpl*-1 mRNA (5′-AGGAATGCTCATCCGAAGAGCTCGACCACGGAGTGCT TCTCGTCGGATACGGAACCGACCCAGAGCACGGAGAC TACTGGATTGT-3′) and the 5.8S rRNA (5′-CTAGCTTCAGCGATGGATCG GTTGCATCGAGTATCGATGAAGAACGCA GCTTGCTGCGTTACTTACCACGAATTGCAGACGCTTAG AGTGGTGAAATTTCGAACGCATAGCACCAACTGGGCCTCC AGTTGGTACGTCTGGTTCAGGGTTGTT-3′). On the next day, the probe was removed from the membrane followed by washing twice with Northern wash buffer 1 (2× SSC and 0.1% SDS) and two wash steps with Northern wash buffer 2 (0.2× SSC and 0.1% SDS) at 65 °C for 15 min each. Subsequently, the membranes were air-dried for 40 min, covered with an imaging plate and exposed for 4 h at RT. The autoradiography signal was detected by using the Thyphoon FLA700 phosphoimager (GE Healthcare) and quantified with the ImageQuant TL, 1D and Array Image Analysis Software (GE Healthcare). For generation of the RNA probes, 150 ng linearized pGEM-4Z plasmid (Promega), containing the respective probe sequence, was in vitro transcribed using and SP6 RNA polymerase (New England Biolabs) according to the manufacturer's instructions. The transcription reaction, supplemented with α-^{32}P-GTP (Hartmann Analytics), was incubated for 40 min at 40 °C. Further, 1.5 µl RNAse-free DNAse I (2 units µl^{-1}, New England Biolabs) was added, followed by incubation for 20 min at 37 °C. Subsequently, 28 µl ultrapure H_2O was added and labelled transcripts were recovered using the mini-Quick Spin RNA Columns (Roche) following the manufacturer's instructions. Finally, 25 µl of the probe was mixed with 25 ml Church buffer (1:1,000).

RNA sequencing and analysis

Determination of mRNA expression was done by sequencing. Age-synchronized day 1 adult hermaphrodites were collected for isolation of total RNA from *C. elegans*. For cell culture experiments, *Ago2*$^{-/-}$ and *Ago2*$^{+/+}$ MEF cells were seeded into 150 cm^2 flasks for collection of samples. After a 3 day growth (to around 70% confluency), either cells were left untreated or ER stress was induced by adding 3 µg ml^{-1} tunicamycin (Sigma-Aldrich) or 500 nM thapsigargin (Sigma-Aldrich) for 6 h. RNA isolation procedure was performed as described above. Total RNA (2 µg, 50–200 ng µl^{-1}, $OD_{260/280}$ 1.8–2.1 and $OD_{260/230}$ >1.5) was sent to the Cologne Center of Genetics (University of Cologne). Quality control and sequencing was performed by the Cologne Center of Genetics. Raw reads were mapped to reference transcriptomes (Ensemble release 91) using HISAT2, and after guided transcriptome assembly with StringTie, quantification and differential expression was performed with Cufflinks. Calculation of *P* values in Cufflinks is performed with two-sided test for significance. In case a transcript has zero fragments in one condition, a one-sided test is performed. Cufflinks uses the Benjamini–Hochberg technique to correct for multiple testing. Hierarchical clustering of *z*-score-normalized FPKM (mean of each three replicates per strain or condition) was computed with R package ComplexHeatmap (version 2.4.2) with default settings[59]. Differential expression was visualized by scatterplots generated by ggplot2 (version 3.3.2). *z*-Score normalization and table organization were conducted with R Studio (version 4.0.3) using dplyr (version 1.0.2) and tidyr (1.1.0) packages. For GO analysis, GO PANTHER v.16.0 overrepresentation test was performed, with the respective ensemble gene IDs that were extracted from the UniProtKB UniRef90 database. We used the total list of transcripts in each experiment as the reference list for the GO PANTHER test. PANTHER calculates raw *P* values with the Fisher's exact test and corrects for multiple comparison by the Benjamini–Hochberg procedure yielding the FDR value, which is displayed in Figs. 3b, 4f and 5d. *FDR <0.05; ** FDR <0.01; *** FDR <0.001; NS, FDR >0.05. The respective FASTA protein sequences were fetched from the UniProtKB UniRef90 database and were submitted to the BUSCA subcellular localization analysis tool[30]. All RNA sequencing, GO term and BUSCA analysis results are summarized in Supplementary Table 4.

RNA–UV crosslink immunoprecipitation (RNA–CLIP)

For CLIP cell culture experiments *Ago2*$^{-/-}$ and *Ago2*$^{+/+}$ MEF cells were seeded into 150 cm^2 flasks for collection of samples. After a 3 day growth (to around 70% confluency), cells were treated with tunicamycin (4 h, 3 µg ml^{-1}, Sigma-Aldrich), UV-crosslinked (Stratalinker UV Crosslinker 1800), 150,000 µJ cm^{-2} on ice, washed in ice cold PBS, pelleted by centrifugation (5 min, 450 RCF) and stored at −80 °C. For immunoprecipitation (IP), the samples were thawed on ice and supplied with 1 ml of lysis buffer (50 mM Tris–HCl, 100 mM NaCl, 1% MP-40 (IGEPAL), 0.1% SDS and 0.5% sodium deoxycholate, pH 7.4) with freshly added protein inhibitor cocktail and RNase inhibitor according to the instructions of the manufacturer. The samples were resuspended in lysis buffer and lysed using a syringe with a 23 gauge and incubated 15 min on ice. The samples were sonicated in the Bioruptor (Diagenode) for 10 min with ten pulses of 30 s on and off. Two microlitres of TurboDNase (2 units µl^{-1}, Thermo Fisher Scientific) was added, and the samples were shaken for 5 min at 37 °C and 1,200 rpm and subsequently centrifuged at 21,000 RCF for 15 min at 4 °C. After centrifugation, 2% of the total volume of the supernatant was put aside for RNA extraction and western blot analysis, respectively (input control, before IP). For the IP, 50 µl Dynabeads (Thermo Fisher Scientific) were coupled with 20 µl Ago2 antibody (Anti-Ago2 monoclonal (2D4), Fujifilm Wako Chemicals, catalogue number 014-22023) and rotated for 1 h at 4 °C. The coupled magnetic Dynabeads® were then added to the samples and rotated overnight at 4 °C. The tubes were placed on the respective magnet tray to bind the magnet tubes at the side of the tube. Again, 20 µl of the supernatant was put aside for RNA extraction and western blot analysis, respectively (input control, after IP). The samples were washed three times with cold wash buffer (20 mM Tris–HCl, 10 mM $MgCl_2$ and 0.2 Tween-20, pH 7.4) and resuspended in 100 µl wash buffer afterwards. Ten microlitres of each sample was put aside for western blot analysis, and 700 µl of TRIzol was added to the samples. RNA extraction was conducted with isopropanol–glycogen precipitation as described above, followed by qRT–PCR against the targets *Nov*, *Mertk*, *C1rl* and *Rpl19*. All antibodies that were used in this study are listed in Supplementary Table 2.

Colony formation assay

We conducted a colony formation assay as described previously by Crowley et al.[60]. In brief, MEF cells were treated with tunicamycin for 4 h and collected by trypsinization. Treated cells were then seeded in six-well plates (800 cells per well) and incubated for 7 days. For staining of colonies, cells were first fixed with 100% methanol (20 min, RT) and rinsed with water. Then, colonies were stained with crystal violet solution (0.5% crystal violet (w/v) in 25% methanol) for 5 min at RT and again rinsed with water. Afterwards, plates were air-dried and imaged using a standard document scanner. Colonies were counted using the cell counter plugin of the ImageJ (1.48 v) software.

Intestinal barrier function assay (Smurf assay)

Age-synchronized animals were grown on *E. coli* OP50 until day 5 of adulthood. On these days, about 30 worms were removed from NGM plates and washed once with M9 buffer. Animals were incubated rotating for 4 h at RT in liquid culture containing 100 µl blue food dye (50 µl 3× concentrated *E. coli* OP50 overnight culture in LB medium; 50 µl 5% w/v Brilliant Blue FCF (Sigma-Aldrich) in H_2O) and 400 µl M9 buffer. After incubation, animals were washed twice with M9 buffer and collected by gravity settling. Subsequently, worms were transferred to agar pads on glass slides, paralysed with 25 mM levamisole (Sigma-Aldrich) and imaged with the Leica SCN400 slide scanner at 40×× magnification. Images were further processed using the Leica Aperio ImageScope software (v12.4.3.5008).

Microscopy

C. elegans work was generally performed using the M80 stereomicroscope with a CLS150× light source (Leica Camera). Fluorescent images

were achieved using the M165 FC stereomicroscope with DFC 340 FX camera (Leica Camera) or the Axio Zoom V16 microscope with the Axiocam 506 mono camera (Carl Zeiss Microscopy GmbH). For imaging of ER structures in *C. elegans*, the confocal microscope TCS SP8 gSTED 3X (Leica Microsystems) was used. To immobilize worms for imaging, animals were treated with 25 mM levamisole (Sigma-Aldrich). Quantification of mCherry-HDEL foci was achieved with the ImageJ (1.48 v) software. If not stated otherwise, day 1 adult worms were imaged.

Quantification, statistical analysis and reproducibility

Statistical details of experiments are described in the legends of the figures in which the relevant results are presented. Statistical analysis was performed using GraphPad Prism 5 and 7. In general, statistical significance was calculated with two-tailed paired Student's *t*-test or one-way/two-way analysis of variance (ANOVA) with post-hoc test. The half-maximal inhibitory concentration (IC_{50}) for tunicamycin treatment in MEF cells was determined with GraphPad Prism 7 using a three-parameter inhibitor versus response non-linear regression calculation (Fig. 5g). Unless stated otherwise, statistical analysis of BioSorter experiments was performed by two-sided pairwise *t*-test of mean values calculated on three independent biological experiments with each entailing at least 200 gated day 1 adult worms per experiment. *P* values were adjusted for multiple comparisons with Holmes method. All representative microscopy images and gel blots were performed in $n = 3$ independent experiments. No statistical method was used to pre-determine sample size. No data were excluded from the analyses. The experiments were not randomized, and the investigators were not blinded to allocation during experiments or outcome assessment.

Reporting summary

Further information on research design is available in the Nature Portfolio Reporting Summary linked to this article.

Data availability

Plasmids and *C. elegans* lines generated in this study will be distributed to other researchers upon request. RNA-sequencing data that support the findings of this study have been deposited in the Gene Expression Omnibus (GEO) under accession codes GSE202291 and GSE161121. Source data are provided with this paper. All other data supporting the findings of this study are available from the corresponding author on reasonable request. The UniProtKB UniRef90 database was used for GO PANTHER and BUSCA bioinformatic analysis.

References

52. Brenner, S. The genetics of *Caenorhabditis elegans*. *Genetics* **77**, 71–94 (1974).
53. Stiernagle, T. Maintenance of *C. elegans*. *WormBook* https://doi.org/10.1895/wormbook.1.101.1 (2006).
54. Laemmli, U. K. Cleavage of structural proteins during the assembly of the head of bacteriophage T4. *Nature* **227**, 680–685 (1970).
55. Timmons, L. & Fire, A. Specific interference by ingested dsRNA. *Nature* **395**, 854 (1998).
56. Timmons, L., Court, D. L. & Fire, A. Ingestion of bacterially expressed dsRNAs can produce specific and potent genetic interference in *Caenorhabditis elegans*. *Gene* **263**, 103–112 (2001).
57. Rual, J.-F., Hill, D. E. & Vidal, M. ORFeome projects: gateway between genomics and omics. *Curr. Opin. Chem. Biol.* **8**, 20–25 (2004).
58. Jagannathan, S. et al. Multifunctional roles for the protein translocation machinery in rna anchoring to the endoplasmic reticulum. *J. Biol. Chem.* **289**, 25907–25934 (2014).
59. Gu, Z., Eils, R. & Schlesner, M. Complex heatmaps reveal patterns and correlations in multidimensional genomic data. *Bioinformatics* **32**, 2847–2849 (2016).
60. Crowley, L. C., Christensen, M. E. & Waterhouse, N. J. Measuring survival of adherent cells with the colony-forming assay. Cold Spring Harb. Protoc. https://doi.org/10.1101/pdb.prot087171 (2016).

Acknowledgements

We thank the Caenorhabditis Genetics Center (funded by NIH Office of Research Infrastructure Programs (P40 OD010440), the ORFM knockout consortium, the Dana-Farber Cancer Institute, Addgene and Geneservice Ltd; A. Antebi, G. Hannon, T. Hayman, E. Jarosch, G. Meister, D. Ron, G. A. Silverman, T. Sommer and D. Wang for antibodies, cDNAs, plasmids, Orsay virus, cells and worm strains; and G. Stellbrink for technical help. We thank the CECAD Imaging facility for support with confocal microscopy and the Cologne Center for Genomics for RNA-sequencing. We also thank A. Franz, G. Riddihough, J. Riemer and D. Vilchez for comments. This work was funded by the Deutsche Forschungsgemeinschaft (DFG, German Research Foundation) under Germany´s Excellence Strategy (EXC 2030) 390661388, FKZ: ZUK81/1; and by the European Research Council (ERC-CoG-616499) to T.H. S.E. received support by the Cologne Graduate School of Aging Research. N.C. is supported by an Alexander von Humboldt Foundation postdoctoral fellowship.

Author contributions

S.E., F.O. and L.-S.S. designed, performed and analysed the experiments. L.-S.S. performed and analysed the RNA-sequencing data together with J.B., S.E. and S.R. A.G. performed the EMS screen. N.C. and S.E. performed the CHX chase assays. T.H. supervised the experimental design and data interpretation. S.E., F.O., L.-S.S. and T.H. wrote the manuscript. All authors (S.E., F.O., L.-S.S, S.R., N.C., A.G., J.L.P., N.H.G., E.A.M., J.B. and T.H.) discussed the results and commented on the manuscript.

Funding

Open access funding provided by Universität zu Köln.

Competing interests

The authors declare no competing interests.

Additional information

Extended data is available for this paper at https://doi.org/10.1038/s41556-022-01025-4.

Supplementary information The online version contains supplementary material available at https://doi.org/10.1038/s41556-022-01025-4.

Correspondence and requests for materials should be addressed to Thorsten Hoppe.

Peer review information *Nature Cell Biology* thanks Cole Haynes and the other, anonymous, reviewer(s) for their contribution to the peer review of this work.

Reprints and permissions information is available at www.nature.com/reprints.

https://doi.org/10.1038/s41556-022-01025-4

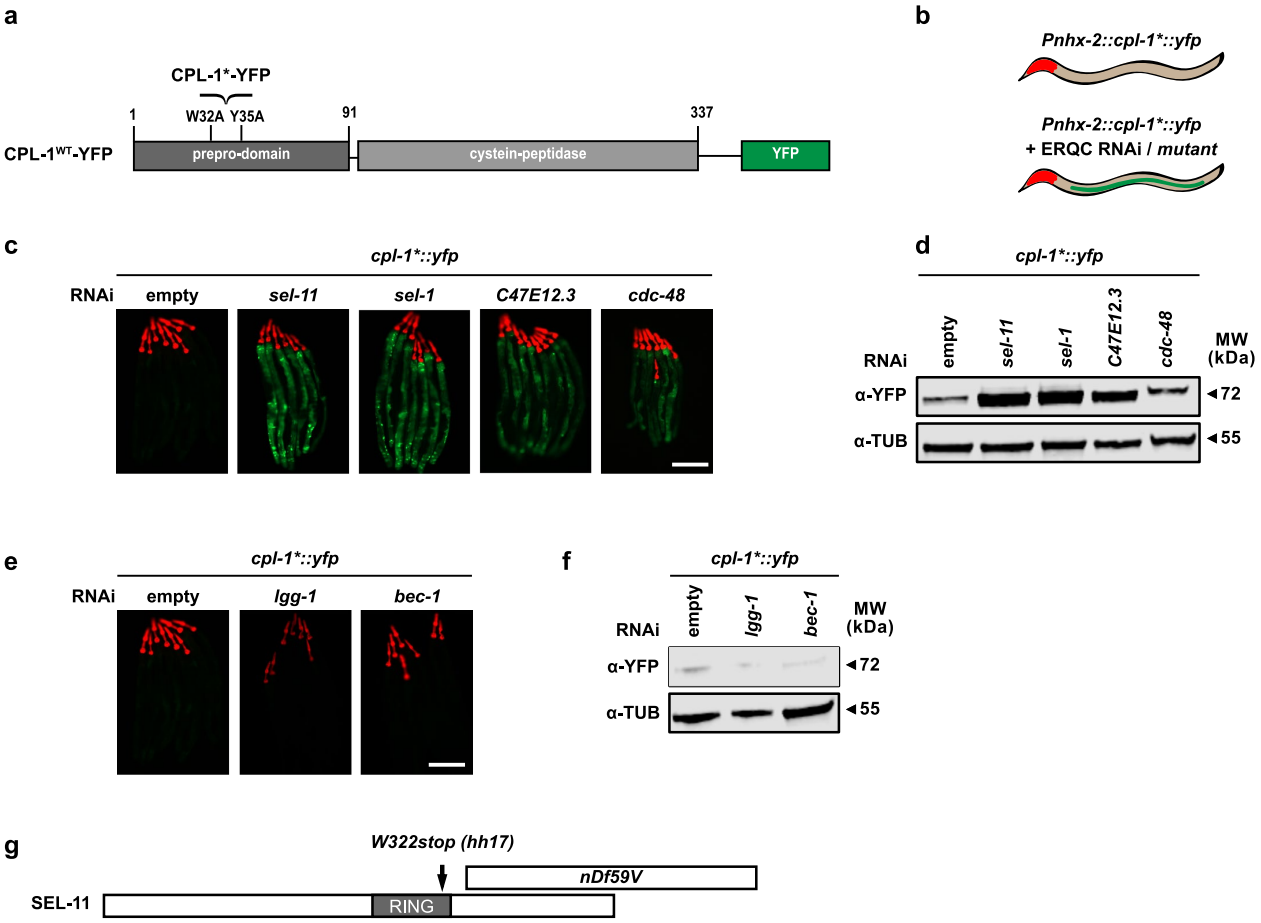

Extended Data Fig. 1 | CPL-1* model substrate to monitor ER quality control in *C. elegans*. (**a**) Schematic overview of mutations inserted into the CPL-1^{WT} encoding transgene for expression of the CPL-1* ERAD substrate. (**b**) Schematic overview of the CPL-1* model substrate for studying ERQC. (**c**) Fluorescence images of worms with mutations in ERAD components expressing *cpl-1**; C47E12.3 (EDEM-1 homologue), empty vector (empty). (**d**) Western blot of worm lysates corresponding to samples shown in (c), detecting CPL-1* (YFP) and tubulin (TUB). (**e**) Fluorescence images of worms expressing *cpl-1** with defects in autophagy. (**f**) Western blot of worm lysates corresponding to the samples in (e), detecting CPL-1* (YFP) and tubulin (TUB). (**g**) Schematic overview of different *sel-11* alleles used in this study; *nDf59*: deletion allele, *hh17*: Introduction of a stop codon at amino acid position 322 of the SEL-11 protein. [(c), (e)] Pharyngeal expression of *Pmyo-2::mCherry* serves as transgenic marker. Scale bar: 200 µm. WT: wild-type. Unprocessed blots are available in the source data.

https://doi.org/10.1038/s41556-022-01025-4

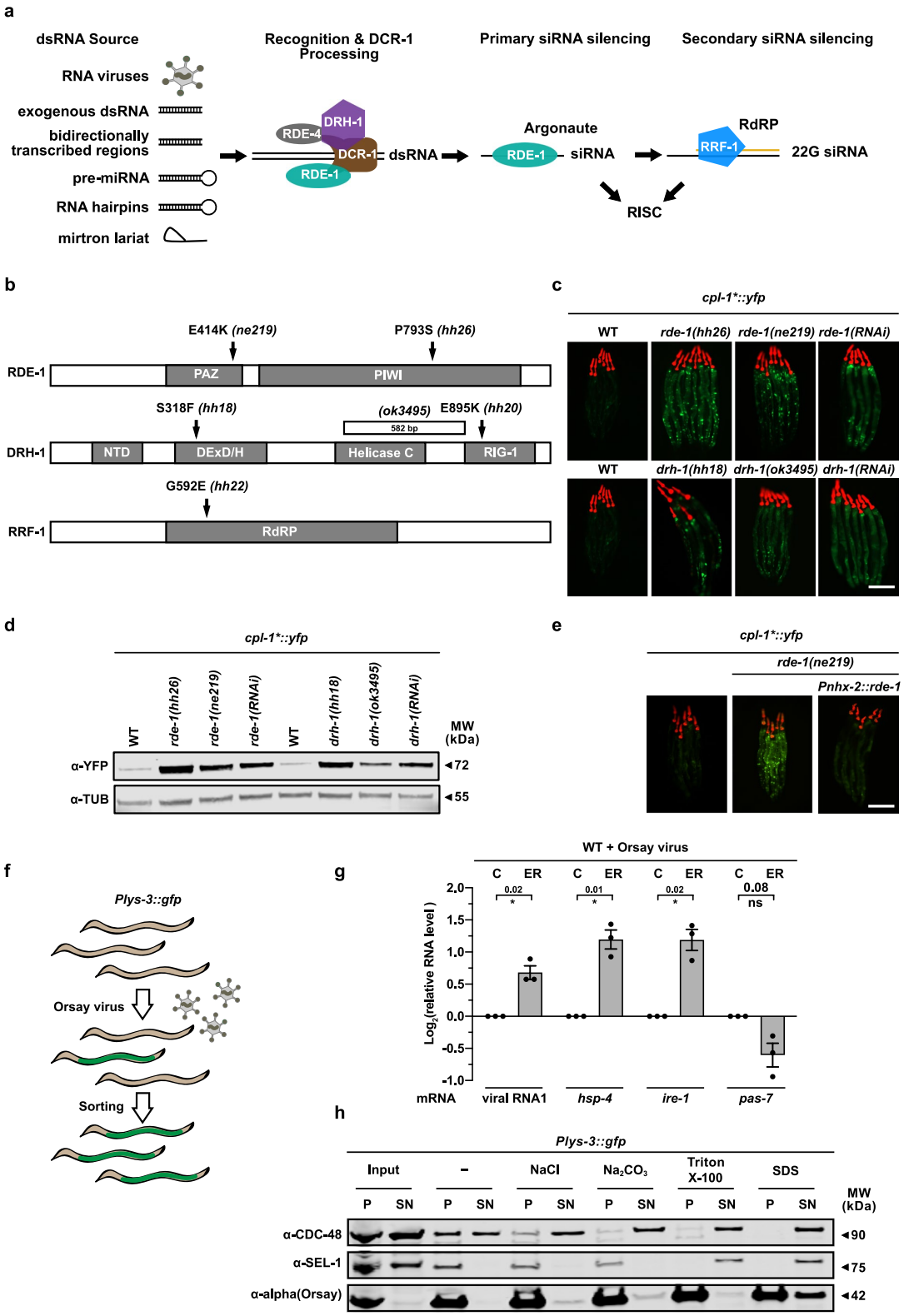

Extended Data Fig. 2 | See next page for caption.

https://doi.org/10.1038/s41556-022-01025-4

Extended Data Fig. 2 | Exogenous RNAi pathway mutants accumulate the CPL-1* protein. (**a**) Scheme of the exogenous RNAi pathway, detecting double stranded RNA (dsRNAs) species from various sources. RDE-4 and DRH-1 are involved in dsRNA recognition, whereas DCR-1 cleaves these RNAs into primary small interfering or micro RNAs (siRNAs/miRNA). These small RNA species are either used for primary siRNA silencing by RDE-1 or engage RDE-1-dependently in amplification by the RNA-dependent RNA polymerase (RdRP) RRF-1. RRF-1 generates secondary siRNAs for potent secondary siRNA silencing. Eventually, siRNAs and their complementary target mRNAs are loaded into the RNA-induced silencing complex (RISC) mediating target mRNA silencing. (**b**) Schematic overview of loss-of-function alleles of *rde-1, drh-1, and rrf-1*. *ne219, hh26, hh18, hh20, hh22*: amino acid substitutions; *ok3495*: deletion allele. NTD: N-terminal domain, RdRP: RNA-dependent RNA polymerase. (**c**) Fluorescence images of worms defective in the exogenous RNAi pathway expressing *cpl-1**. (**d**) Western blot of worm lysates corresponding to samples shown in (c), detecting CPL-1* (YFP) and tubulin (TUB). (**e**) Fluorescence images of *rde-1(ne219)* worms and animals with intestinal *Pnhx-2::rde-1* rescue expressing *cpl-1**. (**f**) Schematic overview of Orsay virus infection in worms expressing the viral infection reporter *Plys-3::gfp*. Infected worms can be detected and sorted by the green fluorescent signal. (**g**) Cellular fractionation of cytosolic (C) and ER fraction (ER) with subsequent RNA purification. Relative mRNA level measured by qRT-PCR. (**h**) Cellular fractionation of microsomes. Western blot detecting SEL-1 (SEL-1), CDC-48 (CDC-48), and Orsay virus alpha capsid protein (alpha (Orsay)). Pellet (P) and supernatant (SN) fractions of *Plys-3::gfp* worm lysates treated with the indicated chemicals after subcellular fractionation. [(c), (e)] Pharyngeal expression of *Pmyo-2::mCherry* serves as transgenic marker. Scale bar: 200 µm. (g) was analyzed by unpaired two-tailed t-tests. Values are depicted as mean ± SEM generated from n = 3 independent experiments, *$p < 0.05$, ns $p > 0.05$. WT: wild-type. Source numerical data and unprocessed blots are available in source data.

https://doi.org/10.1038/s41556-022-01025-4

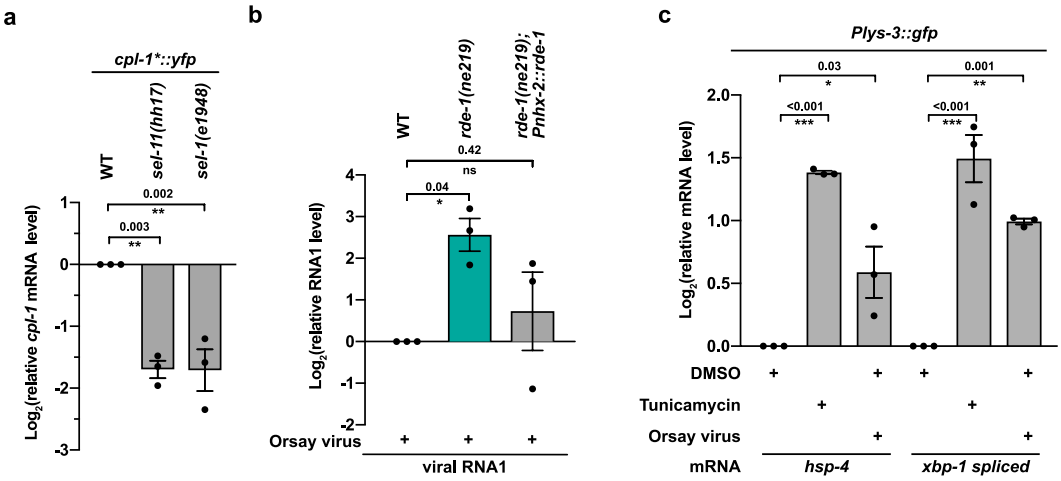

Extended Data Fig. 3 | The exogenous RNAi pathway degrades viral RNA. (**a**) *cpl-1* mRNA level measured by qRT-PCR in worms depleted of the ERAD components *sel-1* or *sel-11*. (**b**) Viral RNA1 level measured by qRT-PCR in *rde-1(ne219)* worms and animals with intestinal *Pnhx-2*::*rde-1* expression. (**c**) *hsp-4* and spliced *xbp-1* mRNA level measured by qRT-PCR in worms infected with the Orsay virus or treated with tunicamycin. [(a)-(c)] were analyzed by one-way ANOVA with Sidak's multiple comparison test. Data are relative to 18 S rRNA. Values are depicted as mean ± SEM generated from n = 3 independent experiments, *p < 0.05, **p < 0.01, ***p < 0.001, ns p > 0.05. WT: wild-type. Source numerical data are available in source data.

https://doi.org/10.1038/s41556-022-01025-4

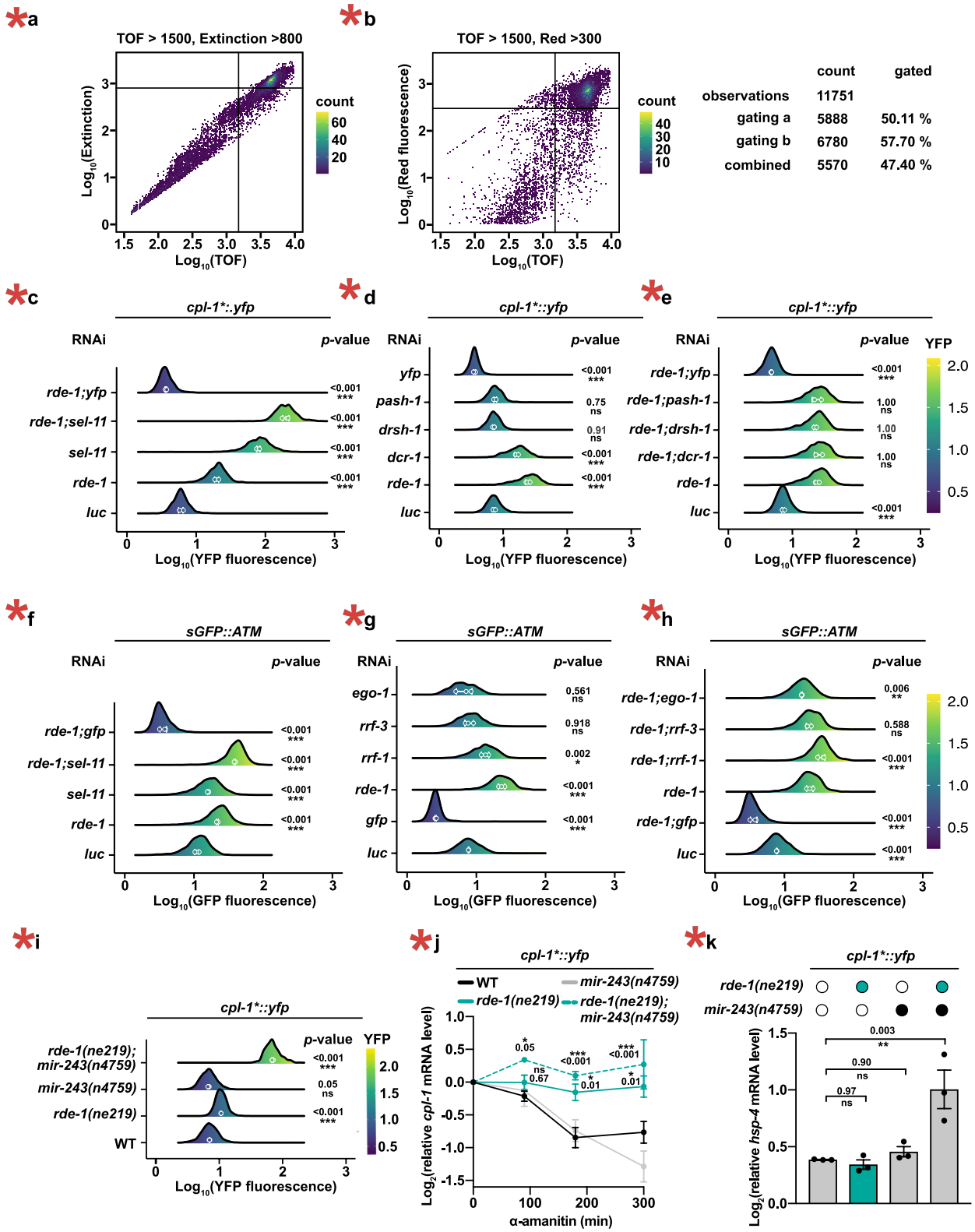

Extended Data Fig. 4 | See next page for caption.

https://doi.org/10.1038/s41556-022-01025-4

Extended Data Fig. 4 | DCR-1 processed dsRNA species and RRF-1 are associated with ERAS. (**a, b**) 2d density hexbin plot (bins = 200) of all Biosorter® raw observations measured in Extended Data Fig. 4c, exemplifying the combined gating method of TOF, Extinction and Red fluorescence, which gates for day 1 adult worms co-expressing either the *ATM* or *cpl-1** reporter with the pharyngeal *Pmyo-2::mCherry* (Red) transgenic marker (**c-e**) Quantification of YFP fluorescence intensity of *cpl-1** expressing worms in RNAi treatments against ERAS and ERAD (c), miRNA maturation and dsRNA processing (d, e). *luc*: luciferase. (**f-h**) Quantification of GFP fluorescence intensity of *ATM* expressing worms in RNAi treatments against ERAS and ERAD (f) and secondary siRNA silencing (**g**). (**i**) Quantification of YFP fluorescence intensity of *cpl-1** expressing worms with lof mutations for ERAS and/or *mir-243*. (**j**) Alpha-amanitin chase assays against *cpl-1** mRNA in *cpl-1** expressing worms with lof mutations for ERAS and/or *mir-243*, measured by qRT-PCR. Data relative to *cdc-42* and *pmp-3* mRNA. (**k**) *hsp-4* mRNA level measured by qRT-PCR in *cpl-1** expressing worms with lof mutations for ERAS and/or *mir-243*. Data relative to *cdc-42* and *pmp-3* mRNA. [(c)-(i)] Measurements were carried out with the BioSorter® using at least 200 animals per replicate, which were merged and displayed in ridgeline density plots. [(c)-(i)] were analyzed by pairwise t-test with Holmes multiple comparison test. (j) was analyzed by a two-way ANOVA with Sidak´s multiple comparison test. (k) was analyzed by one-way ANOVA with Dunnett's multiple comparison test. Values are depicted as mean ± SEM [(j), (k)] or as mean (white circles) ± SD (white error bars) [(c)-(i)] generated from n = 3 independent experiments, *p < 0.05, **p < 0.01, ***p < 0.001, ns p > 0.05. WT: wild-type. Source numerical data are available in source data.

https://doi.org/10.1038/s41556-022-01025-4

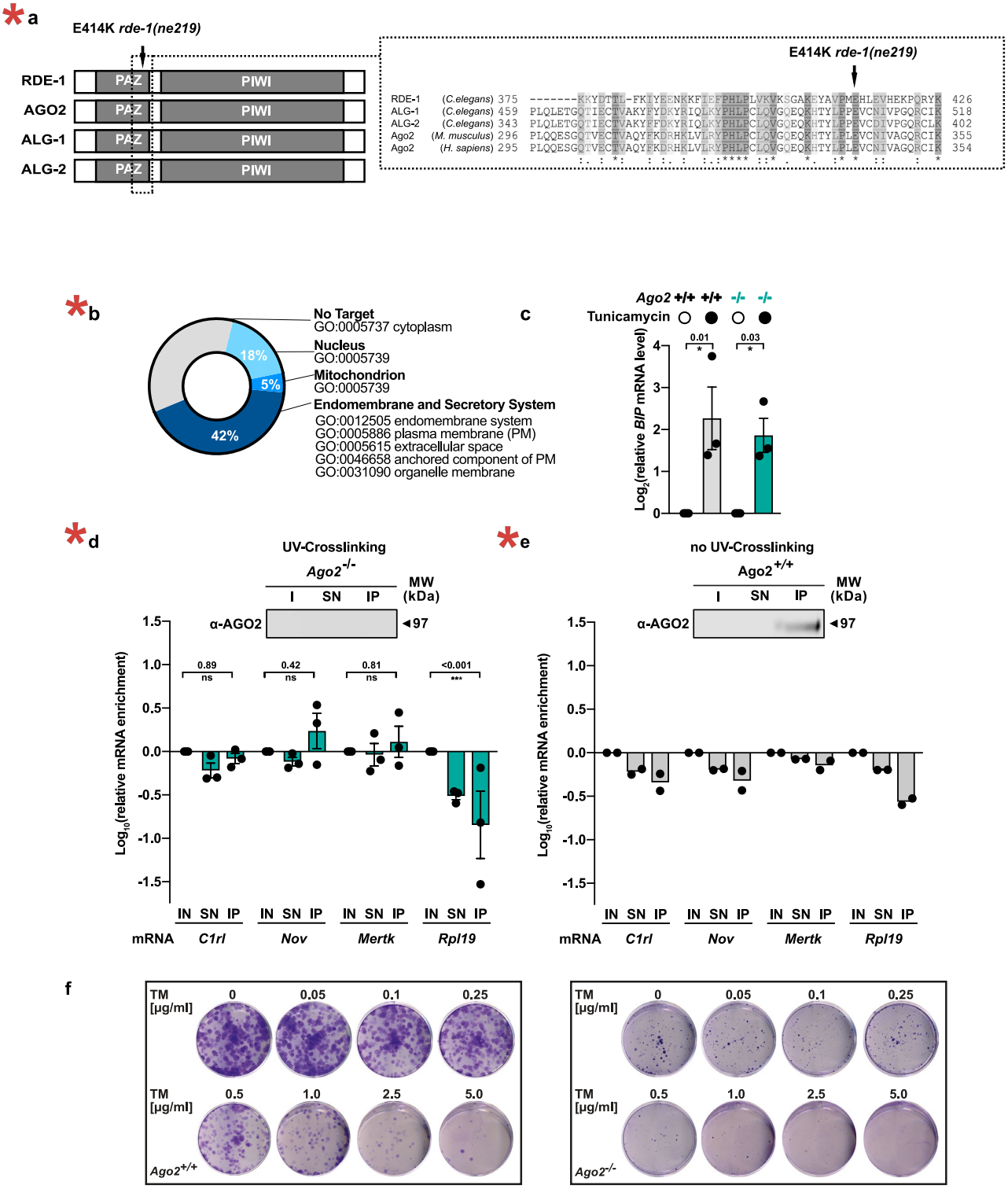

Extended Data Fig. 5 | See next page for caption.

Extended Data Fig. 5 | AGO2 binds to endogenous mRNAs and supports ER stress resistance. (**a**) Schematic illustration of PAZ-PIWI domain containing Argonaute proteins of *C. elegans* (RDE-1, ALG-1, ALG-2) and mammals (AGO2) showing the cross-species conservation of E414 in the PAZ domain, which is mutated to a lysine residue in the E414K mutation of the *rde-1(ne219)* allele. Aasterisk (*) indicates single conserved residues.:(colons) indicate conservation between groups of strongly similar properties, scoring >0.5 in the Gonnet PAM 250 matrix. Period (.) indicates conservation between groups of weakly similar properties, scoring = <0.5 in the Gonnet PAM 250 matrix. The alignment was performed by Clustal-Omega. (**b**) Genes identified in Fig. 5a-c were subjected to BUSCA subcellular localization analysis, showing a targeting of the obtained mRNAs to the endomembrane and secretory system. Results of the BUSCA analysis are summarized in Supplementary Table 4. **(c)** *BiP* mRNA level measured by qRT-PCR at the 0 h timepoint corresponding to the samples shown in Fig. 5h-k. Data relative to 18 S and 28 S rRNA. (**d, e**) Negative control experiments related to UV cross-linking immunoprecipitation (CLIP) experiments in Fig. 5f. CLIP of tunicamycin-treated $Ago2^{-/-}$ (d) or in $Ago2^{+/+}$ MEF cells but without UV cross-linking (e). AGO2 was used as bait with subsequent qRT-PCR against *C1rl*, *Nov*, and *Mertk* target mRNAs in the input (IN), supernatant (SN) and immunoprecipitation (IP) fractions. Data normalized to input fraction. Top panels show western blots against AGO2 for the performed CLIP experiment. (**f**) Images of tunicamycin (TM)-treated $Ago2^{+/+}$ and $Ago^{-/-}$ cell colonies stained with crystal violet. (c) was analyzed by unpaired two-tailed t-tests, [(d), (e)] were analyzed by a two-way ANOVA with Dunnett's multiple comparison test. [(c), (d), (e)] Values are depicted as mean ± SEM generated from n = 3 [(c), (d)] or n = 2 (e) independent experiments, *$p < 0.05$, ***$p < 0.001$, ns $p > 0.05$. Source numerical data and unprocessed blots are available in source data.

https://doi.org/10.1038/s41556-022-01025-4

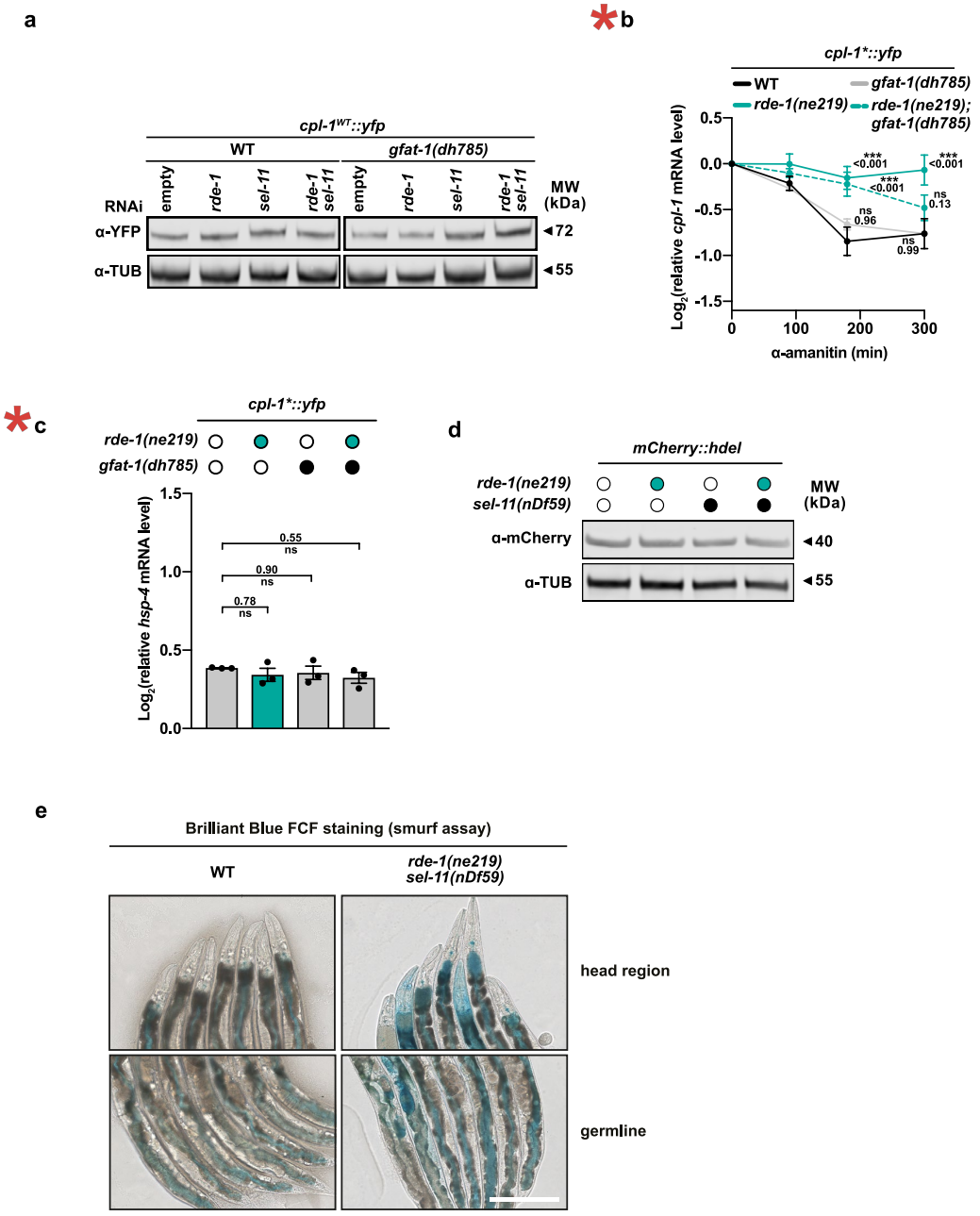

Extended Data Fig. 6 | ERAS and ERAD maintain ER quality control and intestinal integrity. (**a**) Western blot of worm lysates from worms depleted for ERAS and/or ERAD components expressing *cpl-1*^{WT} in the WT (wild-type) or *gfat-1* gain-of-function background detecting CPL-1^{WT} (YFP) and tubulin (TUB). (**b**) Alpha-amanitin chase assays against *cpl-1** mRNA from ERAS mutants and/or animals carrying a *gfat-1* gain-of-function mutation expressing *cpl-1**, measured by qRT-PCR. (**c**) *hsp-4* mRNA level measured by qRT-PCR at the 0 h time point corresponding to the samples shown in (b). (**d**) Western blot of worm lysates corresponding to the data shown in Fig. 6e detecting mCherry::HDEL (mCherry) and tubulin (TUB). (**e**) Images showing the head and germline region of worms with the indicated genotypes after soaking in blue food dye (Brilliant Blue FCF). Blue dye leaking from the intestinal lumen into the body cavity gives rise to the Smurf phenotype. Scale bar: 200 µm. [(b), (c)] Data relative to *cdc-42* and *pmp-3* mRNA. (b) was analyzed by two-way ANOVA with Dunnett's multiple comparison test, (c) was analyzed by one-way ANOVA with Sidak's multiple comparison test. [(b), (c)] Values are depicted as mean ± SEM generated from n = 3 individuals, ***p < 0.001, ns p > 0.05. Source numerical data and unprocessed blots are available in source data.

nature portfolio

Corresponding author(s): Prof. Dr. Thorsten Hoppe

Last updated by author(s): 28.09.2022

Reporting Summary

Nature Portfolio wishes to improve the reproducibility of the work that we publish. This form provides structure for consistency and transparency in reporting. For further information on Nature Portfolio policies, see our Editorial Policies and the Editorial Policy Checklist.

Statistics

For all statistical analyses, confirm that the following items are present in the figure legend, table legend, main text, or Methods section.

n/a	Confirmed	
☐	☒	The exact sample size (*n*) for each experimental group/condition, given as a discrete number and unit of measurement
☐	☒	A statement on whether measurements were taken from distinct samples or whether the same sample was measured repeatedly
☐	☒	The statistical test(s) used AND whether they are one- or two-sided *Only common tests should be described solely by name; describe more complex techniques in the Methods section.*
☒	☐	A description of all covariates tested
☐	☒	A description of any assumptions or corrections, such as tests of normality and adjustment for multiple comparisons
☐	☒	A full description of the statistical parameters including central tendency (e.g. means) or other basic estimates (e.g. regression coefficient) AND variation (e.g. standard deviation) or associated estimates of uncertainty (e.g. confidence intervals)
☐	☒	For null hypothesis testing, the test statistic (e.g. *F*, *t*, *r*) with confidence intervals, effect sizes, degrees of freedom and *P* value noted *Give P values as exact values whenever suitable.*
☒	☐	For Bayesian analysis, information on the choice of priors and Markov chain Monte Carlo settings
☒	☐	For hierarchical and complex designs, identification of the appropriate level for tests and full reporting of outcomes
☒	☐	Estimates of effect sizes (e.g. Cohen's *d*, Pearson's *r*), indicating how they were calculated

Our web collection on statistics for biologists contains articles on many of the points above.

Software and code

Policy information about availability of computer code

Data collection	Image Studio Software v4.0 or v5.0, LI-COR Biosciences Bio-Rad CFX Manager Software 3.1 FlowPilot-Pro™ (v1)

Data analysis	Image Studio Software v4.0 or v5.0, LI-COR Biosciences Bio-Rad CFX Manager Software 3.1 FlowPilot-Pro™ (v1) ImageQuant TL 10.2 (GE Healthcare) GO PANTHER v.16.0 ImageJ (1.48v) Leica Aperio ImageScope software v12.4.3.5008 R Studio (version 4.0.3) R pipelines HISAT2, StringTie and Cufflinks R package ComplexHeatmap (version 2.4.2) R package ggplot2 (version 3.3.2). R package dplyr (version 1.0.2) R package tidyr (1.1.0) R package ggplot2 v.3.6.2 R package ggridges v.3.6.2 R package hexbin v.1.28.2

For manuscripts utilizing custom algorithms or software that are central to the research but not yet described in published literature, software must be made available to editors and reviewers. We strongly encourage code deposition in a community repository (e.g. GitHub). See the Nature Portfolio guidelines for submitting code & software for further information.

Data

Policy information about availability of data

All manuscripts must include a data availability statement. This statement should provide the following information, where applicable:

- Accession codes, unique identifiers, or web links for publicly available datasets
- A description of any restrictions on data availability
- For clinical datasets or third party data, please ensure that the statement adheres to our policy

The authors declare that the main data supporting the findings of this study are available within the article, its Supplementary Information files or in public repositories, which can be accessed with the provided links. Extra data are available from the corresponding author upon request.

Plasmids and C. elegans lines generated in this study will be distributed to other researchers upon request. RNA–sequencing data that support the findings of this study have been deposited in the Gene Expression Omnibus (GEO) under accession codes GSE202291 and GSE161121. Source data have been provided in Source Data. All other data supporting the findings of this study are available from the corresponding author on reasonable request. The UniProtKB UniRef90 database was used for GO PANTHER and BUSCA bioinformatic analysis.

Human research participants

Policy information about studies involving human research participants and Sex and Gender in Research.

Reporting on sex and gender	*Use the terms sex (biological attribute) and gender (shaped by social and cultural circumstances) carefully in order to avoid confusing both terms. Indicate if findings apply to only one sex or gender; describe whether sex and gender were considered in study design whether sex and/or gender was determined based on self-reporting or assigned and methods used. Provide in the source data disaggregated sex and gender data where this information has been collected, and consent has been obtained for sharing of individual-level data; provide overall numbers in this Reporting Summary. Please state if this information has not been collected. Report sex- and gender-based analyses where performed, justify reasons for lack of sex- and gender-based analysis.*
Population characteristics	*Describe the covariate-relevant population characteristics of the human research participants (e.g. age, genotypic information, past and current diagnosis and treatment categories). If you filled out the behavioural & social sciences study design questions and have nothing to add here, write "See above."*
Recruitment	*Describe how participants were recruited. Outline any potential self-selection bias or other biases that may be present and how these are likely to impact results.*
Ethics oversight	*Identify the organization(s) that approved the study protocol.*

Note that full information on the approval of the study protocol must also be provided in the manuscript.

Field-specific reporting

Please select the one below that is the best fit for your research. If you are not sure, read the appropriate sections before making your selection.

☒ Life sciences ☐ Behavioural & social sciences ☐ Ecological, evolutionary & environmental sciences

For a reference copy of the document with all sections, see nature.com/documents/nr-reporting-summary-flat.pdf

Life sciences study design

All studies must disclose on these points even when the disclosure is negative.

Sample size	Sample size determination was done according to standard C. elegans approaches. Exact sample sizes are stated in the according figure legends and Supplementary Information. No statistical method was used to predetermine sample size. Overall at least three biological replicates were performed for each experiment, which is an established norm in the scientific community.
Data exclusions	No data were excluded from the analyses.
Replication	Except for Figure S5f, at least three biological replicates were performed for each experiment.
Randomization	The experiments were not randomized by purpose. Randomization was not applicable in our studies since C.elegans population are inherently isogenic and their distribution to different treatment regimes is per se random.
Blinding	The Investigators were not blinded to allocation during experiments and outcome assessment. All experiments in the study were quantified by automated and objective readout methods for outcome assesment (RT-qPCR, measuring fluorescence, fluorescent foci, etc.).

Reporting for specific materials, systems and methods

We require information from authors about some types of materials, experimental systems and methods used in many studies. Here, indicate whether each material, system or method listed is relevant to your study. If you are not sure if a list item applies to your research, read the appropriate section before selecting a response.

Materials & experimental systems

n/a	Involved in the study
☐	☒ Antibodies
☐	☒ Eukaryotic cell lines
☒	☐ Palaeontology and archaeology
☐	☒ Animals and other organisms
☒	☐ Clinical data
☒	☐ Dual use research of concern

Methods

n/a	Involved in the study
☒	☐ ChIP-seq
☐	☒ Flow cytometry
☒	☐ MRI-based neuroimaging

Antibodies

Antibodies used

Mouse monoclonal anti alpha tubulin (clone B-5-1-2) Sigma Cat# T6074, RRID:AB_477582, dilution 1:5000;
Mouse monoclonal anti Living Colors, (clone JL-8), (anti-GFP) Clontech Laboratories, Inc. Cat# 632380, RRID:AB_10013427, dilution1:5000;
Mouse monoclonal anti Living Colors, DsRed, (anti-mCherry; no clone name provided by Clonetech Laboratories) Clontech Laboratories, Inc. Cat# 632393, RRID:AB_2801258, dilution 1:5000;
Anti-CDC-48.1, Hoppe-lab/Biogenes Berlin, custom antibody, dilution 1:50000;
Anti-SEL-1, Sommer-lab, Berlin, custom antibody, dilution 1:8000;
Anti-Ago2 monoclonal (C34C6)(western bloting), Cell Signaling Cat# 2897, RRID:AB_2096291, dilution 1:10000;
Anti-Ago2 monoclonal (2D4)(UV-crosslinking immunoprecipitation), Fujifilm Wako Chemicals, Cat# 014-22023, RRID:AB_1106837, dilution: 20 µl per CLIP reaction;
Anti-alpha (orsay virus) Wang-lab, Washington, custom antibody, dilution 1:2000;
IRDye® 800CW Donkey anti-Mouse IgG (H + L); LI-COR Biosciences, Cat# 926-32212, RRID:AB_2716622, dilution 1:10000;
IRDye® 800CW Donkey anti-Rabbit IgG (H + L), LI-COR Biosciences, Cat# 926-32213, RRID:AB_621848, dilution 1:10000;
IRDye® 680 Donkey anti-Mouse IgG (H + L), LI-COR Biosciences, Cat# 962-32222, RRID:AB_621844, dilution 1:10000;
IRDye® 680 Donkey anti-Rabbit IgG (H + L), LI-COR Biosciences, Cat# 962-32223, RRID:AB_621845, dilution 1:10000

Validation

Validations of primary and secondary antibodies were done by the stated manufacturer's or by the laboratory they where produced by.
Anti-CDC-48.1, Hoppe-lab/Biogenes Berlin, custom antibody: Franz et al., Mol. Cell., 2014
Anti-SEL-1, Jarosch-lab, Berlin, custom antibody: Denzel et al., Cell, 2014
Anti-alpha (orsay virus) Wang-lab, Washington, custom antibody: Jiang et al., Virology, 2014

Mouse monoclonal anti alpha tubulin (clone B-5-1-2):
Independent Antibody Verification – Demonstrating antibody specificity through the use of multiple antibodies against target in IHC or ICC. (https://www.sigmaaldrich.com/DE/de/technical-documents/technical-article/protein-biology/immunohistochemistry/antibody-enhanced-validation)

Mouse monoclonal anti Living Colors, (JL-8), (anti-GFP):
The quality and performance of this lot of Living Colors A.v. Monoclonal Antibody (JL-8) was tested by Western blot

analysis using lysate made from a HEK 293 cell line stably expressing AcGFP1. After cells were collected and lysed using SDS sample buffer, the lysate (10 µl; equivalent to 35,000 cells) was electrophoresed on a 12% SDSpolyacrylamide gel and transferred to a nitrocellulose membrane. The blot was probed with the Living Colors A.v. Monoclonal Antibody, JL-8 (diluted 1:1,000), followed by a secondary goat anti-mouse antibody conjugated to horseradish peroxidase (HRP). The HRP signal was detected by chemiluminescence. A band of approximately 30 kDa corresponding to AcGFP1 was observed in the lane loaded with the AcGFP1 cell lysate. A band of this size was not detected in the lysate of untransfected HEK 293 cells.

Living Colors® DsRed Monoclonal Antibody:
The quality and performance of this lot of antibody was tested by Western blot analysis using lysate made from a HEK 293 cell line stably expressing DsRed Express. After cells were collected and lysed using SDS sample buffer, the lysate (10 µl; equivalent to 35,000 cells) was electrophoresed on a 12% SDS-polyacrylamide gel and transferred to a nitrocellulose membrane.The blot was probed with the Living Colors DsRed MonoclonalAntibody (diluted 1:500), followed by a secondary goat anti-mouse antibody conjugated to horseradish peroxidase (HRP). The HRP signal was detected by chemiluminescence. A band of approximately 29 kDa corresponding to DsRed Express was observed in the lane loaded with the DsRed Express cell lysate. A band of this size was not detected in the lysate of untransfected HEK 293 cells.

Anti-Ago2 monoclonal (western blotting) (C34C6):
No rating or validation information has been found for Rabbit Anti-Argonaute 2 Monoclonal Antibody, Unconjugated, Clone C34C6.

Anti-Ago2 monoclonal (UV-CLIP) (2D4):
No rating or validation information has been found for Anti-Argonaute 2 Monoclonal Antibody (2D4)

Eukaryotic cell lines

Policy information about cell lines and Sex and Gender in Research

Cell line source(s)	Ago2+/+ and Ago-/- Mouse embryonic fibroblasts were recieved from Greg Hannon, Cambridge, UK.
Authentication	None of the cell lines used in this study were authenticated. However, Ago2-/- MEF cells were tested for absence of Ago2 via western blot.
Mycoplasma contamination	All cell lines used in this study were regularly tested negative for Mycoplasma contamination.
Commonly misidentified lines (See ICLAC register)	According to the ICLAC register, no commonly misidentified cell lines were used in this study.

Animals and other research organisms

Policy information about studies involving animals; ARRIVE guidelines recommended for reporting animal research, and Sex and Gender in Research

Laboratory animals	The study involved Caenorhabditis elegans strains of various genotypes listed in the provided Supplementary Information. C. elegans populations entail predominantly hermaphrodites. The age of the tested organisms is described in the respective method section.
Wild animals	The study did not involve wild animals.
Reporting on sex	All experiments in this study were performed on hermaphrodite C. elegans populations.
Field-collected samples	The study did not involve samples collected from the field.
Ethics oversight	This study only includes work with the nematode C. elegans or with Mouse embryonic fibroblasts. For both no ethical approval or guidance is required.

Note that full information on the approval of the study protocol must also be provided in the manuscript.

Flow Cytometry

Plots

Confirm that:

☒ The axis labels state the marker and fluorochrome used (e.g. CD4-FITC).

☒ The axis scales are clearly visible. Include numbers along axes only for bottom left plot of group (a 'group' is an analysis of identical markers).

☒ All plots are contour plots with outliers or pseudocolor plots.

☒ A numerical value for number of cells or percentage (with statistics) is provided.

Methodology

Sample preparation	1000 age-synchronized worms were grown on L-plates until day 1 adulthood. Worms were washed off in 10 ml of M9 buffer.
Instrument	BioSorter® (Union Biometrica)
Software	FlowPilot-Pro™ (v1)
Cell population abundance	1000 worms per sample
Gating strategy	Unless stated otherwise, gating was performed with TOF >1500, Red >300, Extinction >800. Experiments with smaller sel-11(nDf59) mutant worms were gated with (TOF >1200, Red >300, Extinction >600). Only gated worms were quantified for the fluorescence of interest.

☒ Tick this box to confirm that a figure exemplifying the gating strategy is provided in the Supplementary Information.

A.3 Publication B: Cutting through the stress: RNA decay pathways at the endoplasmic reticulum

(II) Ottens, F.*, **Efstathiou, S***., & Hoppe, T. (2023). Cutting through the stress: RNA decay pathways at the endoplasmic reticulum. In *Trends in Cell Biology*. Elsevier Ltd. https://doi.org/10.1016/j.tcb.2023.11.003

* These authors contributed equally

Trends in Cell Biology

CellPress

Review

Cutting through the stress: RNA decay pathways at the endoplasmic reticulum

Franziska Ottens,[1,2,4] Sotirios Efstathiou,[1,2,4] and Thorsten Hoppe[1,2,3,*]

The endoplasmic reticulum (ER) is central to the processing of luminal, transmembrane, and secretory proteins, and maintaining a functional ER is essential for organismal physiology and health. Increased protein-folding load on the ER causes ER stress, which activates quality control mechanisms to restore ER function and protein homeostasis. Beyond protein quality control, mRNA decay pathways have emerged as potent ER fidelity regulators, but their mechanistic roles in ER quality control and their interrelationships remain incompletely understood. Herein, we review ER-associated RNA decay pathways – including regulated inositol-requiring enzyme 1α (IRE1α)-dependent mRNA decay (RIDD), nonsense-mediated mRNA decay (NMD), and Argonaute-dependent RNA silencing – in ER homeostasis, and highlight the intricate coordination of ER-targeted RNA and protein decay mechanisms and their association with antiviral defense.

Highlights

We illustrate and discuss the relevance of key endoplasmic reticulum (ER)-associated RNA decay pathways – including inositol-requiring enzyme 1α (IRE1α)-dependent mRNA decay (RIDD), RIDD lacking endomotif (RIDDLE), ER-associated RNA silencing (ERAS), regulation of aberrant protein production (RAPP), and ER nonsense-mediated mRNA decay (ER-NMD) – for the unfolded protein response (UPR) and ER homeostasis.

Multiple parallel ER-associated RNA decay pathways may exist to ensure substrate specificity and to efficiently address diverse ER homeostasis and viral challenges.

We summarize recent insights into the intricate interplay of these pathways, and highlight gaps in our knowledge regarding target selectivity, recruitment of degradation machinery, and the physiological relevance of ER-associated RNA decay pathways.

An emerging ER–ribosome-associated quality control (RQC) mechanism involves coordinated ER-associated processes of RNA degradation – IRE1α, Argonaute 2 (AGO2), UPF1 – and protein degradation (LTN1, HRD1, VCP).

RNA decay pathways: emerging gatekeepers of ER homeostasis

Maintaining a balanced proteome is essential for cellular survival and overall organism health [1]. Approximately 30% of cellular proteins are targeted to the ER, a central organelle that orchestrates the translation, folding, and maturation of luminal, transmembrane, and secreted proteins within the endomembrane system [2]. The **signal recognition particle (SRP)** (see Glossary) directs ribosome-associated secretory transcripts to the ER membrane, where the nascent polypeptide chain (NC) enters the ER through the **SEC61 translocon** for co-translational folding [3,4]. The ER quality control (ERQC) network ensures the integrity of the secretory proteome. Misfolded proteins are eliminated from the ER lumen via ER-associated degradation (ERAD), which involves their retro-translocation, ubiquitylation, and proteasomal degradation [5]. ER homeostasis is constantly challenged by exogenous and endogenous perturbations, resulting in increased protein import or accumulation of misfolded proteins. Accumulation of misfolded proteins in the ER lumen activates the unfolded protein response (UPR) (Box 1 and Figure 1A) [6,7], which modulates cytoprotective stress signaling such as the integrated stress response (ISR) (Box 1), the ERQC (Box 1), and the **interferon response**. The UPR helps to restore ER homeostasis by reducing global protein translation and activating transcription factors that upregulate ER protein folding and antiviral defense mechanisms. However, prolonged UPR activation can lead to apoptotic cell death [2].

In addition to its role in UPR-driven transcriptional changes via *XBP1* splicing, IRE1α participates in RIDD, degrading ER-associated mRNAs to halt further translation during ER stress (Box 1). Beyond RIDD, several RNA decay pathways, such as NMD (Box 2) and Argonaute-dependent RNA silencing (Box 3), including regulation of aberrant protein production (RAPP) and ER-associated RNA silencing (ERAS), have emerged as potential regulators of ER homeostasis, preventing ER protein overload during stress [8–14]. All of these pathways are controlled by conserved RNases that influence ER-associated mRNA degradation, but their interplay and impact on ER fidelity is only partially understood. In addition, viral infection depends on the successful biogenesis of

[1]Institute for Genetics, University of Cologne, Cologne, Germany
[2]Cologne Excellence Cluster on Cellular Stress Responses in Aging-Associated Diseases (CECAD), University of Cologne, Cologne, Germany
[3]Center for Molecular Medicine Cologne (CMMC), Faculty of Medicine and University Hospital of Cologne, Cologne, Germany
[4]These authors contributed equally to this work.

*Correspondence:
thorsten.hoppe@uni-koeln.de
(T. Hoppe).

© 2023 Elsevier Ltd. All rights reserved.

Box 1. The unfolded protein response at the ER

When the protein-folding capacity of the ER is overwhelmed, leading to misfolding and accumulation of damaged proteins (ER stress), cells initiate the unfolded protein response (UPR) (see Figure 1A in main text). To counteract stress, the UPR reduces overall translation and increases protein folding, degradation, and processing components [6,7]. The UPR consists of three transmembrane ER stress sensors: activating transcription factor 6 (ATF6), inositol-requiring enzyme 1α (IRE1α), and PKR-like ER kinase (PERK). Normally, these sensors are bound to the ER luminal chaperone BiP and remain inactive. During ER stress, BiP is sequestered by misfolded proteins, activating the sensors and initiating the UPR [7].

Activated ATF6 is translocated to the Golgi apparatus where it is processed to an active transcription factor (ATF6N). This primarily induces the expression of ER quality control (ERQC) factors such as molecular chaperones (e.g., BiP) and ER-associated degradation (ERAD) factors, including the membrane-bound E3 ligase HRD1 [2,5,6]. Activation of the serine/threonine protein kinase PERK leads to targeted phosphorylation of eukaryotic initiation factor 2α (eIF2α), thereby limiting protein translation to reduce ER protein folding load [2,6,7]. However, eIF2α phosphorylation allows specific translation of stress-related transcripts, including the ATF4 transcription factor. ATF4 enhances factors that restore ER homeostasis and cytoprotective processes, although prolonged ER stress can also activate genes associated with apoptosis signaling [2,6,7]. In addition to PERK, three other eIF2α kinases activated by various stress conditions promote eIF2α phosphorylation and translation inhibition, collectively known as the integrated stress response (ISR) [103].

The serine/threonine kinase IRE1α is the most evolutionarily conserved arm of the UPR. Upon activation, IRE1α undergoes oligomerization, autophosphorylation, and activation of its cytoplasmic endoribonuclease domain, linking kinase activity to RNase activity [31,104,105]. IRE1α recognizes the endomotif consensus sequence (CUG^CAG) and removes a 26-nucleotide intronic stem loop from *XBP1* mRNA, generating the active transcription factor XBP1s [36,37]. XBP1s induces the expression of components for pro-survival mechanisms such as chaperones and the ERAD machinery, thereby maintaining ER homeostasis [6,7]. In addition to *XBP1* splicing, IRE1α functions in regulated IRE1α-dependent mRNA decay (RIDD). RIDD cleaves various ER-associated mRNAs, which are further degraded by cellular RNA decay mechanisms, including deadenylation and exonucleolytic decay pathways [24–26,106]. Moreover, upon prolonged ER stress, IRE1α cleaves microRNAs (miRNAs) targeting the protease caspase-2 to promote apoptosis [86].

viral RNA and proteins, a process that is linked to cellular protein networks and is vulnerable to RNA and protein degradation pathways (Box 4) [15–17]. Recent studies demonstrate potent antiviral activities of ERQC, UPR, and interferon response (Box 4) upon non-cytotoxic ER stress treatments, which have increasing relevance for therapeutic intervention [9,15,18–22].

In the past years, increasing evidence for RNA decay pathways as potent players in shaping ER fidelity has emerged. This review provides an overview of ER-associated mRNA decay mechanisms, their functions, and their importance in maintaining ER homeostasis. In this regard, RNA and protein decay mechanisms have so far been considered separately. Here we highlight and discuss the intricate relationships, emerging concepts, and synergies between post-transcriptional and post-translational ERQC, ER homeostasis, and antiviral defense mechanisms.

Regulated IRE1α-dependent mRNA decay in ER homeostasis

In metazoans, IRE1α has a dual function: splicing *XBP1* in the UPR, and performing RIDD (Box 1 and Figure 1A,B). This raises the question of how IRE1α RNase activity is regulated, and how the *XBP1* mRNA is not degraded by RIDD. Recent findings in *Drosophila melanogaster* indicate that, upon ER stress, the RNA-binding protein Pumilio, possibly phosphorylated by IRE1α, shields *XBP1* mRNA from RIDD while still allowing for endomotif-specific *XBP1* splicing [23]. By contrast with metazoans, yeast IRE1 function is specialized. In *Saccharomyces cerevisiae*, IRE1 triggers splicing of the *XBP1* functional ortholog *HAC1* and lacks RIDD activity [24], whereas in *Schizosaccharomyces pombe* IRE1 performs only RIDD [25,26]. This functional specialization is based on the different RNase specificity: stringent in *S. cerevisiae* and promiscuous in *S. pombe* [27]. The interaction of two conserved amino acids at the RNase–RNase interface in the *S. pombe* IRE1 dimer determines the promiscuous RNase activity and modality, and favors IRE1 oligomerization, suggesting that the protomeric orientation of IRE1 may regulate its substrate specificity. Interestingly, these amino acids are conserved in higher eukaryotes, including human IRE1α, possibly explaining its dual function in *XBP1* splicing and RIDD [28].

Glossary

Argonaute: Argonaute proteins are critical for small RNA-guided PTGS. They bind small guide RNA species such as miRNAs and small interfering RNAs (siRNAs) and use them to specifically target host and viral RNAs for repression.
Dicer: a protein that processes long dsRNA into small guide RNA species, such as miRNAs and siRNAs, which are loaded into Argonaute proteins to direct PTGS.
E3 ligase: E3 ubiquitin ligases recruit ubiquitin-loaded E2 ubiquitin-conjugating enzymes to transfer ubiquitin to a protein substrate. E3 ligases interact with both the target protein and E2, providing substrate specificity. In ERAD, E3 ligases typically polyubiquitylate substrates with lysine 48-linked chains for proteasomal degradation.
Interferon response: in vertebrates, a process initiated by the presence of viral dsRNA. This immune mechanism induces both cell-autonomous and cell-non-autonomous antiviral states, promoting antiviral defenses in the infected cell and alerting neighboring cells to augment their immune responses.
RNA-induced silencing complex (RISC): a multi-protein complex central to RNA silencing. RISC binds small guide RNA species, such as miRNAs and siRNAs, and directs them to target mRNAs, facilitating post-transcriptional gene regulation through mRNA degradation or translation repression.
SEC61 translocon: a protein complex, composed primarily of secretory (SEC) proteins, that uses the heterotrimeric SEC61 to form a translocation channel. The SEC61 translocon facilitates the transfer of nascent polypeptides containing a targeting signal peptide sequence from the cytosol to the ER lumen.
Signal recognition particle (SRP): a conserved ribonucleoprotein (protein–RNA complex) that recognizes and targets proteins to the ER. SRP binds to a signal peptide sequence of newly synthesized peptides and recruits the ribosome–nascent chain complex to its cognate SRP receptor in the ER membrane.
Small guide RNA species: these include miRNAs, siRNAs, short hairpin RNAs (shRNAs) and piwi-interacting RNAs (piRNAs); they direct the RISC to target specific mRNA sequences for degradation or translation repression in post-transcriptional gene silencing.

Basal RIDD activity is predominant during physiological stress and increases with the duration and severity of ER stress, whereas acute ER stress dominates adaptive *XBP1* splicing [6,29,30]. IRE1α dimers drive *XBP1* splicing, whereas RIDD requires higher-order oligomerized IRE1α [31,32]. This model is consistent with the above observations in yeast, where specific RNase activity drives *XBP1* splicing and promiscuous activity defines RIDD [28]. Conflicting models question the precise oligomerization requirement for IRE1α activation [33]. However, it is not entirely clear whether IRE1α oligomerization is primarily responsible for activation, or how many molecules need to assemble to trigger IRE1α activity. Recent studies in human cells reveal different IRE1α oligomerization states: pre-assembly into inactive unphosphorylated dimers in unstressed cells, and auto-phosphorylated oligomers that revert to active dimers upon ER stress. The regulation of these states involves the ER luminal domain of IRE1α [34]. Phosphorylated IRE1α oligomers exhibit superior RNase cleavage compared with dimers [35], supporting a 'rheostatic' concept of IRE1α activation [36,37]. Furthermore, in ER-stressed human cells, RIDD also targets endomotif-deficient transcripts in a process termed RIDDLE (RIDD lacking endomotif), demonstrating two RNase modes: specific cleavage by IRE1α dimers and promiscuous, endomotif-independent cleavage requiring phospho-oligomers and minimal C^G sites. Notably, RIDDLE can also further process cleaved RIDD substrates (Figure 1B) [35]. In addition, phosphorylation at IRE1^{S729} is essential for RIDD activity but not for *XBP1* splicing [38]. Another model, the UPRosome, positions IRE1α as a central protein-binding hub that directs it to RIDD through association with RNA decay components and promotes *XBP1* splicing via interactions with factors such as tRNA ligase that adheres to cleaved *XBP1* fragments [30].

IRE1α substrate selection and targeting to the ER membrane remains partially unclear and differs between species. Drosophila shows a relatively promiscuous target selection based on an ER signal peptide sequence, suggesting ER membrane-associated mRNA degradation [24,39,40]. In mammals, RIDD depends on the endomotif (or G^C for RIDDLE targets [35]) along with the translational state of the mRNA [41,42]. In metazoans, unspliced *XBP1* mRNA is transported to the ER by translating ribosomes [43,44]. SRP directs ER-targeted mRNAs to the SEC61 translocon, where IRE1α facilitates *XBP1* splicing and RIDD, and a stable interaction between IRE1α and the SEC61 translocon upon ER stress is important for regulating RNase function [45,46]. Recent studies highlight the interaction of IRE1α with translation components (i.e., ribosomal subunits) and ER protein targeting factors (i.e., SEC61 translocon, SRP) [47]. IRE1α binds ER-directed mRNAs and non-coding RNAs, including ribosomal RNAs, SRP RNA (7SL), and rare tRNAs, suggesting dual mRNA targeting: (i) direct targeting prior to SEC61 translocon association to reduce protein folding load, and (ii) binding of SEC61 translocon-associated ribosomes to degrade mRNAs that produce slow or misfolded polypeptides (Figure 1B). This is supported by IRE1α binding to rare tRNAs, SRP targeting of paused *XBP1* translating ribosomes to the ER, and IRE1α–SEC61 translocon association [43–46]. However, some studies suggest that many RIDD(LE) targets lack ER signal peptide sequences [35,41,48]. How ER-resident IRE1α accesses these mRNAs remains unclear. Further research is needed to explore unconventional models such as IRE1α dynamic foci [49], IRE1α detachment from membrane-anchored oligomers to access cytosolic RIDD targets [50,51], and ER-associated ribosomes also translating non-secretory mRNAs [52]. In general, RNA target accessibility and selectivity at the ER may be influenced by recently described membrane-less organelles enriched in messenger ribonucleoproteins (mRNPs), which regulate transcript translation and degradation at ER contact sites [53,54].

Given the critical role of RIDD in physiology and pathology [29,30,55,56], there is an urgent need to identify, evaluate, and characterize its mRNA targets at the ER. Exploration of alternative sites of IRE1α action is also critical. To understand the impact of RIDD on key cellular pathways – such

Thapsigargin: a non-competitive inhibitor of the sarco-/endoplasmic reticulum Ca^{2+} ATPase (SERCA) that causes an increase in cytosolic calcium levels by inhibiting calcium transport into the ER. This depletion of ER calcium stores induces ER stress and activates the UPR.

Tunicamycin: a mixture of homologous nucleoside antibiotics that blocks N-linked glycosylation during glycoprotein synthesis in the ER. This disrupts protein folding, leading to the accumulation of misfolded proteins, ER stress, and UPR activation.

Ubiquitin–proteasome system: a cellular mechanism for targeted protein degradation. It involves substrate-specific tagging of protein targets with ubiquitin molecules, marking them for proteasomal degradation, and this tagging process is mediated by E3 ligases.

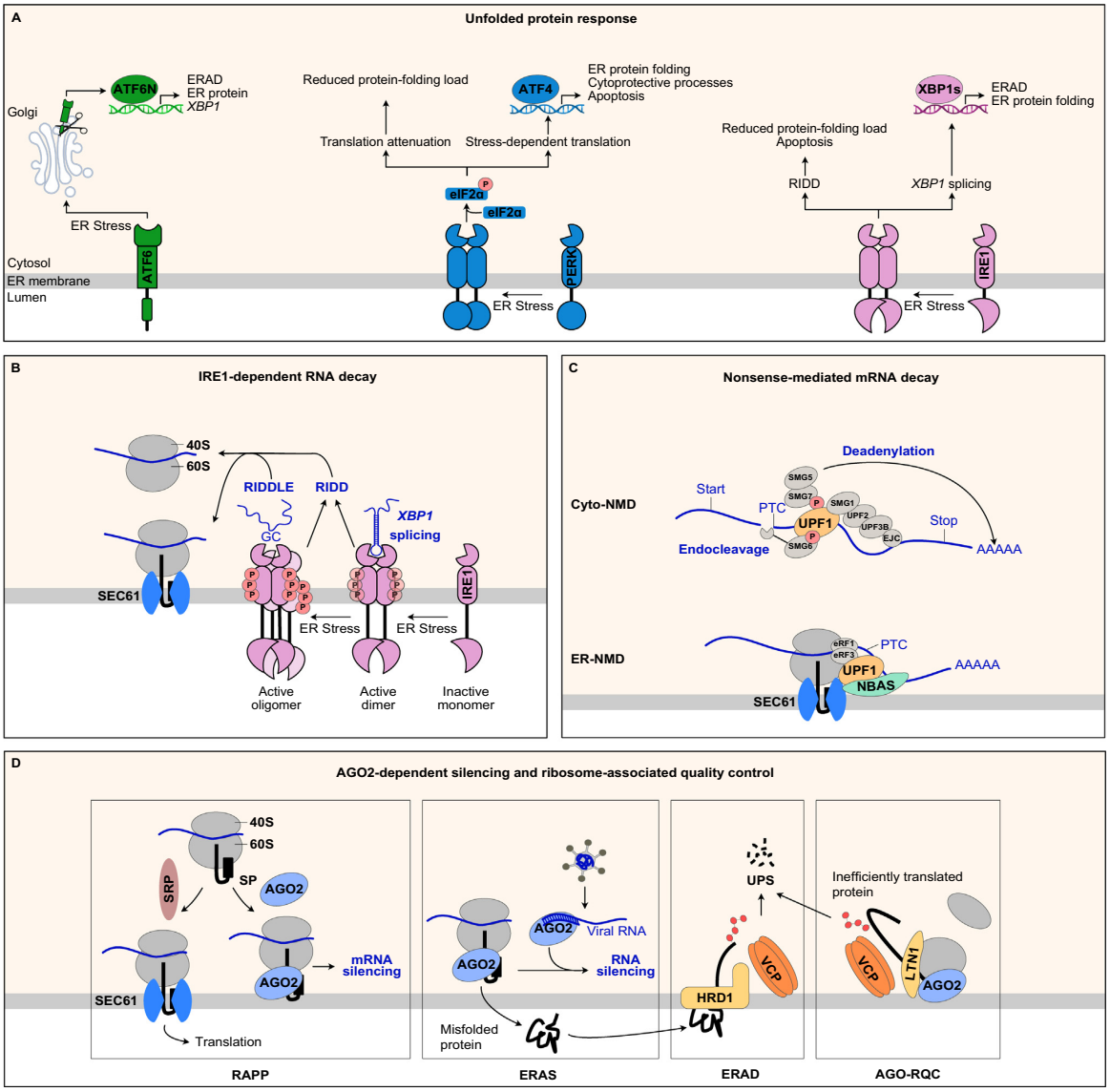

Figure 1. The unfolded protein response (UPR) and endoplasmic reticulum (ER)-associated RNA decay pathways. (A) The three UPR sensors activating transcription factor 6 (ATF6), PKR-like ER kinase (PERK), and inositol-requiring enzyme 1α (IRE1α) are activated upon ER stress and generate the active transcription factors ATF6N, ATF4, and XBP1s. These factors induce cytoprotective gene expression, including ER-associated protein degradation (ERAD). In addition, PERK globally attenuates translation through phosphorylation of eukaryotic initiation factor 2α (eIF2α) and IRE1 acts in IRE1α-regulated mRNA degradation (RIDD). Prolonged ER stress can induce apoptosis. (B) RIDD targets mRNAs before and after SEC61 translocon association. IRE1α (phospho)-dimers cleave stem–loop endomotif-specific RIDD targets, and *XBP1* mRNA and phospho-oligomers degrade RIDDLE (RIDD lacking endomotif) targets at minimal G^C sites, but can also further process RIDD cleavage products. Scheme adapted from [35]. (C) The cytoplasmic nonsense-mediated mRNA decay (Cyto-NMD) machinery factors UPF1/2/3 bridge ribosomes stalled at a premature termination codon (PTC) and the downstream exon junction complex (EJC). Phosphorylation by SMG1 recruits the decay-inducing effectors SMG6 and SMG5/7. For degradation of ER-translated NMD targets (ER-NMD), the syntaxin 18 complex component NBAS binds UPF1 and recruits the early

(Figure legend continued at the bottom of the next page.)

Box 2. Nonsense-mediated mRNA decay

Nonsense-mediated mRNA decay (NMD) is a conserved RNA surveillance mechanism that recognizes and degrades transcripts containing a premature termination codon (PTC) to prevent the accumulation of truncated and aberrant proteins [58,107]. PTCs can result from mutations but can also be incorporated into normal mRNAs during alternative splicing events. In addition, other features within a transcript, including upstream open reading frames (uORFs) and long 3′ untranslated regions (UTRs), can also trigger NMD [60,107]. However, NMD not only degrades defective transcripts, it also affects the transcriptome by directly or indirectly targeting up to 20% of normal mRNAs in eukaryotes [57,58]. NMD is a translation-dependent process, and slowed translation termination at the PTC triggers the formation of a surveillance complex consisting of the SMG1–8–9 kinase complex, DEAD-box helicase UPF1, and the eukaryotic release factors eRF1 and 3 (SURF) [60,107,108]. Components of the SURF complex interact with the core NMD factors UPF2 and UPF3B and a downstream exon junction complex (EJC) that is deposited at exon–exon boundaries during mRNA splicing. Together they form the decay-inducing complex (DECID). DECID formation triggers the dissociation of eRF1 and eRF3, the phosphorylation of UPF1 by SMG1 kinase, and the recruitment of mRNA degradation factors [109,110]. These include the SMG6 endonuclease, which cleaves the mRNA near the PTC and the SMG5/7 heterodimer, initiating mRNA decapping and deadenylation via CCR4-NOT [111–114] (see Figure 1C in main text). This is followed by exonucleolytic decay of the transcript via the 5′-3′ exonuclease XRN1, the 3′-5′ exosome complex, and the exonuclease DIS3L2 [61,115]. Interestingly, UPF1 not only serves as a binding platform for NMD effector molecules, but is also involved in a variety of functionally distinct RNA decay mechanisms, underscoring its central role in cellular mRNA metabolism [88].

as homeostasis, apoptosis, inflammation, and metabolism – it is necessary to elucidate IRE1α activation mechanisms and ribonuclease mode-switching during different levels of ER stress. In addition to RIDD, other RNA decay pathways have emerged as potential regulators of ER homeostasis, discussed in the following sections.

Intertwined dynamics of NMD and the UPR

NMD is an RNA surveillance mechanism that recognizes and targets aberrant mRNAs containing a premature termination codon (PTC) (Box 2 and Figure 1C). The full set of mRNAs targeted by NMD remains unclear. It includes several physiological transcripts, including those encoding UPR factors [57,58]. Thus, NMD not only serves as an RNA surveillance process, but also regulates typical physiological functions. This control influences gene expression, thereby affecting cell viability, cell cycle regulation, antiviral defense, and stress responses [59–62].

NMD and exosome components (Box 2) are also critical for ER homeostasis, as mutations in several *SMG* genes and silencing of SMG6 in worms and mammals induce ER stress and sensitize cells to ER stress signaling by **tunicamycin**. During ER stress, SMG6 levels increase and NMD components localize to the ER [63]. These findings suggest a role for NMD in preventing the accumulation of misfolded proteins that induce the UPR, and conversely, ER-misfolded proteins trigger NMD of deleterious mRNAs to counteract protein misfolding. A mechanistic circuit that prevents full-blown UPR activation under mild stress is critical [2]. The NMD pathway fine-tunes the UPR based on the magnitude and duration of ER stress. This is achieved by directly modulating the transcriptional stability of several UPR-related factors, including IRE1α and components of the PKR-like ER kinase (PERK) pathway [10,11]. In doing so, NMD significantly regulates the UPR by raising the threshold for UPR activation during mild ER stress and ensuring timely UPR termination to protect against prolonged stress. However, the suppression of the UPR by NMD raises the question of how to activate a robust UPR. Ideally, a system by which NMD suppresses the UPR during benign ER stress would include a mechanism that inhibits NMD during severe ER stress to allow for efficient UPR activation. Since NMD is dependent on translation [64], stress-induced inhibition of translation via eukaryotic initiation factor 2α (eIF2α) phosphorylation (Box 1 and Figure 1A) [65] emerges as a candidate for NMD attenuation. Indeed, several studies linking

forming SURF complex [SMG1–UPF1–eukaryotic release factor 1/3 (eRF1/3)] to the ER. Scheme adapted from [8]. (D) Argonaute 2 (AGO2) regulates ER-targeted RNAs and nascent polypeptide chains through regulation of aberrant protein production (RAPP), ER-associated RNA silencing (ERAS), and by cooperating with the ribosome-associated quality control (AGO-RQC) and ERAD components. Protein degradation is mediated by the ubiquitin–proteasome system (UPS). Abbreviations: 40S, small ribosomal subunit; 60S, large ribosomal subunit; SP, signal peptide; SRP, signal recognition particle.

Box 3. Somatic RNA silencing

The somatic RNA silencing pathway is a PTGS system that mediates sequence-specific repression of target RNAs and is orchestrated by two key players: Dicer and Argonaute (AGO). As input, Dicer recognizes a wide range of double-stranded RNAs (dsRNAs) and processes (dices) them into guide RNA species ~20–30 nt long that are competent for AGO loading. Through complementary base pairing of the guide and target RNAs, AGO proteins selectively silence (slice) target mRNAs within the RNA-induced silencing complex (RISC). The somatic RNA silencing pathway includes two well-defined functional manifestations of the RISC: the small interfering RNA (siRNA) and miRNA pathways [116,117]. Its evolutionary roots date back to the last common ancestor of eukaryotes, where it served as an antiviral and siRNA-based defense mechanism against transposable elements and viral deleterious gene sequences, whereas the miRNA pathway of plants and animals appears to have evolved independently [118,119]. The distinction between these pathways is based primarily on three key factors: (i) the origin and structure of the input dsRNA, (ii) the degree of complementarity between the guide RNA and the target RNAs, and (iii) the functional outcome achieved by either mRNA slicing or translation repression [116,117]. Notably, the gene regulatory capacity of somatic RNA silencing transcends the traditional classification of miRNAs and siRNAs and is increasingly recognized for its remarkable versatility [80]. Mammalian genomes encode four distinct AGO proteins, AGO1–4, which share 80% sequence homology. These proteins have a consistent domain structure ranging from the N-terminal (N), MID, PIWI/Argonaute/Zwille (PAZ) to the P-element-induced whimpy tested (PIWI) domain. To achieve catalytic activity, the MID and PAZ domains bind to the 5′ and 3′ ends of the guide RNA, respectively. The N domain unwinds the guide RNA duplex, and the PIWI domain orchestrates cleavage of the target mRNA via a DEDX (X for H or D) catalytic tetrad [120]. AGO2 stands out as the primary mammalian AGO protein with guide RNA-dependent slicer activity, indicating functional similarities to slicer-active AGO proteins found in invertebrates (ceRDE-1, dmAGO1-2). AGO slicer activity is required for siRNA-mediated and direct target mRNA degradation, whereas miRNA-mediated silencing depends on additional downstream RNA decay factors such as CCR4-NOT to mediate target mRNA degradation [121].

ER stress, ER stress-induced NMD inhibition, and translation repression suggest that PERK-eIF2α signaling and associated factors are stabilized upon NMD attenuation [66,67]. However, translation inhibition by eIF2α is not complete (20–45% inhibition) [66], raising the question of whether this mechanism is sufficient to inhibit NMD. An alternative possibility is stress-induced local control of NMD through specific regulation of *ATF4* mRNA stability during translation inhibition (Box 1 and Figure 1A) [68]. Under unstressed conditions, *ATF4* transcripts are degraded by NMD, whereas during stress-induced translation inhibition, *ATF4* escapes NMD [69]. Recently, RIDD was shown to target a regulator of the eIF2α phosphatase, thereby increasing translation inhibition upon ER stress [60]. In addition, NMD components could also be targeted by other RNA decay pathways, such as RIDD, to reduce NMD efficiency in an ER-stress-dependent

Box 4. ER homeostasis, viral defense, and potential synergies

Numerous viruses exploit the host endomembrane system for key stages of their life cycle – including cell entry, replication, and assembly – often triggering the UPR [122]. In tick-borne encephalitis virus (TBEV) infection, there is an early onset of viral replication and UPR induction, while the interferon response, traditionally considered the first line of defense in vertebrates, exhibits delayed activation. However, co-induction of ER stress during infection accelerates and amplifies the interferon response through an IRE1-dependent mechanism [18,123,124]. Strikingly, induction of ER stress with non-cytotoxic concentrations of **thapsigargin** effectively combats several viruses in cell culture and provides protection against lethal influenza A infection in mice and Orsay virus infection in *C. elegans* [9,18–22]. However, the mechanism of action remains largely elusive. UPR-stimulated RIDD may produce mRNA fragments capable of activating interferon signaling [125]. IRE1 shares a functional and evolutionarily related RNase domain with RNase L, which generates RNA fragments comparable to RIDD [126] that potently induce the interferon response [127,128]. In addition, an IRE1β isoform is uniquely expressed in epithelial cells lining the mucosal surfaces of the gastrointestinal and respiratory tracts. IRE1β is less efficient for *XBP1* splicing and more competent for RIDD [129,130]. Collectively, these observations have led to the hypothesis that IRE1β at mucosal surfaces may function in host defense and innate immunity [130–132]. Given that the UPR acts as a potent co-activator of the interferon response in conjunction with viral dsRNA, which also exclusively activates the somatic RNA silencing pathway for antiviral defense, the potential for synergistic effects in the context of ER homeostasis and antiviral defense arises. This scenario creates a conducive environment for simultaneous interferon response and RNA-silencing-mediated antiviral defense, as observed recently [133,134]. In addition, due to their compact genomes, many viruses produce mRNAs with NMD-triggering features such as internal termination codons and long 3′ UTRs [135–137]. Notably, the severe acute respiratory syndrome coronavirus 2 (SARS-CoV-2) N protein interacts with UPF1 and NBAS to inhibit NMD and promote viral replication [135,138,139]. UPF1, NBAS, and other NMD factors are deregulated after viral infection in lung epithelial cells, providing preliminary evidence for an ER-related regulatory mechanism for viral replication and cell survival [138]. In light of the findings from ER-associated RNA decay pathways, it is important to evaluate the interplay between AGO2, IRE1, and NMD in the observed ER-stress-mediated antiviral state.

manner. Taken together, these findings suggest a model in which NMD shapes the UPR by raising the threshold for UPR activation during mild ER stress, and by regulating UPR termination when ER stress subsides. Severe ER stress inhibits NMD, possibly through stress-induced translation inhibition, thereby facilitating increased UPR activation [10,70].

While NMD has been implicated in ER fidelity and the UPR, its regulation of ER-translated transcript stability remains unclear. ER-targeted mRNAs would be susceptible to degradation only after ER-associated translation. Notably, cytoplasmic protein-encoding mRNAs can also be translated by ER-associated ribosomes, and the central NMD factor UPF1 (Box 2) has been shown to interact with both cytoplasmic and ER-bound polysomes [52,71]. In addition, the core NMD factors UPF1/2/3B localize to the SEC61 translocon in human cells [8,72], suggesting a complex ER-NMD role in transcript translation and regulation. SMGL-1 (NBAS in humans) emerged as a novel NMD factor in *Caenorhabditis elegans* [73], localizing to the ER membrane as part of the syntaxin 18 complex for Golgi-to-ER vesicle trafficking [74,75]. UPF1 interacts with components of the syntaxin 18 complex [76], and NBAS, together with core NMD factors, also regulates transcripts encoding factors for membrane trafficking and stress responses [8,77]. NBAS recruits UPF1 to the ER membrane, potentially supporting ER-targeted NMD substrate degradation [8] (Figure 1C). However, further studies are needed to fully understand the direct effects of NBAS on NMD target stability.

In conclusion, NMD is intricately linked to ER function, UPR modulation, and cellular life–death decisions during ER stress. While only a few studies to date suggest an ER-associated NMD machinery that targets mRNAs during ER translation, it is too early to conclude a general role for NMD in ERQC and to evaluate its physiological significance.

Emerging AGO2-centered ERQC

Recently, **Argonaute** 2 (AGO2) has been independently identified by three different research groups as a relevant player in the regulation of ER-targeted gene products [9,12,78,79]. Consistent with its diverse cellular roles, AGO2 exhibits nuclear, cytoplasmic, and ER localization [80]. However, biochemical sedimentation and co-fractionation analyses establish the predominant and consistent presence of AGO2 at the ER membrane, where it forms an **RNA-induced silencing complex (RISC)** with key components of the somatic RNA silencing pathway (Box 3) [81–84]. The rough ER serves as a platform for loading the RISC with **small guide RNA species**, leading to ER-localized and sequence-specific AGO2 RNA degradation activity on target mRNAs [81]. This mechanistic link establishes the rough ER as a central nucleation site for somatic RNA silencing [81,85]. Recent studies indicate that RIDD antagonizes the RISC component **Dicer** by degrading microRNAs (miRNAs) (Box 3) and by directly degrading the mRNA of Dicer itself [86,87]. In addition, AGO2 is a binding partner of UPF1, which participates in functionally distinct RNA decay pathways, including ER-NMD and a Tudor-SN-mediated miRNA decay pathway [88,89]. These examples suggest a mechanistic interplay between ER-associated RNA decay pathways and AGO2. In the following sections, we highlight recent discoveries that establish functional links between AGO2 and the regulation of ER-targeted RNAs and NCs [12].

Regulation of aberrant protein production

During translation of ER-targeted mRNAs, the hydrophobic signal peptide (SP) appears on the NC, leading to SP transfer from the NC-associated complex (NAC) to SRP [90]. Once recruited, SRP drives the localization of the translating ribosome to the SRP receptor at the ER membrane, allowing co-translational translocation of the NC into the ER lumen. SPs with lower hydrophobicity have reduced efficiency in recruiting SRP, which coincides with decreased stability of the encoding mRNA. The extent of reduced SRP binding is directly related to AGO2 recruitment

and mRNA degradation. This process, observed in multiple cell lines and involving multiple mRNAs, has been termed RAPP (Figure 1D) [12]. Furthermore, correlations have been observed between hydrophobic stretches present in NCs without SPs and their regulation by RAPP [14]. Interestingly, the function of AGO2 in RAPP goes beyond its involvement in somatic RNA silencing (Box 3) and does not depend on its slicing activity or on AGO1-3. RAPP function was not abolished by slicing-defective AGO2^{D597A} [91], or knockdown of Dicer and AGO1-3. Notably, studies using mutations in the SP of the secreted immunity factor progranulin have not confirmed the role of AGO2 in RAPP RNA degradation [92], suggesting an incomplete understanding of the substrate specificity and RNA decay factors involved. The *in vivo* regulatory capacity, substrate specificity, and mechanistic details of the involved RAPP effectors are incompletely understood. Since NAC transfers NCs to SRP based on the hydrophobicity of SP, NAC could potentially influence RAPP substrate selection and AGO2 recruitment. Given the dispensability of AGO2 slicer activity for RAPP, the contribution of additional RNA decay factors in regulating substrate specificity needs to be investigated. Similar to the ribosome association of AGO2 in RAPP, another study linked AGO2 to ribosome-associated quality control (RQC) [79].

Quality control of ER-targeted polypeptides

Eukaryotes employ several post-translational PQC mechanisms – including chaperones, the **ubiquitin–proteasome system (UPS)**, and autophagy – to remove misfolded proteins. In addition to post-translational PQC pathways, a pre-emptive surveillance system monitors peptides during ribosomal translation. This pre-emptive RQC system detects aberrant signals from translating ribosomes, such as slow decoding, ribosome pauses, or ribosome collisions. Depending on the severity of the reduced translation processivity, the RQC system initiates mechanisms such as translation repression, mRNA decay, ribosome splitting, and/or NC degradation [93,94]. Upon initiation of ribosome splitting and irreversible interruption of the co-translational process, the **E3 ligase** listerin (LTN1) and the segregase VCP engage to extract, ubiquitylate, and transport the defective NC from the ribosome to the proteasome [93,94], a process with strong similarities to ERAD. ER-localized E3 ligases (ER-E3) such as HRD1 and MARCH6 engage with VCP to extract, ubiquitylate, and transport the defective NC from the ER membrane or lumen to the cytosolic proteasome [95]. While the factors that bridge these two pathways remain unclear, an ER-associated RQC (ER-RQC) has been postulated [96]. Upon RIDD of mRNAs that are engaged in translation, the canonical pre-emptive RQC is recruited for NC degradation [97]. For the degradation of NCs from NMD transcripts, the involvement of the RQC system and UPF1, which has E3 ligase function, is still debated, and preliminary data suggest that EJC components and the SMG6 endonuclease may play a role in NMD-associated RQC [98–102]. Recently, a study observed an AGO-dependent RQC (AGO-RQC) in which ER-localized AGOs recruit LTN1 and VCP to coordinate UPS-mediated degradation of primarily ER-targeted NCs (Figure 1D) [78,79]. The AGO-RQC mechanism is driven by an electrostatic interaction between the positively charged lipid-binding motifs in the N domain of AGOs and the negatively charged lipid PI(4,5)P_2 in the ER membrane. ER-bound AGOs form condensates and recruit LTN1, which cooperates with VCP to direct mainly ER-targeted NCs to the UPS. This led to the proposal of an AGO-centered link between post-transcriptional gene silencing (PTGS) and ER-RQC through the somatic RNA silencing pathway (Box 4). However, the study did not examine the dependence of AGO-RQC on small guide RNAs or AGO2 slicer activity. In addition, it remains uncertain whether the identified targets have correspondingly reduced levels of the encoding mRNAs. Thus, the extent of AGO2's involvement in RNA degradation, whether or not it acts independently of its primary role in PTGS, remains to be determined. Finally, the significant role of VCP in ERAD of ER-targeted NCs has a dramatic potential to affect the interpreted data and was not considered in this study. Without investigating ERAD or the folding state of the NCs, it remains uncertain whether AGO-RQC (AGO2–LTN1–VCP–UPS axis) for ER-targeted NCs relies on ERAD (HRD1–VCP–UPS axis) for its function (Figure 1D).

Indeed, AGO2 was identified as an additional ERQC factor that works in parallel with ERAD to orchestrate widespread ERAS and reduce ER protein-folding burden under ER stress [9].

ERAS supports ER homeostasis and organismal health

In an unbiased screen for ERAD effectors in *C. elegans*, the functional AGO2 ortholog RDE-1 (Box 3), together with additional components of the somatic RNA silencing pathway, were found to be involved in ER-stress-dependent degradation of ER-targeted RNAs [9]. In response to ER stress, RDE-1/AGO2 primarily binds and degrades endogenous ER-targeted mRNAs encoding luminal, transmembrane, and secretory proteins. The coordination of widespread RNA degradation by ERAS is physiologically important because RDE-1/AGO2 loss-of-function mutants are sensitive to ER stress or ERQC disruption, such as impaired ERAD. The cooperation of ERAS and ERAD is crucial, as shown by the increased UPR activation, reduced PQC, and impaired intestinal integrity in *C. elegans* when both ERAD and ERAS are defective. Mechanistically, the mRNA encoding a mutated and misfolded form of the ERAD substrate pro-cathepsin L is an obligate target of ERAS, whereas the mRNA for the properly folded wild-type substrate is degraded only in response to ER stress. ERAS function most likely depends on small guide RNA species. Either substitution of a single conserved amino acid (E414K) in the guide RNA-binding PAZ domain (Box 3) of RDE-1 or knockdown of Dicer completely abolishes ERAS function. Thus, although ERAS and ERAD work together to maintain ER protein homeostasis, their mechanisms of action are distinct. ERAS uses the somatic RNA silencing machinery for mRNA degradation, whereas ERAD uses the UPS for protein degradation (Figure 1D). From an evolutionary perspective, slicer-active AGOs are an ancient antiviral pathway that has been co-opted into a general PTGS system that is now increasingly recognized to regulate ERQC [9,12,78,79]. Notably, in *C. elegans* infected with Orsay virus, viral RNA and proteins are predominantly localized to the ER. Furthermore, a significant reduction in viral RNA levels was observed when subjected to ER stress-inducing conditions, a phenomenon that appears to be conserved in vertebrates [9,18–22]. Although ERAS has been shown to have a substantial *in vivo* RNA regulatory capacity, the details of the factors involved remain largely elusive. While the impact of ER stress on RNA degradation in ERAS is evident, the precise mechanism that governs substrate specificity for ER-targeted mRNAs remains elusive. Further studies are needed to identify the recruited quality control factors in ERAS, the source of the small guide RNA species, and whether ERAS and ERAD simultaneously degrade the mRNA and NC of the same gene product in a pre-emptive AGO-RQC manner. Investigating the interplay between ERAS and other RNA degradation pathways in ER homeostasis and viral defense, and their potential synergies, will shed light on the longstanding and unresolved question of how non-cytotoxic ER stress treatments induce potent antiviral states in invertebrates to vertebrates (Box 4).

Concluding remarks

ER-associated RNA decay pathways have emerged as potent regulators of ERQC. However, significant gaps remain in our understanding of RNA target selection and specificity, the interplay between different ER-associated RNA decay mechanisms, their integration with co-translational protein degradation systems, and their broader implications for organismal physiology, including antiviral defense (see Outstanding questions).

While the ER localization of IRE1α is well established, and there is increasing evidence for AGO2-mediated mRNA degradation at the ER, the ER-NMD pathway and its ER stress-dependent regulation remain poorly defined. Similarly, the target specificity and transcript recruitment to the ER for RIDD and RIDDLE transcripts have been partially elucidated. However, it remains to be determined whether small guide RNA species and classical NMD-inducing sequence features are the driving factors for substrate specificity in the ER-related functions of AGO2 and ER-NMD, respectively. ER-associated mRNA decay pathways appear to be interdependent: RIDD targets components

Outstanding questions

How are target transcripts and key RNA degradation factors recruited to the ER and regulated during ER stress? How is the substrate specificity of different RNA decay mechanisms regulated?

How are the different ER-associated RNA decay pathways interconnected, and to what extent do they shape each other?

What is the exact crosstalk between RNA degradation and protein degradation mechanisms at the ER?

What is the physiological relevance of different RNA decay pathways at the ER?

What is the role of the discussed pathways in ER-associated viral RNA degradation and how do viruses co-opt them to evade antiviral defenses?

of the somatic RNA silencing pathway and coregulates NMD by modulating the ISR. AGO2 physically interacts with UPF1, which is a hub for several RNA decay pathways, including ER-NMD and a miRNA decay pathway. Furthermore, RIDD, AGO2, and potentially NMD all converge on a common ER-RQC system, raising the question of whether the folding state of ER-targeted NCs directly influences the engagement of these ER-associated RNA decay pathways (Figure 2). Substrate specificity in ERAD is achieved through close cooperation between ER-localized PQC factors and ER-E3, such as HRD1 or MARCH6, each of which employs specialized strategies to recognize the diverse array of ER-targeted NCs. In a second step, similar to LTN1-dependent RQC, identified substrates are extracted by VCP and terminally degraded by the UPS. A similar two-step model governing substrate specificity in RNA degradation could be conceptualized. ER-associated RNA decay pathways possessing endonuclease activity, such as RIDD, AGO2 and ER-NMD, employ specialized strategies to recognize a broad spectrum of ER-targeted mRNAs and initiate substrate-specific mRNA degradation. Subsequently, downstream exonucleases such as CCR4-NOT, XRN1, and the exosome take over the bulk RNA degradation process (Figure 2). Although all of the described pathways likely contribute to ER homeostasis by reducing the protein folding load on the ER, their broader physiological impact remains to be determined. By contrast with RIDD, whose physiological role is becoming increasingly well defined as target RNAs are continuously identified, ER-associated AGO2-dependent mRNA decay pathways and ER-NMD lack knowledge about their physiological outcomes. However, the ERAS pathway appears to maintain intestinal integrity, ER homeostasis, and antiviral defense in *C. elegans*. AGO2 and NMD are known to target viral RNAs, and RIDD may be involved in antiviral defense by activating interferon signaling. Viruses co-opt the ER and evade mRNA and protein degradation machinery to facilitate their replication. This suggests an important role for ER-associated RNA and protein degradation pathways in viral defense and a potential for therapeutic intervention.

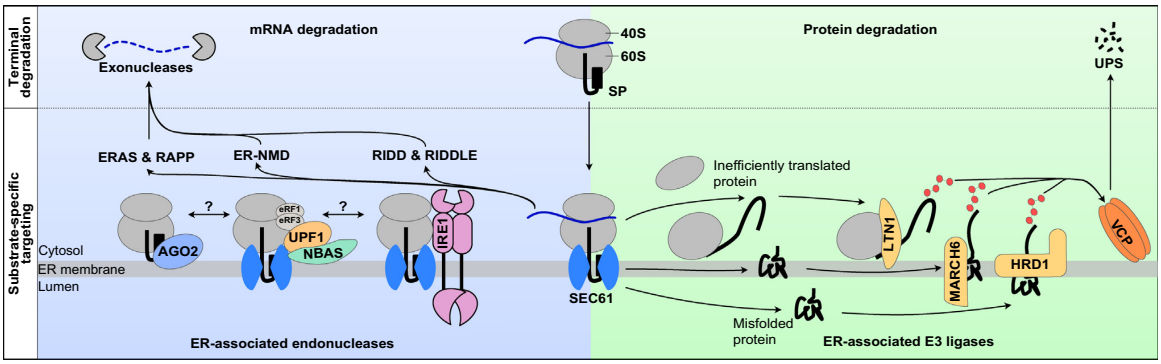

Figure 2. Model of endoplasmic reticulum (ER)-associated RNA decay pathways and their integration with ER quality control (ERQC). ER-targeted gene products are subject to stringent RNA surveillance and protein quality control. Aberrant mRNA and nascent polypeptide chain (NC) features, or ER stress, can trigger substrate-specific recognition and degradation. This process helps alleviate protein-folding overload in the ER and prevents dominant negative effects of aberrant RNAs and proteins. ER-associated RNA decay pathways – such as regulated inositol-requiring enzyme 1α (IRE1α)-dependent mRNA decay (RIDD and RIDDLE), Argonaute 2 (AGO2)-mediated mRNA silencing (ERAS and RAPP), and ER-associated nonsense-mediated mRNA decay (ER-NMD) – contribute to ERQC by mediating substrate-specific mRNA degradation through endonucleolytic cleavage mechanisms. Once mRNAs are destabilized by the ER-associated RNA decay pathways, terminal mRNA degradation is carried out by cytosolic exonucleases. The substrate specificity of NCs is primarily achieved through the combined efforts of ER-localized protein quality control factors and E3 ligases (LTN1, MARCH6, HRD1). Once NCs are unfolded, ubiquitylated (red spheres), and extracted by VCP into the cytosol, terminal protein degradation is mediated by the ubiquitin–proteasome system (UPS). This figure highlights the convergence of these pathways within a common ribosome-associated quality control system (ER-RQC), suggesting a potential link between the folding status of ER-targeted NCs and the engagement of ER-associated RNA decay pathways. However, significant gaps remain in our understanding of the intricate interplay between these pathways, their integration with co-translational protein degradation systems, and their broader physiological implications, including potential roles in antiviral defense. Abbreviations: 40S, small ribosomal subunit; 60S, large ribosomal subunit; SP, signal peptide.

Acknowledgments

We thank the members of the Hoppe laboratory for critical discussion and helpful advice on the manuscript. This work was funded by the Deutsche Forschungsgemeinschaft (DFG, German Research Foundation) under Germany's Excellence Strategy (EXC 2030 – 390661388) and by the European Research Council (ERC-CoG-616499) to T.H. S.E. received support from the Cologne Graduate School of Aging Research. We apologize for not having cited valuable contributions due to size limitations.

Declaration of interests

The authors declare no competing interests.

References

1. Hoppe, T. and Cohen, E. (2020) Organismal protein homeostasis mechanisms. *Genetics* 215, 889–901
2. Vincenz-Donnelly, L. and Hipp, M.S. (2017) The endoplasmic reticulum: a hub of protein quality control in health and disease. *Free Radic. Biol. Med.* 108, 383–393
3. Chartron, J.W. *et al.* (2016) Cotranslational signal-independent SRP preloading during membrane targeting. *Nature* 536, 224–228
4. Voorhees, R.M. and Hegde, R.S. (2016) Structure of the Sec61 channel opened by a signal sequence. *Science* 351, 88–89
5. Wu, X. and Rapoport, T.A. (2018) Mechanistic insights into ER-associated protein degradation. *Curr. Opin. Cell Biol.* 53, 22–28
6. Hetz, C. *et al.* (2020) Mechanisms, regulation and functions of the unfolded protein response. *Nat. Rev. Mol. Cell Biol.* 21, 421–438
7. Preissler, S. and Ron, D. (2019) Early events in the endoplasmic reticulum unfolded protein response. *Cold Spring Harb. Perspect. Biol.* 11, a033894
8. Longman, D. *et al.* (2020) Identification of a localized nonsense-mediated decay pathway at the endoplasmic reticulum. *Genes Dev.* 34, 1075–1088
9. Efstathiou, S. *et al.* (2022) ER-associated RNA silencing promotes ER quality control. *Nat. Cell Biol.* 24, 1714–1725
10. Goetz, A.E. and Wilkinson, M. (2017) Stress and the nonsense-mediated RNA decay pathway. *Cell. Mol. Life Sci.* 74, 3509–3531
11. Karam, R. *et al.* (2015) The unfolded protein response is shaped by the NMD pathway. *EMBO Rep.* 16, 599–609
12. Karamyshev, A.L. *et al.* (2014) Inefficient SRP Interaction with a nascent chain triggers a mRNA quality control pathway. *Cell* 156, 146–157
13. Karamyshev, A.L. *et al.* (2020) Translational control of secretory proteins in health and disease. *Int. J. Mol. Sci.* 21, 2538
14. Hernandez, S.M. *et al.* (2021) Unexpected implication of SRP and AGO2 in Parkinson's disease: involvement in alpha-synuclein biogenesis. *Cells* 10, 2792
15. Ravindran, M.S. *et al.* (2016) Opportunistic intruders: how viruses orchestrate ER functions to infect cells. *Nat. Rev. Microbiol.* 14, 407–420
16. May, J.P. and Simon, A.E. (2021) Targeting of viral RNAs by Upf1-mediated RNA decay pathways. *Curr. Opin. Virol.* 47, 1–8
17. Markiewicz, L. *et al.* (2021) Tricks and threats of RNA viruses – towards understanding the fate of viral RNA. *RNA Biol.* 18, 669
18. Carletti, T. *et al.* (2019) Viral priming of cell intrinsic innate antiviral signaling by the unfolded protein response. *Nat. Commun.* 10, 3889
19. Shaban, M.S. *et al.* (2022) Thapsigargin: key to new host-directed coronavirus antivirals? *Trends Pharmacol. Sci.* 43, 557–568
20. Al-Beltagi, S. *et al.* (2021) Thapsigargin is a broad-spectrum inhibitor of major human respiratory viruses: coronavirus, respiratory syncytial virus and influenza A virus. *Viruses* 13, 234
21. Shaban, M.S. *et al.* (2021) Multi-level inhibition of coronavirus replication by chemical ER stress. *Nat. Commun.* 12, 5536
22. Al-Beltagi, S. *et al.* (2021) Emergent SARS-CoV-2 variants: comparative replication dynamics and high sensitivity to thapsigargin. *Virulence* 12, 2946–2956
23. Cairrão, F. *et al.* (2022) Pumilio protects Xbp1 mRNA from regulated Ire1-dependent decay. *Nat. Commun.* 13, 1587
24. Hollien, J. and Weissman, J.S. (2006) Decay of endoplasmic reticulum-localized mRNAs during the unfolded protein response. *Science* 313, 104–107
25. Guydosh, N.R. *et al.* (2017) Regulated Ire1-dependent mRNA decay requires no-go mRNA degradation to maintain endoplasmic reticulum homeostasis in S. pombe. *eLife* 6, e29216
26. Kimmig, P. *et al.* (2012) The unfolded protein response in fission yeast modulates stability of select mRNAs to maintain protein homeostasis. *eLife* 1, e00048
27. Li, W. *et al.* (2018) Engineering ER-stress dependent non-conventional mRNA splicing. *eLife* 7, e35388
28. Li, W. *et al.* (2021) Protomer alignment modulates specificity of RNA substrate recognition by Ire1. *eLife* 10, e67425
29. Abdullah, A. and Ravanan, P. (2018) The unknown face of IRE1α – beyond ER stress. *Eur. J. Cell Biol.* 97, 359–368
30. Bashir, S. *et al.* (2021) The molecular mechanism and functional diversity of UPR signaling sensor IRE1. *Life Sci.* 265, 118740
31. Han, D. *et al.* (2009) IRE1α kinase activation modes control alternate endoribonuclease outputs to determine divergent cell fates. *Cell* 138, 562–575
32. Ghosh, R. *et al.* (2014) Allosteric inhibition of the IRE1α RNase preserves cell viability and function during endoplasmic reticulum stress. *Cell* 158, 534–548
33. Tam, A.B. *et al.* (2014) Ire1 has distinct catalytic mechanisms for XBP1/HAC1 splicing and RIDD. *Cell Rep.* 9, 850–858
34. Belyy, V. *et al.* (2022) Endoplasmic reticulum stress activates human IRE1α through reversible assembly of inactive dimers into small oligomers. *eLife* 11, e74342
35. Le Thomas, A. *et al.* (2021) Decoding non-canonical mRNA decay by the endoplasmic-reticulum stress sensor IRE1α. *Nat. Commun.* 12, 7310
36. Hooks, K.B. and Griffiths-Jones, S. (2011) Conserved RNA structures in the non-canonical Hac1/Xbp1 intron. *RNA Biol.* 8, 552–556
37. Peschek, J. *et al.* (2015) A conformational RNA zipper promotes intron ejection during non-conventional XBP1 mRNA splicing. *EMBO Rep.* 16, 1688–1698
38. Anthony Tang, C.H. *et al.* (2018) Phosphorylation of IRE1 at S729 regulates RIDD in B cells and antibody production after immunization. *J. Cell Biol.* 217, 1739–1755
39. Coelho, D.S. *et al.* (2013) Xbp1-independent Ire1 signaling is required for photoreceptor differentiation and rhabdomere morphogenesis in drosophila. *Cell Rep.* 5, 791–801
40. Gaddam, D. *et al.* (2013) Comparison of mRNA localization and regulation during endoplasmic reticulum stress in drosophila cells. *Mol. Biol. Cell* 1, 14–20
41. Moore, K. and Hollien, J. (2015) Ire1-mediated decay in mammalian cells relies on mRNA sequence, structure, and translational status. *Mol. Biol. Cell* 26, 2873–2884
42. Oikawa, D. *et al.* Identification of a consensus element recognized and cleaved by IRE1a. *Nucleic Acids Res.* 38, 6265–6273.
43. Yanagitani, K. *et al.* (2009) Cotranslational targeting of XBP1 protein to the membrane promotes cytoplasmic splicing of its own mRNA. *Mol. Cell* 34, 191–200
44. Yanagitani, K. *et al.* (2011) Translational pausing ensures membrane targeting and cytoplasmic splicing of XBP1u mRNA. *Science* 33, 586–589
45. Plumb, R. *et al.* (2015) A functional link between the co-translational protein translocation pathway and the UPR. *eLife* 4, e07426
46. Adamson, B. *et al.* (2016) A multiplexed single-cell CRISPR screening platform enables systematic dissection of the unfolded protein response. *Cell* 167, 1867–1882.e21
47. Acosta-Alvear, D. *et al.* (2018) The unfolded protein response and endoplasmic reticulum protein targeting machineries converge on the stress sensor IRE1. *eLife* 7, e43036
48. Hollien, J. (2013) Evolution of the unfolded protein response. *Biochim. Biophys. Acta Mol. Cell Res.* 1833, 2458–2463

49. Tran, N.H. *et al.* (2021) The stress-sensing domain of activated IRE1α forms helical filaments in narrow ER membrane tubes. *Science* 374, 52
50. Shemorry, A. *et al.* (2019) Caspase-mediated cleavage of IRE1 controls apoptotic cell commitment during endoplasmic reticulum stress. *eLife* 8, e47084
51. Niwa, M. *et al.* (1999) A role for presenilin-1 in nuclear accumulation of Ire1 fragments and induction of the mammalian unfolded protein response. *Cell* 99, 691–702
52. Reid, D.W. and Nicchitta, C.V. (2015) Diversity and selectivity in mRNA translation on the endoplasmic reticulum. *Nat. Rev. Mol. Cell Biol.* 16, 221–231
53. Lee, J.E. *et al.* (2020) Endoplasmic reticulum contact sites regulate the dynamics of membraneless organelles. *Science* 31, 367
54. Ma, W. and Mayr, C. (2018) A membraneless organelle associated with the endoplasmic reticulum enables 3′UTR-mediated protein–protein interactions. *Cell* 175, 1492–1506.e19
55. Bhattacharyya, S. (2014) Can't RIDD off viruses. *Front. Microbiol.* 5, 292
56. Huang, S. *et al.* (2019) Emerging roles for the ER stress sensor IRE1 in metabolic regulation and disease. *J. Biol. Chem.* 294, 18726–18741
57. Wei-Lin Popp, M. and Maquat, L.E. (2013) Organizing principles of mammalian nonsense-mediated mRNA decay. *Annu. Rev. Genet.* 47, 139–165
58. Peccarelli, M. and Kebaara, B.W. (2014) Regulation of natural mRNAs by the nonsense-mediated mRNA decay pathway. *Eukaryot. Cell* 13, 1126–1135
59. Nasif, S. *et al.* (2018) Beyond quality control: the role of nonsense-mediated mRNA decay (NMD) in regulating gene expression. *Semin. Cell Dev. Biol.* 75, 78–87
60. Lykke-Andersen, S. and Jensen, T.H. (2015) Nonsense-mediated mRNA decay: an intricate machinery that shapes transcriptomes. *Nat. Rev. Mol. Cell Biol.* 16, 665–677
61. Kurosaki, T. *et al.* (2019) Quality and quantity control of gene expression by nonsense-mediated mRNA decay. *Nat. Rev. Mol. Cell Biol.* 20, 406–420
62. Ottens, F. and Gehring, N.H. (2016) Physiological and pathophysiological role of nonsense-mediated mRNA decay. *Pflügers Arch. Eur. J. Physiol.* 468, 1013–1028
63. Sakaki, K. *et al.* (2012) RNA surveillance is required for endoplasmic reticulum homeostasis. *Proc. Natl. Acad. Sci. U. S. A.* 109, 8079–8084
64. Carter, M.S. *et al.* (1995) A regulatory mechanism that detects premature nonsense codons in T-cell receptor transcripts *in vivo* is reversed by protein synthesis inhibitors *in vitro*. *J. Biol. Chem.* 270, 28995–29003
65. Joshi, M. *et al.* (2013) Small molecule modulators of eukaryotic initiation factor 2α kinases, the key regulators of protein synthesis. *Biochimie* 95, 1980–1990
66. Wang, D. *et al.* (2011) Inhibition of nonsense-mediated RNA decay by the tumor microenvironment promotes tumorigenesis. *Mol. Cell. Biol.* 31, 3670–3680
67. Li, Z. *et al.* (2017) Inhibition of nonsense-mediated RNA decay by ER stress. *RNA* 23, 378–394
68. Vattem, K.M. and Wek, R.C. (2004) Reinitiation involving upstream ORFs regulates ATF4 mRNA translation in mammalian cells. *Proc. Natl. Acad. Sci. U. S. A.* 101, 11269–11274
69. Gardner, L.B. (2008) Hypoxic inhibition of nonsense-mediated RNA decay regulates gene expression and the integrated stress response. *Mol. Cell. Biol.* 28, 3729–3741
70. Fernandes, R. *et al.* (2019) Nonsense-mediated mRNA decay in development, stress and cancer. *Adv. Exp. Med. Biol.* 1157, 41–83
71. Jagannathan, S. *et al.* (2014) Multifunctional roles for the protein translocation machinery in RNA anchoring to the endoplasmic reticulum. *J. Biol. Chem.* 289, 25907–25924
72. Hein, M.Y. *et al.* (2015) A human interactome in three quantitative dimensions organized by stoichiometries and abundances. *Cell* 163, 712–723
73. Longman, D. *et al.* (2007) Mechanistic insights and identification of two novel factors in the *C. elegans* NMD pathway. *Genes Dev.* 21, 1075–1085
74. Aoki, T. *et al.* (2009) Identification of the neuroblastoma-amplified gene product as a component of the syntaxin 18 complex implicated in Golgi-to-endoplasmic reticulum retrograde transport. *Mol. Biol. Cell* 20, 2639–2649
75. Çivril, F. *et al.* (2010) Structural analysis of the RZZ complex reveals common ancestry with multisubunit vesicle tethering machinery. *Structure* 18, 616–626
76. Brannan, K.W. *et al.* (2016) SONAR Discovers RNA-binding proteins from analysis of large-scale protein–protein interactomes. *Mol. Cell* 64, 282–293
77. Anastasaki, C. *et al.* (2011) Dhx34 and Nbas function in the NMD pathway and are required for embryonic development in zebrafish. *Nucleic Acids Res.* 39, 3686–3694
78. Gao, Y. *et al.* (2023) Argonaute-dependent ribosome-associated protein quality control. *Trends Cell Biol.* 33, 260–272
79. Gao, Y. *et al.* (2022) Lipid-mediated phase separation of AGO proteins on the ER controls nascent-peptide ubiquitination. *Mol. Cell* 82, 1313–1328.e8
80. Li, X. *et al.* (2020) AGO2 and its partners: a silencing complex, a chromatin modulator, and new features. *Crit. Rev. Biochem. Mol. Biol.* 55, 33–53
81. Stalder, L. *et al.* (2013) The rough endoplasmatic reticulum is a central nucleation site of siRNA-mediated RNA silencing. *EMBO J.* 32, 1115–1127
82. Shankar, S. *et al.* (2016) KRAS engages AGO2 to enhance cellular transformation. *Cell Rep.* 14, 1448–1461
83. Höck, J. *et al.* (2007) Proteomic and functional analysis of Argonaute-containing mRNA–protein complexes in human cells. *EMBO Rep.* 8, 1052–1060
84. Barman, B. and Bhattacharyya, S.N. (2015) mRNA targeting to endoplasmic reticulum precedes Ago protein interaction and microRNA (miRNA)-mediated translation repression in mammalian cells. *J. Biol. Chem.* 290, 24650–24656
85. Kim, Y.J. *et al.* (2014) Traffic into silence: endomembranes and post-transcriptional RNA silencing. *EMBO J.* 33, 968–980
86. Upton, J.P. *et al.* (2012) IRE1α cleaves select microRNAs during ER stress to derepress translation of proapoptotic caspase-2. *Science* 338, 818–822
87. Quwaider, D. *et al.* (2022) RNA sequencing identifies novel regulated IRE1-dependent decay targets that affect multiple myeloma survival and proliferation. *Exp. Hematol. Oncol.* 11, 18
88. Kim, Y.K.I. and Maquat, L.E. (2019) UPFront and center in RNA decay: UPF1 in nonsense-mediated mRNA decay and beyond. *RNA* 25, 407–422
89. Elbarbary, R.A. *et al.* (2017) Tudor-SN-mediated endonucleolytic decay of human cell microRNAs promotes G_1/S phase transition. *Science* 356, 859–862
90. Jomaa, A. *et al.* (2022) Mechanism of signal sequence handover from NAC to SRP on ribosomes during ER-protein targeting. *Science* 375, 839–844
91. Liu, J. *et al.* (2004) Argonaute2 is the catalytic engine of mammalian RNAi. *Science* 305, 1437–1441
92. Pinarbasi, E.S. *et al.* (2018) Pathogenic signal sequence mutations in progranulin disrupt SRP interactions required for mRNA stability. *Cell Rep.* 23, 2844–2851
93. Joazeiro, C.A.P. (2019) Mechanisms and functions of ribosome-associated protein quality control. *Nat. Rev. Mol. Cell Biol.* 6, 368–383
94. D'Orazio, K.N. and Green, R. (2021) Ribosome states signal RNA quality control. *Mol. Cell* 81, 1372–1383
95. Christianson, J.C. *et al.* (2023) Mechanisms of substrate processing during ER-associated protein degradation. *Nat. Rev. Mol. Cell Biol.* 11, 777–796
96. Phillips, B.P. and Miller, E.A. (2020) Ribosome-associated quality control of membrane proteins at the endoplasmic reticulum. *J. Cell Sci.* 133, jcs251983
97. Kadowaki, H. *et al.* (2018) Molecular mechanism of ER stress-induced pre-emptive quality control involving association of the translocon, Derlin-1, and HRD1. *Sci. Rep.* 8, 7317
98. Kuroha, K. *et al.* (2009) Upf1 stimulates degradation of the product derived from aberrant messenger RNA containing a specific nonsense mutation by the proteasome. *EMBO Rep.* 10, 1265–1271
99. Chu, V. *et al.* (2021) Selective destabilization of polypeptides synthesized from NMD-targeted transcripts. *Mol. Biol. Cell* 32, ar38

100. Inglis, A.J. *et al.* (2023) Coupled protein quality control during nonsense-mediated mRNA decay. *J. Cell Sci.* 136, jcs261216
101. Hwang, H.J. *et al.* (2021) UPF1: from mRNA surveillance to protein quality control. *Biomedicines* 9, 995
102. Arribere, J.A. and Fire, A.Z. (2018) Nonsense mRNA suppression via nonstop decay. *eLife* 7, e33292
103. Costa-Mattioli, M. and Walter, P. (2020) The integrated stress response: from mechanism to disease. *Science* 368, eaat5314
104. Korennykh, A.V. *et al.* (2009) The unfolded protein response signals through high-order assembly of Ire1. *Nature* 457, 687–693
105. Lee, K.P.K. *et al.* (2008) Structure of the dual enzyme Ire1 reveals the basis for catalysis and regulation in nonconventional RNA splicing. *Cell* 132, 89–100
106. Hollien, J. *et al.* (2009) Regulated Ire1-dependent decay of messenger RNAs in mammalian cells. *J. Cell Biol.* 186, 323–331
107. Fatscher, T. *et al.* (2015) Mechanism, factors, and physiological role of nonsense-mediated mRNA decay. *Cell. Mol. Life Sci.* 72, 4523–4544
108. Karousis, E.D. and Mühlemann, O. (2019) Nonsense-mediated mRNA decay begins where translation ends. *Cold Spring Harb. Perspect. Biol.* 11, a032862
109. Kashima, I. *et al.* (2006) Binding of a novel SMG-1–Upf1–eRF1–eRF3 complex (SURF) to the exon junction complex triggers Upf1 phosphorylation and nonsense-mediated mRNA decay. *Genes Dev.* 20, 355–367
110. Singh, G. *et al.* (2007) Communication with the exon–junction complex and activation of nonsense-mediated decay by human Upf proteins occur in the cytoplasm. *Mol. Cell* 27, 780–792
111. Lejeune, F. *et al.* (2003) Nonsense-mediated mRNA decay in mammalian cells involves decapping, deadenylating, and exonucleolytic activities. *Mol. Cell* 12, 675–687
112. Eberle, A.B. *et al.* (2008) SMG6 promotes endonucleolytic cleavage of nonsense mRNA in human cells. *Nat. Struct. Mol. Biol.* 16, 49–55
113. Huntzinger, E. *et al.* (2008) SMG6 is the catalytic endonuclease that cleaves mRNAs containing nonsense codons in metazoan. *RNA* 14, 2609–2617
114. Loh, B. *et al.* (2013) The SMG5–SMG7 heterodimer directly recruits the CCR4–NOT deadenylase complex to mRNAs containing nonsense codons via interaction with POP2. *Genes Dev.* 27, 2125–2138
115. Mailliot, J. *et al.* (2022) No-nonsense: insights into the functional interplay of nonsense-mediated mRNA decay factors. *Biochem. J.* 479, 973–993
116. Ketting, R.F. (2011) The many faces of RNAi. *Dev. Cell* 20, 148–161
117. Svoboda, P. (2020) Key mechanistic principles and considerations concerning RNA interference. *Front. Plant Sci.* 11, 495350
118. Shabalina, S.A. and Koonin, E.V. (2008) Origins and evolution of eukaryotic RNA interference. *Trends Ecol. Evol.* 23, 578
119. Obbard, D.J. *et al.* (2008) The evolution of RNAi as a defence against viruses and transposable elements. *Philos. Trans. R. Soc. B Biol. Sci.* 364, 99–115
120. Nakanishi, K. (2022) Anatomy of four human Argonaute proteins. *Nucleic Acids Res.* 50, 6618–6638
121. Kuzuo Glu-Öztürk, D. *et al.* (2016) miRISC and the CCR4–NOT complex silence mRNA targets independently of 43S ribosomal scanning. *EMBO J.* 35, 1186–1203
122. Cirone, M. (2021) ER stress, UPR activation and the inflammatory response to viral infection. *Viruses* 13, 798
123. Miorin, L. *et al.* (2012) Formation of membrane-defined compartments by tick-borne encephalitis virus contributes to the early delay in interferon signaling. *Virus Res.* 163, 660–666
124. Överby, A.K. *et al.* (2010) Tick-borne encephalitis virus delays interferon induction and hides its double-stranded RNA in intracellular membrane vesicles. *J. Virol.* 84, 8470–8483
125. Eckard, S.C. *et al.* (2014) The SKIV2L RNA exosome limits activation of the RIG-I-like receptors. *Nat. Immunol.* 15, 839–845
126. Han, Y. *et al.* (2014) Structure of human RNase L reveals the basis for regulated RNA decay in the IFN response. *Science* 343, 1244–1248
127. Manivannan, P. *et al.* (2020) RNase L amplifies interferon signaling by inducing protein kinase R-mediated antiviral stress granules. *J. Virol.* 94, e00205-20
128. Malathi, K. *et al.* (2007) Small self-RNA generated by RNase L amplifies antiviral innate immunity. *Nature* 448, 816–819
129. Imagawa, Y. *et al.* (2008) RNase domains determine the functional difference between IRE1α and IRE1β. *FEBS Lett.* 582, 656–660
130. Iwawaki, T. *et al.* (2001) Translational control by the ER transmembrane kinase/ribonuclease IRE1 under ER stress. *Nat. Cell Biol.* 3, 158–164
131. Bertolotti, A. *et al.* (2001) Increased sensitivity to dextran sodium sulfate colitis in IRE1beta-deficient mice. *J. Clin. Invest.* 107, 585–593
132. Lencer, W.I. *et al.* (2015) Innate immunity at mucosal surfaces: the IRE1–RIDD–RIG-I pathway. *Trends Immunol.* 36, 401–409
133. Li, Y. *et al.* (2016) Induction and suppression of antiviral RNA interference by influenza A virus in mammalian cells. *Nat. Microbiol.* 2, 16250
134. Qiu, Y. *et al.* (2017) Human virus-derived small RNAs can confer antiviral immunity in mammals. *Immunity* 46, 992–1004.e5
135. Wada, M. *et al.* (2018) Interplay between coronavirus, a cytoplasmic RNA virus, and nonsense-mediated mRNA decay pathway. *Proc. Natl. Acad. Sci. U. S. A.* 115, E10157–E10166
136. Balistreri, G. *et al.* (2014) The host nonsense-mediated mRNA decay pathway restricts mammalian RNA virus replication. *Cell Host Microbe* 16, 403–411
137. Ramage, H.R. *et al.* (2015) A combined proteomics/genomics approach links hepatitis C virus infection with nonsense-mediated mRNA decay. *Mol. Cell* 57, 329
138. Granata, V. *et al.* (2023) Modulation of NBAS-related functions in the early response to SARS-CoV-2 infection. *Int. J. Mol. Sci.* 24, 2634
139. Sirpilla, O. *et al.* (2020) SARS-CoV-2-encoded proteome and human genetics: from interaction-based to ribosomal biology impact on disease and risk processes. *J. Proteome Res.* 19, 4275–4290